

# **Medium Access Control and Network Layer Design for 60 GHz Wireless Personal Area Networks**



# **Medium Access Control and Network Layer Design for 60 GHz Wireless Personal Area Networks**

PROEFSCHRIFT

ter verkrijging van de graad van doctor  
aan de Technische Universiteit Delft,  
op gezag van de Rector Magnificus Prof. dr. ir. K.C.A.M. Luyben,  
voorzitter van het College voor Promoties,  
in het openbaar te verdedigen op dinsdag 09 juni 2010 om 12.30 uur  
door

Xueli AN

Elektrotechnisch ingenieur van Technische Universiteit Delft, the Netherlands  
geboren te Harbin, China.

Dit proefschrift is goedgekeurd door de promotor:

Prof. dr. ir. I.G.M.M. Niemegeers

Samenstelling promotiecommissie:

Rector Magnificus	voorzitter
Prof. dr. ir. I.G.M.M. Niemegeers	Technische Universiteit Delft, promotor
Prof. dr. J.R. Long	Technische Universiteit Delft
Prof. dr. ir. P.A.M. Baltus	Technische Universiteit Eindhoven
Prof. dr. ir. S.M. Heemsta de Groot	Technische Universiteit Delft
Dr. ir. P.F.M. Smulders	Technische Universiteit Eindhoven
Dr. R.R. Venkatesha Prasad	Technische Universiteit Delft
Dr. ir. M.J. Bentum	Universiteit Twente
Prof. dr. ir. L.P. Ligthart	Technische Universiteit Delft

Copyright © 2010 by Xueli An

All rights reserved. No part of the material protected by this copyright notice may be reproduced or utilized in any form or by any means, electronic or mechanical, including photocopying, recording or by any information storage and retrieval system, without the prior permission of the author.

ISBN 978-94-6113-003-7

Printed in the Netherlands by Ipskapm Drukkers.

Typeset by the author with the L<sup>A</sup>T<sub>E</sub>X Documentation System.

Author email: [anxueli@gmail.com](mailto:anxueli@gmail.com)

# Acknowledgements

This dissertation presents the research work during my study towards a PhD degree in the Wireless and Mobile Communications (WMC) Group, Delft University of Technology (TU Delft). It would not have been possible without the support and help of many people. My special thanks go to Prof. Ignas Niemegeers, the chairman of WMC and also my promoter, for providing me an opportunity to pursue my doctoral research. I am thankful for his guidance and patience. He opened a door for me to the academic area. I would like to thank my supervisor Dr. R. R. Venkatesha Prasad for motivating and encouraging me to develop my career in the academic area. I would also like to express my gratitude to Dr. Ramin Hekmat. As my supervisor and also as my friend, his guidance and sense of humor helped me to get through a lot of difficulties.

Including my master study, I spent six years in TU Delft. The wonderful working environment, colorful group activities let me have a joyful stay in the Netherlands. I am grateful to Dr. Jos Weber for giving me inspiration and suggestion for my work in the SiGi Spot project. I would like to thank Dr. Gerard Janssen apart from teaching me and helping me on various occasions also helped me to translate part of my thesis into Dutch. I would like to thank Umar Hassan Rizvi, who worked together with me in the SiGi project, for discussions we had and our cheerful friendship. I would also like to thank Siyu Tang, Dajie Liu and Javad Vazifehdan. Our interesting discussions always gave me fresh breath. My sincere thanks go to our secretariat Laura Bauman, Wendy Murtinu-Van Schagen, Marjon Verkaik-Vonk, Dominique Meijer and Stefanie van Gentvoort, for helping me to process all kinds official work. My words of acknowledgement also go to all my Chinese friends, Jinglong Zhou, Yue Lu, Siyu Tang, Yi Wang, Dajie Liu, Qin Tang, Yanying Gu. Our “Wokshop” event highlighted my wonderful life in Delft. I would like to thank Jing Wang, Huijuan Wang and Cheng Guo, for their kind help in these six long years.

I would like to thank all my colleagues from the Ubiquitous Mobile Commu-

nications (UMC) Group, National Institute of Information and Communications Technology (NICT), Yokosuka, Japan and in particular to Lan Zhou, Chin-Sean Sum, Tuncer Baykas, Junyi Wang for their open discussions and comments on my research. My heartfelt gratitude also goes to my dear friends Jing Gao and Yi Jiang, who helped me to experience the joyful life in Japan. Special thanks go to my supervisor in NICT, Dr. Hiroshi Harada. His comprehensive knowledge and research experiences gave me a lot of inspiration. I sincerely thank him for his continual support and encouragement.

Moreover, I would like to thank all my PhD committee members for their time and efforts in reviewing my research work.

This dissertation is dedicated to my parents, Xiangxian Xu and Bingzhe An, for their unconditional love and patience. I would also express my thanks to my grandparents, Jishu Xu and Jinshan Jin, for their endless love and support at every step in my life. I would like to thank my sister Linda An, who is the treasure of my life. Thanks for being there for me and always smiling for me. Special thanks for my fiancé Alexander De Luca, who is not only my life partner, but also my best friend and illuminator, mere words cannot expressed my gratitude for you. Thanks for being with me at the most beautiful season in our life. This thesis is also dedicated to you.

*Delft,  
May 2010*

*Xueli An*

# Summary

The unlicensed frequency band around 60 GHz is a very promising spectrum due to its potential to provide multiple gigabits per second based data rates for short range wireless communication. Hence, 60 GHz radio is an attractive candidate to enable ultra high rate Wireless Personal Area Networks (WPANs), which are expected to support wireless multimedia applications like high-definition video streaming, ultra high speed content download, etc. Till now, the main research effort related to 60 GHz radio is at the physical layer design and channel model investigation. However, the unique properties of 60 GHz radio also create new research challenges for 60 GHz networking. Hence the aim of this dissertation is to provide an in-depth view on the Medium Access Control (MAC) layer and Network layer design for 60 GHz WPANs.

To obtain sufficient link budget for multiple gigabits per second based wireless communication, directional antennas are needed in 60 GHz systems. Although directional antennas exhibit many advantages compared to omni-directional antennas, their deployment is very challenging for the MAC and Network layer protocols. For instance, to set-up directional connections, devices are expected to know the direction of their neighbors. The performance of directional neighbor discovery protocols is investigated in this dissertation to review the impact of directional antennas on the network setup durations. With the knowledge of orientation information of the network components, a resource management scheme, especially for the IEEE 802.15.3 featured WPANs, is proposed to support concurrent transmissions using directional antennas in a Time Division Multiple Access (TDMA) fashion with Quality of Service (QoS) and fairness provisioning. To further improve the transmission efficiency of the MAC layer protocol, standard frame aggregation and low latency frame aggregation mechanisms are investigated to alleviate the impact of transmission overhead. Another issue addressed at the MAC layer in this dissertation is how to support highly-reliable transmissions

using 60 GHz radio. Due to the weak penetration and reflection properties, the Line-of-Sight (LOS) link between two 60 GHz components is easily blocked by obstacles in indoor environments, which is a severe hurdle that influences the reliability of 60 GHz systems. To resolve the link blockage problem, instant decision based beam switching mechanisms and environment learning based beam switching mechanisms are proposed in this dissertation targeting for different usage scenarios.

Furthermore, to support the coexistence of multiple 60 GHz WPANs, a systematic analysis of using synchronization frame to mitigate Co-Channel Interference (CCI) is performed. It has been shown that the link capacity and the guaranteed transmission distance within a WPAN are upper bounded by the CCI. To enable the multi-hop communication among these inter-connected 60 GHz WPANs, the Network layer design is involved in this dissertation. First, a fundamental investigation is provided in ad-hoc networks for using directional antennas in the aspects of topology control and message dissemination. The results provide valuable insights for using directional antennas for multi-hop communication. Second, focusing on the specific network topology of WPANs, the performance of inter-piconet route discovery is examined. Moreover, a joint QoS routing and channel resource allocation mechanism is proposed to resolve the inter-piconet channel resource reservation collision problem.

*Xueli An*



# Samenvatting

De licentievrije frequentieband rond 60 GHz biedt zeer goede mogelijkheden voor draadloze verbindingen met datasnelheden van meerdere gigabits per seconde (Gb/s) over korte afstanden. Daarom is 60 GHz radio een aantrekkelijke optie voor Wireless Personal Area Networks (WPANs) met zeer hoge datasnelheden, waarmee draadloze multimedia toepassingen zoals hoge definitie video en het zeer snel downloaden van gegevens, kunnen worden gerealiseerd. Tot nu toe heeft het onderzoek op het gebied van 60 GHz radio zich geconcentreerd op de kanaalmodellering en het ontwerp van de fysische laag. Echter, de unieke eigenschappen van 60 GHz radio creëren ook nieuwe onderzoeksuitdagingen op het gebied van de netwerkaspecten. Het doel van dit proefschrift is het verschaffen van een diepgaand inzicht in het ontwerp van de Medium Access Control (MAC) en de netwerklaag protocollen voor 60 GHz WPANs.

Om een voldoende ruim linkbudget voor draadloze 60 GHz communicatieverbindingen met meerdere Gb/s te verkrijgen, is het gebruik van gerichte antennes noodzakelijk. Hoewel richtingsgevoelige antennes veel voordelen bieden in vergelijking met rondomgevoelige antennes, leidt de toepassing van deze antennes tot extra uitdagingen bij het ontwerp van de MAC- en netwerklaag protocollen. Bijvoorbeeld, voor het opzetten van een verbinding met richtingsgevoelige antennes moeten de betrokken systemen elkaars relatieve lokaties kennen om de antennebundels goed te kunnen uitrichten. In dit proefschrift wordt de kwaliteit onderzocht van protocollen voor het ontdekken van andere nabije netwerkgebruikers om de invloed van richtingsgevoelige antennes op de tijdsduur die nodig is om een netwerk op te zetten, te karakteriseren. Op basis van de kennis van de antenneoriëntaties van de netwerkgebruikers, wordt een resource management schema voorgesteld (in het bijzonder voor IEEE 802.15.3 WPANs) dat verbindingen met richtingsgevoelige antennes op basis van Time Division Multiple Access (TDMA) met Quality of Service (QoS) en een eerlijke verdeling van de capaciteit ondersteund. Om de transmissie-efficiëntie van het MAC-protocol verder te verhogen, zijn

methoden voor het samenvoegen van standaard frames en “low latency” frames onderzocht, waarmee de te verzenden overheadinformatie kan worden beperkt. Een ander aspect van de MAC-laag dat in dit proefschrift aan de orde komt, is hoe het met hoge betrouwbaarheid verzenden van informatie op 60 GHz kan worden ondersteund. Door de hoge penetratiedemping en de reflectie eigenschappen van 60 GHz signalen, wordt de direct-zicht (Line-of-Sight (LOS)) verbinding tussen twee systemen in een indoor omgeving gemakkelijk geblokkeerd, wat van grote invloed is op de betrouwbaarheid van zo’n verbinding. Om dit blokkeringsprobleem op te lossen, worden voor verschillende gebruikersscenarios methoden voorgesteld op basis van het instantaan schakelen tussen verschillende antennebundels op basis van geleerde informatie over de omgeving.

Om de coëxistentie van meerdere 60 GHz WPANs te ondersteunen, is een systematische analyse van het gebruik van synchronisatie frames uitgevoerd om zo eigen-kanaal interferentie (Co-Channel Interference (CCI)) tegen te gaan. Aange-toond is dat de capaciteit van een verbinding en de gegarandeerde transmissie afstand binnen een WPAN begrensd worden door CCI. Om multi-hop communicatie tussen onderling verbonden 60 GHz WPANs toe te laten, wordt in dit proefschrift ook aandacht besteed aan het ontwerp van de netwerklaag. Ten eerste is fundamenteel onderzoek uitgevoerd naar de invloed van het gebruik van richtingsgevoelige antennes op de netwerktopologie en de verspreiding van berichten in ad-hoc netwerken. De resultaten hiervan geven een waardevol inzicht in het gebruik van richtingsgevoelige antennes voor multi-hop communicatie. Ten tweede is voor de specifieke netwerktopologie van WPANs, de kwaliteit van inter-piconet route-ontdekking onderzocht. Verder wordt een gecombineerd QoS-routerings- en kanaaltoewijzingsmechanisme voorgesteld om het botsingsprobleem tussen inter-piconet-kanaalreserveringsberichten op te lossen.

*Xueli An*



# Contents

<b>Acknowledgements</b>	<b>i</b>
<b>Summary</b>	<b>iii</b>
<b>Samenvatting</b>	<b>v</b>
<b>1 Introduction</b>	<b>1</b>
1.1 Prologue: Revolution through Wireless Communication . . . . .	2
1.2 60 GHz Radio Background . . . . .	6
1.2.1 Worldwide Regulation and Standardization . . . . .	6
1.2.2 60 GHz Radio Vision . . . . .	7
1.2.3 60 GHz Radio Properties . . . . .	8
1.3 Directional Antenna . . . . .	9
1.4 Research Challenges . . . . .	10
1.5 Dissertation Outline . . . . .	12
1.6 Summary of Main Contributions . . . . .	13
1.7 Chapter Summary . . . . .	15
<b>2 Neighbor Discovery using Directional Antennas</b>	<b>17</b>
2.1 Background . . . . .	18
2.2 System Model and Assumptions . . . . .	20
2.3 Antenna Pattern and Link Model . . . . .	21
2.3.1 Directional Antennas . . . . .	21
2.3.2 Radio Propagation Model and Link Probability . . . . .	24
2.4 Analytical Model for Directional Neighbor Discovery . . . . .	27
2.4.1 D-ND Analysis for a Two-Device Model . . . . .	27
2.4.2 D-ND Analysis for a Generic Model . . . . .	30

2.5	Numerical Results . . . . .	34
2.6	Antenna Pattern and Link Model Influence on D-ND . . . . .	37
2.6.1	D-ND Ratio . . . . .	37
2.6.2	D-ND Overhead . . . . .	38
2.6.3	Influence of $p_t$ and $k$ . . . . .	39
2.7	Chapter Summary . . . . .	40
<b>3</b>	<b>Enhanced IEEE 802.15.3 MAC for 60 GHz WPANs</b>	<b>41</b>
3.1	Introduction . . . . .	42
3.2	MAC for 60 GHz WPANs . . . . .	44
3.2.1	IEEE 802.15.3 MAC Overview . . . . .	44
3.2.2	MAC Expectations for 60 GHz WPANs . . . . .	45
3.3	Device Orientation Profile . . . . .	47
3.4	Resource Management . . . . .	49
3.5	Directional Transmission Scheduling (DTS) . . . . .	51
3.5.1	System Model . . . . .	52
3.5.2	Link Coexistence Test . . . . .	52
3.5.3	DTS Procedure . . . . .	52
3.5.4	Spatial Reuse Capability . . . . .	54
3.6	QoS and Fairness Considerations in Resource Allocation . . . . .	55
3.7	Simulation in OPNET . . . . .	57
3.7.1	Simulation Model . . . . .	57
3.7.2	Simulation Results . . . . .	60
3.8	Chapter Summary . . . . .	64
<b>4</b>	<b>Enabling High Performance Transmission in 60 GHz WPANs using Frame Aggregation</b>	<b>65</b>
4.1	Introduction . . . . .	66
4.2	Frame Aggregation in IEEE 802.15.3c . . . . .	67
4.3	Analytical Model . . . . .	68
4.3.1	Imm-ACK . . . . .	69
4.3.2	Standard Frame Aggregation with Blk-ACK . . . . .	70
4.3.3	Low Latency Frame Aggregation with Blk-ACK . . . . .	74
4.4	Performance Evaluation . . . . .	75
4.4.1	Simulation Validation . . . . .	75
4.4.2	Numerical Results . . . . .	76
4.5	Chapter Summary . . . . .	79
<b>5</b>	<b>Resolving Link Blockage Problem in 60 GHz WPANs using Beam Switching</b>	<b>81</b>
5.1	Introduction . . . . .	82
5.2	System Model . . . . .	83

5.2.1	Work Assumptions . . . . .	83
5.2.2	Environment Model . . . . .	83
5.2.3	Human Body Blockage Model . . . . .	84
5.2.4	Propagation Model . . . . .	85
5.3	Proposal to Resolve Link Blockage Problem . . . . .	85
5.3.1	Beam Switching Mechanisms . . . . .	85
5.3.2	Visibility Test . . . . .	86
5.4	Performance Evaluation . . . . .	87
5.4.1	Simulation Specifications . . . . .	87
5.4.2	Simulation Results . . . . .	90
5.5	Chapter Summary . . . . .	92
<b>6</b>	<b>Interference Mitigation for the Coexisting 60 GHz WPANs</b>	<b>95</b>
6.1	Introduction . . . . .	96
6.2	Interference Mitigation Mechanism . . . . .	97
6.3	Analytical Model . . . . .	98
6.3.1	Interference Indication Function Derivation . . . . .	98
6.3.2	Relationship between CCI and Throughput . . . . .	101
6.4	Performance Evaluation . . . . .	104
6.5	Chapter Summary . . . . .	110
<b>7</b>	<b>Impact of Directional Antennas on Multi-hop Networks</b>	<b>111</b>
7.1	Introduction . . . . .	112
7.2	Neighbor Attachment using Directional Antennas . . . . .	113
7.2.1	Neighbor Attachment Policies . . . . .	114
7.2.2	Impact on Interference . . . . .	116
7.3	Probabilistic-based Directional Message Dissemination . . . . .	119
7.3.1	Preliminaries . . . . .	120
7.3.2	Gossiping Using Directional Antennas . . . . .	123
7.3.3	Directional Gossiping Extensions . . . . .	128
7.4	Chapter Summary . . . . .	131
<b>8</b>	<b>60 GHz Multi-hop Communication in Home Networks</b>	<b>133</b>
8.1	Introduction . . . . .	134
8.1.1	Mesh Topology to Support Piconet Coexistence . . . . .	135
8.2	Inter-Piconet Route Discovery . . . . .	137
8.2.1	Mesh Topology Enhancement . . . . .	137
8.2.2	Inter-Piconet Route Discovery Protocols . . . . .	138
8.2.3	Simulation Model . . . . .	139
8.3	Joint QoS Routing and Resource Reservation . . . . .	147
8.3.1	QoS Routing . . . . .	147
8.3.2	Inter-piconet Channel Resource Allocation . . . . .	150

8.3.3	Simulation Model and Results . . . . .	151
8.4	Chapter Summary . . . . .	157
<b>9</b>	<b>Conclusions</b>	<b>159</b>
9.1	Recapitulation . . . . .	160
9.2	Directions for Future Work . . . . .	165
9.3	Epilogue . . . . .	166
<b>A</b>	<b>Occupancy Problem in Directional Neighbor Discovery</b>	<b>169</b>
<b>B</b>	<b>Implementation of Enhanced IEEE 802.15.3 MAC</b>	<b>171</b>
B.1	Root Process Modeling . . . . .	172
B.2	CAP Process Modeling . . . . .	172
B.3	MCTA Process Modeling . . . . .	174
B.4	CTA Process Modeling . . . . .	175
<b>C</b>	<b>IEEE 802.15.3c Physical Layer Specification</b>	<b>177</b>
	<b>Bibliography</b>	<b>181</b>
	<b>List of Abbreviations</b>	<b>191</b>
	<b>Publications by the Author</b>	<b>195</b>
	<b>Curriculum Vitae</b>	<b>199</b>

# Chapter 1

## Introduction

“When it is dark enough, you can see the stars.”

- Ralph Waldo Emerson

*60 GHz radio is a promising technology that can enable wireless transmission data rate in the order of gigabits per second. To position 60 GHz radio technology in the field, a brief history about wireless communication is introduced in this chapter. The background of 60 GHz radio, i.e. worldwide regulation and standardization activities, the target market and applications, and the fundamental propagation properties, etc. are presented. The main focus of this dissertation is to enable high-capacity and high-reliability communication in wireless personal area networks using 60 GHz radio technology. To achieve this goal, the research challenges are identified in this chapter. Finally, the outline and major contributions of this dissertation are provided.*

## 1.1 Prologue: Revolution through Wireless Communication

### Primary Stage

Thousands of years ago, people developed postal systems and used couriers or pigeons to transmit information between towns and cities. Even though the speed of couriers was limited and the accuracy of pigeons was low, those were the primitive attempts of the ancient people to set up a *network* for communication. As far back as the Zhou Dynasty in China (11th-2nd BC), there are records about the use of fire and smoke for military communication<sup>1</sup>. This is just one of the many examples to show how people tried to use a faster medium to transmit information and it could be considered as the embryonic form of telecommunication. *Telecommunication is transmission of signals over a distance for the purpose of communication*<sup>2</sup>. The official beginning of telecommunication can be traced back to the early 19-th century. In 1837, Samuel Morse developed and publicly demonstrated single-wire telegraph. The first transatlantic telegraph underwater cable connecting between North America and Europe was completed in 1866, which marked the beginning of the international telecommunication network. After that, messages could be carried over a long distance. With the invention of telephone by Alexander Graham Bell in 1876, for the first time human voices could be conveyed at velocity of light, and then interactive communication came into the stage. Since then, telecommunication finished its initial stage and grew at an amazing speed. Till now, the Public Switched Telephone Network (PSTN) is the major communication network. As a branch of telecommunication, wireless communication embraced its beginning in 1887, when Heinrich Hertz demonstrated the existence of electromagnetic waves. It validated Maxwell's theory, which was proposed by James Clerk Maxwell in 1873<sup>3</sup>. Guglielmo Marconi transmitted the first transatlantic wireless signals in 1901, which proved that wireless signal could also be sent hundreds of kilometers away. Even though people overcame the distance, and messages could be transmitted within a couple of minutes instead of several weeks by ship, the amount of transmitted information was still limited. At the turn of the twentieth century, wireless communication opened a new era. In 1946, the first public mobile telephone service was launched in the USA, which brought new thrill of carrying voice via radios. It marked the beginning of wireless mobile communication.

### Developing Stage

In the late twentieth century, wireless mobile communication embraced its blooming prosperity. Mobile phones became the most successful personal communi-

---

<sup>1</sup>Holy smoke: In the Vatican, smoke is still used to indicate the results of the selection of the new Pope – *black* smoke for the failed ballot and *white* smoke for the successful election.

<sup>2</sup>Tele in Greek means far, distance.

<sup>3</sup>However, it was a pity that Hertz himself did not foresee the impact of his contribution. When he was asked about the importance of his experiment, he said, "Nothing, I guess."



cation devices. Since the first generation (1G) of mobile cellular networks was launched in early 1980, mobile cellular networks experienced a spectacular evolution, from an analog to a digital system, from the second generation (2G) Global System for Mobile communications (GSM) system to the third generation (3G) Universal Mobile Telecommunications System (UMTS). 3G networks promise a data rate as high as 2 megabits per second (Mbps). Voice is not the only carrying message anymore, a wider range of applications are offered by 3G, for instance mobile TV, video conferencing, etc. This evolution is not going to slow down. It is already moving forward to the fourth generation (4G) mobile network which aims to cater for higher data rates and better Quality of Service (QoS).

Except for mobile cellular networks, wireless communication has been expanded with more branches. According to their geographical coverage, wireless networks are classified into four categories: Wireless Wide-Area Networks (WWAN), which refers to the mobile cellular network, Wireless Metropolitan Area Networks (WMAN), Wireless Local Area Networks (WLAN) and Wireless Personal Area Networks (WPAN). WMAN aims to provide a high-speed broadband wireless access over a large metropolitan area, which is featured by IEEE 802.16 standard<sup>4</sup>. Compared to WWAN and WMAN, WLAN covers a smaller geographical area, e.g. home and office environment, or a couple of buildings. WLAN is featured by the IEEE 802.11 standard, which is also called as Wi-Fi<sup>5</sup>. After mobile cellular networks, Wi-Fi is another successful commercialized wireless technology. It brings an incremental quality in the life pattern of people by replacing cables with radio for wireless internet access. Wi-Fi is widely used for home networks, campus networks and city-wide networks. WPAN is a short range network, which covers an area of few meters. WPAN is typically used for communications among consumer electronic devices close to a person. IEEE 802.15 is denoted for the standardization activities for WPANs. IEEE 802.15 Task Group 1 (TG1), which is also called as IEEE 802.15.1, developed a WPAN standard based on Bluetooth version 1.0 [2]. The IEEE 802.15.3 was formed to specify a Medium Access Control (MAC) and Physical layer (PHY) standard for high-rate WPANs [3]. IEEE 802.15.3 attempted to develop a specification for Ultra-WideBand (UWB) based PHY layer. Unfortunately, this task group was withdrawn in Jan. 2006, due to the fact that the members within this task group could not get an agreement between the two PHY proposals: Multi-band Orthogonal Frequency Division Multiplexing (MB-OFDM) and Direct Sequence UWB (DS-UWB). IEEE 802.15.4 was formed to standardize low-rate WPANs, which is also known as ZigBee [4]. A brief WLAN and WPAN evolution graph is shown in Figure 1.1.

---

<sup>4</sup>IEEE is the abbreviation for Institute of Electrical and Electronics Engineers, which is an international non-profit, professional association for advanced technologies.

<sup>5</sup>Wi-Fi is a trademark of Wi-Fi Alliance [1], which is a global non-profit industry association of the companies dedicated to promote the development of WLANs.

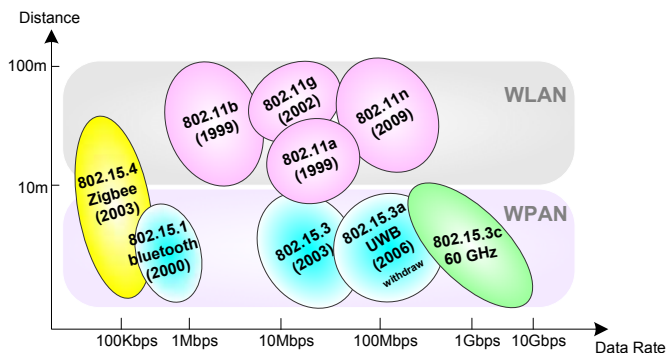


Figure 1.1: WLAN and WPAN evolution.

### Current Stage

Consumers are not easily satisfied with web page surfing using wireless technologies. They desire the flexibility from wireless technology, but also expect the same QoS as wired networks. Video streaming, online gaming, Voice over Internet Protocol (VoIP), etc., all kinds of internet-based multimedia applications open up a fascinating area for the user experience. Meanwhile, they also drive the raise of the wireless data rates. Wi-Fi evolved from IEEE 802.11 a, IEEE 802.11 b, to IEEE 802.11 g, and now, it arrives at IEEE 802.11 n. The supported data rate leaps from 11 Mbps to 600 Mbps.

After the emergence of High Definition TeleVision (HDTV), it rapidly occupies the market. According to a study from IMS research<sup>6</sup>, the number of households HDTV will be increased from 45 million in 2007 to 255 million in 2013, and the Blu-ray Disc market will also experience strong growth within the following years. This means that wireless multimedia applications like uncompressed High Definition (HD) video streaming and ultra high speed downloads might be the next killer applications. The required raw data rate to support transmission of the uncompressed video mode 1080p with resolution  $1920 \times 1080$ , is as high as 2.986 gigabits per second (Gbps) (with 60 frames per second and 24 bits per pixel). High-Definition Multimedia Interface (HDMI) is devised to transmit the uncompressed HD audio/video over a single cable. The typical HDMI cable usage length is within 10 m without using the repeater. The maximum supported bandwidth for HDMI version 1.0 is up to 4.9 Gbps, and the HDMI version 1.3 increased the bandwidth to 10.2 Gbps. Even IEEE 802.11 n is not capable to support such data rate. The consumers' requirements have grown in a formidable rate. To alleviate the data rate bottleneck, new frequency band should be exploited. In this circumstance, 60 GHz radio comes into the picture and exhibits its glamour.

<sup>6</sup><http://www.imsresearch.com/home.html>

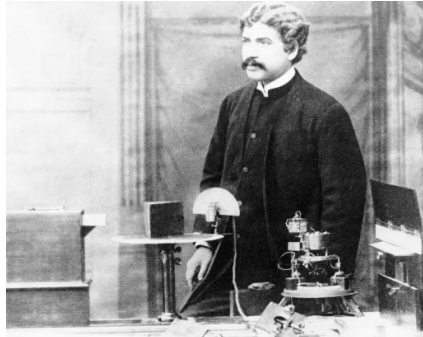


**Figure 1.2:** *J.C. Bose at the Royal Institution, London, 1897 [5].*

## 60 GHz Breakthrough

Although 60 GHz radio is a newly emerging technology, the research about millimeter wave radio can be traced back to one hundred years, when J.C. Bose already conducted experiments using wavelength from 2.5 cm or shorter to 5 mm (60 GHz radio). Figure 1.2 shows J.C. Bose lecturing at the Royal Institution in London, in 1897 [5]. However, his pioneer research was way too early for any applications. It was not until World War II that the invention of radar brought practical uses for microwaves and millimeter wave radio. Traditional 60 GHz Radio Frequency (RF) technology was mainly used for military applications, since it required expensive chip technologies based on compound semiconductors such as Indium Phosphide (InP) and Gallium Arsenid (GaAs) [6]. With the rapid development of Complementary Metal Oxide Semiconductor (CMOS) technology, which is low cost and low power consumption, 60 GHz radio gets more and more attentions. The 60 GHz radio technology is considered a promising candidate to boost wireless communication data rates to the order of multi-Gbps. Due to its great commercial potential, at the beginning of the twenty first century, multiple industry-led effort and international standardization organizations emerged for 60 GHz radio standardization activities, for instance IEEE 802.15.3c [7], WirelessHD [8], etc. The lesson we have learnt from Hertz and Bose is that a hinge factor that drives a successful transformation of a technology from research to industrial products is the desire of the consumers. Essentially, consumers are the strategy maker of the technology trend. With the desires from the consumers, with the maturity of low cost hardware and also with the push from the industry field, 60 GHz radio is under the spotlight of wireless communication stage.

The current research on 60 GHz radio mainly focuses on the channel propagation, front-end and antenna design. However, to apply 60 GHz from research to production, it requires the support of the entire protocol stack. For instance, how to set-up networks, how to organize medium access among multiple devices, these are still open issues for 60 GHz radio. To fill this gap, higher layer protocol design

for 60 GHz WPANs is the main focus of this dissertation. This work is part of SiGi-Spot project (IGC0503), which is funded by the Dutch ministry of Economic affairs within the IOP-GenCom program. The principle goal of the SiGi-Spot is to design low-cost radio technology that utilizes the 60 GHz frequency band for short-range high-speed wireless communication. In the following sections, the background knowledge of 60 GHz radio will be introduced and the research directions will be positioned.

## 1.2 60 GHz Radio Background

### 1.2.1 Worldwide Regulation and Standardization

#### IEEE 802.15.3 c

IEEE 802.15.3 defines a MAC and PHY standardization for high rate WPANs, which aims to enable wireless connectivity of high-speed, low-power, low-cost, multimedia-capable portable consumer electronic devices [3]. In March 2005, the IEEE 802.15.3 Task Group 3c (TG3c) [7] was formed to develop a 60 GHz based alternative PHY for the existing IEEE 802.15.3 standard. It was approved as a standard in Sept. 2009. Three different PHY modes are specified in IEEE 802.15.3 c. The first one is single carrier mode, which aims for low power and low complexity devices. The second is high-speed interface mode, which is for the low-latency bidirectional data transfer. The third one is Audio/video (A/V) mode for the delivery of uncompressed high-definition video and audio. Therefore, 60 GHz radio technology can be adopted for a wide range of consumer devices and applications.

#### IEEE 802.11 ad

The IEEE 802.11 standardization group successfully drives the development of wireless technology in the commercial market. Within the Gigabit gold rush, the IEEE 802.11 formed task group IEEE 802.11 ad [9] to enable 60 GHz WLAN. IEEE 802.11 ad is developed from the IEEE 802.11 VHT (Very High Throughput) study group. It is envisioned to be the successor of IEEE 802.11 n but it provides ten times higher data rate. The main feature being different from IEEE 802.15.3 c is that, IEEE 802.11 ad aims to challenge Gigabit WiFi. The IEEE 802.11 ad featured devices are expected to be compatible with the existing IEEE 802.11 services, facilities, and network structures.

#### WirelessHD

The WirelessHD Consortium was formed in 2006 to define a specification for the next generation wireless digital network interface for consumer electronics and personal computing products [8]. WirelessHD is an industry-led organization

which consists of several leading technology and consumer electronics companies, e.g. Broadcom Corporation, Intel Corporation, LG Electronics Inc., Panasonic Corporation, NEC Corporation, etc. They joined to specify 60 GHz technology based mobile and stationary consumer and enterprise applications. Their main focus is to enable wireless HDMI for streaming compressed and uncompressed A/V at up to 1080p resolution.

### **Wireless Gigabit Alliance**

The Wireless Gigabit Alliance (WiGig) [10] is another industry-led organization promoting multi-Gbps based wireless communications operating over the unlicensed 60 GHz spectrum. WiGig was launched in May 2009 and it is comprised of more than fifteen leading companies that include semiconductor vendors, consumer electronic and personal computer manufacturers. Being different with WirelessHD, WiGig aims to provide a wide range of applications. Many WiGig members are also Wi-Fi Alliance members. It is possible that WiGig aligns itself with IEEE 802.11ad to promote Gigabit Wi-Fi.

### **ECMA**

European Computer Manufacturers Association (ECMA) International is a non-profit association of technology developers, vendors and users [11]. It is dedicated to develop standards for Information and Communication Technology (ICT) and consumer electronics. In December 2008, ECMA published the first edition of the standard ECMA-387, which specifies a PHY, distributed MAC sub-layer, and an HDMI protocol adaptation layer for 60 GHz wireless networks.

#### **1.2.2 60 GHz Radio Vision**

60 GHz radio is the frontier to enable ultra high quality wireless transmission of multimedia applications. The vision of 60 GHz radio is not only the replacement of cable without sacrifice data rate and QoS, but is also envisioned as the hinge to realize smart home, for instance, transport of HD video throughout the “Ambient Intelligence” home with sufficient QoS. Therefore, 60 GHz radio has tremendous commercial values. The IEEE 802.15.3c standardization activities classify the usage models into five categories [12]:

- UM1: Uncompressed Video Streaming
- UM2: Multi uncompressed Video Streaming
- UM3: Office Desktop
- UM4: Conference Ad-hoc
- UM5: Kiosk File-downloading

Within these five categories, UM1 and UM5 are mandatory usage models, and the others are optional. UM1 can be widely used for in-home entertainment programs,

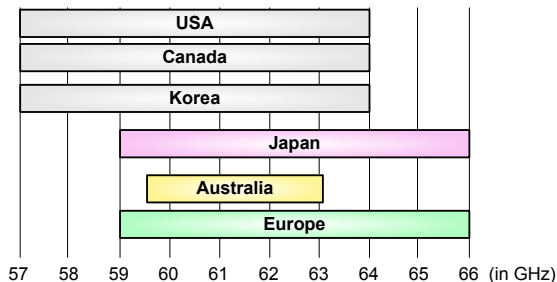


**Figure 1.3:** 60 GHz worldwide spectrum allocation [16].

for instance, wireless streaming high definition video content from set top box, laptop or video recorder to HDTV. In this case, wireless HDMI can be enabled without sacrificing the quality of images. UM1 is expected to be applicable for both Line-of-Sight (LOS) and Non-Line-of-Sight (NLOS) conditions, and the target MAC Service Access Point (SAP) throughput for this usage model is at 1.78 or 3.56 Gbps over 5 to 10 m transmission ranges. UM5 implies the applications of fast content downloading, uploading and synchronization. The target MAC SAP throughput for this usage model is at 1.5 or 2.25 Gbps over 1 m transmission range in LOS condition.

### 1.2.3 60 GHz Radio Properties

60 GHz radio technology is very attractive for broadband mobile telecommunication. Radio operating on this frequency band has some unique properties that make them substantially different from radio on the 2.4 GHz or 5 GHz frequency band.

#### License-free

Abundant unlicensed bandwidth has been allocated worldwide for 60 GHz radio. As shown in Figure 1.3, up to 7 GHz bandwidth is allocated for Europe, Japan, North America, and up to 3.5 GHz bandwidth is allocated for Australia [13–15]. Compared with other license-free applications, this is the largest contiguous block of radio spectrum ever allocated.

#### Oxygen absorption

The millimeter wave region of the electromagnetic spectrum is characterized by high levels of atmospheric radio frequency energy absorption. This means that transmitted energy is quickly absorbed by oxygen molecules in the atmosphere over long distances, like 15 dB/km. In small scale networks, e.g. home network, oxygen absorption is not a big issue.

### High Path Loss

Friis free-space propagation model [17] indicates the fundamental relation between the transmitting power  $P_t$ , receiving power  $P_r$  and the radio wavelength  $\lambda$  as,

$$\frac{P_r}{P_t} = G_t G_r \left( \frac{\lambda}{4\pi d} \right)^2 \quad (1.1)$$

where  $G_t$  and  $G_r$  are the transmitting and receiving antenna gain respectively, and  $d$  is the distance between the transmitting and receiving antennas. Therefore, a free-space path loss derived from Friis model can be expressed as  $20 \log_{10} (4\pi d/\lambda)$ , according to which, the free-space path losses at 1 m for 2.4 GHz, 5 GHz and 60 GHz are 40.05 dB, 46.42 dB and 68 dB, respectively. Therefore, 60 GHz experiences much higher path loss compared to 2.4 GHz and 5 GHz radio.

### Small Size Wavelength

Due to the fundamental relationship between the signal wavelength and the antenna size, the wavelength of 60 GHz is in the order of millimeter (around 5mm), which makes it possible to design small size antennas at 60 GHz band. Therefore, it is convenient to integrate 60 GHz featured transceivers with portable consumer electronic devices.

### Green Technology

It is easy to understand the concern about the harmful influence of radio exposure on human health. Any radio can be harmful if it exceeds the boundary that has been established to insure safe exposure for humans. Therefore, wireless systems should strictly follow the frequency band regulations established by the Federal Communications Commission (FCC) regarding the amount of transmission power. The work in [18] examined the ocular changes of rabbits after exposure at an incident power density of 10 mW/cm<sup>2</sup> using 60 GHz radio and continued the exposure for eight hours, and no ocular damage was recorded. Moreover, 60 GHz systems employ directional antennas to compromise high path loss. To gain the directivity, the directional antenna can focus transmitting power on a desired direction, which results in a significantly small exposure area.

## 1.3 Directional Antenna

To overcome high path loss, high-gain directional antennas are recommended to be used in 60 GHz systems. The main advantages of directional antennas are introduced as follows [19].

- *Transmission range extension:* According to the Friis free-space model mentioned above, it is easy to understand that an increased transmitting or receiving antenna gain results in a longer transmission distance.

- *Capacity increase*: The capacity of a radio link is directly related to the Signal to Interference plus Noise Ratio (SINR). Interference is mainly because of the communications from other close by users. With directional antennas, it is possible to reduce interference levels by nullifying signals from undesired directions. Therefore, transmission capacity can be increased by increased antenna gain and decreased interference level.
- *Spatial reuse*: Because directional antennas focus the transmission power on a certain direction and nullify interference from the other directions, more transmission pairs can be accommodated within a certain area.
- *Multi-path dispersion reduction*: For indoor applications, the multi-path propagation causes delay spread, which limits the maximum bit rate due to inter symbol interference. Using directional antennas suppresses the multi-path dispersion by limiting the transmission power emitting directions.
- *Security*: Omni-directional transmitted signals are easily tapped by intruders. Directional antennas make the interception of broadcasting more difficult, since it limits the effective reception range only to the desired direction.

## 1.4 Research Challenges

Despite the tremendous bandwidth and the promising data rate that 60 GHz radio technology can provide, the unique properties of 60 GHz radio also raise new research questions, which are identified in this section.

### Self-organization of the Network

Self-organization is the ability of ad-hoc networks to create and maintain themselves without relying on any external infrastructure, central dedicated control entity, system administrator, or users. To enable self-organization in ad-hoc network, it requires a framework that encompasses network architecture, protocols, and all the means that allow the individual entity to obtain the interconnection with the network [20]. Hence, within a self-organized network, a device should be capable to detect or organize a network without the awareness from the user's aspect. Neighbor discovery, medium access and network setup are not only the most basic issues for a wireless system to achieve self-organization, but also crucial factors that decide the performance of the system. One of the major impacts from the 60 GHz PHY layer is the use of directional antennas. To setup a directional communication, a device is expected to know its neighbor and the position of its neighbor. Therefore, a conventional neighbor discovery mechanism that employs omni-directional antennas cannot effectively support directional neighbor discovery. How to support the use of directional antennas and how to schedule directional transmissions within a WPAN are open issues.



### Medium Access Control

Medium access is a sophisticated issue to design any wireless system. MAC layer protocols coordinate the devices within a wireless network to let them gain access to the shared medium in an organized and efficient manner. To design an efficient MAC layer protocol for 60 GHz system does not only require to take care of the impact of the 60 GHz featured PHY layer, it also requires to consider the requirements from the applications that are supported in the 60 GHz systems. IEEE 802.11 working group has developed a well-accepted distributed MAC layer protocol, which is already implemented in the commercial WLAN products, but the IEEE 802.11 MAC lacks the consideration of QoS provisioning for the multimedia applications such as video streaming. Although IEEE 802.15.3 working group has developed a centrally controlled MAC layer protocol for high rate WPANs, it is not straightforward to use it for 60 GHz featured WPANs due to the use of directional antennas.

### Connectivity Maintenance

Due to the weak reflection property of 60 GHz radio, communications between 60 GHz components are highly dependent on the Line-of-Sight (LOS) links. Because it is difficult for the 60 GHz radio to penetrate objects, a moving person who passes through the LOS link could easily break the connectivity. This is referred to *link blockage*, which is a typical 60 GHz system problem. Moreover, directional transmission highly relies on the accuracy of the antenna beam-forming. Antenna mis-pointing can easily cause the drop of received power and result in the disruption of the connectivity [21]. How to effectively maintain the connectivity to increase the robustness of the 60 GHz system is very challenging. This problem invokes special concerns of 60 GHz radio properties in the higher layer protocol design.

### System Coexistence

Due to the high path loss, high-speed 60 GHz transmission is only achieved within a short range (e.g. within 10 meters). The use of directional antennas also increases the spatial reuse capabilities of WPANs. Hence, it is possible for multiple 60 GHz WPANs to exist simultaneously within a certain area, for instance a meeting room or an exhibition hall. However, to achieve Gbps-based data rate, 60 GHz radio is fragile to the variance of channel quality and the amount of interference. Especially interference from co-channel systems may easily degrade the performance of 60 GHz systems. Therefore, interference mitigation is an essential factor for the coexisting WPANs to protect high-speed 60 GHz communications. Moreover, as we mentioned earlier, tremendous work has been done concurrently by different industry-led alliances and international organizations to standardize 60 GHz radio technology. In the near future, consumers will embrace 60 GHz based electronic devices with multiple standards. Devices featured by different

standards might not communicate with each other, but they should not interfere with each other. Therefore, how to enable the coexistence of devices with different standards could be problematic but an interesting issue for investigation.

### **Multi-hop Communication**

It is difficult for 60 GHz radio to penetrate walls. Therefore, the concrete walls of a room become natural and reliable boundaries for a 60 GHz WPAN. Although it helps to reduce possible interference from adjacent rooms, it is not easy to enable inter-room communications. Moreover, these hard boundaries make it challenging to support and manage devices with mobility, for instance, to handover from one WPAN to the other WPAN in the neighboring room.

### **QoS Provisioning**

To cater to the multimedia applications requiring tremendous bandwidth, the 60 GHz radio technology is envisaged to be capable to support QoS requirements of these applications. The underlying concepts bandwidth, throughput, delay, jitter, reliability are the basis of the QoS requirements. QoS provisioning can be conveyed from different system layers, for instance, networking, medium access, resource management, etc. Hence, QoS is a crucial factor that should be take special consideration in the system-level design for 60 GHz wireless networks.

## **1.5 Dissertation Outline**

To reduce the complexity of system design, a layer-based architecture is adopted for network protocol stack designs. Each layer offers specified services to its adjacent layers but hides the implementation details of the corresponding service. The Open System Interconnection (OSI) reference model is a primary protocol architecture model used for data communications as shown in Figure 1.4. In this dissertation, the main focus is on the Network layer and MAC layer, which is a sub-layer of the Data Link layer. The outline of the dissertation is depicted in Figure 1.5, which maps the research subjects of this dissertation on the MAC layer and Network layer.

The main body of this dissertation consists of eight chapters. Chapter 2 begins with neighbor discovery process, which is the fundamental process to setup a network and enable network self-organization. The focus of this chapter is on the performance analysis of the neighbor discovery process using directional antennas. Analytically modeling a directional neighbor discovery process is not a trivial issue. To reduce the model complexity, our proposed theoretical model is based on certain assumptions. Thereafter, the influence of the assumptions is illustrated using a simulation tool. Chapter 3 is dedicated to the design of the MAC layer to support 60 GHz WPANs. IEEE 802.15.3 MAC is adopted in this

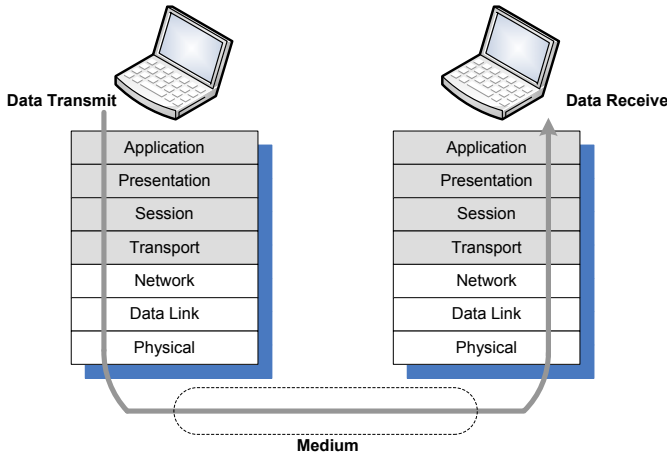


**Figure 1.4:** *OSI seven layer reference model.*

research, but it is not straightforward to use it for 60 GHz radio. Therefore, several enhancement mechanisms are presented to enable directional communication in 60 GHz WPANs. However, this enhanced MAC still cannot achieve high transmission efficiency due to the impact of overhead. Therefore, in Chapter 4, the frame aggregation mechanism is studied to improve MAC transmission efficiency for 60 GHz systems. The main focus of Chapter 5 is to resolve the LOS link blockage problem. A beam switching mechanism is proposed to seek a strong NLOS link as a backup beam path when the LOS link is blocked.

After investigating the medium access, network formation and connectivity maintenance within a single WPAN, Chapter 6 is devoted for the interference mitigation and piconet coexistence issues. To support multi-hop communication among coexisting 60 GHz systems, the fundamental properties using directional antennas for topology control and message dissemination are examined in Chapter 7. In Chapter 8, the multi-hop communication scenario is specified in home and office environment, and the inter-piconet route discovery and communications are studied. Finally, this dissertation is summarized in Chapter 9 with the discussion of future work directions.

## 1.6 Summary of Main Contributions

The main contributions of this dissertation are listed as follows:

1. The performance of the neighbor discovery process using directional antennas has been analytically investigated. Using our proposed analytical model, the 60 GHz system setup time can be estimated according to the device density within the network.

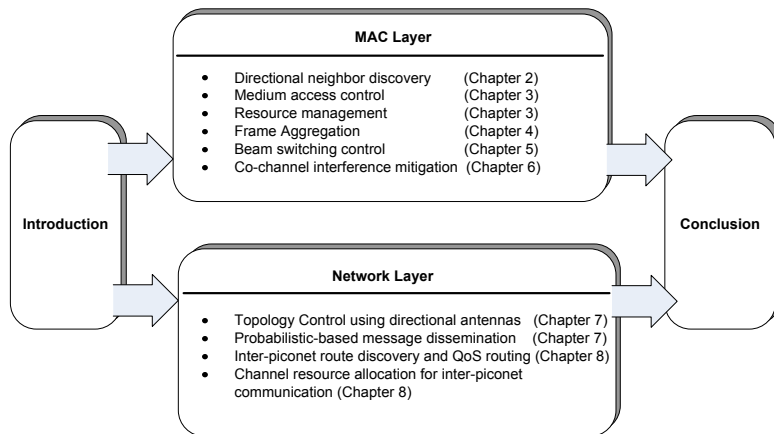


**Figure 1.5:** Research scope and the mapping chapters in the dissertation.

2. To adopt the IEEE 802.15.3 MAC for 60 GHz WPANs, a completed resource management scheme is proposed to support the concurrent directional transmissions.
3. Standard frame aggregation and low latency frame aggregation are employed to increase the MAC transmission efficiency in 60 GHz WPANs. The performance of these two aggregation mechanisms are theoretically analyzed in this dissertation.
4. A beam switching based solution is proposed to resolve the link blockage problem in 60 GHz systems. Targeting for different usage models, two types of beam switching mechanisms are defined and examined in this dissertation: instant decision based beam switching and environment learning based beam switching.
5. To support simultaneously operating 60 GHz WPANs, a thorough study is performed to investigate the use of synchronization frame to mitigate the possible co-channel interference from the adjacent systems.
6. Having the MAC layer design and proposals to maintain one-hop link connectivity, the work is extended from single hop to multi-hop domain. To employ directional antennas for multi-hop communications, a comprehensive investigation is performed to explore the performance of using directional antennas for topology control and message dissemination.
7. The feasibility to support multi-hop communication for in-home networks is studied from two aspects. First, the inter-piconet route discovery process is examined using directional antennas. Second, a joint QoS routing and

channel resource reservation framework is proposed to overcome the inter-piconet channel resource allocation collision problem.

## **1.7 Chapter Summary**

This chapter starts with a brief evolution of wireless telecommunication, and it is shown that the emergence of the 60 GHz radio technology has its inevitability. After introducing the background of the 60 GHz radio, the research challenges are identified and the research directions of this dissertation are also positioned within the field. In the end, the outline and major contributions of this dissertation are provided.



## Chapter 2

# Neighbor Discovery using Directional Antennas

“Equations are more important to me, because politics is for the present, but an equation is something for eternity.”

- Albert Einstein

*Neighbor discovery (ND) is an initial step to enable self-organization in wireless ad-hoc networks. It allows in-range devices to link with each other and form a connected network. To address the ND process in 60 GHz networks, a novel analytical framework is proposed in this chapter to investigate the ND performance using 60 GHz radio. The main difficulty in modeling the ND process in 60 GHz network is the involvement of directional antennas with gain differences between the antenna main lobe and side lobes. Different antenna modes, directional or omni-directional, combining with different ND mechanisms make the analytical work very difficult. In this chapter, we propose a comprehensive theoretical model to demonstrate the performance of using one-way ND and handshake based ND combining with different antenna modes. A number of assumptions are used in the theoretical work to reduce the analysis complexity. Thereafter, we involve a realistic interference-aware link model and the uniform circular array system to revise the analytical model via simulation approach.*

## 2.1 Background

Wireless ad-hoc networks are envisioned to be self-organized, which means, devices are expected to set-up and maintain networks without relying on any external infrastructure, system administrator, or users. Neighbor discovery (ND) is an essential process to realize self-organization in wireless ad-hoc networks [22]. An ND process allows in-range devices to establish links with each other and form a connected network, and cooperates with the medium access, service discovery, and routing protocols that require specific information about neighbors. The required duration and efficiency of an ND process directly affect the network setup time, route establish duration, etc. ND protocols can be generally classified as *direct ND* protocols and *gossip-based ND* protocols [23]. During an ND process, devices broadcast their advertisement messages, which are also called as HELLO messages. If a device directly receives an advertisement message from another device, they are one-hop neighbors. When a direct ND protocol is used, a device only discovers its neighbors via directly receiving their advertisement messages. When a gossip-based ND protocols, devices do not only broadcast their own advertisement messages, but also the information about their neighbors to speed up the ND process. Hitherto, omni-directional antennas are widely addressed in ND protocols [24–26]. An ND process using omni-directional is quite straightforward. Once a device accesses the channel and broadcasts its advertisement message, all the devices that are in the transmission range of the device may receive its advertisement message. If multiple advertisement messages arrive at the receiver simultaneously, none of them can be received. As we mentioned in the previous chapter, directional antennas are widely used in wireless system to increase transceiving gain and reduce interference area [27–31]. To set-up a directional communication, a device does not only need to know who its neighbor is, but it also requires knowing where its neighbor is. Hence, it is necessary for devices to determine the direction of each other before setting up directional communications. Within the indoor environment, there are normally more than one beam path that can be used for communication: one line-of-sight (LOS) path and multiple non-LOS (NLOS) paths. Since 60 GHz radio is prone to the channel variation and LOS blockage phenomenon [32], devices need to trace the best beam path that could provide best quality during the ND process. Hence, gossip-based ND protocols are not suitable to accomplish this. Therefore, direct ND protocols are addressed here for an in-depth study. According to the reply mechanism used in a ND process, direct ND protocols can be further classified as *one-way ND* and *handshake based ND* [33]:

- *One-way ND*: In one-way ND protocols, each device periodically transmits advertisement messages to announce its presence, and discovers its neighbors by receiving advertisement messages from the other devices.
- *Handshake based ND*: In handshake based ND protocols, once a device re-



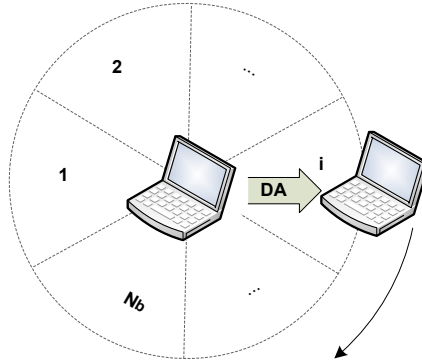


**Figure 2.1:** *Scanning based directional neighbor discovery process illustration.*

ceives an advertisement message, it provides active response to its neighbor. Compared to one-way ND protocols, handshake based ND protocols are more complex to implement, but they are easy to construct symmetric neighborhood by exchanging advertisement messages especially for direction-aware links.

Although directional antennas offer many advantages over omni-directional antennas, their deployment for neighbor discovery is not a trivial matter. For instance, *deafness* is a typical problem caused using directional antennas [31]. The performance of a directional ND (D-ND) process might be affected by this deafness phenomenon when a device, say  $A$ , fails to communicate with the other device  $B$ , because device  $B$  points its antenna main lobe in a direction which is away from  $A$ . A device can also nullify the interference from undesired directions using directional antennas for receiving, which may help to alleviate the advertisement message collisions. Therefore, it is very interesting to know the exact influence of using directional antennas in an ND process. To achieve the best link quality, devices need to find out the best beam path to communicate with its neighbors. Therefore, Directional Advertising (DA) messages are preferred to be transmitted in a *blind* way. Blind means that devices sweep the DA messages in all the possible directions, which helps devices to update the beam path status of their neighbors in time. According to the mechanism used to transmit the DA messages, direct D-ND protocols can be executed in two ways: *randomized D-ND* or *scanning based D-ND*. For a randomized D-ND process, devices randomly pick a direction to transmit their DA messages once they have access to the channel for transmission. In [23], the authors presented several probabilistic models for D-ND protocols, but their approach is only applicable to one-way randomized D-ND processes. For a scanning based D-ND process, if a device is in the transmitting state, it randomly selects a beam sector to transmit its DA message, and moves (counter-)clockwise to transmit the next DA message in the next sector until it covers all the beam

sectors. In [33], authors proposed a simplistic analytical model for handshake and scanning based D-ND. They assumed that in each beam sector only one potential neighbor is present, which makes the analysis only applicable to sparse networks with narrow beam antennas. The one-way scanning based D-ND process is not investigated in their work. D-ND in 60 GHz indoor wireless networks was investigated in [34]. The method used there is also based on one-way randomized D-ND mechanism. Moreover, they assume that reception failure is only caused by packet collisions, in which the effect of the channel is not considered. In [35], authors emphasized on the neighbor location discovery via direct path or non-direct path using linear and circular polarization and different responses to reflections with directional antennas operating in the 60 GHz band.

In this chapter, an in-depth methodology is presented to model the performance of scanning based D-ND protocols by combining a multitude of different ND mechanisms. Thus, we provide a comprehensive study of the ND procedures. Specifically, one-way and handshake based ND mechanisms are combined with different antenna modes, i.e. with directional transmitting and omni-directional listening mode, and directional transmitting and directional listening mode. The D-ND performance is demonstrated in two scenarios. In the first scenario, the performance of a peer-to-peer (two-device) discovery process is investigated using directional antennas. To provide a generic model with multiple devices, in the second scenario we focus on the D-ND processes in a distributed ad-hoc network. The accuracy of our theoretical model is validated with extensive simulations. Moreover, to the best of our knowledge, this work is the first of its kind that provides investigation of the impact of the antenna pattern and the link model on the D-ND performance in 60 GHz wireless networks.

## 2.2 System Model and Assumptions

A two-dimensional network is assumed in this work. All the devices are located on the same horizontal plane. Directional antenna beamwidth is denoted as  $\theta_b$ . According to the antenna beamwidth, the horizontal space around a device is divided into  $N_b$  sectors, where  $N_b = \frac{2\pi}{\theta_b}$ . The D-ND protocols considered could operate in both synchronous and asynchronous systems. To simplify the analysis, a slotted synchronous system is assumed. The duration of each slot  $\tau$  is equal to the transmission time of a DA message. The scanning based mechanism is adopted in this work for D-ND. For one-way D-ND, every  $N_b$  slots are grouped together as a frame, so the time duration of a frame is  $\tau N_b$ . For handshake based D-ND, the duration of each handshake process is defined as the duration for transmitting a DA message and a DA Acknowledgment (ACK) message from the receiver. We assume that a DA ACK is the DA message of the receiver. Every  $2N_b$  slots are grouped together as a frame, and the length of a frame is equal to  $2\tau N_b$ . Therefore, the number of required slots for a ND process can be used as an indicator of ND time. A device is either in the *transmitting* state or *listening*

state. At the beginning of each frame, a device has a probability  $p_t$  to be in the transmitting state or has a probability  $1 - p_t$  to be in the listening state.

To investigate the influence of using directional antennas in ND processes, we define that all the ND-related packets, i.e. DAs and DA ACKs, are transmitted using directional mode. According to the antenna mode used in the listening state, ND processes can be classified into two categories: directional transmitting and omni-directional listening (DO) mode, directional transmitting and directional listening (DD) mode. Once a device is in the directional listening state, it randomly picks up a beam sector to listen and listens to the same direction for the entire frame. According to the combination of ND protocols and antenna modes, there are four D-ND protocols that are examined in the sequel: one-way DO-ND, one-way DD-ND, handshake based DO-ND and handshake based DD-ND.

To quantify the performance of an ND process, we first define the following metrics. *ND ratio* is defined as the ratio between the number of discovered neighbors and the number of all the surrounding neighbors. The ND ratio determines the network topology and robustness. A higher ND ratio means a better connectivity with the entire network. *ND time* is an important metric to characterize the duration of one ND process. It can be viewed as the time spent to let any newly entering device to discover and incorporate with all or most of the neighboring devices. In this work, an ND process is considered as completed if the ND ratio reaches 99%. *ND overhead* is the number of generated DA and DA ACK messages during an ND process.

## 2.3 Antenna Pattern and Link Model

60 GHz radio links are prone to the variations in channel quality. The inaccurate selection of a radio propagation model and the imperfections in antenna patterns with side lobe effects might impact the D-ND performance. To get a better understanding of the D-ND process in a realistic scheme, we first introduce several antenna patterns and link models in this section.

### 2.3.1 Directional Antennas

An antenna *radiation pattern* is defined as a mathematical function or a graphical representation of the radiation properties of the antenna as a function of space coordinates [36]. A *main lobe* of a radiation pattern is defined as lobe containing the direction of maximum radiation. A *side lobe* is any lobe except for the main lobe [36]. Side lobes usually represent radiation in undesired directions. The fundamental properties that can characterize an antenna are radiation intensity, half power beamwidth, directivity and antenna gain [37]:

- Radiation Intensity: The radiation intensity in a given direction  $U(\theta, \phi)$  is defined as the power radiated from an antenna per unit solid angle. The total obtained power is given as  $P_{rad} = \int_0^{2\pi} \int_0^\pi U(\theta, \phi) \sin \theta d\theta d\phi$ , where,

$\theta$  and  $\phi$  are elevation angle and azimuth angle in a spherical coordinate system.

- Half power beamwidth: Within a plane which contains the direction of maximum beam, the angle between two directions in which the radiation intensity is one-half value of them. In this dissertation, the concepts of half power beamwidth and antenna beamwidth are interchangeable.
- Directivity: The directivity of an antenna is defined as the ratio of the radiation intensity in a given direction from the antenna to the radiation intensity averaged over all directions as  $D(\theta, \phi) = 4\pi U(\theta, \phi)/P_{rad}$ .
- Antenna gain: Antenna gain  $G(\theta, \phi)$  is defined as the ratio of the intensity in a given direction, to the radiation intensity that would be obtained if the power accepted by the antenna were radiated isotropically, where  $G(\theta, \phi) = \eta D(\theta, \phi)$ , and  $\eta$  is the antenna dimensionless radiation efficiency.

Adaptive array based directional antenna systems, also known as smart antennas, are composed by a number of antenna elements. The antenna radiation pattern is controlled by the amplitude and phase weights of each individual element. The weights could be varied in time. The main lobe of an adaptive array system is steerable to different directions, which is also called as antenna beam-forming. Antenna beam-forming is achieved by adaptively adjusting the weight of each antenna element. Therefore, adaptive array systems can locate and track the signals. According to the input from each element, the Direction of Arrival (DoA) of the arrival signal is computed using a certain algorithm like MUSIC [38], ESPRIT [39], etc. The DoA information can be cached during the ND process.

### **Idealized Flat-Top Antenna System**

An idealized directional antenna pattern with neglected side lobe is introduced here, which is called “flat-top” antenna system. The antenna gain of the a flat-top antenna system can be denoted as  $G = 10 \log (2\pi/\theta_b)$ . Hence, if the antenna main lobe is directed in the direction  $\theta_s$ , the antenna gain within the range  $[\theta_s - \theta_b/2, \theta_s + \theta_b/2]$  is  $G$ , and the antenna gain outside this range is assumed to be zero. Because flat-top is an idealized antenna pattern, it provides an easy way to model the behavior and influence of directional antennas. It is widely used in the analysis involving directional antennas, for instance in [23] [33].

### **Uniform Circular Array Antenna System**

Uniform Circular Array (UCA) antenna system is a specific case of the adaptive array antenna. For a UCA antenna system, the antenna elements are uniformly arranged on a circle in the  $x - y$  plane. A brief deduction of the antenna gain pattern of a UCA system with  $N$  identical antenna elements is provided here for

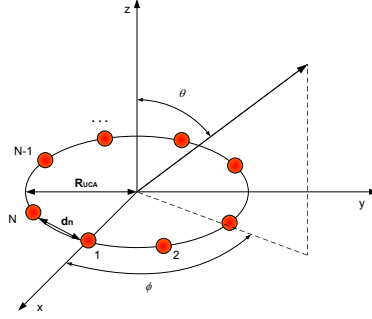


**Figure 2.2:** Uniform circular array system.

the sake of completeness [37]. If each element has the same magnitude, the array factor of a UCA system can be expressed as:

$$(AF)_n = \left| J_o(k\rho) + 2 \sum_{m=1}^{\infty} (j)^{mN} J_{mN}(k\rho) \cos(mN\xi) \right| \quad (2.1)$$

where,

$$\xi = \tan^{-1} \left[ \frac{\sin \theta \sin \phi - \sin \theta_0 \sin \phi_0}{\sin \theta \cos \phi - \sin \theta_0 \cos \phi_0} \right]$$

$$\rho = R[(\sin \theta \cos \phi - \sin \theta_0 \cos \phi_0)^2 + (\sin \theta \sin \phi - \sin \theta_0 \sin \phi_0)^2]^{\frac{1}{2}}, \quad (2.2)$$

and  $J_m(x)$  is the Bessel function of the first kind,  $J_o(k\rho_0)$  is the principal term and the summation part is the residual term. The antenna gain is given by:

$$G(\theta, \phi) = \eta \frac{U(\theta, \phi)}{\frac{1}{4\pi} \int_0^{2\pi} \int_0^\pi U(\theta, \phi) \sin(\theta) d\theta d\phi} \quad (2.3)$$

$$= 4\pi \left[ \left| J_o(k\rho) + 2 \sum_{m=1}^{\infty} (j)^{mN} J_{mN}(k\rho) \cos(mN\xi) \right| \right]^2$$

$$\times \left[ \int_0^{2\pi} \int_0^\pi \left( \left| J_o(k\rho) + 2 \sum_{m=1}^{\infty} (j)^{mN} J_{mN}(k\rho) \cos(mN\xi) \right| \right)^2 \sin \theta d\theta d\phi \right]^{-1}$$

where,  $\eta$  is the dimensionless antenna radiation efficiency. According to (2.3), the antenna gain and beamwidth obtained using 4, 6, 8 elements UCA systems are listed in Table 2.1, which is found by setting  $\theta$  as  $\pi/2$  to only observe the  $x$ - $y$  plane. The space between each adjacent elements  $d_n$  is set as half of the radio wavelength,  $d_n = \lambda/2$ . The main beam is directed at  $\theta_0 = \pi/2$ ,  $\phi_0 = 0$ , and  $\eta = 1$ . The gain patterns of UCA antenna systems are shown in Figure 2.3 (a)

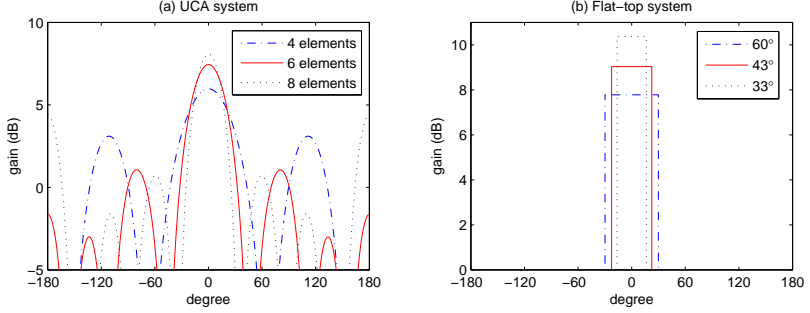


**Figure 2.3:** Antenna gain pattern for different antenna elements. For the UCA system,  $\theta$  is set as  $\pi/2$  to only observe the  $x$ - $y$  plane. The space between each adjacent elements is set as the half of the radio wavelength,  $d_n = \lambda/2$ . The main beam directed at  $\theta_0 = \pi/2$ ,  $\phi_0 = 0$ .

**Table 2.1:** UCA related parameters

Num. elements	Radius	Directivity (dB)	$\theta_{HPBW}$ at x-y plane( $^\circ$ )
4	$0.35\lambda$	5.97	63.24
6	$0.50\lambda$	7.44	43.76
8	$0.65\lambda$	8.08	33.01

with 4, 6 and 8 elements. To enable comparison with the UCA systems, the flat-top antennas are selected with the similar beamwidth as that of UCA systems and their gain patterns are shown in Figure 2.3 (b).

### 2.3.2 Radio Propagation Model and Link Probability

Electromagnetic waves radiated by the transmitter propagate through environments. The received signal power over the wireless channel at the receiver side decreases as the distance between the transmitter and the receiver increases, which is called as *path loss* phenomenon and the path loss radio propagation model can be represented as,

$$P_r(d) = P_t + G_t + G_r - I_L - (PL_0 + 10n \log(d)) \quad (2.4)$$

where  $P_t$  is the transmitting power,  $G_t$  and  $G_r$  are the antenna gains of the transmitter and receiver, respectively.  $I_L$  is the implementation loss.  $PL_0$  is the reference path loss at 1 meter and  $d$  is the transmission distance. Parameter  $n$  is the path loss exponent. The measured path loss exponent for wide-band (e.g. 1 GHz) radio is close to 2 under LOS conditions with directional antennas [40,41].

### Link Model 1 (LM1)

To correctly demodulate and decode a received signal, the received signal power strength is required to be higher than a certain threshold,  $\gamma_{th}$ , which is also called receiving sensitivity. Therefore, the coverage range of a device refers to the area in which the received signal strength from the device is higher than  $\gamma_{th}$ . A maximum transmission range  $r_{th}$  can be calculated as  $r_{th} = 10^{\frac{\kappa}{10n}}$ , where  $\kappa = P_t + G_t + G_r - I_L - PL_0 - \gamma_{th}$ . LM1 defines that all the devices within the radius  $r_{th}$  of the center device are considered as the direct neighbors. Hence the probability of existence of a link between a transmission pair  $i$  and  $j$ , which is also called as link probability, is represented as a simple step function:

$$p_{ij} = \begin{cases} 1 & 0 < \|i - j\| \leq r_{th} \\ 0 & \text{otherwise} \end{cases} \quad (2.5)$$

where,  $\|i - j\|$  is the Euclidean distance between  $i$  and  $j$ .

### Link Model 2 (LM2)

As shown in Figure 2.3, the antenna side lobes play an important role in a UCA system. They may introduce interference to the other transmissions, or be used for communication. Hence a more realistic link model is used in LM2 with consideration of the interference from the other transmitters. To guarantee a required transmission performance for a transmission pair  $(i, j)$ , the Signal to Interference-plus-Noise Ratio (SINR) should be higher than a certain threshold  $\varphi_{th}$ . Therefore, a link exists with a probability,

$$p_{ij} = \begin{cases} 1 & \Delta\mathcal{P} > 0 \\ 0 & \text{otherwise} \end{cases} \quad (2.6)$$

where

$$\Delta\mathcal{P} = 10 \log \frac{\mathbb{P}_r(\|i - j\|)}{N_0 + \sum_{k \in N, k \neq i} \mathbb{P}_r(\|k - j\|)} - \varphi_{th}$$

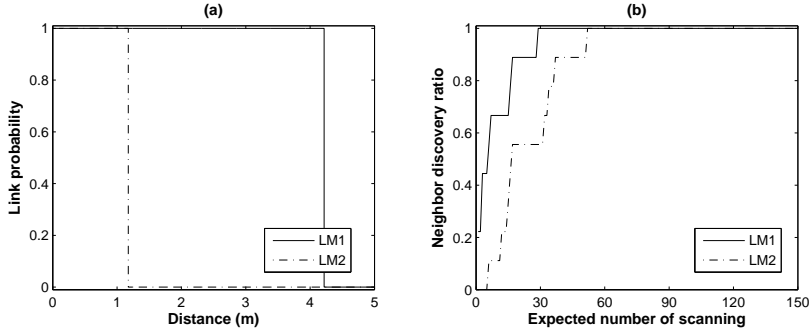
where  $\mathbb{P}_r$  is the received power (in watts),  $N_0$  is the mean noise power (in watts) and  $\sum_{k \in [1, K], k \neq i} \mathbb{P}_r(\|k - j\|)$  is the accumulated interference power from the other  $K$  interfering sources.

### Discussion

To demonstrate the impact of LMs on the link probability, five transmitters are uniformly distributed within a circular network with radius 15 m, in which, a target device is at the center of the network. Without considering the effect of directional antennas, the antenna gains are set to zero. For the target device, the resultant link probability plots using different LMs are shown in Figure 2.4 (a). The link budget related parameter settings are listed in the caption of Figure 2.4.

**Table 2.2:** Defaulted link budget related parameter specifications

Parameter	Value
$P_t$	10 dBm
Center frequency	60 GHz
Bandwidth	1 GHz
Path loss at 1m ( $PL_0$ )	68 dB
Path loss exponent ( $n$ )	2
Temperature	300 K
Implementation loss ( $I_L$ )	1.5 dB
Receiving sensitivity	-72 dBm
SINR threshold	12 dB

**Figure 2.4:** Link model influence on the link probability and the ND ratio. For subplot (a) 5 interfering nodes, network radius 15,  $G_t = G_r = 0$ , (b) 6 elements UCA system, node degree is 10, network radius 5,  $p_t = 0.2$ .

Because 60 GHz radio is very fragile to the co-channel interference, the maximum transmission range that is obtained using LM1 is much longer than the achievable transmission range with the existence of interference.

To obtain some basic ideas of the influence of the adopted LM on the performance of ND process, we study a scenario through simulation. The set up is as follows: ten devices are uniformly distributed within a circular network with a radius of 5 m, and the target device is at the center of the network. Each device is equipped with a 6 element UCA system. The transmission probability is set to 0.2. The ND ratios using different LMs after an one-way DO-ND process are depicted in Figure 2.4 (b), in which LM1 and LM2 exhibit different ND performances. A detailed investigation of the influence of LMs on the ND process is introduced later in this chapter.



## 2.4 Analytical Model for Directional Neighbor Discovery

In this section, a theoretical model is proposed to model the performance of D-ND protocols. Our proposed model is a generic model which can be used for all the systems equipped with directional antennas. Since it is not trivial to model the exact properties of realistic antenna patterns, like the UCA system, the flat-top antenna system and LM1 are used in our theoretical model to alleviate the influence of side lobe effects. Moreover, a full mesh network is assumed, in which all the devices are within the transmission range of each other.

### 2.4.1 D-ND Analysis for a Two-Device Model

The two-device model is a simple and realistic scenario to study a ND process. For instance, when a Blu-ray player sets up connection with an HDTV display for video streaming, or two laptops connect to each other for high speed downloading, the latency of a ND process directly influences the user experience of the consumer products. Therefore, it is necessary to model the ND performance using directional antennas for a two-device model first.

#### One-way DO-ND and DD-ND

For one-way DO-ND, devices transmit with directional antenna, and receive with omni-directional antenna. Let us assume that device  $m$  and device  $n$  are one-hop neighbors. The condition for  $m$  to discover  $n$  in a certain frame is that  $m$  is in the listening state and  $n$  is in the transmitting state, the probability of which is given by  $p_f = (1 - p_t)p_t$ , where  $p_t$  is the probability to be in the transmitting state. Assume one of the two devices discovers its neighbor in the  $i^{th}$  frame, and its neighbor discovers it in the  $j^{th}$  frame, where  $i < j$ . Therefore, this one-way DO-ND process is completed in the  $j^{th}$  frame with probability  $p_{1DO}^{(j)}$ , which is given by

$$p_{1DO}^{(j)} = 2p_f ((1 - p_f)^{j-1} - (1 - 2p_f)^{j-1}). \quad (2.7)$$

The probability for the two devices discovering each other within  $J$  frames is given as  $p_J = \sum_{j=2}^J p_{1DO}^{(j)}$ . Note that the two devices cannot discover each other within the same frame, therefore, it requires at least two frames as such the summation starts from  $j = 2$ . The expected number of slots required for this one-way DO-ND process is given by

$$N_{1DO} = \sum_{j=2}^J N_b j p_{1DO}^{(j)}. \quad (2.8)$$

In the one-way DD-ND case, both transmitting and receiving devices use directional antenna mode. To discover a neighbor, the receiver needs to point its directional antenna in the direction of the transmitter to receive its DA message. The probability of this event is given by  $p_f = \frac{1}{N_b}(1 - p_t)p_t$ . We denote  $p_{1DD}^{(j)}$  as

the probability for the two devices discovering each other in the  $j^{th}$  frame. We use  $N_{1DD}$  as the expected number of slots for the one-way DD-ND process. The two parameters  $p_{1DD}^{(j)}$  and  $N_{1DD}$  can be calculated by substituting  $p_f$  in (2.7) and (2.8).

### Handshake-based DO-ND and DD-ND

In a handshake based mechanism, an active response is provided if a device receives a DA message from the other device. Hence for the two-device model, it is possible for device  $m$  and  $n$  discovering each other within the same frame, and this probability is given by  $p_f = 2(1 - p_t)p_t$ . Let us represent the probability that the two devices discover each other in the  $j^{th}$  frame for the first time as  $p_{2DO}^{(j)}$ , and it is calculated as

$$p_{2DO}^{(j)} = p_f ((1 - p_f)^{j-1}). \quad (2.9)$$

The expected number of slots for a handshake based DO-ND process is expressed as

$$N_{2DO} = \sum_{j=1}^J 2N_b j p_{2DO}^{(j)}. \quad (2.10)$$

Based on the above concepts, it is easy to understand that for the handshake based DD-ND,  $p_f$  is obtained as  $p_f = \frac{2}{N_b}(1 - p_t)p_t$ , and then  $p_{2DD}^{(j)}$  and  $N_{2DD}$  can be obtained by substituting  $p_f$  into (2.9) and (2.10).

**Proposition 2.4.1.** *Within the two-device models, using handshake based D-ND mechanism achieves a faster D-ND process than one-way based mechanism in a slotted system.*

*Proof.* Based on (2.8) and (2.10), the difference in the expected number of slots required for handshake based and one-way DO-ND is expressed as,

$$\begin{aligned} N_{2DO} - N_{1DO} &= \sum_{j=1}^J 2N_b j p_{2DO}^{(j)} - \sum_{j=2}^J N_b j p_{1DO}^{(j)} \\ &= 2N_b p_t (1 - p_t) \sum_{j=1}^J j (3(1 - 2p_t(1 - p_t))^{j-1} - (1 - p_t(1 - p_t))^{j-1}) \\ &= N_b (A + B), \end{aligned} \quad (2.11)$$

where

$$\begin{aligned} A &= 1 - (1 - p_t(1 - p_t))^{J-1} \\ B &= 3((1 - p_t(1 - p_t))^{J-1} - (1 - 2p_t(1 - p_t))^{J-1}). \end{aligned}$$

Since  $A$  and  $B$  are positive, therefore we have  $N_{2DO} - N_{1DO} > 0$ . Similarly, we can also obtain  $N_{2DD} - N_{1DD} > 0$ .  $\square$

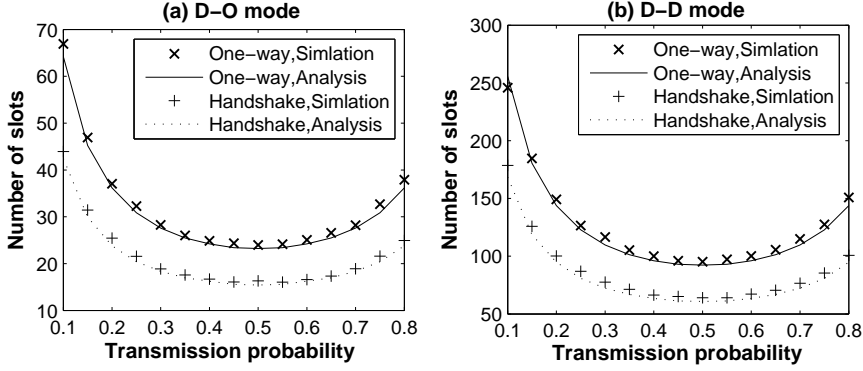


**Figure 2.5:** ND time for the two-device model,  $90^\circ$  antenna beamwidth, 10000 iteration time.

### Simulation Validation

To validate the accuracy of the analytical model, we simulated the four D-ND protocols at the algorithmic level<sup>1</sup> using Matlab (R2007b). The ND process is defined according to the scenario explained in Section 2.2. The analytical and simulation results are compared in Figure 2.5 when the antenna beamwidth is fixed at  $90^\circ$ . The simulation results are based on the average value of 10000 iterations. The one-way and handshake based ND mechanisms are compared when they combine with DO mode and DD mode respectively. They are shown in Figure 2.5(a) and (b). The two subplots show the relationship between the expected number of slots required for an ND process and the transmission probability  $p_t$ . It is shown that, there exists an optimized value for  $p_t$ . If the transmission probability is too small, the two devices are both in the listening state in most of the time. If the transmission probability is too high, the two devices might miss the DA messages from each other because they are both in the transmitting state. It is also observed that, the handshake based ND protocol is superior to the one-way ND protocol in both DO mode and DD mode. Comparing Figure 2.5 (a) and (b), we can also see that using the DD mode leads to a longer ND time than that of using the DO mode.

A two-device model for different D-ND protocols has been presented. However, it is not straightforward to extend the analytical model from two devices to multiple devices model. To deduce a model for a D-ND process with multiple devices, we focus on the ND process of a target device instead of obtaining the ND time and ND ratio for all the devices within the network.

<sup>1</sup>In this work, the physical layer simulation is not considered, that means, in a certain time slot, if a DA message is transmitted without experiencing any DA collision, it can be received by all the receiving devices in the range with probability 1.

## 2.4.2 D-ND Analysis for a Generic Model

### One-way DO-ND

To construct a scenario involving multiple devices, a circular full mesh network is used in this. Let the device  $m$  be the target device. It is located in the center of the network. Let the node degree (the number of direct neighbors of the device in the network) of the target device be  $k$ , and the  $k$  neighbors are uniformly distributed within the circular network. Using one-way DO-ND, device  $m$  can detect its neighbors by receiving DA messages from them. In a certain frame  $i$ , the probability that device  $m$  is in the listening state and its  $w$  neighbors are in the transmitting state with probability  $p_t$  is denoted as  $p_w$ , and is given by,

$$p_w = (1 - p_t) \binom{k}{w} p_t^w (1 - p_t)^{k-w}. \quad (2.12)$$

**Proposition 2.4.2.** Denote  $n_{i,x}$  as the number of DA messages that arrive at device  $m$  in the  $x^{th}$  slot of the  $i^{th}$  frame, so we have  $\sum_{x=1}^{N_b} n_{i,x} = w$ . For a certain combination  $\mathcal{N}_i = [n_{i,1}, \dots, n_{i,N_b}]$ ,  $l_{i,z}$  is denoted as the number of elements, which are equal to  $z$ , in  $\mathcal{N}_i^2$ . We have  $\sum_{z=0}^{\max(\mathcal{N}_i)} l_{i,z} = N_b$ . The probability to obtain a given  $\mathcal{N}_i$  on the condition that all the elements in it appear in an arbitrary order is given by,

$$p_i = \frac{w!}{\prod_{z=1}^{\max(\mathcal{N}_i)} l_{i,z}!} \frac{N_b!}{\prod_{x=1}^{N_b} n_{i,x}!} N_b^{-w}. \quad (2.13)$$

*Proof.* For the proof please refer to Appendix A. □

If multiple DA messages arrive in a time slot simultaneously ( $z > 1$ ), these messages collide with each other and cannot be received by the receiver. Hence, the average number of received DA messages in one frame is given by,

$$n_{rt} = \sum_{w=0}^k \sum_{i=1}^{\varpi} l_{i,1} p_i p_w, \quad (2.14)$$

where,  $\varpi$  is the total number of occupancy combinations of  $\mathcal{N}_i$ , which is a function decided by node degree  $k$  and the number of slots in one frame  $N_b$ . The number of distinguishable occupancy of  $\mathcal{N}_i$  is denoted as  $A_{w,N_b}$ , where  $A_{w,N_b} = \binom{w+N_b-1}{N_b-1}$  [42]. The relation between  $A_{w,N_b}$  and  $\varpi$  is given by,

$$A_{w,N_b} = \sum_{i=1}^{\varpi} \frac{w!}{\prod_{z=1}^{\max(\mathcal{N}_i)} l_{i,z}!} \quad (2.15)$$

---

<sup>2</sup>For instance, if device  $m$  receives three DA messages from two time slots within one round of scanning,  $l_{i,3} = 2$ .

Therefore, the probability for device  $m$  to detect  $k'$  neighbors within consecutive  $J$  frames is formulated as:

$$P(J, k') = \sum_{j=0}^{k'} \sum_{x=0}^{k'-j} P(J-1, k'-j) \rho(x+j) \frac{\binom{k'-j}{x} \binom{k-k'+j}{j}}{\binom{k}{x+j}}, \quad (2.16)$$

where,  $\rho(x+j)$  is the probability of device  $m$  receiving  $x+j$  DA messages within the  $J^{th}$  frame, in which  $x$  messages are from known neighbors and  $j$  messages are from unknown neighbors, and  $\rho(x) = \sum_{w=1}^k \sum_{i=1}^{\infty} 1_{(t_i, 1=x)} p_i p_w$ , where  $1_{(\Omega)}$  is an indicator function, and it is equal to 1 if  $\Omega$  is true, otherwise, it is equal to 0.

### Handshake based DO-ND

Using handshake based DO-ND, device  $m$  can detect its neighbors in two scenarios: first,  $m$  is in the listening state and receives DA messages from its neighbors; second,  $m$  is in transmitting state and receives DA ACKs from its neighbors. We denote device  $m$  receiving  $n_h$  DA messages in a frame. The number  $n_h$  can be expressed as  $n_h = n_{rt} + n_{tr}$ , where  $n_{rt}$  and  $n_{tr}$  are the number of DA messages received when device  $m$  is in the listening state and transmitting state respectively.  $n_{rt}$  can be obtained from (2.14), and  $n_{tr}$  is derived here. When device  $m$  is in the transmitting state, it sweeps its DA messages in all the possible direction. Once its neighbors receive the DA messages, they reply to it with DA ACK. Therefore, device  $m$  could also discover its neighbors during the transmitting state. The number of received DA ACKs depends on the number of successful transmissions in one frame, and also depends on the number of neighbors that reply to the DA messages in a certain slot. For the sake of simplicity in analysis, we assume that a device always replies to the received DA messages from its neighbors. Let  $p_x$  be the probability for  $x$  neighbors within a certain beam sector of device  $m$ , and  $y$  out of the  $x$  neighbors are in the listening state, where

$$p_x = \binom{k}{x} \frac{1}{N_b}^x \left(1 - \frac{1}{N_b}\right)^{k-x} \binom{x}{y} (1-p_t)^y p_t^{x-y}. \quad (2.17)$$

The condition for device  $m$  to receive one DA ACK is that only one out of  $y$  neighbors that are in the listening state replies to  $m$ , because if more than one neighbors transmit replies to  $m$ , DA ACKs collide. The only reason that the other  $(y-1)$  neighbors cannot reply is because they do not correctly receive DA message from  $m$ . For instance, they receive more than one DA message at the same time from other neighbors, the probability of which is denoted as,

$$p_y = \binom{y}{1} p_s (1-p_s)^{y-1}, \quad (2.18)$$

where  $p_s$  is the probability for a neighbor that is in the listening state correctly receiving a DA message from device  $m$  in a certain time slot. For a device, say  $n$ , on condition that  $m$  is in the transmitting state and  $n$  is in the listening state,  $n$  receives DA message from device  $m$  if there are no other devices transmitting in the direction of device  $n$ . Therefore, we have,

$$p_s = \left(1 - \frac{p_t}{N_b}\right)^{k-x-1} \left(1 - \frac{1}{N_b}\right)^{x-y}. \quad (2.19)$$

Hence, the average number of received DA messages when device  $m$  is in the transmitting state is,

$$n_{tr} = \sum_{x=1}^k \sum_{y=1}^x p_t p_x p_y. \quad (2.20)$$

### One-way DD-ND

For the one-way DD-ND, both transmitter and receiver use directionality. At the beginning of a frame, if a device is in the listening state, it randomly chooses a beam sector to listen to. If multiple DA messages arrive at a device simultaneously, only the packets from the listening direction can be received. The average number of received DA messages in one frame can be modified according to (2.14) as,

$$n_{rt} = \sum_{w=0}^k \sum_{i=1}^{\infty} \sum_{x=1}^{N_b} 1_{|n_{i,x}| \geq 1} \binom{n_{i,x}}{1} \left(1 - \frac{1}{N_b}\right)^{n_{i,x}-1} \frac{1}{N_b} p_i p_w, \quad (2.21)$$

in which, according to the definition in Section 2.4.2,  $n_{i,x}$  is the number of DA messages that arrive at device  $m$  in the  $x^{th}$  slot of the  $i^{th}$  frame.

### Handshake based DD-ND

In the same way as that of handshake based DO-ND, devices can detect neighbors in both transmitting and listening state using handshake based DD-ND. When device  $m$  is in the listening state, the number of received DA messages is obtained according to (2.21). Figure 2.6 is taken for example to deduce the number of received DA ACKs when device  $m$  is in the transmitting state. Within a certain frame, we assume that device  $m$  is in the transmitting state and one of its neighbors, say device  $n$  is in the listening state and listens to the direction where device  $m$  is covered as shown in Figure 2.6. Being different from the handshake based DO-ND protocol, not all the devices that are in the transmitting state transmit in the direction of device  $n$  and thus can cause DA collisions at device  $n$ . Because  $n$  selects a certain direction to listen to and thus nullifies interference from the other directions, only devices within listening direction of  $n$  may interfere the reception of the DA message from  $m$ . As shown in Fig. 2.6, the white area,  $I$ , is the intersection area between the receiving sector of device  $n$  and the circular network, which can be considered as the potential interfering area for device  $n$ . If the other

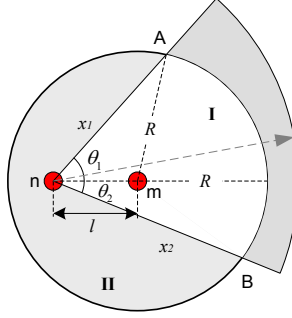


**Figure 2.6:** *Effective interfering area illustration.*

transmitting devices are located in this area, and they point in the direction of  $n$ , device  $n$  cannot receive a DA message from  $m$  due to a DA collision. The average size of the potential interfering area is given by,

$$S = \frac{1}{2} \int_0^R \int_0^\theta \left( lx_1 \sin \theta_1 + R^2 \arcsin \left( \frac{x_1 \sin \theta_1}{R} \right) + lx_2 \sin \theta_2 + R^2 \arcsin \left( \frac{x_1 \sin \theta_2}{R} \right) \right) f(\theta_1) f(l) d\theta_1 dl \quad (2.22)$$

where  $R$  is the network radius. The summation of  $\theta_1$  and  $\theta_2$  is the antenna beamwidth  $\theta$ , and  $l$  is the distance between device  $m$  and device  $n$ .  $f(\theta_1)$  and  $f(l)$  are the distribution for the angle  $\theta_1$  and distance  $l$ , where  $f(\theta_1) = 1/(2\pi)$  and  $f(l) = 2l/R^2$ . Receiving beam sector of device  $n$  intersects with the circular network at point  $A$  and point  $B$ . The distance from device  $n$  to  $A$  is  $x_1$ , and the distance from device  $n$  to  $B$  is  $x_2$ , where  $x_1$  and  $x_2$  are the solutions of the polynomial equations,

$$\begin{cases} x_1^2 + l^2 - R^2 = 2 \cos \theta_1 x_1 l \\ x_2^2 + l^2 - R^2 = 2 \cos \theta_2 x_2 l. \end{cases} \quad (2.23)$$

In a certain time slot when device  $m$  transmits a DA message to  $n$ , the condition for correct reception of this DA message by device  $n$  is that device  $n$  listens in the direction of  $m$  and no other devices within the listening direction of  $n$  transmit in  $n$ 's direction. The probability of this event is given by,

$$p_s = \sum_{x=0}^{k-1} \frac{1}{N_b} \binom{k-1}{x} \left( \frac{S}{\pi R^2} \right)^x \left( 1 - \frac{p_t}{N_b} \right)^x \times \left( 1 - \frac{S}{\pi R^2} \right)^{k-x-1} \quad (2.24)$$

When device  $m$  is in the transmitting state, the expected number of DA ACKs received,  $n_{tr}$ , can be calculated according to (2.17), (2.18) and (2.20).

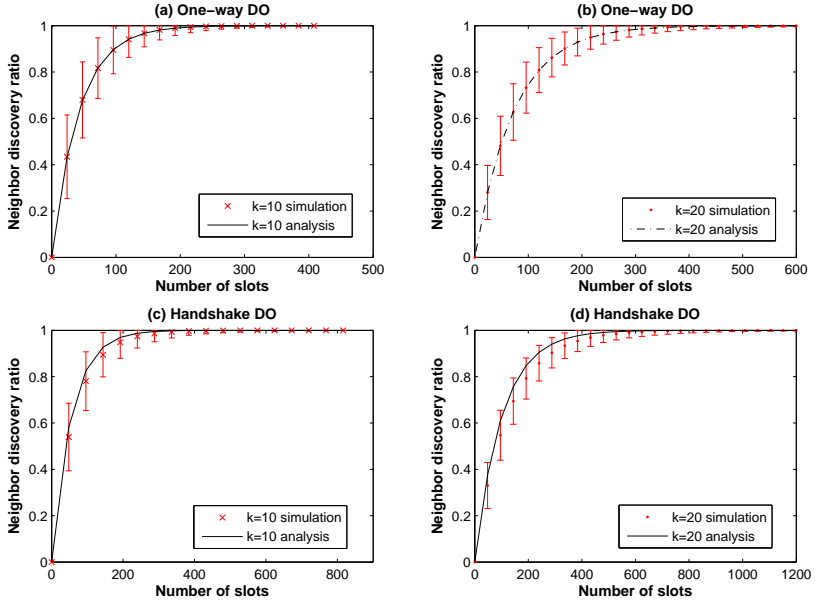


**Figure 2.7:** Simulation validation for the ND ratio of one-way and handshake-based DO-ND, 10000 iterations,  $\theta = 60^\circ$ ,  $p_t = 0.3$ .

## 2.5 Numerical Results

Simulation study is used to verify the analysis employed thus far. According to the assumptions used in the analytical model, a two-dimensional circular network is formed in simulation scenarios, in which all the devices are within the transmission range of each other. The target device is located in the middle of the network, and all the other devices are uniformly distributed within the network. The devices are assumed to be equipped with flat-top antennas. The ND ratio mentioned in this section refers to the ND ratio of the target device in the middle of the network.

Figure 2.7 compares the performance of using one-way and handshake based D-ND mechanisms using DO mode with different node degrees. The simulation results are plotted with mean values and 95% confidence intervals. These figures illustrate a good accuracy of our proposed analytical model. From Figure 2.7, it is observed that the handshake based mechanism performs worse than the one-way mechanism, which is different from the results of the two-device model. It is because that there is a possibility for multiple listening devices being in the same beam sector and transmit multiple DA ACKs simultaneously, especially when the transmission probability is low. Hence, DA ACK collision compromises the D-ND performance.

The optimal transmission probability  $p_{opt}$  is obtained to maximize the number



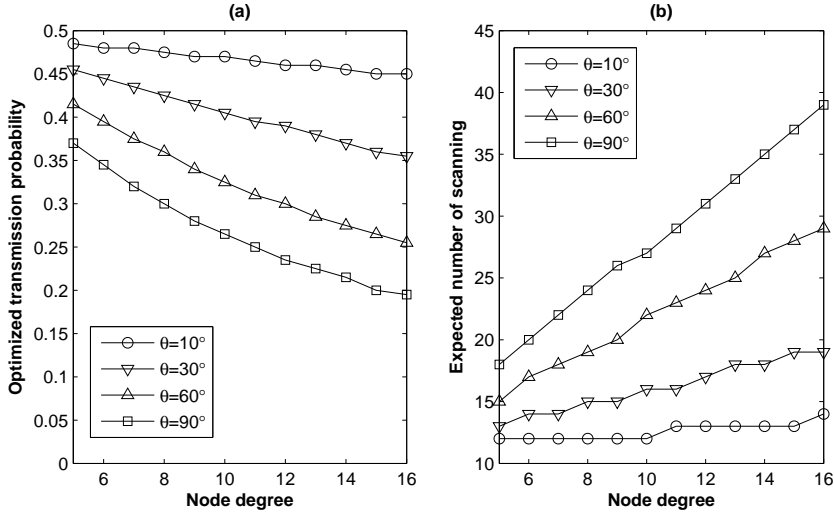


**Figure 2.8:** Relationship between node degree, the optimized transmission probability and expected number of scanning with variant antenna beamwidth.

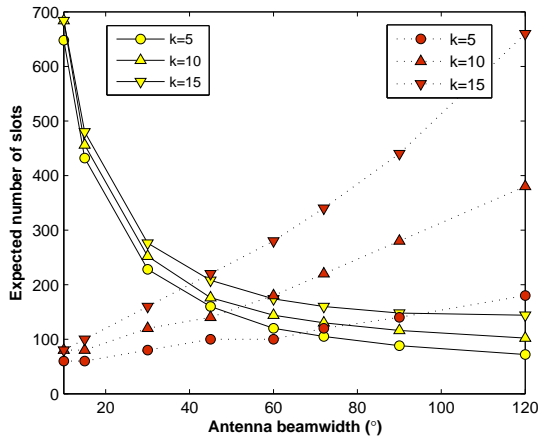


**Figure 2.9:** Antenna beamwidth influence on the ND performance,  $p_t = 0.2$ .

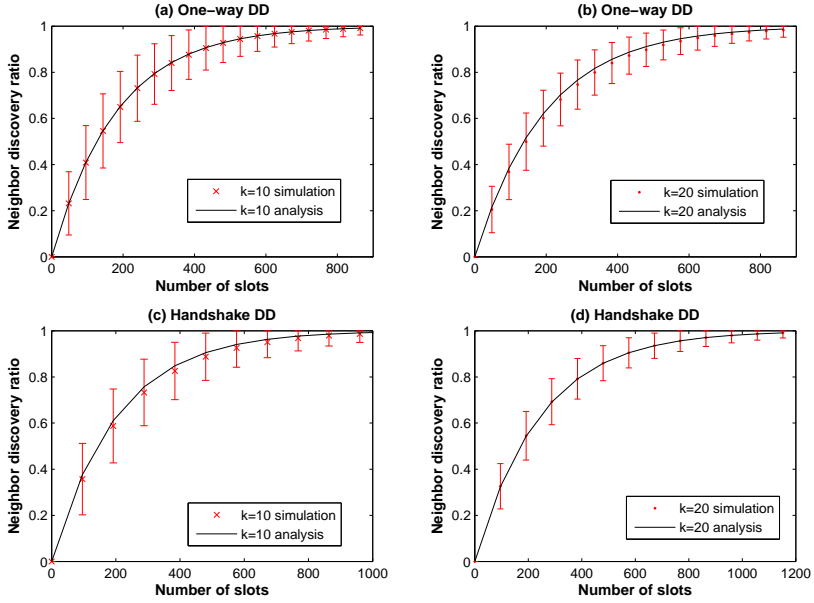


**Figure 2.10:** Simulation validation for the ND ratio of one-way and handshake-based DD-ND, 10000 iterations,  $\theta = 60^\circ$ ,  $p_t = 0.3$ .

of detected neighbors in one frame. The relationship between the node degree and  $p_{opt}$  is depicted in Figure 2.8 (a). Once a new device joins the network and obtains the basic knowledge of the network, for instance the node degree<sup>3</sup>, it could be used to estimate the optimized transmission probability to achieve a better ND performance. Figure 2.8 (b) shows the number of scanning required for a particular node degree using the optimal transmission probability. Here, the expected number of scanning is defined to be equivalent to the expected number of frames required for a ND process. It is observed that, using  $p_{opt}$  significantly reduces the expected number of scanning.

The influence of antenna beamwidth on the ND duration is shown in Figure 2.9. With the increase in the antenna beamwidth, although the expected number of scanning increases, the entire ND time, which is related to the number of expected slots used for a ND process decreases.

The analytical results for the ND ratio obtained using one-way DD-ND and handshake based DD-ND are depicted in Figure 2.10, which are compared with the results from the simulation. These two figures also indicate a good accuracy of our proposed analytical model. In Fig. 2.11, the four D-ND protocols, one-way DO, one-way DD, handshake DO, and handshake DD, are compared together in terms of ND ratios using simulations. Each generated result is the mean of 10000

<sup>3</sup>In IEEE 802.15.3c featured WPAN, once a device associates with the piconet controller (PNC), it is informed by the PNC the number of devices with the WPAN [7].

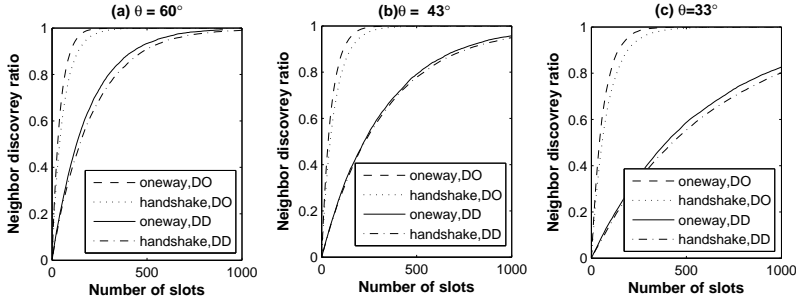


**Figure 2.11:** ND ratio comparison using flat-top directional antennas,  $k = 10$   $p_t = 0.3$ .

iterations. The node degree is fixed at 10 and the transmission probability is 0.3. As shown in Fig. 2.11, it is observed that, in general, using DO mode has higher ND ratio than using DD mode. The smaller the antenna beamwidth is the bigger is the ND performance difference between DO mode and DD mode. Moreover, when antenna mode is fixed (DO or DD), the one-way mechanism has a higher ND ratio than the handshake based mechanism.

## 2.6 Antenna Pattern and Link Model Influence on D-ND

To illustrate the influence of antenna pattern on the performance of ND processes, simulations are carried out using a UCA antenna system and LM2 link model to compare with the results obtained using the flat-top antenna system and LM1 link model on the condition that all the devices are within the transmission range of each other.

### 2.6.1 D-ND Ratio

In Figure 2.12, one-way DO, handshake based DO, one-way DD, and handshake based DD are compared together using UCA antenna systems with different number of antenna elements. In Fig. 2.12, it is observed that the DD mode performs better than the DO mode in all the scenarios, which is different from the results from Fig. 2.11. This is because, the UCA system and the flat-top system have a large difference in terms of the antenna gain pattern due to the influence of side lobes, which is shown in Fig. 2.3. Note that the antenna beamwidth used for these two antenna patterns are similar here. For the UCA system, the side lobes play an important role in the D-ND process. If a side lobe has sufficient gain, it can also be used to discover a neighbor that is not pointed by the main lobe. Meanwhile, a side lobe may also generate interference to disturb the transmissions amongst the other links, if the amount of interference is high. The performance between one-way and handshake based mechanisms is very close for DD mode with a 6-

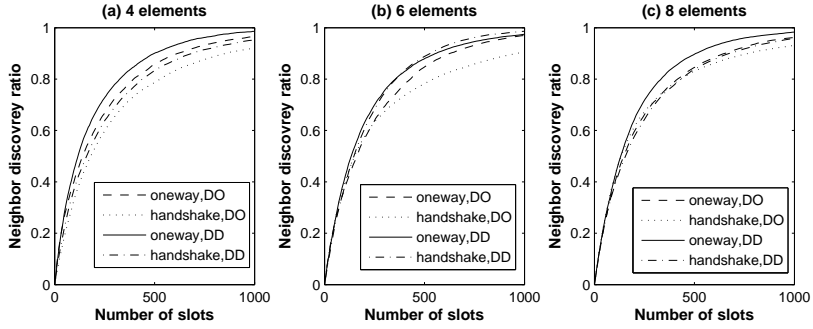


**Figure 2.12:** The influence of the number of antenna elements of UCA systems on ND ratio,  $p_t = 0.3$ ,  $n = 2.5$ ,  $k = 10$ ,  $R = 5$  m.

element UCA system and using DO mode with an 8-element UCA system. Except these two scenarios, one-way mechanism performs better than handshake based mechanism and this can be also observed in Fig. 2.11.

### 2.6.2 D-ND Overhead

In Figure 2.13 (a) and (b), the overheads are compared using different D-ND mechanisms using the UCA system and the flat-top system respectively, in which the results show the mean with 95% confidence intervals. When the flat-top system is used in the simulation, the following properties are observed. First, the amount of overhead generated increases with the decrease of antenna beamwidth using all the D-ND mechanisms. Second, using DD mode generates more overhead than using DO mode for both one-way and handshake based mechanisms. Third, using DO mode, handshake based mechanism generates slightly more overhead than one-way mechanism. Fourth, using DD mode, the amount of overhead generated using one-way mechanism is higher than using handshake based mechanism. To explain the above observations, the expected numbers of scanning using the UCA system and the flat-top system are plotted in Figure 2.13 (c) and (d). Although the expected ND time obtained using one-way mechanism is faster than using handshake based mechanism shown in Figure 2.11, the expected number of scanning obtained using one-way mechanism is higher than the handshake based mechanism as shown in Figure 2.13 (d). The expected number of scanning relates to the number of DA messages transmitted during a ND process. As shown in Figure 2.13 (d), when the DO mode is used, one-way and handshake based mechanism have similar number of expected scanning, which implies that the number of generated DA messages are also similar. For the handshake based mechanism, except for the DA messages, it also generates DA ACK messages. This leads to increase in overhead compared to the one-way DO. When the DD mode is used, the expected number of scanning obtained using one-way mechanism is much hi-

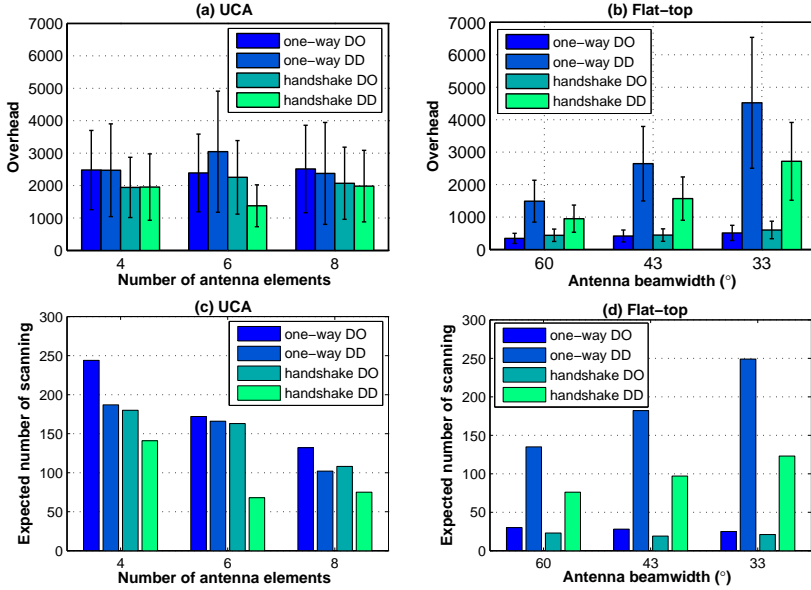


**Figure 2.13:** Overhead and expected number of scanning comparison between UCA system and flat-top system,  $p_t = 0.3$ ,  $k = 10$ ,  $n = 2.5$ ,  $R = 5$  m.

gher than the handshake based mechanism. Hence the generated DA messages dominate the amount of the overhead.

Compared to the flat-top systems, the overhead using UCA systems does not change much with for varying number of antenna elements. Moreover, contrary to this, in the flat-top systems the expected number of scanning decreases with the decrease in antenna beamwidth. This is because of the influence of antenna side lobes. As shown in Figure 2.3, when the number of antenna elements is less, the influence of the side lobes is higher, which decreases the D-ND performance due to the interference generated from the side lobes within a ND process. It is also seen that the one-way mechanism results in a higher number of scanning compared to the handshake based mechanism.

### 2.6.3 Influence of $p_t$ and $k$

The influence of transmission probability,  $p_t$ , and the node degree,  $k$ , on the expected number of scanning are depicted in Fig. 2.14, in which a 6 elements UCA system is used in the simulation. The optimized transmission probabilities for the D-ND processes can be observed in Figure 2.14 (a). Compared to Figure 2.8 (a), the optimized transmission probability obtained using the UCA system is lower than the flat-top system with the same antenna beamwidth. This is also because

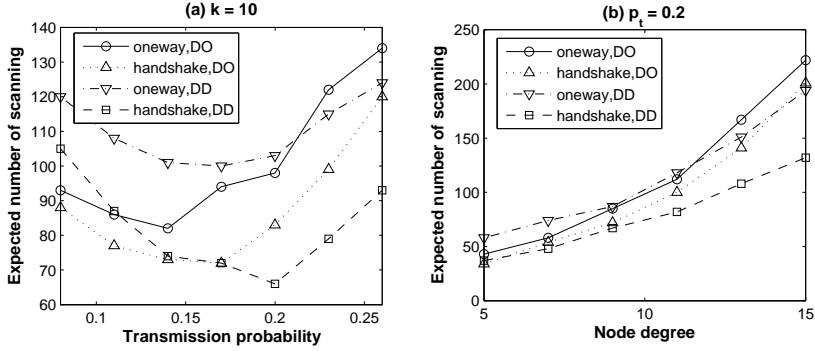


**Figure 2.14:** *Transmission probability influence on the expected number of scanning, 6 elements UCA system*

of the interference generated by side lobes. As shown in Figure 2.14 (b), the expected number of scanning increases with the increase in node degree, and the expected number of scanning obtained using handshake DD-ND is the lower bound compared to the other mechanisms.

## 2.7 Chapter Summary

In this chapter, the performance of ND processes using directional antennas was investigated. A comprehensive analysis was proposed to demonstrate the ND performance using different ND mechanisms (one-way ND and handshake based ND) and different antenna modes (DO mode and DD mode). Our analytical model is based on the flat-top antenna pattern and full mesh networks. The accuracy of our model was validated via extensive simulations. Moreover, to revise the influence of the antenna pattern and link model impact on D-ND processes, the D-ND performance was investigated using UCA system with an interference-aware link model. The results indicated that there are indeed some gap between the analytical model and the realistic scenario, which is due to the effect of side lobes in UCA system. With the advances in antenna technology, this gap can be reduced and our analytical model provides a guideline to use directional antennas with less side lobe impact.

# Chapter 3

## Enhanced IEEE 802.15.3 MAC for 60 GHz WPANs

“It is not knowledge, but the act of learning, not possession but the act of getting there, which grants the greatest enjoyment.”

- Carl Friedrich Gauss

*The IEEE 802.15.3 standard defines a well-accepted MAC layer protocol for high rate WPANs. However, it is not straightforward to adapt the IEEE 802.15.3 MAC for 60 GHz featured WPANs. The main research challenges to use the IEEE 802.15.3 MAC for 60 GHz WPANs are identified in this chapter, in which, one of the main difficulties is to schedule directional transmissions. In this chapter, a complete resource management scheme is proposed to resolve the directional transmission scheduling problem based on the IEEE 802.15.3 MAC. Moreover, the IEEE 802.15.3 MAC is lack of fairness consideration and multi-class traffic support. Hence in this chapter, a QoS-aware transmission scheduling algorithm with fairness consideration is devised to support heterogeneous services in 60 GHz WPANs.*

## 3.1 Introduction

Wireless medium is in an open environment, which means, multiple devices can gain access to the medium at the same time. Basically, a MAC layer protocol defines certain rules to let the devices within a network access the shared medium in an organized and efficient manner [43]. Hence, MAC protocols play an important role for the channel resource management and coordination. MAC layer protocols can be generally divided into two categories: contention-based MAC protocol and contention-free MAC protocol. Contention-based MAC protocol is also called as random access protocol. It defines that all the devices in the network contend to gain access to the medium. ALOHA is a classical contention-based MAC protocol. It was the first MAC protocol for packet radio networks, which was proposed in 1970 [44]. ALOHA defines that whenever a node has packets to transmit, it transmits them immediately without checking the status of the channel. If the transmission collides with other transmissions, it will be retransmitted after a random back-off period. The maximum throughput for ALOHA is proven to be 18.4% [44]. If the system is slotted and all of the transmissions happen only at the beginning of each slot, the maximum throughput of the system can be improved to 36.8%, and this MAC protocol is called as slotted ALOHA. Carrier Sense Multiple Access (CSMA) is another example for contention-based MAC protocol. To reduce data collisions, CSMA defines that, devices sense the channel before data transmission, which is also called as physical channel sensing. To solve the hidden/exposed node problem, which is suffered by all the contention-based wireless networks, CSMA with Collision Avoidance (CSMA/CA) uses a handshake process of Request-to-Send and Clear-to-Send (RTS-CTS) packets before data transmission, which is also called virtual channel sensing. CSMA/CA is also adopted in IEEE 802.11 MAC protocol [45]. Contention-free MAC protocol is also called as scheduled MAC protocol. For instance, Time Division Multiple Access (TDMA) is a typical contention-free MAC protocol, which defines that several users are allowed to share the same channel by dividing it into different time slots, and each transmission pair is allocated with a dedicated time slot to avoid collisions due to medium access contention. Compared to the contention-based MAC, contention-free MAC protocols are more suitable for the services with QoS requirements because of its capability to limit transmission delay and jitter.

In Chapter 1, the properties of 60 GHz radio have been introduced. To obtain sufficient link budget for multiple Gbps data rates, directional antennas are necessary in 60 GHz systems. Although directional antennas provide higher antenna gain and less interference range compared to omni-directional antennas, designing a MAC protocol for directional antennas is not a trivial issue. As mentioned in the previous chapter, the major issue caused using directional antennas is the so-called *deafness*. Extensive work has been done to design CSMA/CA based MAC protocols using directional antennas in ad hoc networks [27, 30, 31, 46–48, 48–50]. The works, like [49, 50], propose to use circular directional RTS packets to prevent deafness by sweeping its antenna's main lobe to transmit RTS packets in all the



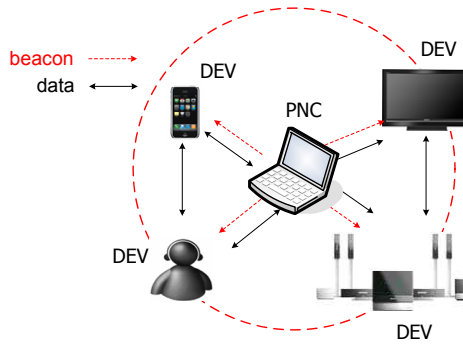


**Figure 3.1:** *IEEE 802.15.3 based piconet components*

possible directions. TDMA is a feasible way to coordinate directional transmissions. Because each transmission pair has guaranteed time for channel access. Hence, deafness is not an issue in TDMA systems.

The use of directional antennas brings the feasibility to enable spatial reuse in a TDMA system. The fundamental approach to schedule concurrent transmissions is based on the criteria of SINR estimation, e.g. [51]. If the coexistence of multiple radio links satisfies their respective SINR restrictions, these links can be scheduled at the same time for concurrent transmissions. The distance between a transmission pair is the crucial factor to calculate SINR. The approaches proposed in [51] are generic models considering only the omni-directional antennas. Using directional antennas, except for the distance between transmitter and receiver, the antenna pointing direction also influences the resulted SINR. The work in [52] proposed a scheduling algorithm using antenna array, in which, the directional information of a device is used to assist SINR estimation. However, their work is only for a star-topology network, e.g. multiple terminal devices communicate with a base station. The dynamic transmission scheduling for peer-to-peer communication is not supported in their work. In [53], the authors have separated the interference area piecewise according to the antenna's main lobe and side lobes. However, their analytical model is based on a cone and sphere antenna radiation pattern. If a realistic directional antenna pattern with side lobes is considered, their work is less efficient.

The IEEE 802.15.3 standard defines a central controlled network topology and the TDMA based MAC protocol for WPANs. Due to the small scale network size, the central controlled network topology can efficiently manage the channel resource and QoS requirements. However, it is not straightforward to use the IEEE 802.15.3 MAC for 60 GHz featured PHY [54]. The MAC design challenges for 60 GHz WPANs are identified in this chapter. To overcome these challenges, several enhancements on top of the IEEE 802.15.3 MAC are proposed.

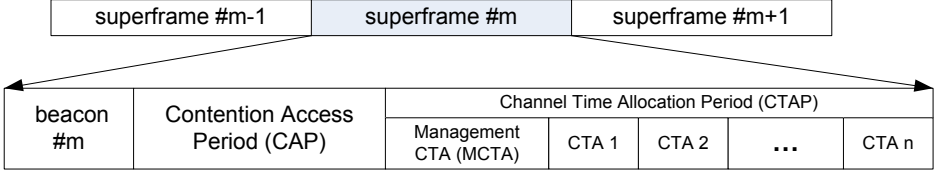


Figure 3.2: IEEE 802.15.3 defined superframe structure

## 3.2 MAC for 60 GHz WPANS

### 3.2.1 IEEE 802.15.3 MAC Overview

A piconet is the fundamental topology for the IEEE 802.15.3 WPANS. It consists of a PicoNet Coordinator (PNC) and several slave Devices (DEVs) within the radio coverage range of the PNC, as shown in Figure 3.1. The PNC provides the basic timing for the piconet by broadcasting beacons. Moreover, the PNC is also responsible to manage the QoS, power save modes and access control to the piconet. When a PNC capable device is powered on, it firstly scans the possible channels to choose an idle channel to establish a piconet. To join in a piconet, a DEV needs to associate with the PNC. During the association process, the PNC provides a unique identifier for the DEV, and the PNC also acquires the capabilities of the DEV. The Channel time in a piconet is based on the superframe, which contains three major parts: the beacon, the Contention Access Period (CAP) and the Channel Time Allocation Period (CTAP) as shown in Figure 3.2.

- Beacon

The PNC periodically broadcasts beacon packets, which contain the channel time allocation and piconet management information. The devices in the piconet synchronize themselves with the PNC by receiving beacons.

- Contention Access Period

The CAP is used for asynchronous data or communication commands transmissions. The medium access mechanism during the CAP is CSMA/CA. During the CAP, a device is allowed to transmit one data frame (except for the Imm-ACK frame) at a time with a backoff mechanism being applied.

- Channel Time Allocation Period

The CTAP is composed of the Channel Time Allocation blocks (CTAs) and the Management CTAs (MCTAs). The CTAs are used for commands, isochronous streams and asynchronous data. The peer-to-peer QoS can be guaranteed in CTAs using a TDMA based medium access mechanism. In the MCTA period,

devices request to reserve dedicated channel access time in the CTAP by sending Channel Time Request (CTR<sub>q</sub>) frames to the PNC. The PNC acknowledges the devices by replying Channel Time Response (CTR<sub>p</sub>) frames. The medium access mechanism in MCTAs is based on slotted ALOHA. The IEEE 802.15.3 standard is defined for omni-directional antennas based WPANs.

### 3.2.2 MAC Expectations for 60 GHz WPANs

The IEEE 802.15.3 MAC is designed for omni-directional antennas. To enable spatial reuse using directional antennas, the key issues that need to be addressed are directional information management and directional transmission scheduling. For instance, to enable directional communication, the devices should know where to point and whom to point. Therefore, how to acquire a neighbor's directional information is a crucial concern. Moreover, the adaptive array antenna system provides certain advantages such as the feasibility to support antenna beam-forming and it may also enable the spatial reuse capability within a WPAN. How to efficiently use directional antennas in WPANs is an open issue.

A MAC functional block for an adaptive array antenna system is proposed as shown in Figure 3.3, in which, it contains the major functional modules at the MAC layer and the interface with the adjacent PHY and Network layer. To enable the use of directional antennas for the IEEE 802.15.3 MAC, the following functions are expected at the MAC layer.

#### Antenna Beam-forming Control

Beam-forming is a signal processing technique used to steer the transmitting or receiving signals to different directions by phasing the antenna array elements [55]. As shown in Figure 3.3, when the system down-converts the signal, the direction of the received signal is computed by a DoA algorithm. The information supplied from the DoA module is processed by an adaptive array algorithm, which computes the appropriate weights that result in an optimum radiation pattern toward the desired signal. The adaptive array based beam-forming is attractive for 60 GHz communication due to the following reasons. First, within the usage models defined in Section 1.2.2, applications defined in UM2 UM3 and UM4 require that devices have self-organization capability to construct and maintain networks in ad-hoc mode, which means, devices within a network can autonomously discover their neighbors and set up links without interventions from users. Therefore, devices should acquire the neighbor's direction information for communication. A mis-pointing of antenna may easily reduce the received power and disturb the connectivity. Hence, accurate direction estimation is a crucial factor to guarantee high speed transmission in 60 GHz systems. How to perform high accuracy beam-forming is out of the scope of this work. The main focus of this chapter is at the MAC layer design to cooperate the directional antenna features at the PHY layer.

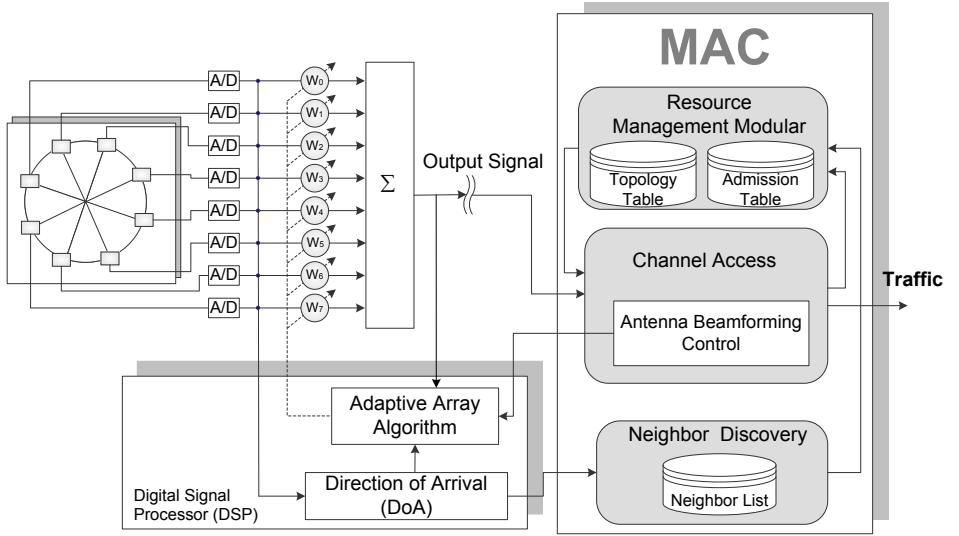


**Figure 3.3:** Functional block for the MAC layer module and the interfaces with eight-element adaptive array system.

### Directional Neighbor Discovery (D-ND)

The ND process is not specified in the IEEE 802.15.3 MAC, but it is embedded in the device and PNC association process. When a new device joins in a piconet, the PNC adds the new device's address in the beacon to inform the other devices in the piconet. However, to realize directional transmission, being aware of the existence of a device is not enough. Devices should know where to point and when to point. Therefore, a distributed, self-organized ND process is essential to enable directional communication in WPANs. During the distributed ND process, devices sequentially transmit their advertising messages to cover all the possible directions. To build symmetrical link, a device that receives an advertising packet from its neighbor should provide active response to the transmitter. An advertising packet contains a device's address, piconet ID and the transmitting beam sector number. The packet preamble contains the training sequences for the purpose of beam-forming. During a ND process, all the advertising and corresponding response messages are transmitted directionally. Although the frequently executed ND process could update the network statue in time, it also involves more overhead. Therefore, it is defined that the ND process is not a compulsory component in each superframe. A ND process could be triggered in several situations:

- Null neighbor list: After a device joins a piconet, the ND process is first triggered in the CAP due to its empty neighbor list.

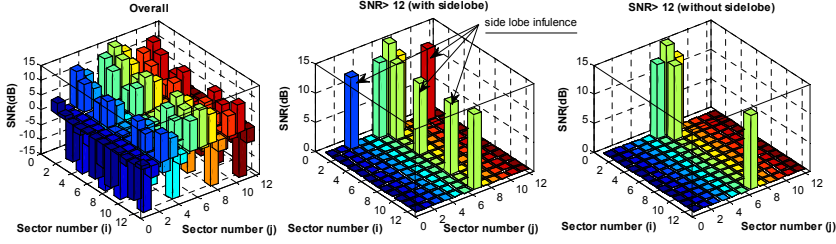


**Figure 3.4:** *Neighbor direction relation illustration*

- **Link quality degradation:** Directional links are vulnerable to the environment changes and highly rely on LOS link communication. However, LOS link is easily shadowed by a moving person or any obstacles. If the link quality is degraded, the ND process is triggered automatically to trace other feasible beam path to continue communication.
- **Periodical update:** To pro-actively update any changes in the piconet, the ND process should be triggered periodically by a pre-defined ND timer, which should be designed according to the dynamic property of a piconet.

### 3.3 Device Orientation Profile

#### Device Orientation Profile Definition

Using omni-directional antennas, all the devices within the transmission range are one-hop neighbors. In contrast, the concerned neighbor relationship becomes more sophisticated using directional antennas, which is also discussed in Chapter 2. To demonstrate the directional neighbor relationship, a neighbor detection process is simulated between two devices, e.g. transmitter  $i$  and receiver  $j$ , which are equipped with 4-element UCA system. For each device, its azimuth plane is equally divided into  $N_B$  sectors, where  $N_B = \left\lceil \frac{360}{\theta_{HPBW}/2} \right\rceil$ , where  $\lceil \cdot \rceil$  denotes the ceiling function<sup>1</sup>. If a 4-element UCA system is used, according to Table 2.1,  $N_B$  is 12. The two devices are separated by 10 meters. Device  $j$  is located in the 1<sup>st</sup> sector of  $i$ , and device  $i$  is located in the 7<sup>th</sup> sector of  $j$ . The transmitter steers its antenna's main lobe and transmits its advertising packets from the center of each sector. The receiver also sequentially steers its listening direction. Therefore, the whole process induces a  $12 \times 12$  SNR vector using the specified propagation model and corresponding parameter settings introduced in

<sup>1</sup>The number of beam sectors should be decided by the antenna beam-forming accuracy. More beam sectors might provide higher accuracy for neighbor direction detection, but it also prolongs the ND process.

Section 2.3.2. On condition that the SNR threshold is 12 dB, the overall SNR vector is plotted in Figure 3.4 (a). The SNR vector using UCA system is depicted in Figure 3.4 (b), from which it is observed that, the highest SNR is resulted when the two devices use main lobes to point each other, which should be used for directional communication. When the side lobe effect cannot be neglected, it increases the interference area of directional transmissions. Using more advanced antenna technique, the side lobe can be restrained within the neglected range, so the SNR vector using idealized flat-topped directional antenna pattern is also demonstrated, which has the same main lobe gain with the 4-element UCA system but without the side lobe effect. The SNR vector of the flat-topped antenna system is shown in Figure 3.4 (c).

*Device orientation profile* is denoted as the collection of sectors from where the directional link can be established with sufficient SNR for communication. As shown in Figure 3.4 (b), for device  $j$ , its neighbor  $i$ 's orientation profile is denoted as  $\nu_j(i)|_{i \rightarrow 1} = \{3, 6, 7, 8, 11\}$ , which means, when device  $i$  points to its 1<sup>st</sup> beam sector, device  $j$  can hear device  $i$  when its main lobe points to the  $x^{th}$  sector, where  $x \in \nu_j(i)|_{i \rightarrow 1}$ . Using the flat-topped directional antenna system, it has  $\nu_j(i)|_{i \rightarrow 1} = \{6, 7, 8\}$ . Therefore, when a directional antenna with neglecting side lobes is used, it can be concluded that, when device  $j$  receives a self-advertising packet from its neighbor  $i$ ,  $j$  computes the DoA  $\theta_{ji}$  and maps it into a orientation profile as  $\nu_j(i) = \{\epsilon_j(i) - 1, \epsilon_j(i), \epsilon_j(i) + 1\}$ , in which,  $\epsilon_j(i)$  is the sequence number of the beam sector where device  $i$  is located relative to  $j$  and  $\epsilon_j(i) = \left\lceil \frac{\theta_{ji}}{\theta_{HPBW}/2} \right\rceil$ . After updating its neighbor list, device  $j$  replies  $i$  with a self-advertising response packet, which records its own address, piconet ID and the transmitting beam sector number. Devices within a piconet report any updates of its neighbor list to the PNC through Information Commands. Therefore, the PNC maintains the entire direction-aware piconet topology. For a piconet, the involved devices are limited to the consumer electronic devices, e.g. HDTV, video recorder, laptop, etc, and the effective operation range is within 10 meters. Therefore compared to the achievable network throughput in the order of Gbps, the topology updating related Information Commands overhead could be neglected.

### Device Orientation Profile Management

The device orientation profile is managed and maintained via neighbor list. An example of a neighbor list is shown in Table 3.1. After a device detects a new neighbor, it adds a new entity in its neighbor list, in which the neighbor's ID, the relative direction  $\epsilon_i(j)$ ,  $\epsilon_j(i)$ , and the probed link quality are recorded. Each entity is associated with a timer to limit the effective duration of neighbor information. When the timer is expired, the associated neighbor information is erased from the neighbor list. A device could detect a neighbor through LOS link or through a NLOS link, for instance reflection from the ceiling or the walls. However, not all the NLOS links can provide sufficient SNR for high data communication. If a

**Table 3.1:** *A neighbor list example of device  $i$* 

Neig. ID ( $j$ )		3	5
Beam path 1 (Strongest)	$\epsilon_i(j)$	1	2
	$\epsilon_j(i)$	3	6
	SNR(dB)	15	14.5
	Expire Time	$t_{31}$	$t_{51}$
Beam path 2 (Backup)	$\epsilon_i(j)$	3	-
	$\epsilon_j(i)$	6	-
	SNR(dB)	10	-
	Expire Time	$t_{32}$	-
Ori. Profile		$\nu_i(3)$	$\nu_i(5)$

NLOS link with good quality is detected during the ND process, the device also records it in the neighbor list as a backup choice. In case a LOS link is blocked by a person or any obstacle, the device may steer the beam to a backup link to continue the connectivity. This issue will be addressed in Chapter 5.

### 3.4 Resource Management

To achieve multi-Gbps throughput, it is crucial for the network resource being arranged in an efficient way. A piconet has a central-controlled network topology, in which the PNC manages the channel resource and schedules peer-to-peer communication within the piconet. All the other non-PNC devices request channel access time from the PNC. Therefore, the PNC can easily monitor the overall system capacity and control traffic flows within the piconet. The PNC should dynamically allocate channel resource to optimize the system performance. The essential tasks for resource management are resource allocation and admission control. The resource management module designed in this work is shown in Figure 3.5. The main functionalities of this resource management module are explained as follows.

- Channel Access Request

Devices within a piconet transmit the CTRq command frames to reserve channel access time from the PNC. In a CTRq, it records the transmitter, receiver addresses and the channel access time length. To facilitate directional transmission scheduling, the transmitting beam sector sequence number and receiving beam sector sequence number are also recorded in the CTRq. The resource management module is invoked by receiving the CTRq command frames.

- Request Admission Control

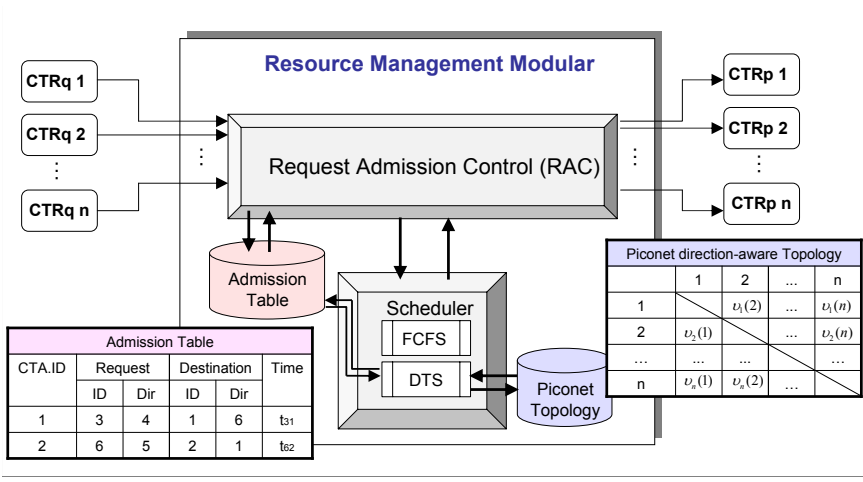


Figure 3.5: PNC-based resource management block diagram

Because of the limited channel resource, the PNC cannot admit all the requests for channel access. To ensure the QoS requirements from the users within the piconet, the PNC should admit new arrival channel access requests based on certain criteria, such as the available bandwidth, power restriction, etc. The request admission control module is designed for this purpose. It is triggered by receiving CTRq frames from the devices within the piconet. The PNC estimates the channel resource according to the channel utilization circumstance. A channel access request is admitted if it subjects to the equation (3.1) and (3.2),

$$L_{overhead} + \sum_{i=1}^m L_{CTA_i} \leq L_{sf_{max}} \quad (3.1)$$

where  $L_{sf_{max}}$  is the time duration of the superframe with the maximum length, which is specified as  $65535 \mu s$  in the standard [3],  $L_{overhead}$  is the channel access time used for the beacon, the CAP and the MCTA,  $L_{CTA_i}$  is the channel access time arranged for the  $i^{th}$  CTA block and  $m$  is the total number of arranged CTA blocks.  $L_{CTA_i}$  is calculated as  $L_{CTA_i} = n_{q,i} \times \bar{\tau}_i$ , where  $n_{q,i}$  is the number of packets queueing in the buffer and  $\bar{\tau}_i$  is the average time to transmit a packet. To keep the fairness of scheduling, a certain length of CTA is limited by equation (3.2):

$$L_{CTA_i} \leq \delta (L_{sf_{max}} - L_{overhead}) \quad (3.2)$$

where  $\delta$  is a proportion factor within the range  $(0, 1)$ , which is used to avoid a certain device selfishly occupying all the channel resource. The request admission control process invokes a scheduling algorithm in the scheduler module to make transmission scheduling decisions. After processing the channel access request, the



request admission control module generates a CTRp command frame, in which the channel time allocation decision (acceptance or reject) is recorded to acknowledge the requiring device.

- Scheduler

The channel resource can be allocated using different transmission scheduling algorithms. According to the required traffic load and QoS constraints, the request admission control module can invoke different scheduling algorithms within the scheduler. First-Come-First-Served (FCFS) is one of the most straightforward algorithms. It simply defines that if the requested channel access time is less than the available channel resource, the request is admitted. When the traffic load is low, it makes no difference to use different transmission scheduling algorithms, because the channel resource is sufficient to allocate all the requests. When the traffic load increases, different transmission scheduling algorithms exhibit dissimilar performance. The PNC can either use a low complexity algorithm (e.g. FCFS) to make fast decisions when the traffic load is low, or use a high complexity algorithm to optimize the usage of channel resource when traffic load is high. Therefore, the scheduler module contains multiple scheduling algorithms to allocate channel resource in different traffic load circumstance.

- Admission Table

The PNC maintains an admission table to record the scheduled transmissions within its piconet. The admission table is broadcasted through beacon frames to inform the devices about the scheduling results within the current superframe. The PNC can estimate the piconet traffic load according to the channel time reservations registered in the admission table. In each entity of the admission table, it records the transmitter ID, transmitting beam sector, receiver ID, receiving beam sector, the allocated CTA block ID and the channel access time. After a transmission is scheduled, the admission table is updated correspondingly.

- Piconet Topology Database

Devices acquire their neighbor profiles during the ND process and inform the PNC of their neighbor profiles to assist the PNC in constructing the piconet topology. The PNC maintains a database which records the entire piconet topology information as shown in Figure 3.5. The DTS algorithm could schedule concurrent transmissions using the direction-aware topology information recorded in the database.

## 3.5 Directional Transmission Scheduling (DTS)

Directional antennas provide the spatial diversity for wireless systems by concentrating energy on certain directions and restraining interference from other directions. If multiple transmissions could take place simultaneously without interfering with each other, these links coexist in the same channel. In this section a

Directional Transmission Scheduling (DTS) algorithm is proposed on top of the IEEE 802.15.3 MAC to enable spatial reuse TDMA in WPANS.

### 3.5.1 System Model

First, the network model and some notations used in the following content are introduced here. The network graph  $G(V, E)$  characterizes the piconet topology, where  $V$  represents the set of devices and  $E$  represents the set of links. If device  $j$  is within the transmission range of device  $i$ , it is denoted as  $l_{ij} = 1$ , otherwise  $l_{ij} = 0$ ,  $\forall l_{ij} \in E$  and  $\forall i, j \in V$ . Bi-directional links are assumed in this work. Thus, if  $l_{ij} = 1$ , then  $l_{ji} = 1$ . For each link  $l_{ij}$ , the set of its interfering links is represented as  $\Gamma_{l_{ij}}$ , which means that the set of links cannot coexist with  $l_{ij}$ .

### 3.5.2 Link Coexistence Test

During the distributed ND process, the PNC obtains the direction-aware topology of its piconet. Therefore, the PNC could estimate the interference between links using device orientation profiles. The core idea of DTS is Link Coexistence Test (LCT). The basic principle of LCT is that, for two links, if the transmitter of each link does not interfere with the receiver of the other link, the two transmission links can coexist. For instance for directional link  $l_{ji}$ , transmitter  $j$  and receiver  $i$  use their antenna's main lobes to point each other. In this circumstance, all the neighbors located within  $\nu_i(j)$  are forbidden to transmit to  $i$ . Otherwise, collision happens at  $i$  side. For another link  $l_{kl}$ , if  $\epsilon_i(k) \in \nu_i(j)$  and  $\epsilon_k(i) \in \nu_k(l)$ , link  $l_{ji}$  and link  $l_{kl}$  cannot coexist. To guarantee sufficient geographic separation between two links, the above condition can be modified as:

$$\text{Coexist.Code} = [[\nu_i(j) \cap \nu_i(k) \neq \phi] \& [\nu_k(i) \cap \nu_k(l) \neq \phi]]^c \quad (3.3)$$

where  $A^c$  represents the complement of set  $A$ , and  $(A^c)^c = A$ . If the `Coexist.Code` is false, link  $l_{ji}$  and link  $l_{kl}$  can not be allocated in the same CTA block. Therefore,  $\Gamma_{l_{ij}} = \Gamma_{l_{ij}} \cup \epsilon_{kl}$  and  $\Gamma_{l_{kl}} = \Gamma_{l_{kl}} \cup l_{ji}$ .

### 3.5.3 DTS Procedure

Assume that  $K$  represents the set of already scheduled CTA blocks by the PNC. In the  $\kappa^{th}$  arranged CTA block ( $\kappa \in K$ ),  $m$  links are already scheduled in it, and the scheduled link set is represented as:

$$\Lambda_\kappa(m) = [l_{t_1 r_1}, l_{t_2 r_2}, \dots, l_{t_m r_m}], \quad (3.4)$$

where,  $\forall t_x, r_x \in V, \forall x \in [1, m]$ . The PNC receives a channel access request from device  $i$  to reserve channel access time  $t_{ij}$  for link  $l_{ij}$ . If the requiring link  $l_{ij}$  satisfies  $l_{ij} \notin \bigcup_{x=1}^m \Gamma(e_{t_x r_x})$ , this link can coexist with the links already scheduled in the  $\kappa^{th}$  CTA block. If the required channel access time  $t_{ij}$  is smaller than the

---

**Algorithm 1** The DTS algorithm
 

---

```

1: procedure DTS(request from link  $i \rightarrow j$ )
2:   reason.code = FAIL
3:   while reason.code == FAIL &&  $K \neq \phi$  do
4:      $\kappa \leftarrow \text{rand}(K)$ 
5:      $\Lambda_\kappa(m) \leftarrow [e_{t_1 r_1}, e_{t_2 r_2}, \dots, e_{t_m r_m}]$ 
6:     for all  $x \in m$  do
7:       if  $\nu_j(i) \cap \nu_j(t_x) \neq \phi$  &&  $\nu_{t_x}(j) \cap \nu_{t_x}(r_x) \neq \phi$  then
8:          $\text{LinkCoexitFlag} \leftarrow \text{FAIL}$ 
9:       end if
10:      if  $\nu_{r_x}(t_x) \cap \nu_{r_x}(i) \neq \phi$  &&  $\nu_i(j) \cap \nu_i(r_x) \neq \phi$  then
11:         $\text{LinkCoexitFlag} \leftarrow \text{FAIL}$ 
12:      end if
13:    end for
14:    if  $\text{LinkCoexitFlag} \neq \text{FAIL}$  then
15:      if  $t_{ij} - L_{CTA_\kappa} < SF_{\text{remainder}}$  then
16:         $\Lambda_\kappa(m+1) \leftarrow \Lambda_\kappa(m) \cup l_{ij}$ 
17:         $m \leftarrow m + 1$ 
18:         $L_{CTA_\kappa} \leftarrow \max(t_{t_x r_x})$ 
19:        reason.code = SUCCESS
20:      end if
21:    end if
22:    if reason.code = FAIL then
23:       $K \leftarrow K \cap \bar{\kappa}$ 
24:    end if
25:  end while
26:  if reason.code = FAIL &&  $t_{ij} \leq SF_{\text{remainder}}$  then
27:    reason.code = SUCCESS
28:  end if
29: end procedure

```

---

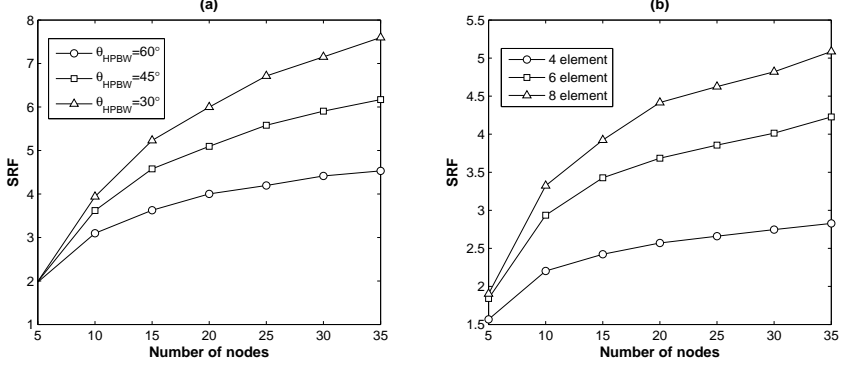


**Figure 3.6:** Relationship among SRF, antenna beamwidth and the number of nodes using flat-topped antenna system and UCA antenna system, with  $\varphi_{th} = 12$  dB.

current CTA duration  $L_{CTA_\kappa}$ , the channel access request is accepted and the PNC arranges link  $l_{ij}$  in this CTA. If  $t_{ij}$  is bigger than  $L_{CTA_\kappa}$  but  $t_{ij} - L_{CTA_\kappa}$  is smaller than the superframe remainder, the request is also accepted by the PNC and the length of this CTA block  $L_{CTA_\kappa}$  adapts to the length of  $t_{ij}$  and  $\Lambda_x(m+1) = \Lambda_\kappa(m) \cup l_{ij}$ . Otherwise, link  $l_{ij}$  cannot be arranged in this CTA. If link  $l_{ij}$  cannot be arranged in any already allocated CTA blocks, the PNC schedules a new CTA block for  $l_{ij}$  on condition that there is sufficient channel resource. The algorithm pseudo code is shown in Algorithm 1.

### 3.5.4 Spatial Reuse Capability

Using the DTS algorithm, multiple transmissions can be admitted by the PNC for simultaneous communication. A Spatial Reuse Factor (SRF) is defined to evaluate the spatial reuse capability of a wireless system. SRF represents the maximum number of simultaneously scheduled links in a piconet. The piconet capacity is directly influenced by the SRF. A higher piconet capacity can be achieved with a higher SRF value. A simulation model is designed in Matlab to investigate the performance of the spatial reuse capability using different directional antennas. A circular network is deployed in the simulation. The network diameter is the same as the maximum achievable transmission range using direction antennas. Therefore, the devices form a full-mesh network. The number of devices varies from 5 to 35. Links are scheduled according to the LCT. During the simulation, it is assumed that there are  $M$  transmission pairs coexisting with each other. To guarantee a required transmission performance, the SINR for a transmission pair  $(t_i, r_i), \forall i \in [1, M]$  should be higher than a certain threshold as defined in (2.6).

To provide an upper bound for the SRF, it is assumed that each device is equipped with an idealized flat-topped pattern antenna without considering the side lobes. The relationship among SRF, antenna beamwidth and the number

of nodes in the piconet is shown in Figure 3.6 (a), which reveals that the SRF increases with the number of nodes but decreases with the antenna beamwidth. Each value is obtained by averaging 1000 iterations. To demonstrate the realistic situation, the UCA system is also used to measure the SRF value. The performance of UCA system is shown in Figure 3.6 (b). Compared to Figure 3.6 (a), the SRF achieved using the UCA system is lower than the SRF obtained using the flat-topped antenna system, which is due to the side lobe effect.

### 3.6 QoS and Fairness Considerations in Resource Allocation

Due to the diversity of the emerging multimedia applications, e.g. high definition video streaming, fast data transfer, on-line gaming, etc., it is necessary for the 60 GHz WPANs to support multi-class traffics with different QoS constraints. Two kinds of traffic are specified in the IEEE 802.15.3 standard: asynchronous traffic and isochronous traffic. The medium access mechanism for CTAP is TDMA based. Therefore, the basic QoS requirements for the isochronous traffic can be warranted by limiting the delay and reducing jitter of a continuous data stream. According to the different QoS requirements, e.g. end-to-end delay, packet loss ratio, etc., the isochronous traffic can be further categorized into different QoS classes. However, multi-class traffic supporting is an open issue in the IEEE 802.15.3 standard. The standard defines that once an isochronous stream is created, it is only terminated when the source or destination device sends the stream termination request to the PNC. If the channel resource is not sufficient, high priority traffic might wait until the preoccupied channel resource is released from low priority traffic. To overcome this problem, a dynamic resource allocation scheme is proposed in this section, which can differentiate the multi-class traffic with fairness consideration. Before explaining the concepts of QoS provisioning and fairness, a number of notations used in the following content is introduced first. For a certain isochronous traffic flow  $i$ , its *service profile* is defined as  $\tau_i = [\xi_i, T_{deadline,i}, T_{backlogged,i}]$ , where,

- $\xi_i$  is the QoS class index, which represents the *service priority* of a traffic flow. Service differentiation is indicated by the value of  $\xi_i$ , which is preassigned at application layer and  $\xi_i \in [1, m_s]$ . Parameter  $m_s$  is the total number of the supported service types. A higher value of  $\xi_i$  indicates a more stringent requirement of QoS. In this work,  $m_s$  is set to 8.
- $T_{deadline,i}$  is the associated delivery deadline time for traffic flow  $i$ . For the isochronous traffic, the data frames should be delivered to the destination before the deadline time. Otherwise, they are dropped, which results in a poor quality of the user experience, e.g. the discontinuity of video streams.
- $T_{backlogged,i}$  is the backlogged time of flow  $i$ , which characterizes the traffic queuing delay. It is defined that  $T_{backlogged,i} = N_{refuse,i} \times \overline{L_{sf}}$ , where,

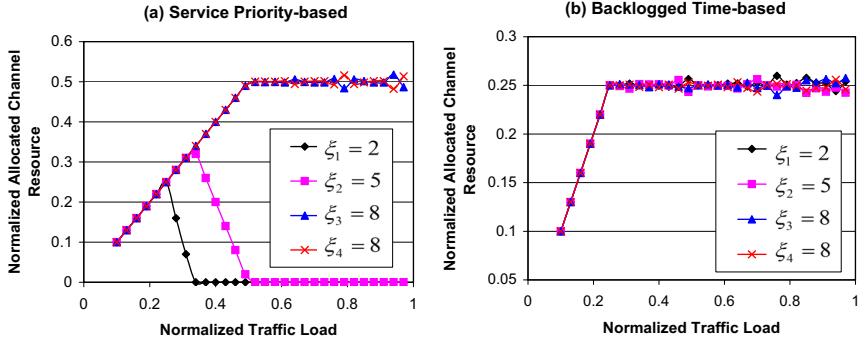


**Figure 3.7:** The comparison between pure service priority based and backlogged time based scheduling algorithms

$N_{refuse,i}$  is the number of times that the channel access request is rejected by the PNC in a row, and  $\overline{L_{sf}}$  is the average superframe length. Because a real-time data frame should be delivered before its deadline time,  $T_{backlogged,i}$  is always smaller than  $T_{deadline,i}$ .

In the resource management domain, fairness refers to the ability of a network to provide equal channel resources to all the users and avoid a certain selfish user occupying the channel exclusively. However, equal resource sharing is unfair for the users with different QoS classes and requirements. Hence, fairness should be warranted based on the QoS criteria. Figure 3.7 illustrates the performance of channel resource allocation using a pure service priority based scheduling algorithm (Figure 3.7.a) and a pure fairness-guaranteed algorithm (Figure 3.7.b). Four traffic flows with different service priorities are considered. In Figure 3.7, the x-axis represents the normalized traffic load for each flow, which is equal for all the flows. The normalized traffic means that the traffic load for each flow is normalized to the total traffic that can be handled by the radio channel. Using the pure service priority based scheduling algorithm, the channel access requests are sorted based on service priority  $\xi$ . A traffic flow with a higher  $\xi$  always has a higher scheduling priority. Using the pure fairness-guaranteed algorithm, the channel access requests are sorted based on the traffic backlogged time of each flow. A traffic flow with longer waiting time has a higher priority for scheduling. Figure 3.7.a indicates that the resource differentiation is the main aim for the service priority based scheduling algorithm, but fairness cannot be guaranteed. Figure 3.7.b shows that the fair resource allocation is the main aim, but different services cannot be distinguished from each other.

A well designed scheduling algorithm is expected to make dynamic decisions according to the network and service properties, which cannot be decided based on a single factor. To take both QoS and fairness into the same scheme, for a

certain traffic flow  $i$ , its normalized *scheduling priority factor* is defined as,

$$\chi_i = \frac{\xi_i}{N_S} \sigma + \frac{T_{backlogged,i}}{T_{deadline,i}} (1 - \sigma). \quad (3.5)$$

Here,  $\sigma$  is a constant value within the range of  $[0, 1]$ , which is a predefined value used to adjust the importance between the service priority and the queuing state.  $\chi_i$  is within the range of  $[0, 1]$ . The closer the value of  $\chi_i$  to 1, the higher the scheduling priority is. In this way, the scheduling priority can be dynamically calculated based on the service priority and the weighted queuing delay. When the traffic load is heavy, the system does not simply sacrifice the QoS of low priority services to guarantee high priority services. It balances the entire QoS requirements for heterogeneous services.

During the resource reservation period, the PNC receives a batch of channel access requests from the devices. After sorting the requests according to the scheduling priority factor  $\chi_i$ , the PNC could use different transmission scheduling algorithm to allocate channel resource. The proposed scheduling priority assignment mechanism is combined with FCFS, which is denoted as QoS-aware and Fair FCFS Transmission Scheduling (QFTS). The scheduling priority assignment mechanism is combined with the DTS algorithm, which is denoted as QoS-aware and Fair Directional Transmission Scheduling (QFDTS).

## 3.7 Simulation in OPNET

The simulation work is deployed in the Optimized Network Engineering Tools (OPNET<sup>TM</sup>) Modeler [56]. OPNET employs a hierarchical structure to model communication networks, which is comprised by network, node and process models. The network model defines the overall simulated system that includes communication links, devices or sub-networks. A device can be mapped into a specific node model that represents its internal protocol structure. The OPNET node model uses an analogous concept of layer-based protocols described by the OSI reference model. In the node model, each layer has a corresponding processor module, and these modules only exchange data with the adjacent layers over packet streams [56]. The enhanced IEEE 802.15.3 MAC layer protocol is implemented in OPNET. The node model constructed in this work is shown in Figure 3.8.

### 3.7.1 Simulation Model

#### MAC Layer

The enhanced IEEE 802.15.3 MAC is implemented as a set of process models and encapsulated in several processors. The main processor is termed as WPAN\_MAC, as shown in Figure 3.8, which includes the IEEE 802.15.3 specified MAC layer protocol and our proposed resource management scheme. The PNC-based re-

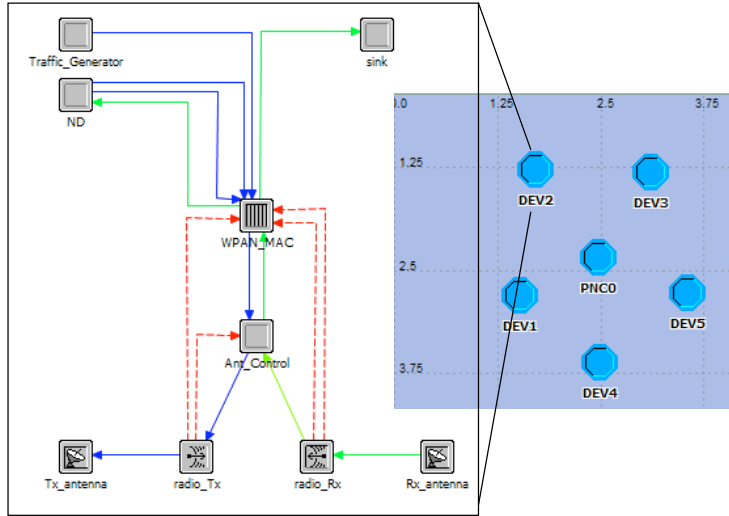


**Figure 3.8:** *WPAN node and network model in OPNET.*

source management module is triggered by receiving the CTRq frames from devices during the MCTA period. The ND processor contains the neighbor discovery protocol, and the ND related packets are only transmitted during the CAP. The Ant\_Control processor is designed to control the antenna mode (omni-directional or directional) and the antenna pointing direction. For the implementation details please refer to Appendix B.

### Higher Layer

The Traffic\_Generator processor produces the raw traffic data which is encapsulated as MAC Service Data Units (MSDU) at the MAC layer. The inter-arrival time of the generated packets satisfies the exponential distribution. The Sink processor is responsible to deal with the arrival packets from the MAC layer and record the collected statistics. Each transmission pair is associated with an isochronous flow. Therefore, the sources reserve the time from CTAP for transmissions.

### 60 GHz based PHY Layer

In OPNET, the PHY layer is modeled by the Radio Transceiver Pipeline stages. Each pipeline stage specifies a certain wireless channel characteristics, e.g. transmission delay, antenna gain, propagation delay, etc. A link budget is created for each packet arriving at the receiver. In order to simulate mmWave-based WPANs, a realistic 60 GHz PHY model is constructed in our simulation. The 60 GHz featured PHY layer is specified through *antenna pattern* and *modulation*



**Table 3.2:** *Parameter specifications used in the simulation*

Parameters	Value
Beacon frame	832 bits
MSDU length	1024 byte
Imm_ACK frame	80 bits
SIFS	0.2 $\mu$ s
BIFS	1.5 $\mu$ s
RIFS	1.8 $\mu$ s
Slot time	1.4 $\mu$ s
Guard band	0.1 $\mu$ s
CAP Duration	1 ms
MCTA Duration	0.15 ms
Max superframe duration	65535 $\mu$ s
Min superframe duration	2000 $\mu$ s
High data rate	1 Gbps
Low data rate	0.3 Gbps
Carrier frequency	60 GHz
The maximum transmission power	10 mW
Queue size	Infinite
Retransmission limit	3
Proportion factor $\sigma$	0.5

*curve.*

OPNET supplies an antenna pattern editor to customize the user-defined antenna patterns. The antenna module specifies the properties of antennas that are used by radio transmitters or receivers. The antenna system has unique significance to influence transmission and reception by means of antenna gain pattern and the main lobe pointing direction. The antenna used in this work is a flat-topped directional antenna. More sophistic antenna models could be tested in the future research. The main lobe of the directional antenna is 13 dBi and the antenna beamwidth is 30°.

OPNET uses modulation curves to specify the modulation and coding scheme. These curves plot the Bit Error Rate (BER) of a signal as a function of the effective SNR. The modulation curve could be edited by a modulation curve editor. An Orthogonal Frequency Division Multiplexing-Quadrature Phase Shift Keying (OFDM-QPSK) scheme proposed in [57] is adopted in this work at the PHY layer. The channel model is based on the free-space radio propagation model. The link budget of the channel model is introduced in 2.3.2.

### 3.7.2 Simulation Results

Simulation is carried out to evaluate the performance of the proposed schemes and the results are presented in this section. The related parameter specifications are listed in Table 3.2.

#### Performance of the DTS Algorithm

In this simulation, six devices are randomly deployed in the piconet and the network topology is shown in Figure 3.8. Device 0 is assigned as the PNC. There are three transmission pairs:  $0 \leftrightarrow 1$ ,  $2 \leftrightarrow 3$ , and  $4 \leftrightarrow 5$ . The devices in the same transmission pair transmit packets with each other. The network throughput and packet end-to-end delay are compared using DTS and FCFS as shown in Figure 3.9. Figure 3.9 (a) depicts that the DTS algorithm dramatically increases the system throughput compared to the FCFS algorithm. The relationship between the packet end-to-end delay and the mean traffic arrival rate is shown in Figure 3.9 (b). Based on Figure 3.9 it can be observed that, when the traffic load is lower than 0.04 million packets/sec, there is no performance difference between DTS and FCFS. Therefore, using FCFS is better than DTS because of its lower algorithm complexity. When the traffic load is within the range from 0.08 to 0.1 million packets/sec, the two algorithms can still achieve the same throughput, but FCFS leads to a longer delay. The network throughput is saturated when the traffic arrival rate is around 0.1 million packets/sec using FCFS and it is saturated when the traffic arrival rate is around 0.36 million packets/sec using DTS.

Figure 3.9 (c) compares the number of admitted channel access requests between DTS and FCFS. In this simulation, each device randomly picks up a destination and transmits a traffic flow which is generated at 0.16 Gbps. Compared to FCFS, the DTS algorithm exploits the spatial reuse capability from directional antennas, hence it can arrange more admissions in one superframe. The linear increase of the DTS curve is because the current piconet is still not saturated. From the above results it can be seen that, the DTS algorithm dramatically increases the piconet capacity and reduces the packet end-to-end delay using spatial reuse TDMA.

#### Performance of the DTS with QoS and Fairness Consideration

To model the performance of the DTS algorithm with QoS and fairness consideration, some additional assumptions are considered:

- *Piconet topology*: The network configuration is based on a single piconet including a PNC and a number of slave devices. The PNC selection policy is out of the field of this work. Therefore, in each simulation a device is predefined as the PNC. The piconet size is  $10\text{m} \times 10\text{m}$ . Six devices are randomly placed in the network. All the devices are within the transmission range of each other.

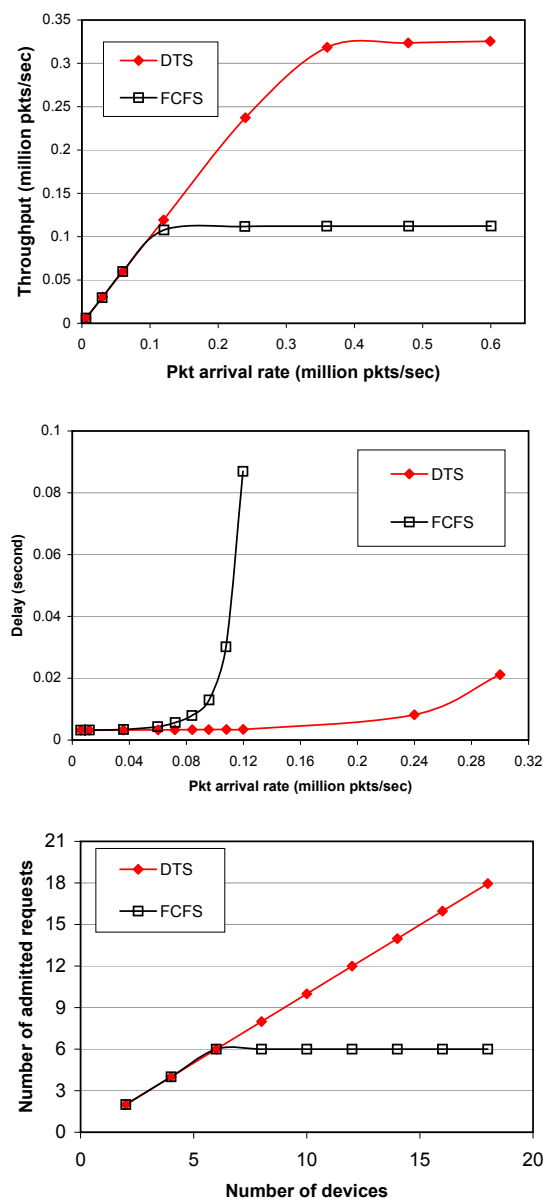


Figure 3.9: Throughput and delay comparison between FCFS and DTS

**Table 3.3:** Traffic flow's service priority and deadline time

Link	Service Priority	Deadline(ms)
0 $\rightarrow$ 1	2	1000
1 $\rightarrow$ 0	5	100
2 $\rightarrow$ 3	8	40
3 $\rightarrow$ 2	5	100
4 $\rightarrow$ 5	8	40
5 $\rightarrow$ 4	2	1000

- *Superframe length:* Superframe length is adapted according to the traffic load but within a range of  $[L_{sfmin}, L_{sfmax}]$ , where  $L_{sfmin}$  and  $L_{sfmax}$  are the minimum and maximum supported superframe durations. For traffic flow  $i$ , the maximum required channel access time  $T_{reqmax,i}$  is limited by  $T_{reqmax,i} \leq \frac{\lambda_i}{R} L_{sfmax}$ , where  $\lambda_i$  is the traffic load on flow  $i$ ,  $R$  is the achievable transmission data rate of the radio channel.
- *Traffic load:* In each simulation all the traffic flows have the same traffic load. Different traffic flows have different service priorities and associated deadline times, which are specified in Table 3.3.

To compare the fairness characteristics of different scheduling algorithms, a fairness factor is defined based on the weighted traffic backlogged time:

$$f(k) = \frac{\left(\sum_{i=1}^N k_i\right)^2}{N \sum_{i=1}^N (k_i)^2}, \quad (3.6)$$

where  $k_i = \frac{T_{backlogged,i}}{T_{deadline,i}}$ .  $N$  is the number of scheduled transmissions in one superframe. It is defined that  $\frac{0}{0} = 1$  to avoid the situation when the channel resource is sufficient and all the channel access request can be admitted.  $f(k)$  is within the range from 0 to 1. If the channel resource is fairly scheduled by the PNC, the value of  $f(k)$  approaches 1. As shown in Figure 3.10 (a), QFTS is more fair than FCFS. Especially when the traffic load becomes higher, the improvement of the fairness is bigger. The similar results are also observed from Figure 3.10 (b) and (c), in which, QFDTS performs better than DTS.

Job Failure Ratio (JFR) is a metric used to characterize the dropped packets due to reaching the delivery deadline time. The relation between JFR and the traffic load is shown in Figure 3.11. In general, JFR is monotonously increased with the increase of the traffic load. In Figure 3.11 (a), QFTS always has a lower JFR than FCFS. For the DTS-based algorithms, the situation is more complex. When the antenna beamwidth is  $30^\circ$ , as shown in Figure 3.11 (c), QFDTS exhibits better performance than DTS for all the traffic loads. When the antenna beamwidth is  $60^\circ$ , as shown in Figure 3.11 (b), QFDTS performs better when the

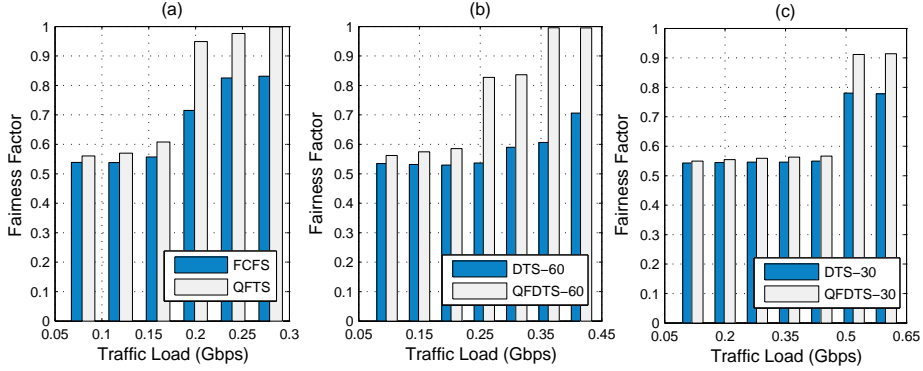


Figure 3.10: Fairness Comparison

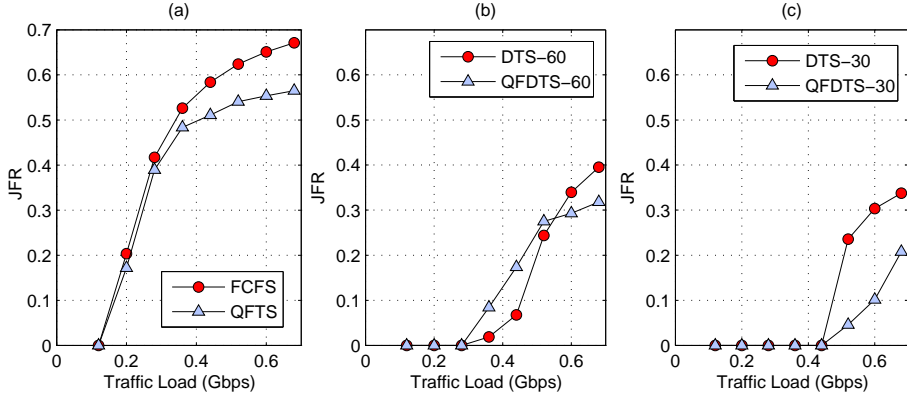
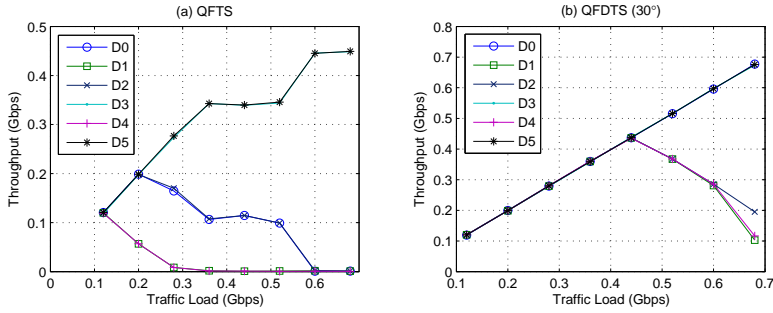


Figure 3.11: JFR Comparison

traffic load is higher than 0.55 Gbps. That is because for DTS, its performance is related to the geographical deployment of the devices, e.g. spreading equally in the network or congesting together. When the antenna beamwidth becomes wider, the spatial reuse capability becomes worse. If some high priority traffic flows are preassigned in certain CTA blocks, the amount of scheduled concurrent links could be lower than the random assignment without considering the priority. Therefore, when directional antennas are used in the network, our proposed resource allocation scheme works better when the antenna beamwidth is narrow.

In Figure 3.12, it provides the comparison between QFTS and QFDTS about the throughput of each traffic flow. This figure indicates that, both QFTS and QFDTS can differentiate the resource allocation for the multi-class traffic flows. Compared to QFTS, QFDTS achieves much higher throughput by exploiting the



**Figure 3.12:** *Throughput Comparison*

spatial reuse capability from adaptive antenna array systems.

## 3.8 Chapter Summary

To adopt the IEEE 802.15.3 MAC for 60 GHz WPANs, a number of enhancement proposals are provided in this chapter. The main contributions of this chapter are three-fold. First, a direction information management mechanism was proposed for the devices within a piconet to obtain the orientation profiles of their neighbors. The PNC collects the orientation profiles of the slave devices within its piconet to maintain the entire direction-aware piconet topology, which is used to schedule the concurrent transmissions within its piconet. Second, the resource management scheme has been addressed on top of the IEEE 802.15.3 MAC. The proposed resource management scheme exploits the spatial reuse capability in 60 GHz WPANs using directional antennas. Third, a QoS-aware transmission scheduling algorithm with fairness consideration is devised to support heterogeneous services in WPANs. The IEEE 802.15.3 MAC, resource management scheme, and 60 GHz PHY layer have been implemented in OPNET. Simulation results indicated that a substantial performance improvement, in terms of throughput and delay, is gained using our proposed MAC enhancement mechanism.

# Chapter 4

## Enabling High Performance Transmission in 60 GHz WPANs using Frame Aggregation

“Give people a little bit more bandwidth and they’ll find something for which that bandwidth is not nearly enough.”

- Paul Green

*To achieve ultra high rate communication in WPANs using 60 GHz radio, the frame aggregation is devised in IEEE 802.15.3c to increase the MAC transmission efficiency. In this chapter, a novel statistical model is proposed to analyze the behavior of two types of frame aggregation mechanisms: standard frame aggregation and low latency frame aggregation. Through our proposed model, the performance of the frame aggregation mechanisms can be fully understood in terms of the transmission delay and system capacity. The accuracy of the proposed analytical model is validated by extensive simulation studies. This chapter provides helpful insights into using 60 GHz radio to achieve ultra high performance transmission.*

## 4.1 Introduction

At the MAC layer, the traffic from upper layers is fragmented into MAC Service Data Units (MSDUs) for transmission. Automatic repeat request (ARQ) protocols use retransmission mechanism to increase transmission reliability in error-prone wireless channel. There are three retransmission mechanisms defined in the IEEE 802.15.3 MAC: No Acknowledgment (no-ACK), Immediate Acknowledgment (Imm-ACK) and Delayed Acknowledgment (Dly-ACK). The transmitted frames with no-ACK policy do not need to be acknowledged by the receivers. No-ACK policy shall be used for broadcasting and multicasting frames. When using Imm-ACK policy, each transmitted frame shall be acknowledged by the receiver with an ACK frame. Using Dly-ACK policy, instead of acknowledging each frame, the transmitter sends a burst of frames and the receiver acknowledges them together with a Dly-ACK frame. Dly-ACK shall be used for stream data frames, for instance, isochronous connections.

As specified in the IEEE 802.15.3 standard, multiple data rates are supported at the PHY layer. To increase the receiving reliability, the packet preamble and headers are transmitted using basic data rate and the data payloads are transmitted using high data rate [3]. When the Gbps-based ultra high speed modulation scheme is considered, the proportion of the channel access time used to transmit data payload is severely impacted. The MAC transmission efficiency can be defined as the effective channel time used to transmit data frames. While using typical settings for 60 GHz system, the MAC efficiency for Imm-ACK using 512 bytes payload is only around 12.7%, which will be explained in this chapter. It is far below the requirement to support high performance transmissions. Although Dly-ACK mechanism could moderately improve the MAC efficiency [58], the overhead induced by packet preamble and header still cannot be avoided. To further reduce the impact of packet overhead, the frame aggregation is devised in the IEEE 802.15.3c MAC to improve data transmission efficiency. There are two concerned aggregation mechanisms in IEEE 802.15.3c: *standard frame aggregation* and *low latency frame aggregation*. With using standard frame aggregation, several subframes are grouped together and encapsulated by one PHY and MAC header for transmission. Although standard frame aggregation could significantly improve the transmission efficiency, it degrades the transmission delay due to the aggregation process, especially when the traffic load is low. To guarantee the performance of delay-constraint applications, the low latency frame aggregation mechanism is devised to resolve this problem [59].

In this chapter, a statistical model is proposed to evaluate these two aggregation mechanisms. By means of our proposed model, it is able to provide explicit expressions for the aggregation process used in IEEE 802.15.3c. Our work is useful to understand the transmission delay and capacity properties of the standard and low latency frame aggregation. The accuracy of the proposed analytical model is validated by extensive simulation studies.



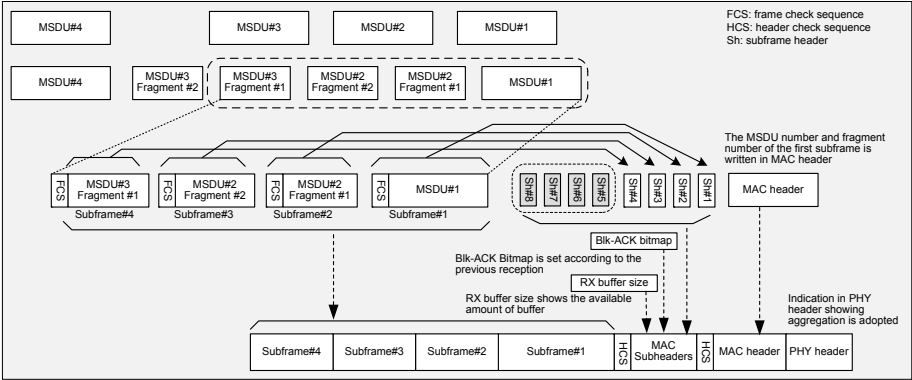


**Figure 4.1:** *Standard frame aggregation illustration at the transmitter side [7].*

## 4.2 Frame Aggregation in IEEE 802.15.3c

To support high-speed data streaming or low latency bidirectional data transmissions, two frame aggregation mechanisms are designed in IEEE 802.15.3c: standard frame aggregation and low latency frame aggregation.

### Standard Frame Aggregation

The standard frame aggregation procedure at the transmitter side is illustrated in Figure 4.1. The transmitter maps a MSDU into a subframe payload once it receives it from the Frame Convergence SubLayer (FCSL). If a MSDU exceeds the predetermined subframe length, the MSDUs are fragmented and mapped into multiple subframes. MSDUs are distinguished from each other using their unique MSDU numbers. Several subframes are grouped together as an aggregated frame. If the aggregation mechanism is adopted for transmission, it is indicated in the PHY header. A subheader is created for each subframe, which contains the necessary information to assist the receiver to retrieve the original data. The number of aggregated subframes is predefined. If a subframe is not used in the current frame, the subframe length field is set to zero. All the subheaders are combined together and form the MAC subheader. To avoid buffer overflow, the transmitter and the receiver inform each other the available buffer size. This information is helpful for the transmitter to adjust the subframe number and the length.

Instead of transmitting a MSDU frame and responding with an Imm-ACK frame, the transmitter transmits an aggregated frame. Once the receiver receives an aggregated frame, it validates each subframe by checking the associated Frame Check Sequence (FCS). Based on the received status of each subframe, it responds to the transmitter with a Block ACK (Blk-ACK), in which a bitmap field in the MAC subheader of Blk-ACK is used to indicate the subframes that are not

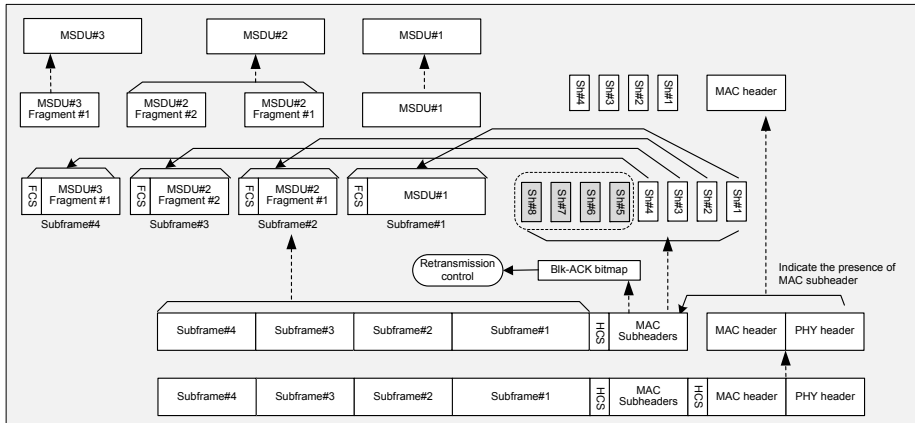


**Figure 4.2:** *Frame de-aggregation illustration at the receiver side [7].*

received correctly. After receiving a Blk-ACK, the transmitter retransmits them in the next aggregated frame. The de-aggregation process at the receiver side is shown in Figure 4.2.

### Low Latency Frame Aggregation

For the standard frame aggregation mechanism, multiple subframes are aggregated into a single frame. An aggregated frame is transmitted only when it already contains sufficient number of subframes. Therefore, this mechanism involves extra waiting delay to produce an aggregated frame, especially when the traffic load is low. The low latency aggregation mechanism is proposed to overcome this drawback. It defines that, if the transmitter does not receive enough MSDUs from the FCSL, it just transmits empty subframes with zero length with No-ACK policy until the arrival of an MSDU or the expiration of the pre-defined CTA duration timer. In this way, the radio link between the transmitter and receiver is kept alive, and the transmission delay for a certain sub-frame is reduced.

## 4.3 Analytical Model

In this section, the analytical model is presented for Imm-ACK, standard frame aggregation with Blk-ACK and low latency frame aggregation with Blk-ACK in detail. Let  $\kappa$  denote a Modulation and Coding Scheme (MCS) at PHY layer. For a memoryless channel, it can be assumed that bit errors are not correlated and they are uniformly distributed within a packet. Under this assumption, the resultant Packet Error Rate (PER) for a packet with length  $l$  (in bits) is given as  $P_e^\kappa(l) = 1 - (1 - e_\kappa)^l$ , where  $e_\kappa$  is the BER using MCS  $\kappa$ .

### 4.3.1 Imm-ACK

To increase the transmission reliability, packet preamble, header and ACKs are transmitted using basic/low rate MCS  $\kappa_l$  and data frames are transmitted using high rate MCS  $\kappa_h$ . With using Imm-ACK policy, the probability for a successful transmission of a data frame with length  $l$  bits is expressed as,

$$P_{succ}(l) = \left(1 - P_{e,data}^{\kappa_h}(l)\right) \left(1 - P_{e,o}^{\kappa_l}(l_h + l_{ack})\right), \quad (4.1)$$

where,  $l_h$  refers to the length for packet preamble and header, and  $l_{ack}$  is the length for an ACK frame.  $P_{e,data}^{\kappa_h}(l)$  denotes the probability of transmission error for data frames, and  $P_{e,o}^{\kappa_l}(l_h + l_{ack})$  is the probability of transmission error for packet header or ACK. Consequently, the average life time for a data frame existing in the system is calculated as:

$$\begin{aligned} \bar{\tau} = & \sum_{i=0}^{n_r} P_{succ}(l)(1 - P_{succ}(l))^i (i \times t_{fail} + t_{succ}) \\ & + (1 - P_{succ}(l))^{n_r+1} (n_r + 1) t_{fail}, \end{aligned} \quad (4.2)$$

where,  $n_r$  is the retransmission limit,  $t_{succ}$  and  $t_{fail}$  are the time duration for a successful transmission and a failed transmission, respectively, which are given as:

$$\begin{aligned} t_{succ} &= t_p + \frac{l_h + l_{ack}}{R_l} + \frac{l}{R_h} + 2t_{SIFS} \\ t_{fail} &= t_p + \frac{l_h}{R_l} + \frac{l}{R_h} + t_{RIFS}, \end{aligned} \quad (4.3)$$

where,  $t_p$  is the packet preamble duration,  $R_h$  is the high data rate,  $R_l$  is the low/basic data rate.  $t_{SIFS}$  and  $t_{RIFS}$  are the Short Inter-Frame Space (SIFS) length and Retransmission Inter-Frame Space (RIFS) length, respectively. The maximum life time of a frame is  $\bar{\tau}_{max} = (n_r + 1) \times t_{fail}$ , which represents the situation that the frame is dropped due to the retransmission limit.  $\bar{\tau}$  could be considered as the transmission delay, especially when the channel quality is good.

Denote the proportion of the CTAP within one superframe as  $\rho$ , where  $\rho = T_{CTAP}/T_{SF}$ ,  $T_{CTAP}$  is the time duration of one CTAP, and  $T_{CTAP} = T_{SF} - T_B - T_{CAP}$ , where  $T_{SF}$  is the superframe duration,  $T_{CAP}$  is the CAP duration, and  $T_B$  is the transmission time of a beacon packet. The maximum achievable throughput  $C_{Imm}$  within CTAPs can be approximated as,

$$C_{Imm} = \frac{\rho l}{\bar{\tau}} \left(1 - (1 - P_{succ}(l))^{n_r+1}\right). \quad (4.4)$$

### 4.3.2 Standard Frame Aggregation with Blk-ACK

#### Throughput Modeling

Using standard frame aggregation, several subframes are aggregated together and encapsulated within one PHY and MAC header. Additionally, an aggregated frame also has MAC subheaders which are used to specify the information of each subframe. During the transmission process, if the packet headers or the Blk-ACK is not received correctly, the entire aggregated frame has to be retransmitted. On the condition that an aggregated frame is received correctly but a number of subframes within the aggregated frame are damaged, the incorrectly received subframes are retransmitted in the next aggregated frame. Let  $l_{blk-ack}$  and  $l_{ah}$  be the Blk-ACK frame length and the packet header length for an aggregated frame, and  $l_{ah} = l_h + l_{sub-h}n_{blk}$ , where,  $l_{sub-h}$  is the length of the subframe header, and  $n_{blk}$  is the number of grouped subframes in one aggregated frame. Let  $P_{e,o}^{\kappa_l}(l_o)$  denote the probability that transmission error happens at the packet header of an aggregated frame or Blk-ACK, where  $l_o = l_{ah} + l_{blk-ack}$ . Therefore, the average life time of an aggregated frame could be derived as,

$$\begin{aligned} \bar{\tau}_a = & \sum_{i=0}^{n_r} (1 - P_{e,o}^{\kappa_l}(l_o)) P_{e,o}^{\kappa_l}(l_o)^i (i \times t'_{fail} + t'_{succ}) \\ & + P_{e,o}^{\kappa_l}(l_o)^{n_r+1} (n_r + 1) t'_{fail}, \end{aligned} \quad (4.5)$$

where

$$\begin{aligned} t'_{succ} &= t_p + \frac{l_{ah} + l_{blk-ack}}{R_l} + \frac{ln_{blk}}{R_h} + 2t_{SIFS} \\ t'_{fail} &= t_p + \frac{l_{ah}}{R_l} + \frac{ln_{blk}}{R_h} + t_{RIFS}. \end{aligned} \quad (4.6)$$

Let  $\overline{n_{agg}}$  be the average number of transmissions to transmit an aggregated frame, and  $\overline{n_{agg}}$  is obtained as,

$$\begin{aligned} \overline{n_{agg}} = & \sum_{i=0}^{n_r} \left( 1 - P_{e,o}^{\kappa_l}(l_o) \right) P_{e,o}^{\kappa_l}(l_o)^i (i + 1) \\ & + P_{e,o}^{\kappa_l}(l_o)^{n_r+1} (n_r + 1). \end{aligned} \quad (4.7)$$

If an aggregated frame is incorrectly received, the retransmission counter for each subframe in the aggregated frame is increased by one. Therefore,  $\overline{n_{agg}}$  is subject to  $\overline{n_{agg}} \leq n_r + 1$ . On the condition that an aggregated frame is correctly received, for a certain subframe in the aggregated frame, it has a PER of  $P_{e,sub}^{\kappa_h}(l_{sub})$ , where  $l_{sub}$  is the packet length for a subframe. For simplicity,  $l_{sub}$  is assumed to be a fixed value. The maximum achievable throughput  $C_{agg}$  using standard frame

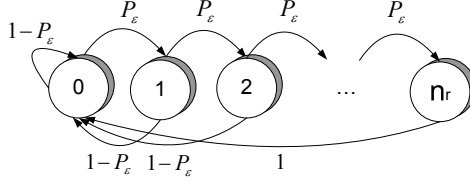


**Figure 4.3:** Markov chain model for the retransmission process.

aggregation can be expressed as,

$$C_{agg} = \frac{\rho n_{blk} l_{sub}}{\bar{\tau}_a} \left( 1 - P_{e,o}^{\kappa_l} (l_o)^{n_r+1} \right) \left( 1 - P_{e,sub}^{\kappa_h} (l_{sub}) \right). \quad (4.8)$$

### Delay Modeling

The aggregated frame structure influences the transmission delay from two aspects: aggregation delay and delivery delay. An aggregated frame is produced only if there are at least  $n_{blk}$  subframes in the buffer. If the number of subframes in the buffer is smaller than  $n_{blk}$ , the transmitter has to wait until there are sufficient subframes to make an aggregated frame. Hence, extra delay may be involved within the aggregation process, which is also called as aggregation delay. This aspect will be discussed together with the low latency aggregation mechanism in the next section. In this section, the traffic load is assumed to be saturated, which means that there are always enough number of subframes in the buffer of the transmitter.

For the subframes that are damaged during the transmission of an aggregated frame, they are retransmitted in the next aggregated frame until they reach the retransmission limit. To identify different MSDUs, each MSDU is assigned a unique MSDU sequence number. Subframes are aggregated according to their associated MSDU sequence numbers. To reduce transmission delay, a subframe with a lower MSDU sequence number should always be put in front of a subframe with a higher MSDU sequence number. Therefore, the retransmitted subframes should be in front of the newly arrived subframes. The retransmission process  $s(t)$  can be modeled as a one-dimensional Discrete-Time Markov Chain. Its state transition graph is shown in Figure 4.3, which describes the retransmission circumstance of a subframe with the influence of its transmission failure ratio  $P_e$ , where

$$P_e = (1 - P_{e,o}^{\kappa_l} (l_o)) P_{e,sub}^{\kappa_h} (l_{sub}) + P_{e,o}^{\kappa_l} (l_o). \quad (4.9)$$

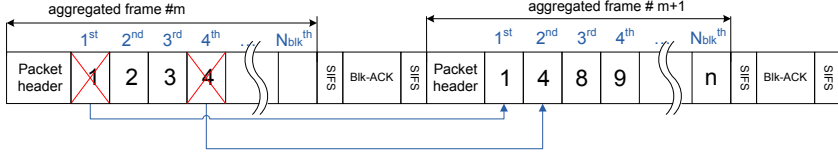


**Figure 4.4:** *Subframe retransmission illustration.*

The transition probability matrix  $\mathbf{P}$  is given as

$$\mathbf{P}_{ij} = \begin{cases} P_e & \text{if } j = i + 1 \text{ and } i \neq n_r, \\ 1 - P_e & \text{if } j = 1 \text{ and } i \neq n_r, \\ 1 & \text{if } j = 1 \text{ and } i = n_r, \\ 0 & \text{otherwise.} \end{cases} \quad (4.10)$$

The steady state vector of this Markov Chain is given as  $\pi = [\pi_0, \pi_1, \dots, \pi_{n_r}]$ . It follows that  $\pi_j = \sum_{i=1}^{n_r+1} \mathbf{P}_{ij} \pi_j$  and  $1 = \sum_{i=1}^{n_r+1} \pi_i$ . If a subframe is transmitted within one aggregated frame, the probability that it leaves system in the next aggregated frame due to successful transmission or reaching the retransmission limit is denoted as  $P_v$ , and the probability that it is still required to be transmitted in the next aggregated frame is denoted as  $P_o$ , where

$$\begin{aligned} P_v &= \pi_0 \\ P_o &= 1 - P_v. \end{aligned} \quad (4.11)$$

For a subframe, its position in an aggregated frame could be different for each retransmission, hence the transmission delay involved by each retransmission could vary from time to time. For instance as shown in Figure 4.4, Subframe 1 and 4 in the  $m^{th}$  aggregated frame are not correctly received and they are retransmitted in the next aggregated frame. For Subframe 4, its position in the next aggregated frame is decided by the status of its previous subframes. For instance, if Subframe 2 and 3 are received correctly or dropped due to the retransmission limit, their positions are vacant in the next aggregated frame. Therefore, Subframe 4 is retransmitted at the second position. To model the subframe transmission delay, a two-dimensional Discrete-Time Markov Chain model with two stochastic processes  $\{s(t), b(t)\}$  is proposed here, where  $s(t)$  is the retransmission process, and  $b(t)$  represents the index of the position of a subframe in an aggregated frame. The two processes  $\{s(t), b(t)\}$  have finite state spaces. For each state  $(m, k)$ ,  $m$  is within the range of  $[0, n_r]$  and  $k$  is within the range of  $[1, n_{blk}]$ . The state transition graph for the two-dimensional Discrete-Time Markov Chain is shown in Figure 4.5. For a certain subframe, when it is encapsulated in an aggregated frame for the first time, it has a probability  $\sigma(x)$  to be put at position  $x$ , which is denoted as  $b(0) = x$  and  $x \in [1, n_{blk}]$ . The probability  $\sigma(x)$  depends on the number

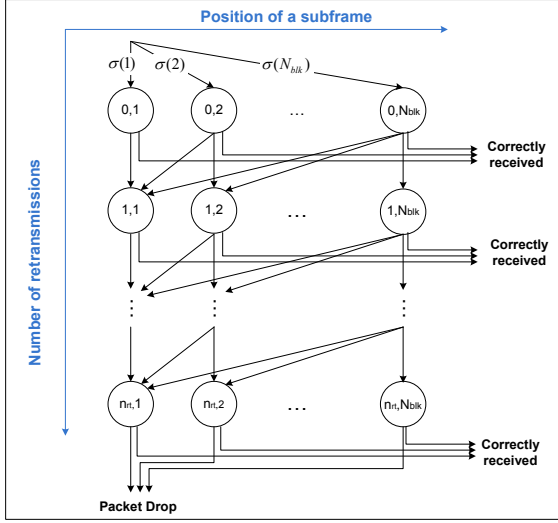


**Figure 4.5:** Two-dimensional discrete-time Markov chain of  $\{s(t), b(t)\}$ .

of retransmitted subframes from the previous aggregated frame, and conversely, the number of retransmitted subframes is smaller than  $x$ . Consequently, it can be obtained that

$$\sigma(x) = \sum_{i=0}^{x-1} \binom{n_{blk}}{i} P_o^i P_v^{n_{blk}-i} \frac{1}{n_{blk} - i}. \quad (4.12)$$

When the channel quality is high,  $\sigma(x)$  is a uniform distribution. When a subframe is incorrectly received at stage  $m$ , it moves to the next stage  $m+1$  on the condition that  $m$  is smaller than  $n_r$ , otherwise, it is dropped. When there is a transition from state  $(m-1, k')$  to state  $(m, k)$ , the value of  $k$  is constrained by  $k \leq k'$ . Therefore, the possible state  $k$  of process  $b(t)$  in the  $m^{th}$  stage is constrained by its initial state  $b(0)$  as  $k \leq b(0)$ . The one-step transition probability for a subframe to be in state  $(m, k)$  is given as

$$\mathbf{P}'_{m,k|b(0)=x} = P_\epsilon \sum_{i=k}^x \mathbf{P}'_{m-1,i} P_o^{k-1} P_v^{i-k} \binom{i-1}{i-k}, \quad (4.13)$$

where,  $k \in [1, b(m-1)]$  and  $m \in [1, n_r]$ . The initial value of one-step transition probability is given as

$$\mathbf{P}'_{0,k|b(0)=x} = \begin{cases} 1 & \text{if } k = x \\ 0 & \text{otherwise} \end{cases}. \quad (4.14)$$

As mentioned before, if the transmission error happens at the packet header of an

aggregated frame or Blk-ACK, the entire aggregated frame should be retransmitted. The factor  $\psi(u, m)$  is denoted as the probability that  $u$  out of  $m$  transmitted aggregated frames are incorrectly received, where

$$\psi(u, m) = \binom{m}{u} P_{e,o}^{\kappa_l}(l_o)^u \left(1 - P_{e,o}^{\kappa_l}(l_o)\right)^{m-u}. \quad (4.15)$$

If a subframe is correctly received at state  $(m, k)$ , its transmission delay is obtained as

$$D(m, k, u) = t'_{fail}u + t'_{succ}(m - u) + \frac{l_o}{R_l} + \frac{kl}{R_h}. \quad (4.16)$$

On condition that the initial position of a subframe is  $x$ , the average transmission delay to correctly receive this subframe is calculated as

$$D|_{b(0)=x} = (1 - P_\epsilon) \sum_{k=1}^x \sum_{m=0}^{n_r} \sum_{u=0}^m \mathbf{P}'_{m,k} \psi(u, m) D(m, k, u). \quad (4.17)$$

Let  $D_{drop}$  be the time duration to drop this subframe due to the retransmission limit, and it is given by

$$\begin{aligned} D_{drop} &= \sum_{i=0}^{n_r+1} \psi(n_r + 1 - i, n_r + 1) P_{e,data}^{\kappa_h}(l)^i \\ &\times \left( t'_{fail} \times (n_r + 1 - i) + t'_{succ} \times i \right). \end{aligned} \quad (4.18)$$

Finally, the average life time of a subframe is derived as

$$\overline{D}_{agg} = \sum_{x=1}^{n_{blk}} \sigma(x) D|_{b(0)=x} + D_{drop}. \quad (4.19)$$

### 4.3.3 Low Latency Frame Aggregation with Blk-ACK

When the traffic load is saturated, there is no difference between standard and low latency frame aggregation. When the traffic load is low, the standard frame aggregation should wait to collect  $n_{blk}$  subframes to generate an aggregated frame. Therefore, the waiting time for the arrival of subframes from the FCSL involves extra transmission delay. The Poisson process is used to model the arrival of MSDUs. Using standard aggregation mode, the aggregation time  $T_{n_{blk}}$  is denoted as the interval from the arrival of the first MSDU to the arrival of the  $n_{blk}^{th}$  MSDU, which is given as  $T_{n_{blk}} = \sum_{k=1}^{n_{blk}-1} \tau_k$ , where  $\tau_i$  is the time interval between the  $i^{th}$  arrived MSDU and the  $(i+1)^{th}$  arrived MSDU. This extra delay should be considered while using standard aggregation mechanism. For low latency aggregation mechanism, if there is no MSDU in the buffer of FCSL, empty subframes are sent out without waiting for the arrival of MSDUs from the upper layers. The



**Table 4.1:** *Parameter specifications in the simulation*

Parameters	Value
MAC subheader length	38 bytes
Beacon frame	832 bits
Imm-ACK frame	25 bytes
Blk-ACK frame	26 bytes
Preamble length	3.26 $\mu$ s
SIFS	2.5 $\mu$ s
CCA	9 $\mu$ s
RIFS	1.8 $\mu$ s
CAP Duration	1 ms
Superframe duration	65.535 ms
Retransmission limit	3
Subframe length	1024 bytes
Number of subframes in one aggregated frame	8

probability to send an empty subframe is denoted as  $P_{empt} = e^{-\lambda\tau}$ , where,  $\lambda$  is the MSDU arrival rate, and  $\tau$  is the time duration to transmit a subframe, which is given as  $\tau = l_{sub}/R_h$ . Therefore, within an aggregated frame, each subframe position has a probability  $P'_v$  to be empty, and has a probability  $P'_o$  to be occupied, which means that the subframe at this position still needs to be retransmitted in the next aggregated frame.  $P'_v$  and  $P'_o$  are derived based on (4.11) as

$$\begin{aligned} P'_v &= P_v(1 - P_{empt}) + P_{empt} \\ P'_o &= P_o(1 - P_{empt}). \end{aligned} \quad (4.20)$$

Therefore, the delay model for the low latency aggregation mechanism can be obtained by substituting (4.20) into (4.12)- (4.19).

## 4.4 Performance Evaluation

### 4.4.1 Simulation Validation

A Matlab based simulator is constructed to validate the accuracy of our analytical model. The 60 GHz featured physical layer is specified in Appendix C. In the following simulation, QPSK is used as the modulation scheme for the transmission of data frames,  $\frac{\pi}{2}$  Binary Phase Shift Keying (BPSK) is used as the basic/low rate modulation scheme. The LOS channel model is adopted. According to Table C.1, the achievable data rates for using  $\frac{\pi}{2}$  BPSK and QPSK are 1.61 Gbps and 3.23 Gbps, respectively. The simulation related parameters are specified in Table 4.1. Each simulation result is the average value of the transmission of  $10^4$

**Table 4.2:** *Frame life time comparison between analytical and simulation results*

SNR (dB)	Analytical(ms)	Simulation(ms)
5.7	0.145	0.145
5.9	0.137	0.138
6.1	0.126	0.128
6.3	0.096	0.094
6.5	0.043	0.061
6.7	0.023	0.022
6.9	0.016	0.017
7.1	0.015	0.015

aggregated frames. Figure 4.6 validates the initial position probability, which is denoted as  $\sigma(x)$  in (4.12), within an aggregated frame in different channel quality scenarios. In Table 4.2, the analytical results are compared with the simulation results in terms of frame life time. The simulation results confirm the accuracy of our analytical model.

#### 4.4.2 Numerical Results

In Figure 4.7, with varied subframe length, the analytical results between non-aggregated mode (with Imm-ACK) and standard aggregation mode (with Blk-ACK) are compared together in terms of saturated system throughput. As shown in this figure, the system throughput has remarkable improvement using the standard aggregation mechanism. When subframe length is 512 bytes, the MAC efficiency of the conventional IEEE 802.15.3 MAC with Imm-ACK only achieves 12.70%. In comparison, the standard aggregation with Blk-ACK mechanism can achieve 52.76%. When the subframe length is 2048 bytes, the MAC efficiency is increased from 36.25% (Imm-ACK) to 80.28% (standard aggregation with Blk-ACK). Therefore, the standard frame aggregation scheme could effectively support isochronous streaming with high bandwidth requirements. Although the standard frame aggregation mechanism increases the transmission efficiency substantially, the aggregated structure involves extra delay for transmissions, which is illustrated in Figure 4.8. Especially when the channel quality becomes worse, a frame requires a longer time to be transmitted using the aggregation mechanism. Therefore, the aggregation mode is not suitable to be used when the channel quality is low.

Figure 4.9 illustrates the influence of the retransmission limit  $n_r$ . When the channel quality is low, the increase of  $n_r$  can help to improve system throughput but at the price of increased transmission delay. Therefore, retransmission mechanism is necessary for capacity-constrained application, e.g. content downloading, but it could be optional for delay-constrained application, like video streaming. In Figure 4.10, the impact of different modulation schemes is illustrated when

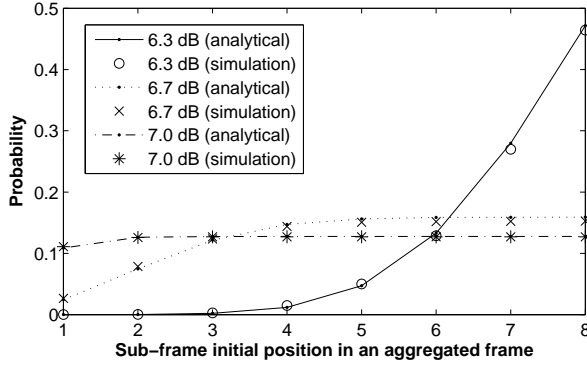


Figure 4.6: Probability of the initial position of a subframe in an aggregated frame.

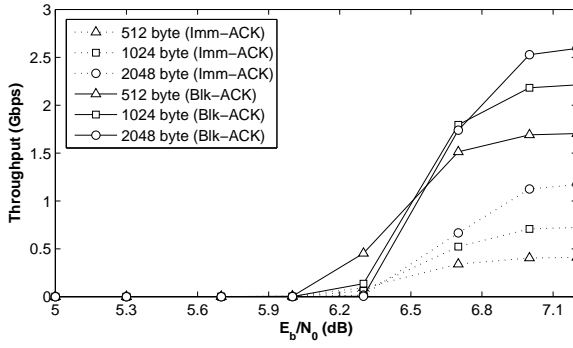


Figure 4.7: Throughput comparison between Imm-ACK and standard aggregation with Blk-ACK.

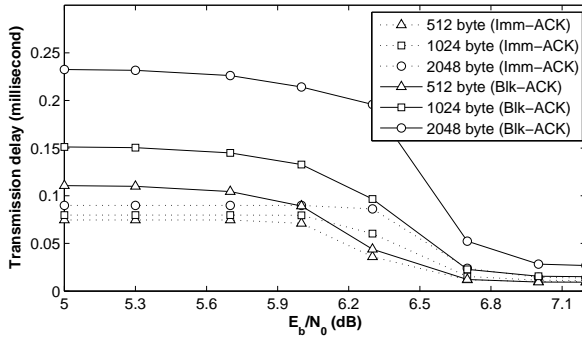
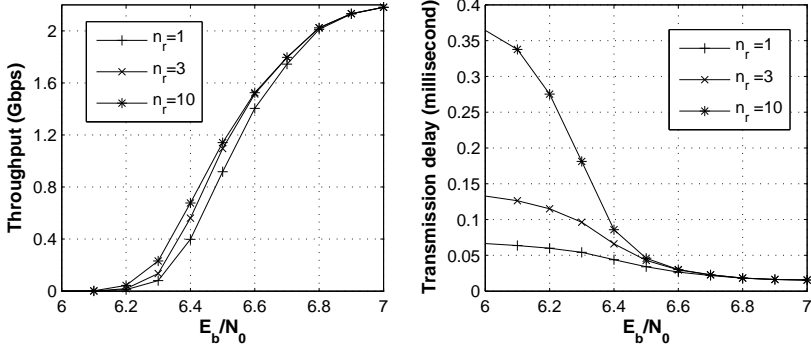
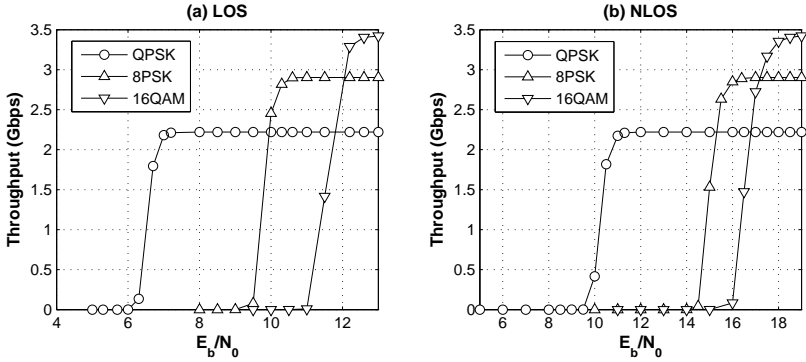


Figure 4.8: Frame life time comparison between Imm-ACK and standard aggregation with Blk-ACK.



**Figure 4.9:** Retransmission times influence, 1024 bytes, QPSK, standard aggregation with *Blk-ACK*.



**Figure 4.10:** Modulation scheme comparison, 1024 bytes, standard aggregation with *Blk-ACK*.

the subframe length is fixed at 1024 bytes. High rate modulation scheme can be used to achieve higher throughput, but they have stringent requirements on the channel quality. Moreover, the throughputs in LOS and NLOS channel model are depicted in sub-figure (a) and (b), respectively.

Comparison of the transmission delay between standard and low latency frame aggregation is depicted in Figure 4.11. With using standard frame aggregation, the transmission delay is decreased with the increase in the traffic load due to the reduced aggregation time. For the low latency aggregation, its transmission delay is slightly affected by the traffic load. This is because, with the increase of traffic load, the possible packet retransmission increases the averaged transmission delay of subframes. Using the low latency aggregation mechanism may scarify channel bandwidth by sending empty subframes, but it is suitable for delay-constrained applications.

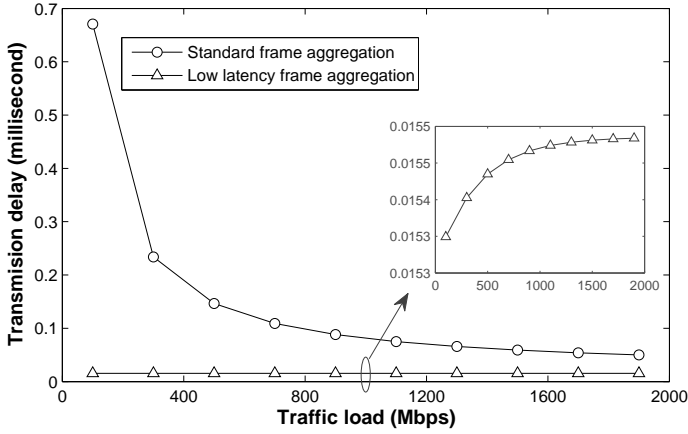


**Figure 4.11:** Transmission delay comparison between standard and low latency aggregation mechanism, with 1024 bytes subframe length, and 7 dB SNR,  $n_r = 3$ .

## 4.5 Chapter Summary

In this chapter, an analytical model has been given to investigate the performance of the standard and low latency frame aggregation mechanisms proposed in IEEE 802.15.3c. This model can provide a detailed performance of the frame aggregation mechanisms, and its accuracy has been validated through extensive simulation studies. It is shown that the standard frame aggregation mechanism can dramatically improve the MAC transmission efficiency. However, this performance improvement is at the cost of the prolonged transmission delay. Therefore, the low latency frame aggregation mechanism is devised for delay-sensitive applications. Based on our analytical results, the low latency frame aggregation mechanism dramatically decreases the transmission delay compared to the standard frame aggregation mechanism.



# Chapter 5

## Resolving Link Blockage Problem in 60 GHz WPANs using Beam Switching

“Intelligence is the ability to adapt to change.”

- Stephen W. Hawking

*The Line-of-Sight (LOS) link is easily blocked by a moving person in the indoor environment, which is one of the severe problems in 60 GHz systems. Beam-forming is a feasible technique to resolve link blockage by switching the beam path from the LOS link to a Non-LOS (NLOS) link. This chapter proposes a solution to resolve this problem using Beam Switching (BS). In this chapter two kinds of BS mechanisms are defined and evaluated: instant decision based BS and environment learning based BS. These two mechanisms are examined in a typical indoor WPAN scenario. Extensive simulations have been carried out, and the simulation results reveal that combining the Direction of Arrival (DoA) with the received signal to noise ratio could make better decision for beam switching.*

## 5.1 Introduction

Due to the weak diffraction and reflection capability of 60 GHz radio, a directional 60 GHz link relies on the Line-of-Sight (LOS) communication. According to the research in [60], the received signal strength could be shadowed around 20 dB when a person crosses the LOS link. Hence, the LOS link can be easily blocked by a moving person in indoor environment, which is termed as *human body blockage effect* or *LOS link blockage problem* [61].

To understand the LOS blockage effect, firstly, it is essential to understand the impact of human activities on 60 GHz systems. This subject is fully investigated in [62], in which the authors have reported that the fading caused by human blockage has several properties: the attenuation speed is fast, the fading duration is long, and the fading amplitude is strong, which means that the LOS link blockage could be easily detected by the dramatically decreased signal strength and there is sufficient time to adopt certain anti-blockage mechanisms to maintain connectivity. In [60, 63, 64], the authors have investigated the use of system diversity to reduce link blockage probability. In [32], a multi-hop solution is proposed to circumvent link blockage using intermediate devices as relays. The IEEE 802.15.3c activities consider the use of beam-forming technique to switch the LOS link to a Non-LOS (NLOS) link when the direct link is blocked [65]. In a residential environment, there normally exist one LOS link and several NLOS links which can be used as alternative paths. Therefore, before establishing a link for communication, the transmitter and the receiver could negotiate a backup choice. Once the LOS link is blocked, they switch to the backup NLOS link together to maintain the connectivity. Being different from relying on system diversity or intermediate relaying devices, beam-forming does not require support from other hardware or devices to resolve the link blockage problem. Therefore, this chapter is motivated to investigate how to select a backup NLOS link to support high performance Beam Switching (BS). To the best of our knowledge, this is the first effort working on this subject.

The main contributions of this chapter include the following aspects. The BS based mechanisms are proposed to resolve link blockage problem in 60 GHz systems. The BS mechanisms are further classified into two categories: *instant decision* based BS and *environment learning* based BS. The instant decision based BS refers to the mechanisms which only use the current available information to select backup links, for instance, the received Signal-to-Noise Ratio (SNR), Direction of Arrival (DoA) of a beam path, etc. The environment learning based BS uses the previous success or failure BS experiences to assist the backup beam path selection. The environment learning based BS is suitable for the usage model like uncompressed video streaming [7], in which, devices like HDTV, Blu-ray player, are always stationed at certain positions. Our proposals are evaluated in a residential environment. Extensive simulations have been carried out. This work provides valuable insights to support beam-forming in 60 GHz WPANs.



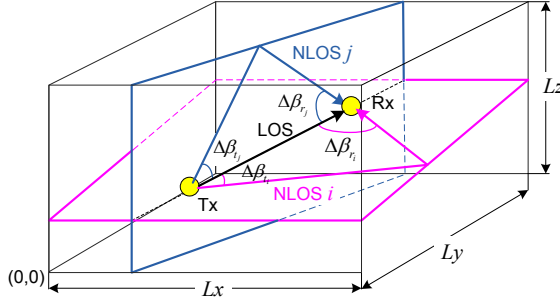


**Figure 5.1:** Illustration of ray tracing approach to find first order reflection beam paths in three-dimensional residential environment.

## 5.2 System Model

### 5.2.1 Work Assumptions

During data transmission, the transmitting and receiving both use directional antennas. The received signal strength from multi-path is negligible. Therefore, when a person passes through the LOS link, the transmission is terminated. When the LOS link is blocked, the transmission pair switches their antenna's main lobe to an alternative NLOS path according to certain negotiations beforehand. Due to the high reflection loss, the reflections higher than first order normally cannot be used for transmission. Hence only the first order reflection beam paths are considered as the backup candidates. After beam switching, devices should keep probing the channel status of the LOS link. To maximize the system throughput, the moment the LOS path is unblocked, it should be capable to switch the beam path back to the LOS path. In this chapter, devices are assumed to be equipped with directional antennas that could steer to any direction. In reality, the steering range of directional antennas might be constrained to a certain number, which leads to a reduced number of backup NLOS links.

### 5.2.2 Environment Model

The geometrical optics method is used to compute the significant paths between the transmission pair in a predefined three-dimensional environment with size  $L_x \times L_y \times L_z$ , as shown in Figure 5.1. The coordinates of the transmitter and receiver are  $[t_x, t_y, t_z]$  and  $[r_x, r_y, r_z]$ , respectively. According to the scenario depicted in Figure 5.1, the first order reflections from the four walls and roof, apparently, are significant paths, which are considered as the possible beam paths in the following study. Before data communication starts, devices execute neighbor discovery process to discover surrounding devices and probe channel status. Normally, there is one LOS link between a transmission pair and also several NLOS links with

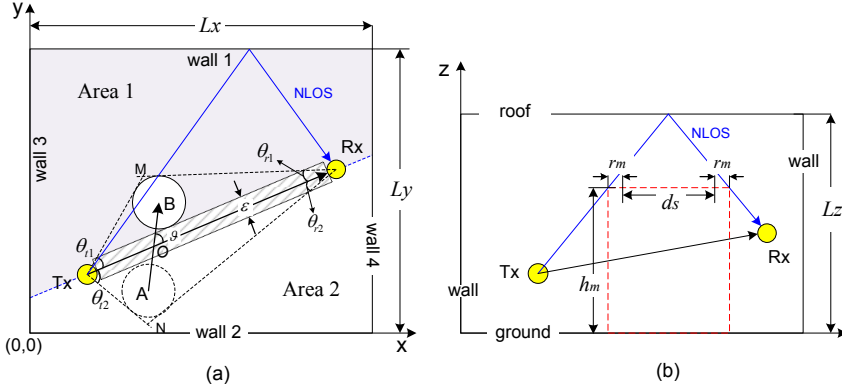


**Figure 5.2:** Human activity influence on the link connectivity illustration.

degraded channel quality. Each beam path can be characterized by the received SNR  $\gamma_i$ , the signal's transmitting direction and receiving direction. Therefore, a three-tuple profile factor is defined as  $\langle \gamma_i, \Delta\beta_{t_i}, \Delta\beta_{r_i} \rangle$  for a certain NLOS path  $i$ , where  $\Delta\beta_{t_i}$  and  $\Delta\beta_{r_i}$  are the transmitting and receiving spatial angle differences between the LOS link and the  $i^{th}$  NLOS path, as illustrated in Figure 5.1.

### 5.2.3 Human Body Blockage Model

This section explains the methodology used to model human activity. A person is represented by a cylinder with radius  $r_m$  and height  $h_m$ . The transmitter and receiver are deployed lower than the height of a person. Hence the LOS link could be easily blocked by a person. When a person crosses a LOS link, it affects the radio link by the attenuation of the received signal strength and the duration of shadowing. According to the methodology used in [62], a link blockage event is detected when the attenuation is higher than a certain threshold, which means that when a person moves into a certain area, his body shadows the received signal strength and the radio link blockage is detected. This area, which is termed as *shadowing area* in this work, is defined as a rectangle with length  $d_{tr}$  and width  $\epsilon$  as shown in Figure 5.2 (a), where  $d_{tr}$  is the distance between the transmitter and the receiver on the XY-Plane. The tolerance of the radio link to the signal strength attenuation is different when different modulation and coding schemes are used, which leads to a different length of  $\epsilon$ . For simplicity, we assume  $\epsilon$  to be a fixed value. The person moves according to the Random Way Point (RWP) mobility model with a certain speed and pausing time.

### 5.2.4 Propagation Model

The radio propagation on the LOS link is modeled using the link budget presented in Section 2.3.2. After the first order reflection, the signal strength is degraded due to the reflection loss. The Fresnel reflection coefficient for perpendicular polarization wave can be expressed as,

$$\eta_{\perp} = \frac{\cos \theta_1 - \sqrt{\omega - \sin^2 \theta_1}}{\cos \theta_1 + \sqrt{\omega - \sin^2 \theta_1}} \quad (5.1)$$

where  $\theta_1$  is the incident angle,  $\omega$  is dielectric constant which can be set as  $6.5 - 0.7j$  for concrete structure [66]. The amplitude of the signal response after reflection is given as:  $\nu = \left(\frac{\lambda}{4\pi d}\right) |\eta_{\perp} \sqrt{G_t G_r}|$ . Hence, the received power from NLOS link is given by  $P'_r(d) = P_r(d) + 20 \log \eta_{\perp}$ .

## 5.3 Proposal to Resolve Link Blockage Problem

To support beam switching during data transmission phase, the transmitter and the receiver negotiate a backup NLOS link before establishing an isochronous link. Devices use directional antennas to detect their surrounding neighbors and probe the corresponding channel states. A weight factor  $\varsigma$  is associated with each detected beam path. Except for the LOS link, a path with the highest weight factor is selected as the backup choice. In this section, several mechanisms are introduced to define the BS weight factor  $\varsigma$ .

### 5.3.1 Beam Switching Mechanisms

#### Instant Decision based Beam Switching

The most straightforward way is to select an alternative path with the highest SNR. Intuitively, this path can provide the best channel quality. Hence the measured SNR  $\gamma_i$  (in dB) from a certain detected beam path  $i$  is used to compute its weight factor  $\varsigma_i$  as

$$\varsigma_i = 1 - \left| \frac{\gamma_i - \gamma_o}{\gamma_o} \right|, \quad (5.2)$$

where  $\gamma_o$  is the highest measured SNR from all the detected beam path. With the existence of the LOS link,  $\gamma_o$  is the measured SNR from the LOS link. This mechanism is denoted as SNR based Beam Switching (SNR-BS).

In certain circumstances, if the NLOS link is geographically close to the LOS link, the selected backup link is probably also blocked by the same person. Therefore, to involve spatial diversity in the alternative path selection process, the

weight factor is adjusted as:

$$\varsigma_i = \left(1 - \left| \frac{\gamma_i - \gamma_o}{\gamma_o} \right| \right) \sin\left(\frac{\Delta\beta_{t_i}}{2}\right) \sin\left(\frac{\Delta\beta_{r_i}}{2}\right), \quad (5.3)$$

where  $\Delta\beta_{t_i}$  and  $\Delta\beta_{r_i}$  are within the range  $[0, \pi]$ . This method involves the beam path spatial property by taking the DoA of a beam path into consideration. Therefore, this mechanism is denoted as Directional-SNR based Beam Switching (DSNR-BS).

### Environment Learning based Beam Switching

In a residential environment, the consumer electronic devices, like HDTV, Blu-ray player, are always placed at fixed positions. Hence, they could learn from the beam switching successes and failures to assist the antenna beam-forming. One simple approach that can be easily implemented is the Exponential Moving Average (EMA) technique. Using this approach, the weight factor of each NLOS path candidate is computed based on the previous weight factor and the current measured data as,

$$\varsigma_i(n+1) = [(1 - \alpha)\varsigma_i(n) + \alpha M_i(n)] \Big|_{M_i(n) \neq \phi}, \quad (5.4)$$

where  $\alpha$  is a constant smoothing factor which influences the learning rate by characterizing the importance of the recent measurement data and  $M_i(n)$  is the  $n^{th}$  beam switching result using beam path  $i$ , where

$$M_i(n) = \begin{cases} 1 & \text{switching success} \\ 0 & \text{switching failure} \\ \phi & \text{path } i \text{ is not selected.} \end{cases} \quad (5.5)$$

When  $M_i(n) = \phi$ , the initial value of  $\varsigma_i$  can be obtained using SNR-BS or DSNR-BS.

### 5.3.2 Visibility Test

A geometric approach is used in the simulation to test the visibility of the beam paths. A link is *visible* if it is not blocked by any obstacle. Using different BS mechanisms, communication links (e.g. the LOS link) and backup links (e.g. a NLOS link) are selected before the data transmission phase. When a person passes through the LOS link, the transmitter and receiver switch to the backup NLOS link to maintain the connectivity. If the LOS link and NLOS link are not shadowed by the person at the same time, it is defined as a successful beam switching. Different methods are used to test the visibility of the paths reflected via the walls and the roof, which are illustrated in Figure 5.2 (a) and (b), respectively. As shown in Figure 5.2 (a), it is the plan view of the indoor scenario, in which

the transmitter and the receiver are on the line  $l_1 : y = k_1x + b_1$ , and  $l_1$  separates the room into two parts: Area 1 and Area 2. A person moves from  $A$  to  $B$  according to the trajectory  $l_2 : y = k_2x + b_2$ , and he crosses  $l_1$  at point  $O$ . Take the tangents from the transmitter and the receiver to circle  $A$  and  $B$ , they enclose two triangles  $\Delta TxRxM$  with angles  $(\theta_{t1}, \theta_{r1})$  and  $\Delta TxRxN$  with angles  $(\theta_{t2}, \theta_{r2})$ , which are considered as the influenced area by the person. Hence if a NLOS path  $i$  within Area  $\varpi$  is reflected via a wall, where  $\varpi \in [1, 2]$ , and it satisfies  $\Delta\beta_{ti} \leq \theta_{t\varpi}$  or  $\Delta\beta_{ri} \leq \theta_{r\varpi}$ , this NLOS path is also blocked by the same person. The threshold angles are given as

$$\theta_X = \arcsin\left(r_m / (d_X^2 + (0.5\epsilon + r_m)^2)^{\frac{1}{2}}\right) + \arctan((0.5\epsilon + r_m) / d_X), \quad (5.6)$$

where

$$X = \begin{cases} t1 : & d_{t1} = d_{to} + \kappa \\ t2 : & d_{t2} = d_{to} - \kappa \\ r1 : & d_{r1} = d_{tr} - d_{to} - \kappa \\ r2 : & d_{r2} = d_{tr} - d_{to} + \kappa, \end{cases}$$

in which,  $d_{to}$  denotes the distance between  $Tx$  and crossing point  $O$  at XY-plane,  $\kappa = (0.5\epsilon + r_m) \cot(\vartheta)$ , and  $\vartheta$  is the angle between  $\overrightarrow{AB}$  and  $\overrightarrow{TxRx}$ .

As shown in Figure 5.2 (b), it depicts the plane that is perpendicular to the XY-plane and intersects with XY-plane in line  $l_1$ . It illustrates the NLOS path reflected via the roof. According to the reflection law, the position of the reflection point via roof is influenced by the heights of the transmitter and the receiver. If the person's crossing point is within the range of  $d_s$  as shown in Figure 5.2 (b), he does not block the NLOS path reflected from the roof, which is considered as a successful beam switching. If the crossing point is uniformly distributed on the LOS link, the successful beam switching ratio  $p$  when the path gets reflected via the roof is obtained as

$$p = \frac{2(L_z - h_m)}{2L_z - (t_z + r_z)} - \frac{2r_m}{((t_x - r_x)^2 + (t_y - r_y)^2)^{\frac{1}{2}}}. \quad (5.7)$$

Based on the above equation, it can be concluded that putting the transmitter and the receiver at higher positions could help to decrease the probability of link blockage.

## 5.4 Performance Evaluation

### 5.4.1 Simulation Specifications

A Matlab based simulation environment has been developed to model our proposed scenario. All the proposed models are integrated as shown in the flow chart in Figure 5.3. The related simulation parameters are listed in Table 5.1. The radio

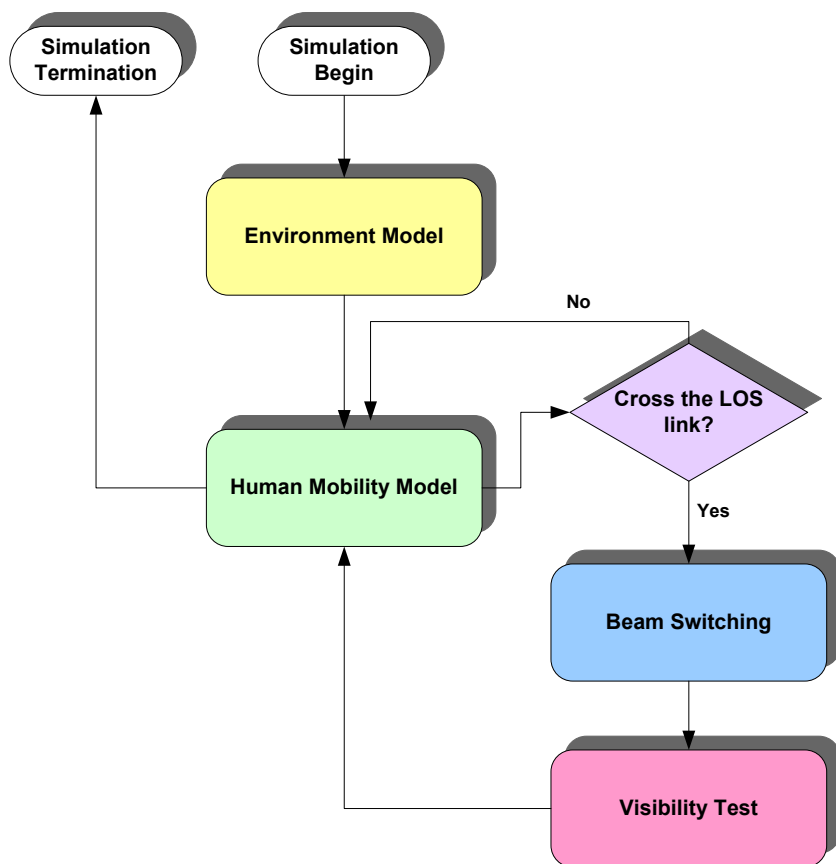


**Figure 5.3:** *Flowchart for the simulation design.*

**Table 5.1:** *Defaulted simulation parameters*

Parameter	Value
Room weight, length and height $[L_x, L_y, L_z]$	[10 m, 10 m, 3 m]
RWP uniform speed distribution	[0, 1 m/s]
RWP uniform pausing time distribution	[0, 10 s]
Shadowing area width $\epsilon$	0.1 m
Human body radius $r_m$ and height $h_m$	0.5 m, 1.75 m
Transmitter and receiver height	1 m
Transmit power $P_t$	10 dBm
Path loss at 1 m	-68 dB
Implementation loss $I_L$	1.5 dB
Path loss exponent $n$	2
Directional antenna gain	13.8 dBi

**Table 5.2:** *Modulation and coding scheme dependent parameters*

Modulation	SF	FEC type	Rec. sensitivity	Data rate
$\pi/2$ BPSK	64	RS(255,239) <sup>a</sup>	-70 dBm	25.3 Mbps
$\pi/2$ BPSK	4	RS(255,239)	-61 dBm	405 Mbps
$\pi/2$ BPSK	1	LDPC(672,504) <sup>b</sup>	-59 dBm	1300 Mbps
$\pi/2$ QPSK	1	LDPC(672,336)	-58 dBm	1730 Mbps
$\pi/2$ QPSK	1	LDPC(672,504)	-56 dBm	2590 Mbps
$\pi/2$ QPSK	1	LDPC(672,588)	-54 dBm	3020 Mbps

<sup>a</sup>Reed Solomon Code<sup>b</sup>Low Density Parity Check Code

propagation model mentioned in Section 2.3.2 is used to compute the received SNR from different beam paths. In one simulation run, a person moves according to the RWP mobility model, and he crosses the LOS link for 10000 times in total. All the depicted simulation results are based on the average value of the 10000 iterations. The link visibility  $p_s$  is defined as the proportion of the successful switching in one simulation run. The specifications listed in Table 5.2 are used to model the capacity of NLOS links, in which, 25.3 Mbps is used as the basic rate used to transmit command packets to probe the channel status. Therefore if the received signal strength from a NLOS link is lower than -61 dBm, it cannot be used as a backup link. According to the received signal strength at beam path  $i$ , the achievable data rate  $R_i$  can be estimated based on Table 5.2. The achievable capacity using NLOS path  $i$  is defined as  $C_i = R_i \times p_s$ .

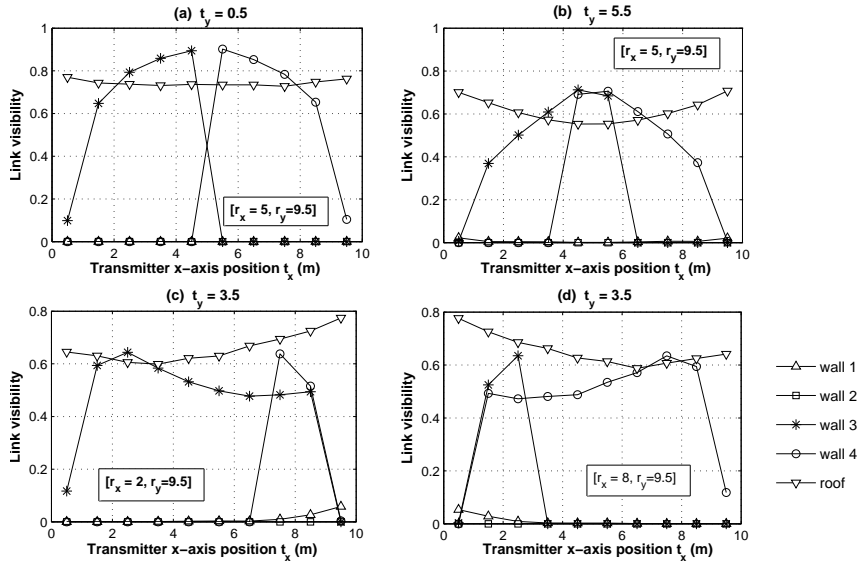


Figure 5.4: Link visibility comparison using different beam paths.

## 5.4.2 Simulation Results

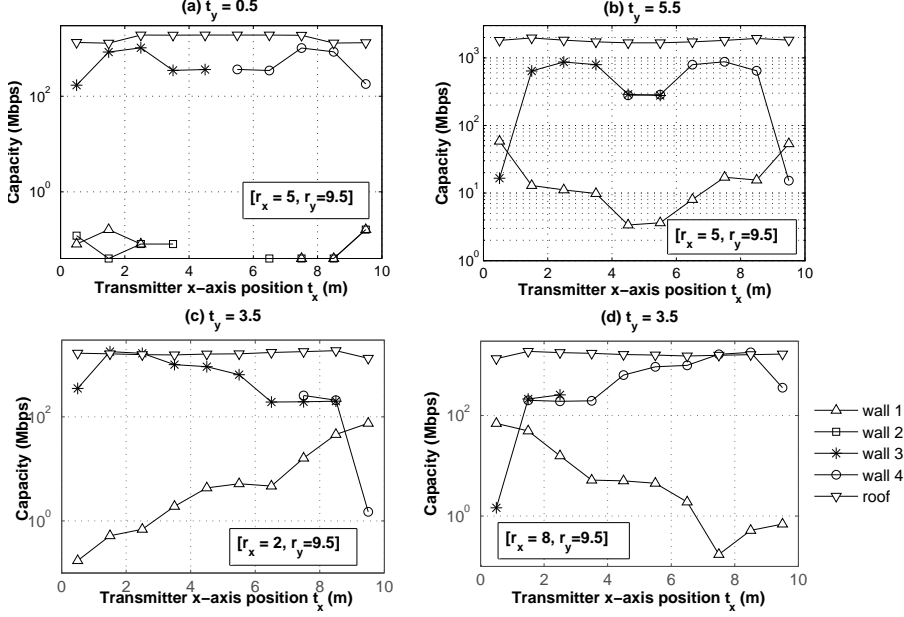
### Performance comparison between different beam paths

Figure 5.4 depicts the link visibility, using all the first order reflection paths with variant transmitter and receiver positions. In Figure 5.4 (a) and (b), the receiver is fixed at  $[5, 9.5]$  and transmitter is put at  $[t_x, t_y]$ , in which,  $t_x$  varies from 0.5 to 9.5 with step size 1, and  $t_y$  is set as 0.5 and 5.5 in different scenarios. As shown in Figure 5.4 (a) and (b), the beam paths reflected from wall 3, wall 4 and the roof exhibit the best performance alternately at different positions. In Figure 5.4 (c) and (d), the receiver position is at  $[2, 9.5]$  and  $[8, 9.5]$ , respectively. For the transmitter, its y-coordinate is fixed at 3.5 and  $t_x$  varies from 0.5 to 9.5 with step size 1. In sub-figure (c) and (d), the reflection via the roof exhibits the best performance in most of the tested positions.

The performance of the capacity that can be achieved using different beam paths is shown in Figure 5.5. The reflection from the roof is superior to the others in all the examined positions although its link visibility is not always the highest. What should be noticed is that compared to the LOS link, the achievable capacity is degraded due to the path loss and reflection loss. Therefore, for certain bandwidth-constrained application, for instance wireless video streaming, the video format should be adapted to a lower bandwidth requirement format. This involves cross-layer optimization which is out of the scope of this chapter.

Another interesting observation is that, according to (5.7), the switching suc-





**Figure 5.5:** Link capacity comparison using different beam paths.

cess ratio using the path reflected via the roof should not be influenced by the transmitter and receiver's position. However as shown in Figure 5.4, the link visibility for the reflection via the roof varies with different positions. This is because, (5.7) is derived based on the assumption that a person crosses the LOS link uniformly. However, using the RWP model, the spatial positions of a person are not uniformly distributed. For instance as shown in Figure 5.6, it records the y-coordinate of the person's crossing points in one simulation run. The crosses are the data collected from the simulation, and the line is the fitted curve, which shows that the person has a higher probability to be at the middle of the room than at the margin of the room when the RWP model is used.

### Performance comparison between different BS mechanisms

Figure 5.7 compares the overall beam switching performance using instant decision based BS (SNR and DSNR) and the environment learning based BS (SNR-EMA and DSNR-EMA). The receiver is put at  $[5, 9.5]$  and the transmitter has a variable position as illustrated in Figure 5.7. It is observed that for the instant decision based mechanisms, D-SNR has a better link visibility than the SNR based BS, which indicates the benefit of involving directional information to make beam switching decision. For the environment learning based mechanisms, SNR-EMA and DSNR-EMA have similar performance, but DSNR-EMA is slightly super-

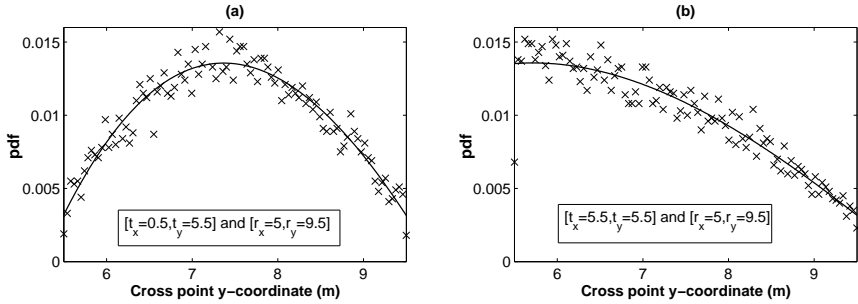


**Figure 5.6:** The probability density function (pdf) for the y-coordinate of the crossing point on the LOS link.

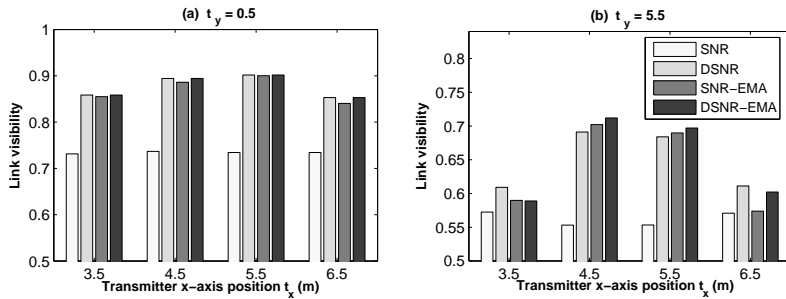


**Figure 5.7:** Performance comparison between the instant decision based policies and the EMA based policies, with  $\alpha = 0.1$ ,  $[r_x = 5, r_y = 9.5]$ .

ior to SNR-EMA. In an unknown environment, they are envisioned to trace the beam path that has a high link visibility. Using the EMA approach, the beam path selection is controlled by the smoothing factor  $\alpha$ . Figure 5.8 compares the smoothing capability with different  $\alpha$ . Each simulation point is averaged over 10000 simulation runs. The smaller  $\alpha$  has a higher dependency on the previous beam switching performance, which leads to a faster convergence to the stable status if the environment is fixed. Finally, it can be concluded that, for the devices with fixed positions, long-term environment learning is robust to the instant decision. For the portable devices without fixed positions, the instant decision based BS is a better choice, and D-SNR can provide better performance than SNR based BS.

## 5.5 Chapter Summary

In this chapter, several Beam Switching (BS) mechanisms have been investigated to support beam-forming once the communication link is blocked by a moving

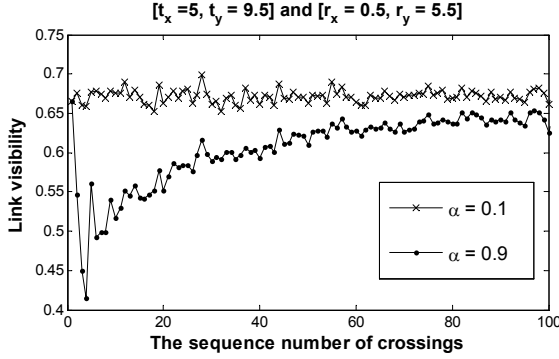


**Figure 5.8:** *The influence of smoothing factor using DSNR-EMA.*

person or any obstacle. The BS mechanisms have been classified into two categories: instant decision based BS and environment learning based BS. The instant decision based BS uses the current available information to make BS decision, e.g. the measured SNR or DoA. The mechanism to select a backup link with the highest SNR is denoted as SNR-BS. The mechanism to select a NLOS link which is geometrically far away from the LOS link and keeps the SNR as high as possible is denoted as DSNR-BS. The environment learning based BS uses the earlier switching experiences to make a BS decision. The link visibility and the achievable system capacity have been assessed using different BS mechanisms, and it can be concluded that combining the directional information of a beam path with the received SNR makes a better decision for BS.



# Chapter 6

## Interference Mitigation for the Coexisting 60 GHz WPANs

“Measure what is measurable, and make measurable what is not so.”

- Galileo Galilei

*60 GHz WPANs are capable of providing multi-Gbps transmission data rate for short-range wireless communication. However, the 60 GHz link is very fragile to the co-channel interference. An interference mitigation mechanism is addressed in this chapter, which employs PNC-capable devices within a piconet to relay synchronization (sync) frames. In this way, the protection range of a primary piconet can be extended. Based on the study in this chapter, it is illustrated that the system performance is significantly improved by using sync frames, in terms of throughput and the guaranteed transmission distance. Moreover, the optimized beacon and sync frame range are also investigated when multiple piconets coexist.*

## 6.1 Introduction

Due to the stringent link budget for 60 GHz system to achieve Gbps-based transmission data rate, 60 GHz link is fragile to the variance of the channel quality and the amount of interference. The work in [67] has evaluated the error performance and the throughput of their proposed 60 GHz channel model, with the existence of Co-Channel Interference (CCI). Their channel model is based on the actual measurements in [68]. It is reported that, an undesired CCI may easily compromise to the quality of the 60 GHz system. To mitigate the CCI, the IEEE 802.15.3 MAC layer protocol defines that a PNC may periodically request the channel status from the devices in its piconet, and estimate the channel quality according to the number of transmitted channel status request frames and the number of received response frames. If the channel experiences intolerable interference, the PNC moves its piconet to another channel with less interference. If the channel status is not updated with time, the communication within a WPAN may be interrupted by the other close-by WPANs.

To support the use of 60 GHz radio, IEEE 802.15.3c plans four channels with central frequencies of 58.32, 60.48, 62.64, 64.80 GHz, as shown in Figure 6.1. This channelization is also adopted by the other 60 GHz standardization activities, for instance ECMA [11] and WirelessHD [8]. Due to the limited number of channels, instead of simply switching from one channel to another channel to avoid CCI, it is worthy to investigate how to optimize the coexistence of WPANs in the same channel. It is especially important for the usage models which lack channel resource, for instance, in an office room or exhibition hall scenarios. For this reason, this chapter is dedicated for the study of interference mitigation mechanism without considering channel switching.

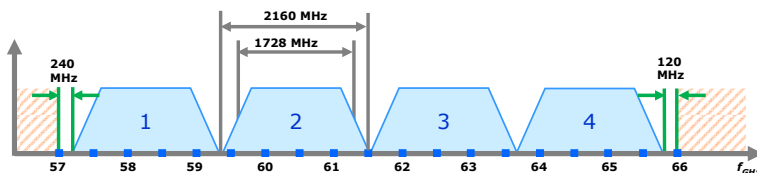


Figure 6.1: IEEE 802.15.3c channel plan [69].

To support the simultaneous operation of WPANs, some works have been done [70–74]. The coexistence of IEEE 802.15 WPAN and IEEE 802.11 WLAN was studied in [70]. The authors analyzed the probabilities of channel conflicts between IEEE 802.11b and IEEE 802.15.1 based networks. The work in [71] addressed the coexistence of two types of Ultra Wide Band (UWB) based WPANs: DS-UWB and Multiband OFDM. The work in [72] was devoted for the coexistence of Bluetooth based WPANs. In [73], the authors have proposed an adaptive frequency hopping scheme to enable the coexistence issue that involves the Bluetooth and IEEE 802.11b technologies. In [74], the authors have analyzed the

interference in a cognitive network with the coexistence of the primary user and multiple cognitive users. However, to the best of our knowledge, there is no work that has provided special treatment to the interference mitigation for the coexistence of 60 GHz WPANs.

In this chapter, *synchronization* (sync) frames are used to mitigate the inter-piconet interference for the 60 GHz WPANs. The novelty of this work relies on the following aspects. Our work is the first attempt to quantify the performance of using sync frames to support coexistence of the 60 GHz WPANs. An analytical model is derived in this chapter to reveal the relation between CCI and the system capacity via the BER derived from a 60 GHz featured physical layer and a realistic 60 GHz channel model. Due to the complexity in analysis, the conventional methods to model the interference for coexisting systems normally do not consider the shadowing effect in radio propagation model, e.g. [70,72]. This gap is closed in our analytical model wherein the log-normal shadowing radio propagation model is used. Secondly, based on the proposed theoretical model, the effectiveness of using sync frames is illustrated in terms of the throughput and the guaranteed transmission distance. Thirdly, a lower bound on the guaranteed transmission distance is provided with a number of coexisted piconets.

## 6.2 Interference Mitigation Mechanism

To control a piconet, the PNC periodically broadcasts beacons, which contain the timing and management information of the piconet. Devices within a piconet reserve channel resource from the PNC and access the channel in a TDMA fashion. In this way, collision-free communication can be guaranteed. If there are two PNCs which are out of the transmission range of each other, they could select the same channel to construct their piconets. If the two piconets are close enough, the communication within one piconet could be disturbed by the interference from the other piconet, which is considered as the *hidden PNC problem*. For example as shown in Figure 6.2 (a), PNC  $v$  is denoted as the primary PNC, and DEV  $m$  is a slave device of PNC  $v$ . Because PNC  $n$  is outside the transmission range of PNC  $v$ , it cannot sense the beacons from PNC  $v$ . Therefore, it could begin its own piconet by transmitting beacons on the same channel. DEV  $m$  is located in the overlapping area of these two piconets, therefore, transmission collisions could happen at DEV  $m$  side. The IEEE 802.15.3c standard defines a new frame format to mitigate the interference from co-channel systems, which is called as sync frame. It provides a method to exchange information among the independent piconets. In the standard, it defines that it is mandatory for the PNC-capable devices to transmit sync frames, and it is optional for non-PNC capable devices. The coverage range of a piconet is extended using the surrounding slave devices to forward sync frames. Sync frames can be considered as copies of beacons, which contain the timing information of a piconet. For a device, if it receives a beacon or a sync frame from a piconet, it cannot become a PNC to establish its own piconet.

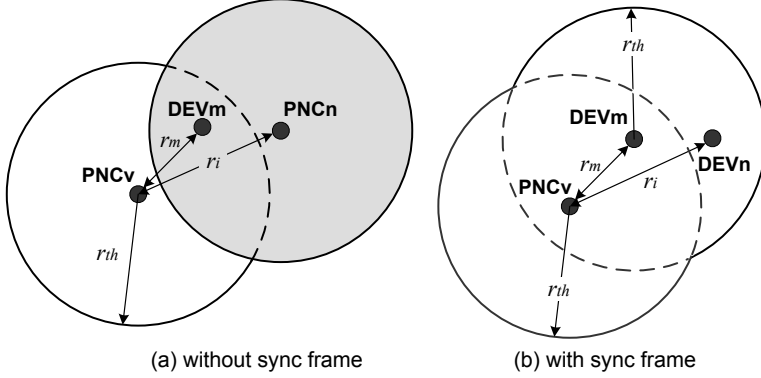


**Figure 6.2:** Piconet interference and corresponding mitigation mechanism illustration. PNC v: primary PNC. PNC n: interfering PNC. DEV m: a slave device of PNC v.

For instance as shown in Figure 6.2 (b), DEV  $n$  receives sync frames from DEV  $m$ , so it either joins PNC  $v$ 's piconet via dependent piconet structure [3], or it joins the other piconets.

## 6.3 Analytical Model

### 6.3.1 Interference Indication Function Derivation

When a device is powered on, first it scans the possible channels to detect if there are any surrounding piconets. If the device receives a beacon within a certain scanning time  $T_{scan}$ , it associates with the detected PNC to join in its piconet, where  $T_{scan}$  is the time duration to transmit  $n_b$  beacons. Otherwise, it assumes that the channel is free, and it can become a PNC by broadcasting its own beacons. To study the interference situation with the existence of a single interfering source, PNC  $v$  is assumed to be the primary PNC and it is located at the center of an area with radius  $R$ . Its beacon range is denoted as  $r_{th}$ , and we have  $r_{th} < R$ .

In Chapter 2, a path loss model was introduced in (2.4) to describe the propagation of radio, in which,  $P_r(d)$  represents the received signal strength (in dB) at the receiver that is  $d$  meters away from the transmitter, where,  $P_r(d) = P_t + G - PL_0 - 10n \log_{10}(d)$ , where  $P_t$  is the transmission power,  $G$  is antenna gain,  $PL_0$  is the reference path loss at 1 m, and  $n$  is the path loss exponent.

Several studies have shown that the received signal power strength varies around the predicted mean power value obtained by path loss model, and this variation can be modeled by a log-normal distribution [75, 76]. Hence, in this chapter, a log-normal shadowing model is used to calculate the received signal



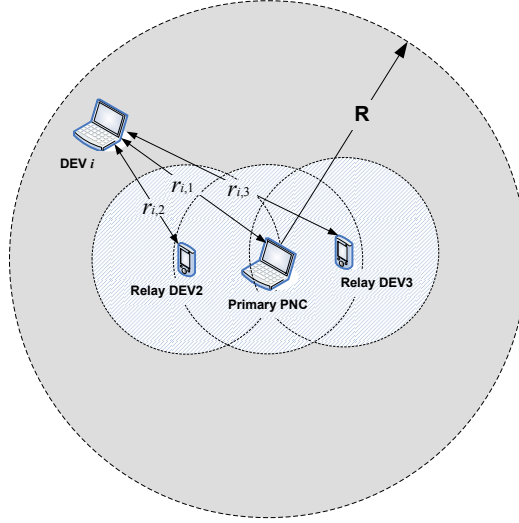


**Figure 6.3:** Scenario illustration for a single interfering device.

power strength,

$$P_r(d) = P_t + G - PL_0 - 10n \log_{10}(d) + X_\sigma, \quad (6.1)$$

where,  $X_\sigma$  is a zero mean Gaussian random variable with standard deviation  $\sigma$ . The measured standard deviation  $\sigma$  is about 1 dB [6]. Hence, the received power can be denoted as a Gaussian random variable  $P_r(d) \sim \mathcal{N}(\mu(d), \sigma)$  with mean  $\mu(d) = P_t + G - PL_0 + 10 \log_{10}(d^{-n})$  and standard deviation  $\sigma$ . To correctly receive a signal, the received signal strength should be higher than a certain threshold  $\gamma_{th}$ , which is also called as receiving sensitivity. Therefore, the probability that a link exists between the transmitter and receiver can be expressed as [77]<sup>1</sup>,

$$\begin{aligned} p(d, n) &= \Pr[P_r(d) - \gamma_{th} > 0] \\ &= \frac{1}{\sigma\sqrt{2\pi}} \int_0^\infty \exp\left[-\frac{(t - 10 \log_{10}(\hat{d}^{-n}))^2}{2\sigma^2}\right] dt \\ &= \frac{1}{2} \left(1 - \operatorname{erf}\left(\frac{10n \log_{10}(\hat{d})}{\sqrt{2}\sigma}\right)\right), \end{aligned} \quad (6.2)$$

<sup>1</sup>In [78], the error function  $\operatorname{erf}(\cdot)$  is defined as  $\operatorname{erf}(z) = \frac{2}{\sqrt{\pi}} \int_{-\infty}^z e^{-t^2} dt$ , and

$$\frac{1}{\sigma\sqrt{2\pi}} \int_{-\infty}^x \exp\left[-\frac{(t - \mu)^2}{2\sigma^2}\right] dt = \frac{1}{2} \left(1 + \operatorname{erf}\left(\frac{x - \mu}{\sqrt{2}\sigma}\right)\right).$$

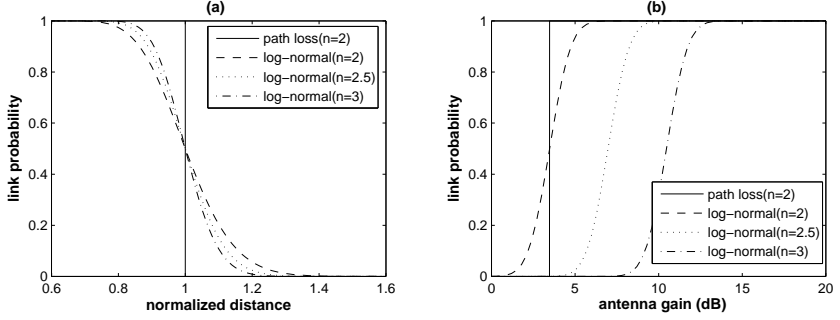


**Figure 6.4:** The normalized distance and antenna gain influence on the link probability, the defaulted parameters are listed in Table 2.2.

where  $\hat{d}$  is defined as the normalized distance and it is given by  $\hat{d} = d/r_{th}$ .  $r_{th}$  is the beacon range without considering the log-normal shadowing effect, and  $r_{th} = 10^{\frac{\varpi}{10n}}$ , in which  $\varpi = P_t + G - PL_0 - \gamma_{th}$ . The impact of the normalized distance on the link probability is shown in Figure 6.4 (a) and the impact of the antenna gain is shown in Figure 6.4 (b) when  $d$  is set to 5 m.

Device  $m$  is a slave device of PNC  $v$ . Assume that PNC  $v$  is at the origin of a polar coordinate system. The polar coordinates of device  $m$  are given by  $(r_m, \alpha_m)$ . The link between  $v$  and  $m$  is considered as the target link with  $m$  as the transmitter and  $v$  as the receiver. Except for the target transmission pair, there is another device (here  $i$ ), which is randomly placed and is uniformly distributed within the circular area with polar coordinates  $(r_i, \alpha_i)$ . The probability for device  $i$  to become an interfering PNC is,

$$p_c = \left[ \prod_{k=0}^{m_s} (1 - p_{ik}(r_{ik}, n_{ik})) \right]^{n_b}, \quad (6.3)$$

where,  $m_s$  is the number of slave devices relaying sync frames within the primary piconet, for the scheme without using sync frames,  $m_s = 0$ .  $r_{i0}$  is the distance from device  $i$  to PNC  $v$  and  $r_{ik}$  is the distance from device  $i$  to the  $k^{th}$  relaying device, where  $k \in [1, m_s]$ . Denote the polar coordinates of the  $k^{th}$  relaying device as  $(r_k, \alpha_k)$ , hence  $r_{ik}$  is expressed as  $r_{ik} = (r_i^2 + r_k^2 - 2r_i r_k \cos(\alpha_i - \alpha_k))^{\frac{1}{2}}$ . Because the channel quality between device  $i$  and the PNC or relaying devices might be different,  $n_{ik}$  is used to specify the path loss exponent for each link.

The CCI can be quantified as the ratio of the undesired signal power and the desired signal power. On the condition that device  $i$  is an interfering device, and the distance between device  $i$  and PNC  $v$  is  $r_i$ , where  $r_i$  is short for  $r_{i0}$ , the CCI (in dB) is represented as  $\zeta(r_i, r_m) = P_r(r_i) - P_r(r_m)$ .  $P_r(r_m)$  is the received power (in dB) from the target transmitter and  $P_r(r_m) \sim \mathcal{N}(\mu(r_m), \sigma_t)$ ,  $P_r(r_i)$  is the received power (in dB) from the interfering source and  $P_r(r_i) \sim \mathcal{N}(\mu(r_i), \sigma_i)$ .

To achieve a certain level of BER,  $\zeta$  should be smaller than a required threshold  $\zeta_{th}$  [67]. Therefore, device  $i$  has a probability  $\xi_c$  to disturb the received signal at PNC  $v$ , which is given by,

$$\begin{aligned}\xi_c(r_i, r_m) &= \Pr[\zeta(r_i, r_m) > \zeta_{th}] \\ &= \frac{1}{2} \left( 1 + \operatorname{erf} \left( \frac{10 \log_{10}(\hat{r}_i) - \zeta_{th}}{\sqrt{2(\sigma_i^2 + \sigma_i^2)}} \right) \right),\end{aligned}\quad (6.4)$$

where  $\hat{r}_i = r_m^{n_t}/r_i^{n_i}$ , factor  $n_t$  is the path loss exponent for target link between  $m$  and  $v$ , and  $n_i$  is the path loss exponent for the interfering link between  $n$  and  $v$ . Here, an interference indication function  $\mathbb{F}(\cdot)$  is defined to express the possible interference caused within the network as,

$$\mathbb{F}(r_m) = \int_0^{2\pi} \int_0^R p_c(x) \xi_c(x, r_m) f(r_i) f(\alpha_i) dr_i d\alpha_i, \quad (6.5)$$

where  $f(r_i) = 2r_i/R^2$  and  $f(\alpha_i) = 1/2\pi$ . To demonstrate the performance of  $\mathbb{F}(r_m)$  using sync frames, three slave devices of PNC  $v$  are used to relay sync frames, and they are placed at equal distances from each other on the circumference of the circle of 8 m from  $v$ . The values of  $\mathbb{F}(r_m)$  are compared using and without using sync frames while varying path loss exponent for the interfering link. The results are shown in Figure 6.5. It is observed that the sync frames can effectively reduce the interference level. The beacon range influence is depicted in Figure 6.6 when the transmission distance of the target link  $r_m$  is fixed at 5 m. What needs to be noticed here is that we denote the sync frame range to be same as beacon range. Bigger the beacon range, lower is the interference level.

### 6.3.2 Relationship between CCI and Throughput

The piconet coexistence scenario employed in the following work is shown in Figure 6.7. Except the target transmission pair, the other devices are uniformly distributed within the circular network. Because PNC  $v$  is at the center of the entire network, it is expected to experience the highest amount of interference. Within a co-operating system, the CCI for a system with multiple interfering sources can be represented as,

$$\zeta(r_m) = 10 \log_{10} \frac{\sum_{i=1}^N \mathbb{P}(r_i)}{\mathbb{P}(r_m)}, \quad (6.6)$$

where  $\mathbb{P}(r_m)$  is the desired signal strength (in watt) and  $\mathbb{P}(r_i)$  is the received signal strength (in watt) from the  $i^{th}$  interfering source. The distance between the interfering device and the target receiver is  $r_i$ . For an individual interfering source  $i$ ,  $\mathbb{P}(r_i)$  could be represented as a log-normal variable with mean  $\omega_i$  and standard deviation  $\nu_i$ , where  $\omega_i = \exp(\mu_i + \sigma_i^2/2)$  and  $\nu_i = (\exp(\sigma_i^2) - 1)\exp(2\mu_i + \sigma_i^2)$ .

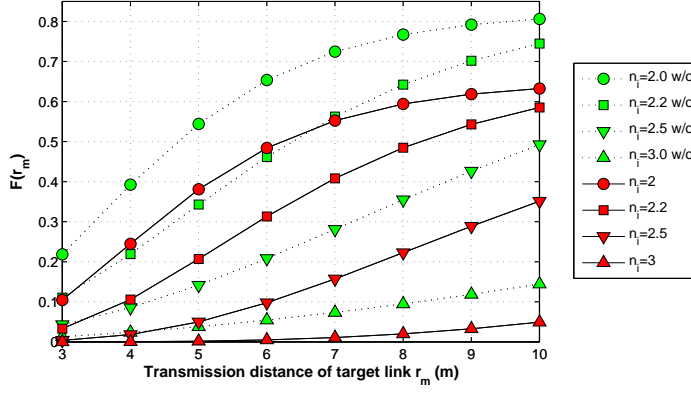


**Figure 6.5:**  $\mathbb{F}(r_m)$  comparison between using sync frames and without using sync frames, 3 relaying devices,  $\gamma_{th} = -70$  dBm,  $\zeta_{th} = -15$  dB,  $\sigma_t = 1.3$ ,  $\sigma_i = 2.7$ ,  $n_t = 2$ ,  $d_{th} = 10$  m,  $R = 30$  m,  $n_b = 3$ .

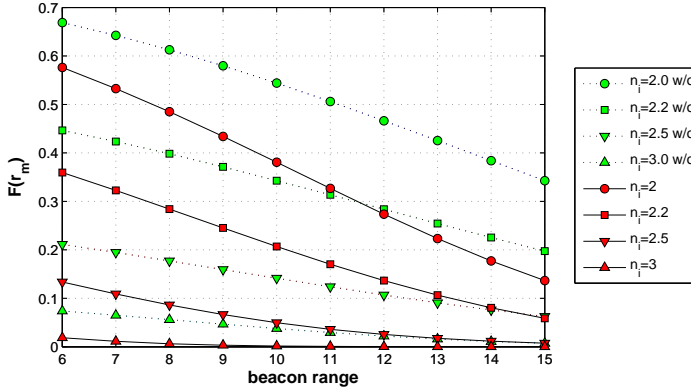


**Figure 6.6:** Beacon range influence on  $\mathbb{F}(r_m)$ , the same parameter specification as the previous figure, the target transmission distance is 5 m.

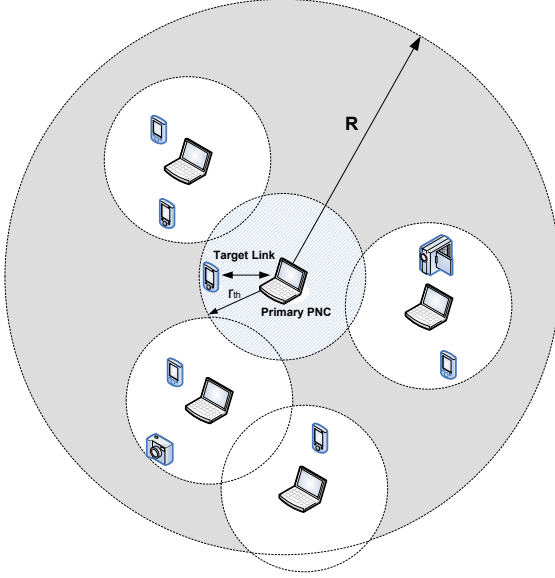


**Figure 6.7:** *Piconet coexistence scenario.*

The summation of  $N$  log-normally distributed interfering power can be assumed as a log-normally distributed variable  $\mathbb{L} \sim \text{Log-}\mathcal{N}(\mu_l, \sigma_l)$  [79]. Fenton-Wilkinson (FW) model [80] has a good accuracy when the standard deviation of log-normal components are less than 4 dB [77, 80]. Therefore, when the FW approximation model is used, it can be obtained,

$$\mu_l = 2 \ln u_1 - \frac{1}{2} \ln u_2, \sigma_l = (\ln u_2 - 2 \ln u_1)^{\frac{1}{2}}, \quad (6.7)$$

where

$$u_1 = \sum_{i=1}^N \exp(\omega_i + \nu_i^2/2)$$

$$u_2 = \sum_{i=1}^N \exp(2\omega_i + 2\nu_i^2) + 2 \sum_{i=1}^{N-1} \sum_{j=i+1}^N \exp(\omega_i + \omega_j) \exp\left(\frac{1}{2}(\nu_i^2 + \nu_j^2)\right). \quad (6.8)$$

The CCI level  $\zeta$  and the selected MCS  $\kappa_i$  determine the achievable BER  $e_{\kappa_i}$  at the target link as  $e_{\kappa_i} = f_{\kappa_i}(\zeta)$ . The mapping function  $f_{\kappa_i}(\cdot)$  is decided by the physical layer specifications presented in Appendix C, according to which, the resultant BER and CCI performance are shown in Figure 6.8. It interprets that, for instance, to achieve the target BER as high as  $10^{-4}$ , the CCI should be lower than -15.5 dB in the LOS channel model and -14.6 dB in the NLOS channel model using  $\pi/2$ -BPSK modulation scheme. For a memoryless channel, the bit errors can

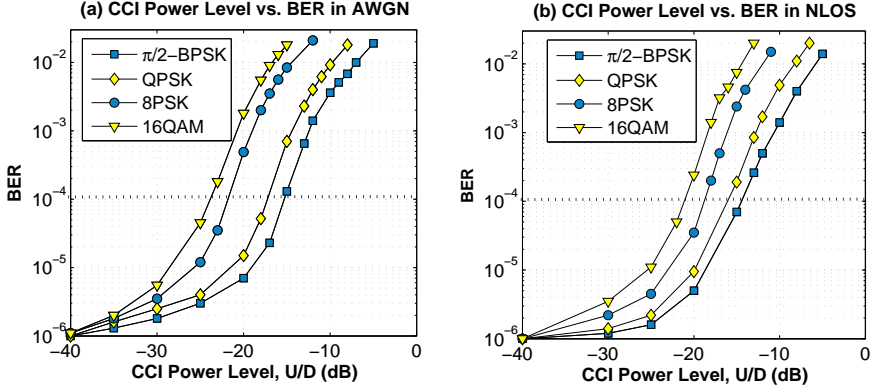


**Figure 6.8:** CCI power level in residential LOS and NLOS channel.

be assumed as non-correlated and they are uniformly distributed within a packet. Under this assumption, the resultant PER is expressed as  $P_e^{\kappa_i}(l) = 1 - (1 - e_{\kappa_i})^l$ , where  $l$  is the frame length (in bits). Therefore, the system throughput without considering any automatic repeat request technique can be approximated as

$$C = (1 - \eta)R_{\kappa_i}(1 - P_e^{\kappa_i}(l)), \quad (6.9)$$

where  $R_{\kappa_i}$  is the transmission data rate using MCS  $\kappa_i$ , and  $\eta$  is the proportion of overhead,  $\eta = \frac{t_o}{l/R_{\kappa_i} + t_o}$ , where  $t_o$  is the time duration for overhead which includes the packet preamble, packet header, and minimum inter-frame spacing length.  $R_{\kappa_i}$  is given by  $R_{\kappa_i} = S_{BW}L_m r_c \frac{L_{sub} - L_{gi}}{L_{sub}}$ , where  $S_{BW}$  is the Nyquist bandwidth,  $L_m$  is the modulation level,  $r_c$  is the coding rate.  $L_{gi}$  and  $L_{sub}$  are the length of the guard interval and the Frequency Domain Equalization (FDE) sub-block for operation in the NLOS channel. The achievable data rate using different modulation scheme is listed in Table C.1.

## 6.4 Performance Evaluation

Simulation studies are carried out in Matlab. The physical layer and channel model are based on the specifications presented in Appendix C. A circular network with  $N$  devices is generated, where  $N > 2$ . The position of the target transmission pair is fixed, in which, PNC  $v$  is located at the center of the network, and its target transmitter is located  $r_m$  meters away. The position of the other  $N - 2$  devices are sequentially generated, and they are uniformly distributed within the circular network. Two network topology formation mechanisms are considered in the simulation i.e., with or without sync frames:

- *Network topology formation without using sync frames:* For this scenario,

after a device is generated, it associates with the closest PNC that it can reach. If there is no surrounding PNC, it becomes a PNC and generates its own piconet<sup>2</sup>.

- *Network topology formation with using sync frames*: For this scenario, after a device is generated, it associates with the closest PNC. If this device is not within the beacon range of any piconets and it receives sync frames from the relaying devices, it associates with the closest relaying device. If this device is not within the coverage range of any beacon or sync frames, it becomes a PNC.

After formatting the network topology, each PNC outside the primary piconet is assumed as the transmitter in its piconet, and it selects its closest slave device as the receiver. The FW model is used to approximate the interference power. Assume that all the transmission pairs communicate simultaneously to create the worst interference situation for the target link in the center. Therefore, the capacity of the target link could be considered as a lower bound for the link capacity with transmission distance  $r_m$ . It is assumed that, all the transmission pairs can select the MCS that provides the highest data rate according to their current CCI level. Each simulation is iterated 10000 times, and the results are taken as the mean value.

### Impact of Transmission Distance

The cumulative distribution function (cdf) of the CCI at PNC  $v$  is shown in Figure 6.9 when the transmission distance of the target link  $r_m$  is fixed at 0.8 m. It is observed that, the CCI performance is dramatically improved using sync frames in both LOS and NLOS channel model. Figure 6.10 (b) illustrates the influence of the CCI on the guaranteed transmission distance of the target link, in which, the achievable throughput is plotted in the case that  $r_m$  is varied from 0.05 m to 6 m. In each simulation, the throughput is calculated based on the mean CCI and the MCS that provides the highest throughput. The guaranteed maximum transmission distance of the target link is denoted as  $r_{max}$ , which is obtained with the targeted BER as  $10^{-4}$ . The factor  $r_{max}$  is the transmission distance threshold. If  $r_m > r_{max}$ , the link is disconnected. Without using sync frames,  $r_{max}$  is 1 m for LOS channel, and 3.05 m for NLOS channel. Using sync frames,  $r_{max}$  is 1.85 m for LOS and 6 m for NLOS. This shows that  $r_{max}$  significantly increases when sync frames are used. Due to the fact that PNC  $v$  is expected to experience the highest amount of interference,  $r_{max}$  can be viewed as the lower bound of the guaranteed transmission distance within a piconet.

---

<sup>2</sup>All the devices are assumed as PNC-capable devices.

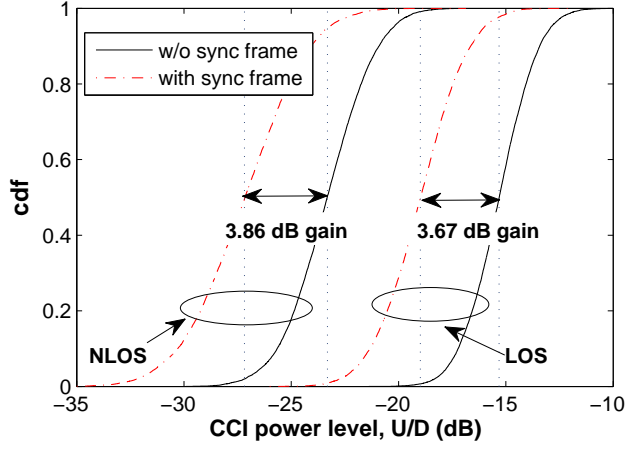


**Figure 6.9:** Interference level and achievable throughput, the same parameter specification as Figure 6.5, moreover,  $N = 100$ ,  $n_i = 2.7$ ,  $r_m = 0.8$  m,  $t_o = 2.5$   $\mu$ s,  $l=2048$  bytes,  $S_{BW} = 1728$  MHz.

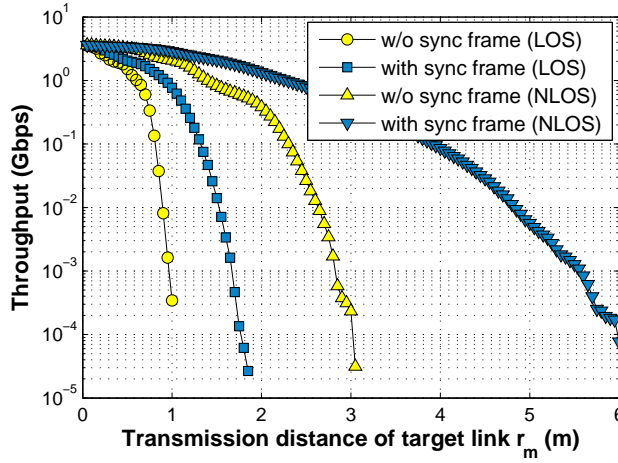


**Figure 6.10:** Transmission distance of the target link and achievable throughput, the same parameter specification as Figure 6.9.



### Impact of Beacon Range

Every PNC should protect its devices from the interference caused by the other piconets. Intuitively, a bigger beacon/sync frame range can provide better protection of the link quality of the target transmission pair. However, to achieve a longer beacon range, it normally requires a higher transmission power or to use a MCS that provides lower data rate. A longer beacon range also results in fewer coexisting piconets within a certain area, which leads to the decrease of the entire network throughput. Moreover, the devices that are on the edge of the beacon range may not have enough link margin to communicate with the PNC using high data rates. Hence, the beacon range can not be increased blindly. It is important to know what the appropriate beacon range is. This aspect will be examined in the following studies.

The impact of the beacon range is shown in Figure 6.11 with and without using sync frames. The target transmission distance is fixed at 0.8 m, and the beacon range is varied from 6 m to 15 m. To show the influence of the node density, the number of nodes within the entire network is varied from 50 to 110 in each subplot. Figure 6.11 (a) depicts the achievable throughput at the target link, which is denoted as  $C_{target}$  (Gbps) in subplot (a). The plots with using sync frames exhibit better performance than the plots without using sync frames, which also indicates that, using sync frames, a smaller beacon/sync frame range is required to achieve the same  $C_{target}$  as that without using sync frames. Within subplot (a), it is also observed that, the achieved  $C_{target}$  without using sync frames is increased with the increase of the node density. In comparison,  $C_{target}$  obtained using sync frames does not simply decrease with the increase in the node density. This is because when the node density is increased, the number of relaying devices in a single piconet is also increased. It leads to a bigger coverage range of a piconet, which could help to push the interfering sources farther. To provide a better understanding of this phenomenon, the averaged interfering distance and the number of interfering sources are plotted in subplot (b) and (c). The distance between each interfering source  $i$  and the target receiver PNC  $v$  is denoted as  $r_i$ . The averaged interfering distance is defined as  $\bar{r} = \frac{1}{n} \sum_{i=1}^n r_i$ , where  $n$  is the number of the interfering sources. As shown in subplot (b) and (c),  $\bar{r}$  is increased with the increase in the beacon range, but  $n$  is decreased with increase in the beacon range. It is interesting to observe that for a certain beacon range,  $\bar{r}$  and  $n$  are both increased with the increase in the node density, which means when node density is high, more piconets can be generated within a certain area and the average distance between the interfering source and the target receiver becomes longer. What should be noticed is,  $\bar{r}$  and  $n$  have an opposite impact on  $C_{target}$ . When  $n$  is fixed, a bigger  $\bar{r}$  means a smaller CCI which results in a bigger  $C_{target}$ . If  $\bar{r}$  is fixed, a bigger  $n$  means a higher amount of CCI which results in a smaller  $C_{target}$ . As shown in subplot (c), another interesting observation is, with using sync frames, the number of interfering sources is not sensitive to the changes of the node density, especially when the beacon range is longer than 9 m.

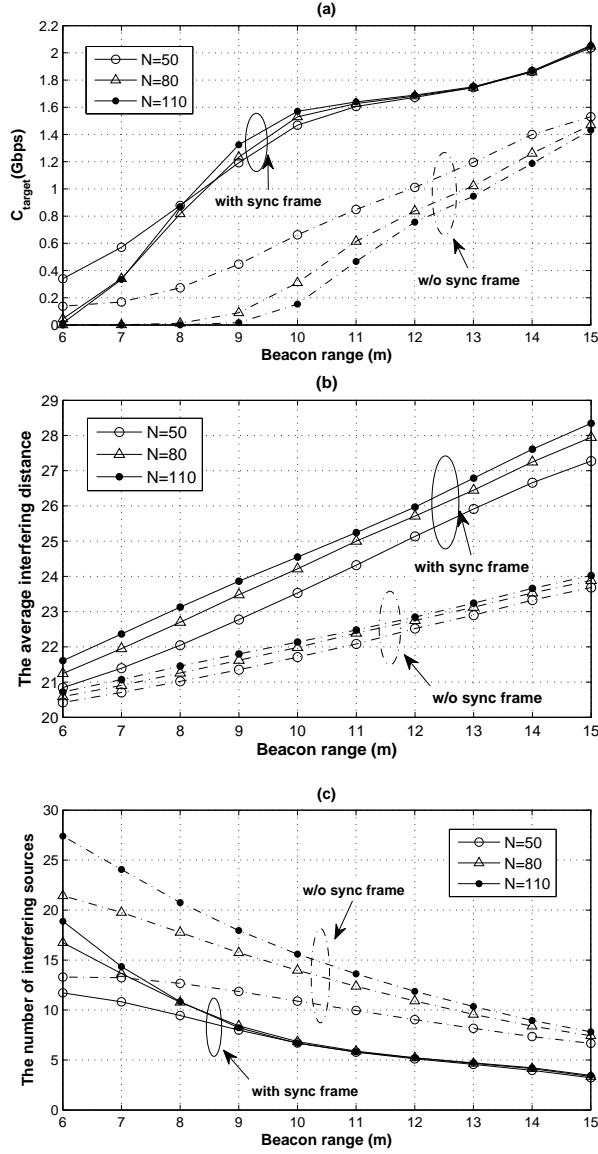


**Figure 6.11:** Node density influence on the target transmission pair capacity, with  $R = 30$  m,  $r_m = 0.8$  m, LOS.

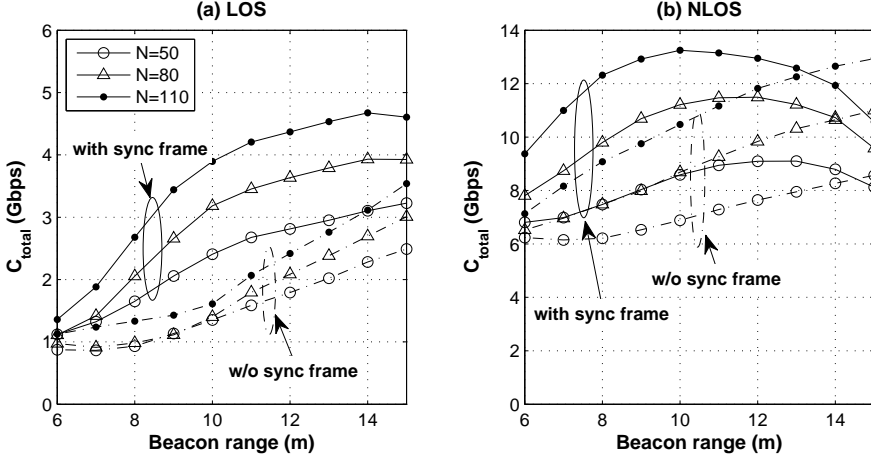


**Figure 6.12:** The entire system capacity comparison between LOS and NLOS channel models,  $R = 30$  m,  $r_m = 0.8$  m.

In comparison, the node density has a bigger impact for the plots without using sync frames. Therefore, coming back to subplot (a), for the plots without using sync frames,  $C_{target}$  is decreased with increase in the node density, which indicates that  $n$  dominates the changes of  $C_{target}$ . For the plots with using sync frames,  $C_{target}$  is affected by  $n$  when the beacon range is shorter than 9 m. When the beacon range is longer than 9 m,  $n$  does not vary with change in the node density, hence  $C_{target}$  is mainly influenced by  $\bar{r}$ . Therefore, on the contrary without using sync frames,  $C_{target}$  is increased with increase in the node density.

Figure 6.12 depicts the capacity of the entire network, with and without using sync frames. To demonstrate the channel model impact on the system capacity, it is assumed that the communication within a piconet is always LOS, but the channel model among the piconets can be LOS or NLOS, which are depicted in subplot (a) and (b), respectively. It is observed that, compared to the LOS environment, the interference sources have less impact on  $C_{total}$  when they are in the NLOS environment. When sync frames are used to format the network topology, the optimized beacon ranges to achieve the highest  $C_{total}$  are observed within our simulated beacon range in both subplot (a) and (b). For instance as shown in subplot (b), for the plots with using sync frames, the optimized beacon range is 10 m when  $N = 110$ , 12 m when  $N = 80$ , and 13 m when  $N = 50$ . This is because of an increased beacon range resulting in a decreased number of coexisting piconets, which decreases the spatial reuse capability. For the plots that do not exhibit the optimized beacon range, it indicates that the increased beacon range leads to the increase of per piconet throughput, which dominates the variance of  $C_{total}$ .

For a summary, the relationships among the target transmission distance, bea-

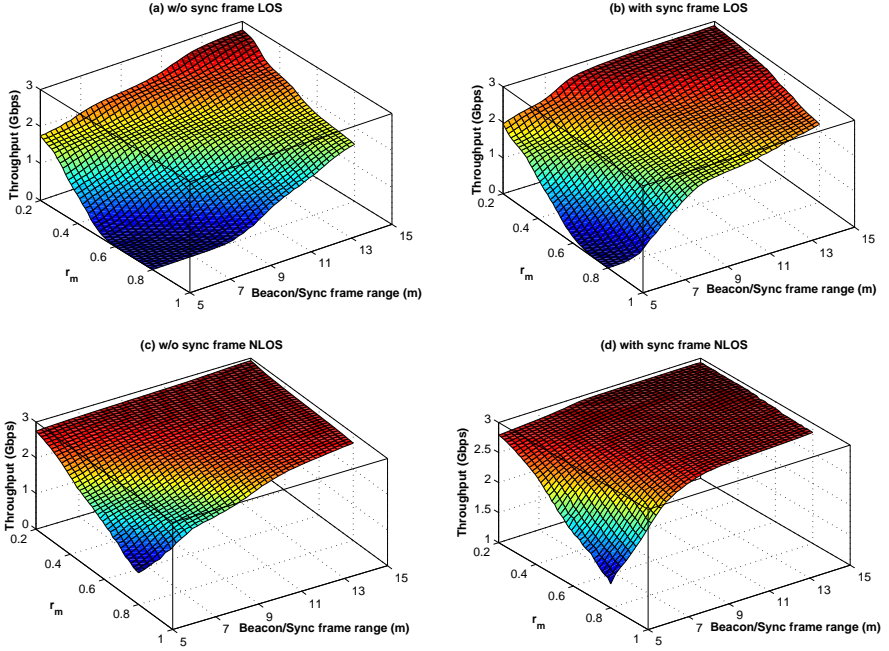


**Figure 6.13:** Relationship between the target transmission distance, beacon range and the achievable target link capacity, using sync frames, with  $R = 30$  m,  $N = 100$ .

con range, and the achievable target link capacity are depicted as 3-dimensional plots in Figure 6.13, which provides an overview of the performance of using sync frames and without using sync frames.

## 6.5 Chapter Summary

In this chapter, the effect of using synchronization (sync) frames has been investigated to mitigate Co-Channel Interference (CCI) in 60 GHz WPANs. The sync frames extend the piconet coverage range to improve the channel quality of the protected piconet. An analytical model has been provided to analyze the performance of using sync frames in terms of the interference indication function and throughput. The piconet coexistence performance has been studied in terms of the aggregated throughput of the coexisting piconets and the related beacon/sync frame range. Based on our study, it is shown that, sync frames can dramatically increase the channel quality within a WPAN. Moreover, it has been found that if beacon/sync frames range is properly selected, devices within a certain WPAN can be effectively protected from CCI, while keeping the spatial reuse capability as high as possible.

# Chapter 7

## Impact of Directional Antennas on Multi-hop Networks

“If numbers aren’t beautiful, I don’t know what is.”

- Paul Erdős

*Except for the 60 GHz system, directional antennas are also widely adopted in the other wireless telecommunication systems. Although directional antennas have certain unique advantages compared to omni-directional antennas, its deployment for communication is not a trivial issue. In Chapter 2, we have already studied the directional antennas and its characteristics for neighbor discovery processes, which is in the one-hop domain with small number of devices. Here, we are motivated to study the impact of directional antennas in a more general scenario, in which, the devices are connected via multi-hop fashion and the number of devices is relatively large.*

## 7.1 Introduction

Directional antennas are capable to provide sufficient gain for the required link budget to achieve ultra high speed communication in 60 GHz system. In Chapter 2, the performance of directional neighbor discovery processes have been discussed. Chapter 3 has presented how to support directional transmission within an IEEE 802.15.3 based WPAN. These are the issues referring only to the one-hop communication. This chapter is motivated to investigate the use of directional antennas in multi-hop networks. Multi-hop communication is a wide research area. It is difficult to cover all the details. Hence two aspects are selected to reveal the impact of using directional antennas in multi-hop networks.

### Neighbor Attachment Policy

During a neighbor discovery process, devices discover and link with their one-hop neighbors to form a connected network. However, due to the physical factor constraints, for instance long transmission distance or low channel quality, not all the neighbors are suitable for direct communication. Certain neighbor attachment strategies can be followed to limit the number of carefully selected neighbors. Because interference has a direct impact on the capacity of a network, we begin with the effect of neighbor attachment policies on the interference in ad-hoc networks, with and without using directional antennas. A neighbor attachment mechanism in ad-hoc networks directly affects the link-layer network topology. By adjusting some controllable parameters, such as transmission power and antenna direction, different topologies can be formed. A properly designed topology can reduce power consumption, remove low quality links and improve routing efficiency in a multi-hop network. Especially some innovative physical layer techniques, like antenna beam-forming, introduce new possibilities for neighbor attachment. With using high-gain directional antennas, more neighbors can be detected in a specific direction, while at the same time the interference with nodes outside the main antenna lobes is reduced. The state-of-the-art literature related to topology control focuses mainly on life-time extension, hop-count reduction, or performance optimization (e.g. [81]), without taking into account effects of neighbor attachment on the amount of interference experienced in the network. The aim of this chapter is to fill this knowledge gap by comparing four widely used neighbor attachment policies based on their interference imprint. Consequently, the suitability of each neighbor attachment policy is identified in this chapter to support different types of applications in ad-hoc networks.

### Probabilistic-based Message Dissemination

Compared to omni-directional antennas, directional antennas can use the transmission power more efficiently by concentrating the energy on a certain direction and nullifying the interference from other directions. However, using directional

antennas for broadcasting is a problematic issue, because a node should sweep a packet in all the possible directions. The generated redundant overhead may impact on the network performance. To alleviate this problem, the second aspect that will be investigated in this chapter is probabilistic-based message dissemination within multi-hop networks using directional antennas. In [82], the authors proposed a relay node selection mechanism to reduce broadcasting overhead, which defines that only the farthest neighbor in a certain direction forwards broadcasting packets. However, their work assumed a preliminary neighbor discovery process, so each node knows if it is the farthest neighbor of the node from which it receives the packets. In [31], the authors investigated directional routing protocols in ad-hoc networks. To reduce routing overhead, they proposed to avoid forwarding route request in the direction where the channel is busy. In [83], Shen *et al.* discussed a probabilistic-based approach for directional message forwarding, but in a simple way. Compared to the related work, our work has the following contributions:

- Multiple probabilistic-based message dissemination mechanisms are investigated based on various network graphs: random graph, lattice graph and random geometric graph.
- The message dissemination performance is provided for using different combinations of the transceiver antenna mode and variant antenna beamwidth. The appropriate antenna beamwidth range for using different antenna modes is examined in this work.
- Several directional probabilistic-based extension schemes are discussed and compared to each other. It is shown that a combination of two optimization mechanisms could further enhance the message dissemination performance.

To the best of our knowledge, this is the first time that directional antennas are comprehensively evaluated in probabilistic-based broadcasting protocols.

## 7.2 Neighbor Attachment using Directional Antennas

To position our research, firstly, an overview of the main approaches that have been investigated to study interference in ad-hoc networks is provided. In [84] authors have looked at the impact of interference on the connectivity properties of a dense network with random deployment of nodes. This line of work is pushed forward in [85] where authors discussed the effect of interference on the link quality and connectivity of large networks. Although much attention is given to the connectivity problem in ad-hoc networks, the impact of the interference on the capacity are discussed only by approximation. Also, in the calculation of interference in [85], the dependency of interference on the location of nodes inside the network is not considered. In [86] authors presented an approach to preserve network connectivity based on the principle of maintaining the number

of physical neighbors of every node equal to or slightly below a specific threshold value. They show that the interference remains bounded under this approach. Here we show that the interference always remains bounded in ad-hoc networks regardless of the node degree. This finding matches with previously found results in [87]. In [88], authors gave algorithms to construct a network topology for wireless ad-hoc networks, but the link interference in the resulted topology is either minimized or approximately minimized. To minimize the interference, many researches (e.g. [89]) have suggested the construction of topologies that require low transmission power. However, it is shown that minimizing interference on the link level is not the sufficient condition to guarantee maximum Signal-to-Interference ratio (SIR), and consequently maximum capacity. In summary, topology control policies published so far do not take into account the amount of the interference experienced in the network in a realistic manner. Due to the impact of interference on channel capacity, without proper interference estimation, the capacity calculation methods provided in the literature lack accuracy as well.

### 7.2.1 Neighbor Attachment Policies

The neighbor attachment policies considered in this chapter are described briefly here.

**Policy 1:** Nodes are equipped with omni-directional antennas. Any node considers all other nodes within its maximum transmission range (its coverage area) as its neighbors.

**Policy 2:** Nodes are equipped with directional antennas with beamwidth  $\alpha$ . Each node sweeps its surroundings sector by sector, and establishes neighboring relations with all nodes that are discovered in this way. Considering additional gain of the directional antennas in comparison to omni-directional antennas, this policy generally results into more discovered neighbors (at farther distances) than the first policy.

**Policy 3:** Nodes are equipped with omni-directional antennas. All nodes run a local algorithm to construct a Minimum Spanning Tree (MST) [90]. Each node links only its adjacent nodes on the MST as its neighbors.

**Policy 4:** This policy uses omni-directional antennas, together with an angular parameter  $\alpha$  to select neighbors [91]. The neighbor selection process consists of two phases. In the first phase each node, e.g. node  $u$ , increases its transmission power gradually to find the closest neighbors one by one. New neighbors are added until there is at least one neighbor in any cone of angle  $\alpha$  centered at node  $u$ , or the maximum transmission power has been reached. Phase one may produce a considerably higher number of neighbors than the number of neighbors that are strictly required for network connectivity. Therefore, in the second phase of neighbor selection some links are pruned.



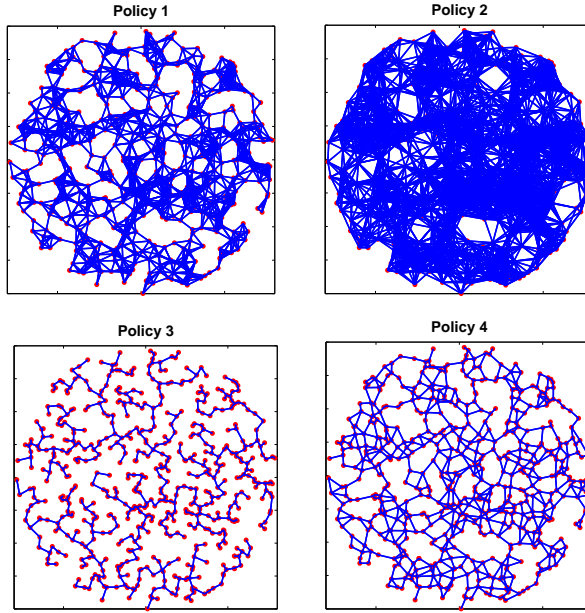


**Figure 7.1:** Example of link-layer network topology for the considered neighbor attachment policies, with 600 nodes uniformly distributed over a circular area of normalized radius 8. Here  $\eta=4.0$  and  $\alpha = 60^\circ$  (for policies 2 and 4).

Assume that node  $u$  has two neighbors  $v$  and  $w$ . Node  $w$  will be removed from the neighbor list of node  $u$  if the power required to send a packet from  $u$  to  $w$  directly is more than the power required to send the packet from  $u$  to  $w$  via  $v$ .

For the connection between nodes a simple path loss propagation model is assumed in which the received signal power at distance  $d$  is proportional to  $d^{-\eta}$ , where  $\eta$  is the path loss exponent. This assumption results in a circular coverage area of radius  $r$  around each node with an omni-directional antenna. Let  $P$  be the power received at distance  $r$ . In other words,  $P$  is the minimum required power for correct reception of signals. For convenience in notation and ease of interpretation, all the distances used in this chapter is normalized to  $r$  and all powers to  $P$ . Figure 7.1 shows an example of the network topologies obtained for each of the neighbor attachment policies described above in a network consisting of 600 nodes which are uniformly distributed over a circular area of normalized radius 8. This figure clearly shows the impact of neighbor attachment policies on the resulting network topologies. The number of links and the average number of neighbors per node (called mean degree) are strongly affected by the attachment policies. In Section 7.2.2 it will be shown that how these variations affect the

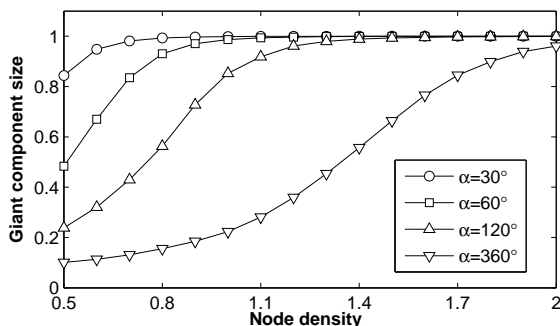


**Figure 7.2:** The relationship between the giant component size and the node density, for different antenna beamwidths. Each point in this figure is the mean value taken over 1500 independent simulation runs when the corresponding numbers of nodes are uniformly distributed over a circular area of normalized radius 8.

experienced interference in the network.

Here a few words are spent to briefly describe the impact of using directional antennas on the network topology and network connectivity characteristics. This brief description will help to interpret the results provided in Section 7.2.2. As the antenna beamwidth reduces, the directional antenna gain usually increases. This increased gain would mean that the nodes at farther distances could become neighbors. Consequently, this effect can increase the link density, the mean degree, and improve the network connectivity. Figure 7.2 shows an example of the influence of antenna beamwidth on network connectivity. In this figure the giant component size [77] is used as an indicator for connectivity in the network. The largest connected cluster in a network of nodes spread over a certain geographical area is called the giant component. Giant component size is the fraction of nodes in the network that are connected to each other in single-hop or multi-hop fashion. Obviously, when the giant component size is 1, the entire network is connected. Figure 7.2 is obtained through simulation and it shows how full connectivity can be reached at lower node densities when directional antennas with narrow beamwidths are used.

## 7.2.2 Impact on Interference

### Interference and Capacity

In the previous chapter, the relation between interference and system capacity is reviewed based on a certain PHY layer and channel model. In this section, a more general relationship between interference and capacity is discussed here. Signal to Interference ratio (SIR), which is also known as carrier-to-interference ratio (C/I), is defined as the ratio between the power of wanted signal to the power of sum of interfering signals. In radio communication, the capacity of the networks

can be directly linked to the expected value of SIR using the Shannon channel capacity formula [92] to obtain an upper bound of the capacity:

$$W = B \log_2(1 + E[\text{SIR}]), \quad (7.1)$$

where  $B$  is the channel bandwidth (in Hz) and  $E[\text{SIR}]$  is the expected signal to interference ratio.  $W$  (in bits per second) indicates the upper bound on the capacity of the wireless channel. When the expected value of SIR decreases, the capacity of the link between two nodes decreases as well.

### Simulation Model

There are  $N$  nodes randomly but uniformly distributed within a circular area. The topology imposed by the neighbor attachment policy will be used to send packets along the shortest path in multi-hop fashion between any two nodes in the network. The interference situation does not need to be the same for all nodes in the network. A receiving node in the center of the area is used as the target node for investigation, which can be expected to experience the highest amount of interference in the network. CSMA/CA with reservation is considered at the MAC layer. Whenever a transmission link is established between a source node, and a neighboring destination node, the MAC protocol will prohibit a portion of nearby nodes in the network from simultaneous transmission. At any instant of time, assuming that all nodes always have data to be transmitted to any other node, only  $n$  nodes obtain access to the medium. In other words,  $n$  is the number of transmission pairs that can be formed simultaneously in the network. The fraction of the nodes that gain access to the medium at any time interval in the entire network is then  $n/N$ , which is also called as interfering node density in the following of study.

### Simulation Results

In this section the simulation results are presented regarding the amount of interference caused by deploying each neighbor attachment policy in a network of randomly but uniformly distributed nodes. The question addressed here is whether any of the considered neighbor attachment policies has significant advantage or disadvantage in terms of experienced interference in the network. This point is investigated with power control as well as without power control. In the former case, each packet is transmitted with the minimum required power to be received correctly by the intended neighboring node. In the latter case, all packets are transmitted with maximum power. Figure 7.3 summarizes our results, which indicates the relationship among interfering node density, expected interference power and expected SIR for each neighbor attachment policy. All results presented in the subplots of Figure 7.3 correspond to the networks formed by a circular area of normalized radius 8. The node densities vary from 1 to 8, which correspond roughly to networks of 200 to 1600 nodes. Each point presented in this figure

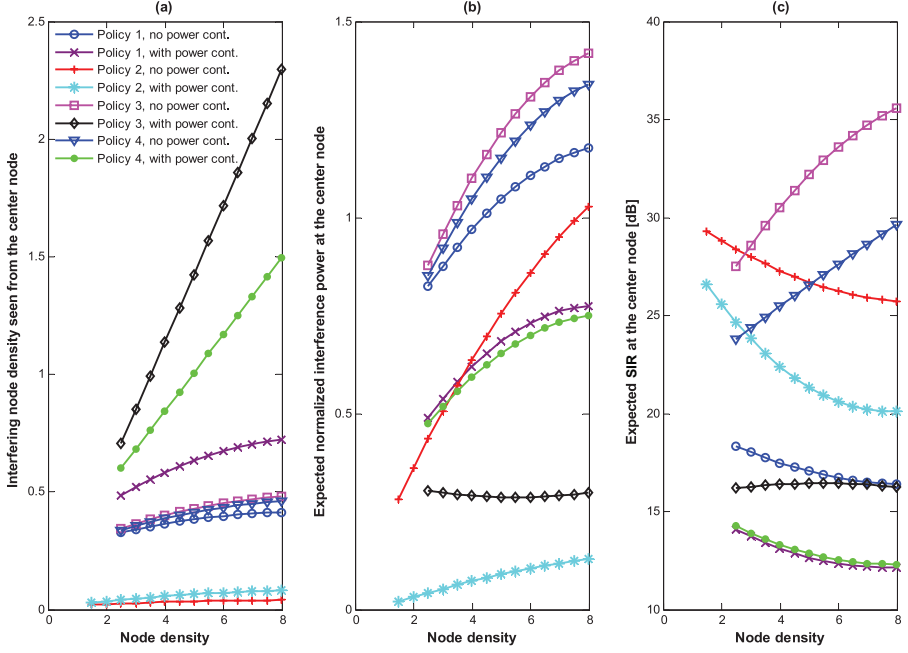


**Figure 7.3:** *Interfering node density, normalized interference power, and SIR as function of the node density for a node in the center of a circular area of normalized radius 8. Each point is the expected value taken over 1500 independent simulation runs of the corresponding configuration. Assumed is: CSMA/CA with reservation at the MAC layer,  $\eta=4.0$ ,  $\alpha = 60^\circ$  for policies 2 and 4, and 10.4 dB processing gain in plot (c).*

is found by taking the expected value over 1500 different network configurations. Subplot (a) in Figure 7.3 shows the interfering node density seen from the center node. In subplot (b) the aggregate interference power has been computed at the center node, assuming the path loss propagation model with  $\eta = 4.0$ . The interference power here is normalized to  $P$ , the minimum required power for correct reception of radio signals. Subplot (c) shows the expected SIR for the center node, when this node receives a packet from one of its randomly chosen neighbors. In calculation of SIR, a processing gain of 11 (10.4 dB) [45, 77] is assumed.

Based on Figure 7.3, several interesting properties have been observed. First, for all the policies without using power control, the interfering node density tends to level-off towards an upper limit independent of the node density. This is due to the function of the MAC protocol. The portion of area that is occupied by a transmission pair is directly related to the size of the coverage radius of a node, which is a fixed value in case of no power control. When the density of nodes increases, more nodes will fall within the prohibited transmission areas. As a result, the density of interfering nodes is not expected to increase linearly with

the increase of the node density. Second, for all policies with power control, the density of the interfering nodes tends to increase linearly with the increase of the node density. This is again related to the working of the MAC protocol. In contrast to the case when no power control is used, the size of the prohibited transmission area for each source-destination pair tends to decrease at high node densities; allowing room for higher density of interfering nodes. Third, a high density of the interfering nodes does not necessarily mean high interference power. For example, policy 3 with power control results in the highest interfering node density, while it produces relatively low interference power (see subplots (a) and (b)). Fourth, all scenarios produce less interference when power control is used. Also using directional antenna reduces the interference. However, a low value of interference does not always mean a high value for SIR, or the best network capacity. For example, policy 3 without power control provides the best SIR for high node densities, while it is suffering from the highest amount of interference power in comparison with other policies. It is known that in policies 3 and 4 nodes attach only to their closest neighbors. Obviously, the expected distances to the closest neighbors are reduced by increasing the node density. A consequence of this fact is the increase of the wanted signal power relative to the interference power when no power control is used. This explains the improvement of SIR for the related cases in subplot (c) of Figure 7.3. Finally, it is observed that for policies 1 and 2, with or without power control, the amount of interference is increased, and SIR is decreased by increasing node density. From all policies, policy 2 without power control provides the best SIR at low node densities. At high node densities policy 3 without power control offers the best SIR. Therefore, if maximization of SIR at the physical layer is desired, usage of power control is not preferable.

In this section, neighbor attachment influence on SIR with and without using directional antennas has been presented. In the next section, the message dissemination within multi-hop networks with using directional antennas will be addressed.

## 7.3 Probabilistic-based Directional Message Dissemination

Gossiping is a well-known probabilistic mechanism for information dissemination within communication networks. Using the gossiping approach, each node in the network forwards packets with a pre-specified probability  $p$ , which is called as *gossiping probability*, or has a probability  $1 - p$  to discard it. Compared to flooding, it is a simple alternative to mitigate the amount of generated overhead, which is termed as *broadcast storm problem* [93]. Hence, gossiping is more efficient and scalable than flooding. Gossiping is widely used to facilitate routing protocols and optimize broadcasting process in ad-hoc networks. Extensive work has been done on this topic, e.g. [93–98]. In [94], Haas *et al.* has presented GOSSIP, which introduces a parameter  $k$  to tune the gossiping probability. They define that all

the nodes located within  $k$  hops from the source node always forward packets with probability 1. In [95], Kyasanur *et al.* proposed a gossip-based protocol which automatically adapts gossiping probability according to the network topology. Cartigny and Simplot [98] combined the forwarding probability with distance information to let a gossiping process to be aware of the network density. All the work mentioned above is based on omni-directional antennas. Therefore, this section is devoted to study the gossiping based protocol using directional antennas.

### 7.3.1 Preliminaries

#### Percolation Theory and Phase Transition Phenomenon

Percolation theory is used to model the behavior of a random medium. Considering the medium as a number of nodes in a network, percolation probability  $\xi(p)$  is defined as the probability that a given node belongs to an infinite cluster. There exists a critical threshold  $p_c$  for gossiping probability  $p$  [99]. If the gossiping probability is larger than  $p_c$ , it is almost sure to guarantee the dissemination of information in the entire network, such that

$$\xi(p) \begin{cases} = 0 & \text{if } p < p_c, \\ > 0 & \text{if } p > p_c. \end{cases} \quad (7.2)$$

This phenomenon is termed as *bimodal* or *phase transition* behavior in percolation theory [96,99]. This phenomenon is also observed from gossip-based protocols [94]. In [83], the authors declared that if the network is sufficiently large, the gossiping probability  $p$  of omni-directional and directional broadcasts over a network are the same as the percolation threshold of *site percolation*. The explicit expression of the percolation probability is hard to get. It varies according to the network topology, but approximations can be obtained via simulation. For instance in [94], the author illustrated the transition threshold of gossiping probability for omni-directional broadcasting. In this work, the bimodal behavior is indicated using different transmission and reception antenna modes.

#### Graph Type

Three types of graphs are used in this work, which are shown in Figure 7.4.

- Random graph (T1)

A random graph  $G_{p_r}(N)$ , consists of  $N$  nodes, in which each link between two nodes is chosen independently and with probability  $p_r$ . The existence of a link in a random graph does not depend on the position of the transmission pairs. Therefore, a node's position within the network does not influence the network connectivity. In order to demonstrate the directional gossiping protocols on a random graph,  $N$  nodes are randomly generated and they are uniformly distributed in a circular network with radius  $R$ . Each node selects its neighbors from

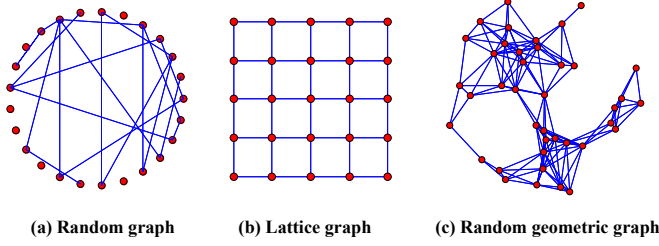


**Figure 7.4:** *Graph type illustrations.*

the  $N - 1$  nodes with a probability  $p_r$ . The mean node degree in random graph is calculated as  $E[d] = (N - 1) \cdot p_r$ .

- Lattice graph (T2)

Lattice graph is also known as square grid graph. A  $5 \times 5$  lattice graph is shown in Figure 7.4 (b), in which nodes are deployed as square grid.

- Random geometric graph (T3)

Random geometric graph  $G_{p_{ij}}(N)$  could be considered as a variation of the random graph, in which a link exists according to a variable probability  $p_{ij}$  instead of a fixed probability  $p_r$ . Random geometric graph is a good model for ad-hoc wireless networks, because the probability of the existence of a link can be specified by the radio propagation model. For simplicity, we define that a node  $i$  has probability 1 to connect to the neighbors within its transmission range  $d$ ,

$$p_{ij} \begin{cases} = 1 & \text{if } \|i - j\| \leq d, \\ = 0 & \text{if } \|i - j\| > d. \end{cases} \quad (7.3)$$

where,  $\|i - j\|$  represents the Euclidean distance between node  $i$  and  $j$ . To construct a random geometric graph,  $N$  nodes are uniformly distributed over a circular area with radius  $R$ . Each node links with all the other nodes within its transmission range.

### Antenna Mode

For directional antenna systems, two operating modes, omni-directional mode and directional mode, can be used for transmitting and receiving. When different antenna modes are applied in a neighbor discovery process, devices can have different neighborhood relationship as explained in Table 3.2. To investigate the performance of message dissemination using directional antennas, the same as in Section 2.2, two antenna modes are used to characterize the employed transceiver: directional transmitting and omni-directional listening (D-O) mode and directional transmitting and directional listening (D-D) mode. Considering a flat-top

pattern directional antenna, the antenna gain is obtained as,  $G = 10 \log(2\pi/\theta)$  (unit: dB), where  $\theta$  is the antenna beamwidth.

### Performance Metrics

In this work, the performance of various gossiping schemes is examined based on the following metrics.

- Giant component size (GCS): GCS indicates the connectivity of a network, which is introduced in Section 7.2.1.
- Overhead: Overhead refers to the total number of generated packets in one run of simulation<sup>1</sup>. The amount of overhead indicates the efficiency of a gossiping protocol.
- Path length: During the gossiping process, the messages are transmitted from the source and disseminated to the rest of the network via different routes. The path length refers to the hop count of the longest path in the network, which could represent the latency of the gossiping process.
- Delivery ratio: We denote  $\Pr[A_N(L)]$  as the delivery ratio, which represents the probability that all the nodes within the network are informed when the path length is  $L$ .  $\Pr[A_N(L)]$  could be considered as the percolation probability in a network with a finite size.

### Assumptions

1. To achieve a homogeneous gossiping environment, the source is located at the center of the network when the random geometric graph and lattice graph are used. For random graph and random geometric graph, all the nodes are uniformly distributed within the network.
2. During the gossiping process, a node could receive multiple messages from different routes. A node only reacts to the first received packet, and simply discards all the packets after the first one.
3. All the constructed networks are completely connected. Moreover, a perfect medium access is assumed to eliminate the MAC layer influence. We consider that the network is at the initialization phase, so a node has no information about its surrounding neighbors.
4. All the simulation results are averaged based on 1000 iterations.

---

<sup>1</sup>We define one run of simulation as the period from the moment that the first packet is transmitted from the source till the gossiping process dies out or the entire network is informed.



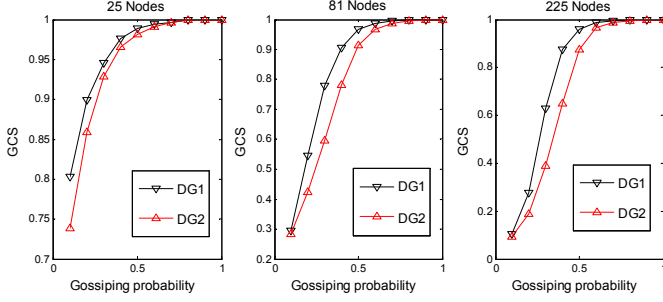


**Figure 7.5:** Performance comparison between DG1 and DG2 in variant size of networks,  $\theta = 90^\circ$ , D-O mode.

### 7.3.2 Gossiping Using Directional Antennas

The original gossiping protocol defines that after a node receives a packet, it has a probability  $p$  to forward the packet, or has a probability  $1-p$  to discard the packet. When directional antennas are used, the azimuth plane of a node is divided into  $N_B$  beam sectors, where  $N_B = 2\pi/\theta$ . According to different forwarding manners, two basic Directional Gossiping (DG) mechanisms are defined here: (a) per-sector based DG and (b) per-node based DG.

- Per-sector based DG (DG1): After a node receives a packet, it generates a probability  $p_i$  for each beam sector, where  $i \in [1, N_B]$ . A packet is forwarded from beam sector  $i$ , if  $p_i < p$ .
- Per-node based DG (DG2): After a node receives a packet, it only generates one probability  $p_v$ . If  $p_v < p$ , it forwards a packet in each beam sector. Otherwise, it does not forward it at all.

In order to guarantee that there are packets sent out from the source, the source has probability 1 to transmit from each beam sector.

#### DG Mechanism Comparison

The performance of DG1 and DG2 in a random geometric graph is examined. Nodes use directional antennas for transmitting and omni-directional antenna for receiving or listening. The mean network density is kept around 10.5, and scale up the total number of nodes from 25 to 225. The simulation results are shown in Figure 7.5. In general, DG1 exhibits a higher GCS than DG2, which means DG1 can inform more nodes in one execution of gossiping process. Therefore, DG1 is more reliable than DG2. In the following simulation, only DG1 is used to examine the directional gossiping performance.

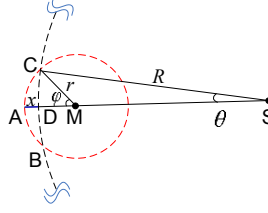


**Figure 7.6:** *The illustration of the border effect.*

### Network Graph Influence

In this section, the performance of the directional gossiping process is evaluated in several network graphs. To compare different network graphs, the node degree is used as the guide line. Node degree refers to the number of direct neighbors of that node in the network. Therefore, each type of network is formed with the same or similar mean node degree for performance comparison. In a large scale network, the mean node degree can be simply approximated as  $(N \left(\frac{r_\theta}{R}\right)^2 - 1)$ , where  $r_\theta$  is the normalized transmission range using directional antenna with beamwidth  $\theta$ ,  $N$  is the total number of nodes in the network, and  $R$  is the normalized radius of the circular network. When the network radius  $R$  is not large enough, the border effect should be taken into consideration and the mean node degree is approximated as:

$$E[d] \approx \left( \int_0^{R-r_\theta} f(x)dx + \int_{R-r_\theta}^R \phi(r_\theta + x - R)f(x)dx \right) \times \left[ N \left( \frac{r_\theta}{R} \right)^2 - 1 \right], \quad (7.4)$$

where  $f(x)$  is the position probability density functions of the node, and  $f(x) = 2x/R^2$ . Function  $\phi(\cdot)$  represents the proportion of the effective coverage area of a node at the network border area. As shown in Figure 7.6, if a node is located at  $M$  and the coverage range of this node is denoted as circle  $M$  with radius  $r$ . This node is at the border area of a circular network  $S$  with radius  $R$ . Circle  $M$  and  $S$  intersect at point  $B$  and  $C$ . Line  $MS$  intersects with Circle  $M$  and  $S$  at point  $A$  and  $D$ , respectively. As indicated in the figure,  $\|AD\| = x$ ,  $\|DM\| = r - x$ , and  $\|MS\| = R - r + x$ , where  $x \in (0, r]$  and the norm represents the Euclidean norm. Moreover,  $\|CD\| = d$  and  $\angle AMC = \varphi$ , where,

$$\begin{aligned} \varphi &= \arccos \left( \frac{r^2 + (r-x)^2 - d^2}{2r(r-x)} \right) \\ d &= \left( 2R^2 - 2R^2 \left( 1 - \frac{2rx - x^2}{2R(R-r+x)} \right) \right)^{\frac{1}{2}} \end{aligned} \quad (7.5)$$

The intersection area of Circle  $M$  and  $S$  is calculated as

$$S_{SM}(x) \approx r^2(\pi - \varphi) + (r - x)r \sin(\varphi) \quad (7.6)$$

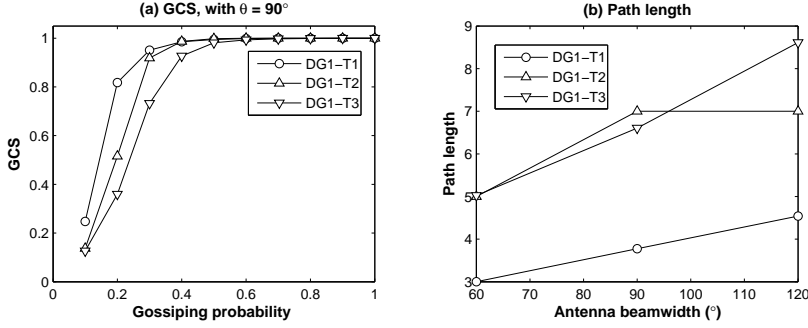


**Figure 7.7:** Network graph influence on directional gossiping performance, based on *D-O* mode,  $N = 225$ ,  $R = 8.36$ .

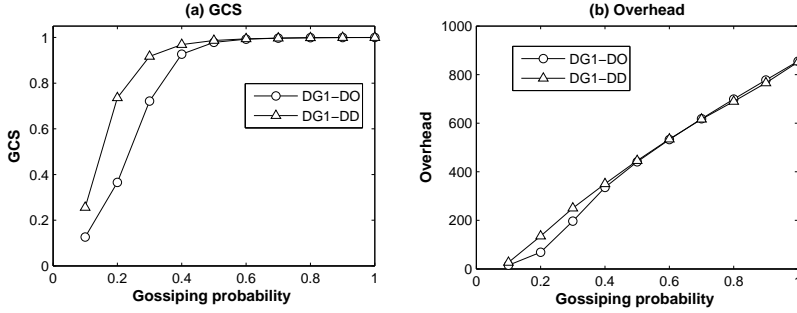


**Figure 7.8:** Transceiver mode impact on the directional gossiping performance in random geometric graph,  $N = 225$ ,  $R = 8.36$ , and  $\theta = 90^\circ$ .

Therefore, the proportion of the effective coverage range of the node is given by  $\phi(x) = S_{SM}(x)/(\pi r^2)$ . Therefore,

$$\phi(d) \approx \left(1 - \frac{\varphi}{\pi}\right) + \frac{1}{\pi} \left(1 - \frac{d}{r_\theta}\right) \sin(\varphi). \quad (7.7)$$

In a lattice graph, the distances between the adjacent nodes are 1. While using  $90^\circ$  directional antennas, the mean node degree is 10.68 for lattice graph, which is measured from the simulation. For the random geometric graph, the network radius is set to 8.36 to get similar mean node degree as the lattice graph using  $90^\circ$  directional antennas, in which the mean node degree is 10.69 according to (7.4). For random graph, the link selection probability  $p_r$  is set to 0.0477. According to the above setting, the influence of the network graph on the directional gossiping performance is illustrated as shown in Figure 7.7. In Figure 7.7 (a), the GCS values using DG1 are compared in different network graphs with  $90^\circ$  directional antenna. In Figure 7.7 (b), the gossiping probability is set to 1 and the path length

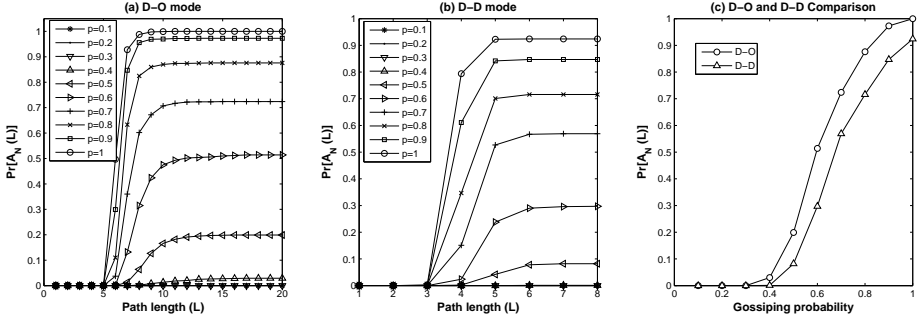


**Figure 7.9:** Influence of the gossiping probability on the probability that all the nodes within the network are informed, with  $N = 225$ ,  $R = 8.36$ , and  $\theta = 90^\circ$ .

performance is obtained as a function of antenna beamwidth. The DG1 algorithm in random graph exhibits the highest GCS and the shortest path length. That is because, in random graph, the connection between any two nodes depends on the link selection probability  $p_r$ . Therefore, the possibility for a node to be reached by the source is independent of the position of the node. In the random geometric graph, the distance between a node and the source influences the latency that the node is informed. For instance, if a node is far away from the source, it has to wait until the packet reaches the node via multiple relaying nodes. Therefore, the message dissemination speed is faster in random graph than in random geometric graph. The performance of DG1 in the lattice graph is in between the other two graphs.

### Transceiver Antenna Mode Influence

Directional broadcasting is not as efficient as omni-directional broadcasting, since a node duplicates a broadcasting packet and transmits one in each beam sector in directional broadcasting. However, the directional antennas can achieve longer transmission range, and hence more neighbors could be covered by one round of sweeping. The performance using different transceiver antenna modes (D-O and D-D) is demonstrated in Figure 7.8. D-O and D-D induce similar amount of overhead in the gossiping progress, but using D-D mode achieves higher GCS compared to D-O mode, especially when the gossiping probability is low. That is because the gossiping performance can be compensated by the increase in the transmission range although D-D mode limits the transmitting and the receiving directions.

Figure 7.9 (a) depicts the relationship between the gossiping probability, the resultant path length and the delivery ratio using DG1. From this figure it can be observed that, to achieve the same delivery ratio  $\Pr[A_N(L)]$ , a lower gossiping probability leads to a longer path length. When the gossiping probability is lower

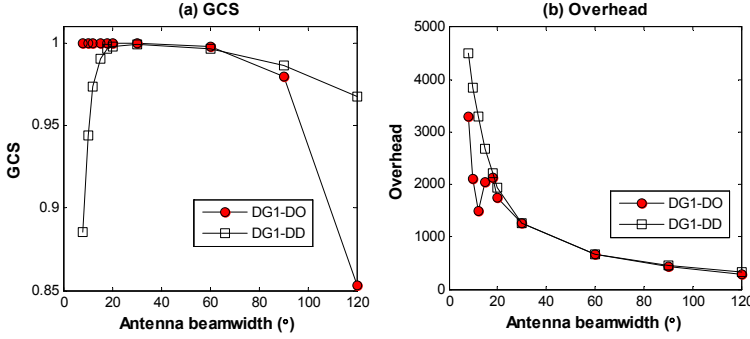


**Figure 7.10:** Performance comparison between D-O mode and D-D mode with variant antenna beamwidth, gossiping probability  $p$  is 0.5,  $N = 225$ ,  $R = 8.36$ .

than 0.3, the network cannot be totally covered at all, which verifies the bimodal behavior of the directional gossiping process. In contrast to Figure 7.9 (a), the resultant path length and the delivery ratio using D-D mode with varying gossiping probabilities is plotted in Figure 7.9 (b). From this figure we can observe that, compared to D-O mode, using D-D mode for directional gossiping results in shorter path length. Similar to D-O mode, when the gossiping probability is lower than 0.4, the network cannot be totally informed at all, which also validates the bimodal behavior of the directional gossiping performance in D-D mode. Figure 7.8 indicates that, using D-D mode could achieve higher GCS than using D-O mode, especially when the gossiping probability is low. However, an interesting observation from Figure 7.9 is that, the probability  $\Pr[A_N(L)]$  measured using D-D mode is lower than using D-O mode. For instance, when the gossiping probability  $p = 1$ , the probability to fully inform the network is only 92.4% using D-D mode. In contrast, D-O mode can fully inform the network with probability 100%. Therefore, we can conclude that, compared to D-O mode, using D-D mode has a faster message dissemination speed and fair message coverage capability, but it is difficult for D-D mode to completely cover the entire network, which means, when the gossiping probability is high, the resultant GCS using D-D mode could be quite close to 100% but difficult to reach 100%.

To better illustrate the phase transition behavior, the results for  $\Pr[A_N(L)]$  of the longest path length using D-O mode and D-D mode are plotted in Figure 7.9 (c), which confirms the critical threshold  $p_c$  in the percolation theory mentioned in (7.2).

### Antenna Beamwidth Influence

The influence of antenna beamwidth on DG1 algorithm in the random geometric graph using D-O mode and D-D mode is shown in Figure 7.10 when the gossiping probability is set to 0.5. These two transceiver antenna modes behave in a

piecewise manner. When antenna beamwidth is narrow, like  $\theta < 20^\circ$ , D-O mode exhibits higher GCS than D-D mode, and also higher overhead. It should be noticed that, the lower amount of overhead using D-D mode is because of the dying out of the gossiping process other than the efficient transmission. When antenna beamwidth is within the range  $20^\circ \leq \theta \leq 60^\circ$ , using D-O mode and using D-D mode achieve similar connectivity and overhead. When antenna beamwidth is bigger than  $60^\circ$ , using D-D mode obtains better connectivity and both transceiver antenna modes have similar amount of overhead. Therefore, using D-D mode is not suitable for small antenna beamwidth. When antenna beamwidth is within a moderate range, using D-D mode is better than D-O mode, because they can use the similar amount of overhead to achieve the same connectivity, but D-D mode results in shorter path length.

### 7.3.3 Directional Gossiping Extensions

To increase the efficiency of a gossiping process, some gossiping extension ideas are proposed in the literature. In this section, two gossiping extension mechanisms are introduced based on DG1: distance and angle based optimization and  $k$ -hop based gossiping algorithm.

#### Distance and Angle based Optimization (DG3)

After receiving a packet, the distance between the transmitter and the receiver can be estimated according to the received signal strength. In [93], the authors have proposed a distance-based broadcasting optimization scheme. They proposed that, if the estimated distance is smaller than a certain distance threshold, the received packet will not be broadcasted from the receiver. This idea is extended in [83], in which the authors have declared that a node that covers a bigger range has a higher probability of forwarding. They have proposed a forwarding probability calculation method, which depends on the source-destination distance and the packet forwarding direction. In our work, this distance and angle based optimization scheme is combined with the gossiping mechanism. Therefore, each node could have different gossiping probability depending on the distance and relative direction between a node and its previous transmitter.

When a node receives a packet from beam sector  $n_r$ , based on the received signal strength, the node estimates the distance  $D$  between the transmitter and itself. This node computes a gossiping probability for each beam sector, which is a product between the basic gossiping probability and a weighting factor. The weighting factor  $w_i$  for beam sector  $n_i$  is expressed as:

$$w_i = 1 - \left( \sqrt{1 - \left( \frac{D \sin(\Delta n_i \theta)}{r_\theta} \right)^2} - \frac{D \cos(\Delta n_i \theta)}{r_\theta} \right)^2, \quad (7.8)$$

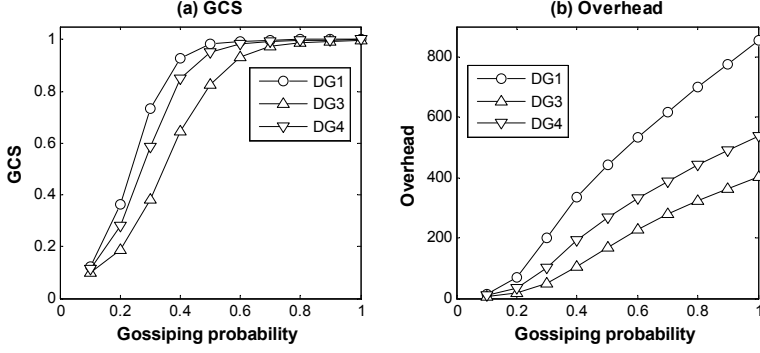


**Figure 7.11:** Performance comparison between DG3 and DG4, D-O mode,  $N = 225$ ,  $R = 8.36$ ,  $\theta = 90^\circ$ .

where  $\Delta n_i = \min[|n_i - n_r|, N_B - |n_i - n_r|]$ ,  $\Delta n_i$  is the beam sector difference between the receiving sector  $n_r$  and the forwarding sector  $n_i$ .  $r_\theta$  is the normalized transmission range. Weighting factor  $w_i$  should be a value that is bigger than 0. If the calculated value of  $w_i$  is smaller than 0,  $w_i$  is simply reset to 0. The forwarding probability is calculated as  $p_f = p \cdot w_i$ .

#### Simplified Distance and Angle based Optimization (DG4)

DG4 is a simplified version of DG3. Based on the estimated distance, a node estimates a threshold angle  $\theta_{TH}$ , where  $\theta_{TH} = \arccos\left(\frac{D}{2r_\theta}\right)$ , if the packet forwarding direction  $\theta_i$  is bigger than  $\theta_{TH}$ , the weighting factor  $w_i$  is 1, otherwise,  $w_i$  is set to 0,

$$w_i = \begin{cases} 1 & \theta_i > \theta_{TH} \\ 0 & \text{otherwise} \end{cases}, \quad (7.9)$$

where  $\theta_i = \Delta n_i \theta - \frac{1}{2} \theta$ . The forwarding probability is calculated as  $p_f = p \cdot w_i$ .

Figure 7.11 (a) and (b) show the comparison results of DG1, DG3 and DG4 in random geometric graph using D-O mode. It is observed that, DG4 achieves slightly lower GCS than DG1, but it significantly reduces the amount of overhead. For instance, when the gossiping probability is 0.7, the resultant GCSs using DG1 and DG4 are 99.72% and 99.36%, respectively. But the resultant overhead using DG4 is only 62.78% of the amount of overhead generated using DG1. DG1 performs better than DG4 and DG3 in terms of GCS. However, when the gossiping probability is high, e.g.  $p > 0.8$ , the resultant GCSs are all close to 1, but DG3 has the lowest overhead.

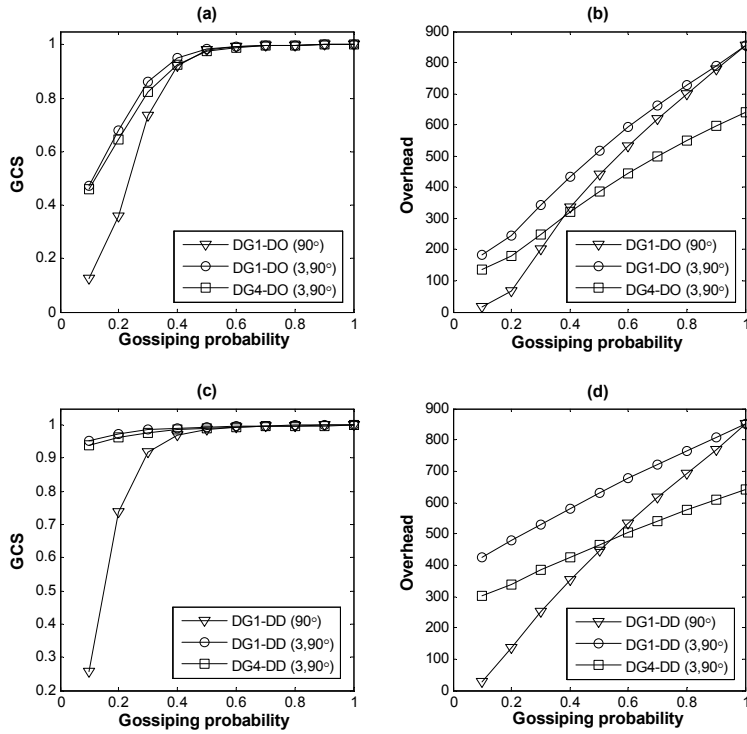


**Figure 7.12:** Performance comparison between  $k$ -hop based scheme and the original gossiping protocol,  $N = 225$ ,  $R = 8.36$ , and  $\theta = 90^\circ$ .



### DG4 Combined with 'k-hop'

The source node is located in the center of the network, and the other nodes are uniformly distributed within the network. If the source has a smaller number of neighbors, the gossiping process could probably die very fast. To avoid this phenomenon, the authors in [94] proposed a  $k$ -hop gossiping protocol. They set the gossiping probability to be 1 for the first  $k$  hops from the source, and then the gossiping process continues with probability  $p$  from the  $k + 1$  hop. This mechanism is combined with DG1 and denoted as  $DG1(k, \theta)$ . Moreover, it is combined with DG4 and denoted as  $DG4(k, \theta)$ . These two extended schemes are compared to the original DG1 as shown in Figure 7.12. Figure 7.12 (a) and (b) show the results from the schemes using D-O mode, and Figure 7.12 (c) and (d) show the results from the schemes using D-D mode. It is observed that, compared to DG1, the  $k$ -hop scheme enhances the message delivery ratio but also increases the amount of overhead. As we mentioned before, the optimization scheme DG4 could effectively reduce the overhead, but it also reduces the message delivery ratio. When the  $k$ -hop scheme and DG4 are combined together as  $DG4(k, \theta)$ , the new scheme achieves the similar delivery ratio as  $DG1(k, \theta)$ , but the resultant overhead is much lower. Therefore, the scheme  $DG4(k, \theta)$  inherits the benefit of  $k$ -hop scheme and DG4. Figure 7.12 (a) and (c) also indicate that, using D-D mode with the optimization scheme has better performance than using D-O mode.

## 7.4 Chapter Summary

In this chapter, the fundamental properties of using directional antennas in multi-hop ad-hoc networks have been investigated. First, the impact of neighbor attachment policies on SIR has been studied using and without using directional antennas. It has been shown that, by choosing a suitable antenna beamwidth, directional antennas can reduce the amount of interference in the network. Further, it has been observed that although power control or directional antennas can reduce the amount of interference, they do not necessarily produce the best SIR. Given the direct link between high SIR and high capacity, it can be concluded that the neighbor attachment policies that focus on interference reduction may fail to improve capacity in ad-hoc networks. Second, a comprehensive investigation on the probabilistic-based message dissemination mechanisms has been presented using directional antennas. The message dissemination performance has been evaluated from different aspects: directional gossiping mechanism, network graph type, transceiver antenna mode, et cetera. Our work could help to mitigate some misconceptions regarding the performance of using directional antennas. It has been shown that using DD antenna mode does not always perform worse than DO antenna mode. The work in this chapter provides valuable insights for using directional antennas in multi-hop connected ad-hoc networks.



# 60 GHz Multi-hop Communication in Home Networks

“An experiment, like every other event which takes place, is a natural phenomenon; but in a scientific experiment the circumstances are so arranged that the relations between a particular set of phenomena may be studied to the best advantage.”

- James Clerk Maxwell

*Due to the high path loss, 60 GHz WPANs usually have very limited coverage range. This chapter focuses on the methods to extend the coverage range of 60 GHz systems via multi-hop communication crossing several inter-connected WPANs. Inter-piconet communication is possible through the bridge devices. While extending the range of WPANs, bridge devices become the capacity bottlenecks for these inter-connected piconets. An unoptimized resource allocation mechanism involving the bridges could degrade system performance severely. In this chapter the inter-piconet route discovery and establishment are investigated. To resolve the inter-piconet resource allocation problem, a joint QoS routing and resource reservation framework is proposed.*

## 8.1 Introduction

The multi-hop communication for IEEE 802.15.3 based WPANs can be classified as: intra-piconet communication and inter-piconet communication. For the intra-piconet multi-hop communication, the source device and destination device are within the same piconet, but out of the transmission range of each other. The intra-piconet multi-hop communication is not difficult to handle and it is a well-studied topic, for instance, [100,101]. The PNC can allocate channel resource route by route instead of node by node [100]. Due to the high path loss, the transmission range of 60 GHz radio is normally limited within 10 meters. Although directional antennas are used to compensate the high path loss, it is still difficult for the 60 GHz radio to penetrate the walls and obstacles. For instance, the attenuation of the transmission of 60 GHz radio through a 15 cm thick concrete wall can be as high as 36 dB [102]. Although the concrete walls and floors of a building are natural and reliable boundaries for a piconet, which reduce the possible interference from adjacent rooms, it is very difficult to let the devices within different rooms to communicate with each other. Using *radio relaying devices* (RRDs) to relay signals from room to room is a feasible approach to resolve this problem. RRDs are also called as *bridge devices*, and these two concepts are interchangeable in this chapter. RRDs are supposed to be low cost devices which are easily mounted through walls<sup>1</sup>. RRDs provide an infrastructure that does not require the support from backbone network to enable inter-room communication. To keep the design simplicity, RRDs are envisioned as reduced function devices, which may be only featured with PHY and MAC layer, and simply relay signals from room to room, for instance as shown in Figure 8.1. The static deployment of RRDs within the indoor environment provides a wireless infrastructure to enable 60 GHz based wireless mesh networks. Therefore, the room-to-room communication can be considered as inter-piconet communication via RRDs, which is the main concern for this chapter.

This chapter is motivated to evaluate the feasible network topology to support piconet coexistence, based on which the inter-piconet route discovery, route establishment and multi-hop communication are studied.

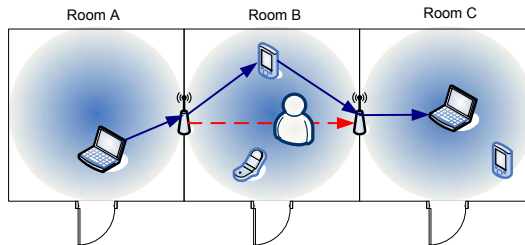


**Figure 8.1:** Indoor radio relaying devices deployment scenario.

<sup>1</sup>RRD devices are also called as “via” devices in [103]

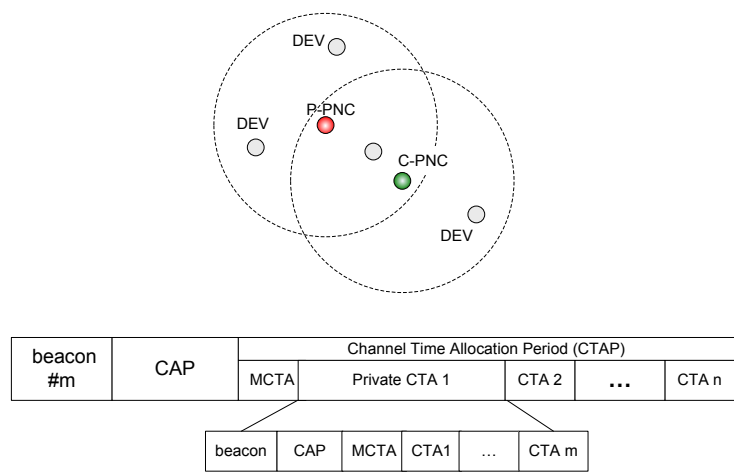


**Figure 8.2:** *Parent-child piconet topology and superframe structure.*

8.1.1 Mesh Topology to Support Piconet Coexistence

The first step to enable inter-piconet communication is to define how to coordinate the coexisted piconets. There are two approaches which have been proposed in the IEEE related standardization activities to support inter-piconet communication:

Topology 1: Parent-Child Piconet Topology

IEEE 802.15.3 defines a parent-child piconet architecture to support inter-piconet communication [3]. The parent-child piconet architecture is shown in Figure 8.2. A parent piconet refers to a piconet that allocates channel access time for another piconet. A child piconet is formed under a parent piconet. It is considered as a subsidiary piconet attaching to its parent piconet. A parent piconet is possible to have more than one child piconet. The PNC of the child piconet, which is called as child PNC, must be a member of the parent piconet. The child PNC requires channel access time for the child piconet from its parent PNC. The parent PNC may allocate a private CTA block for the child piconet if the channel resource is sufficient. The multi-hop communication is possible to use child PNC to relay traffic from parent to child piconet, or vice versa. The parent and child piconets share the same superframe as shown in Figure 8.2. During the time that the channel access is allocated for the parent piconet, the devices in the child piconet keep silent, and vice versa. Hence, the assigned per-piconet channel recourse is inversely proportional to the number of child piconets attached to a parent piconet. This architecture can effectively support the coexistence of parent and child piconets, but it limits the channel resource utilization efficiency. This issue is also discussed in [104].

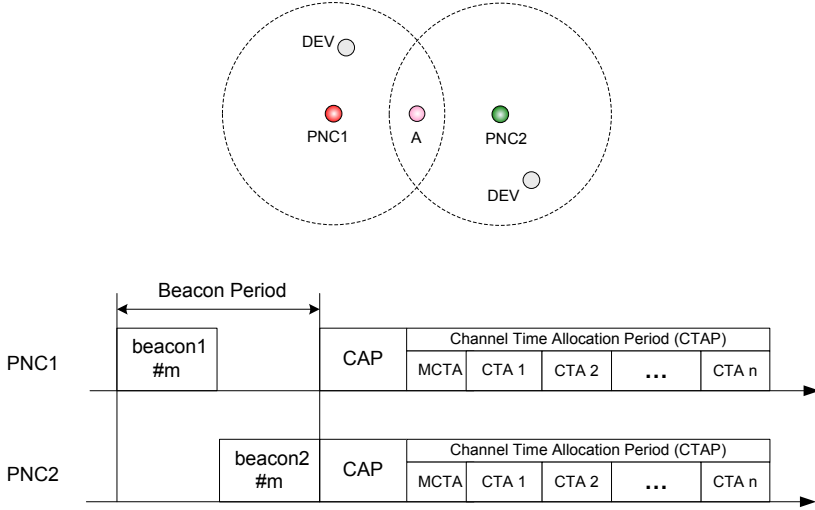


**Figure 8.3:** *Beacon alignment mechanism.*

### Topology 2: Beacon Alignment

To support piconet coexistence and meanwhile not to lose the utilization efficiency of channel resource, the IEEE 802.15 Task group 5<sup>2</sup> related activity has proposed a beacon alignment based piconet coordination mechanism in [105]. The main difference between this approach and the parent-child piconet topology is that, a bridge device which is used to connect the adjacent piconets is a non-PNC device that is located in the overlapped area of two piconets. As shown in Figure 8.3, two independent piconets operate simultaneously and they overlap partially. Device *A* is a member of PNC1 and it is located within the overlapped area of the two piconets. Once device *A* receives a beacon from PNC2, it notices the existence of the other piconet. It triggers device *A* to act as a bridge between the two piconets. Device *A* uses Application Specific Information Element (ASIE) [3] to relay timing information from high capability (senior) PNC to low capability (junior) PNC. Once a junior PNC receives an ASIE from a bridge device, it synchronizes itself with the senior PNC according to the timing recorded in the ASIE, and the junior PNC aligns its beacon after the beacon from the senior PNC in the beacon period. This process operates during the CAP of a superframe. Senior PNC is responsible to decide beacon period length and allocate the CAP and CTAP durations. In a more general case if more than two piconets are involved, beacons are aligned according to the set theory: two piconets could use the same beacon slot if they have an empty set of common reachable devices. This piconet coordina-

<sup>2</sup>The IEEE 802.15.5 is formed to enable mesh networking for WPANs. Mesh networks are capable to extend WPAN coverage range and enhance the reliability via route redundancy.

tion mechanism could effectively synchronize adjacent piconets and avoid beacon collision at the bridge devices. The main cost of this method is the overhead used for synchronization. When the number of piconets increases, the amount of the relayed timing information is also increased. Compared to the parent-child topology, this method could use channel resource more efficiently because adjacent piconets do not need to share the same superframe. However, it might involve possible interference for the devices that can receive from both piconets. Without the cooperation among the adjacent piconets, possible interference may happen and degrade the system performance. The authors in [104] have extended the work from [105] by proposing a channel resource allocation algorithm to resolve collisions within the overlapped area of adjacent piconets. They have proposed to separate the channel access time for the devices which are within the overlapped area of the two piconets and the devices which are only within a certain piconet. Their work could mitigate the interference for adjacent piconets, but it is on the price of the reduced channel utilization efficiency.

In this work, the second topology is selected to investigate multi-hop communication for the following two reasons. First, the main aim of this work is to support room-to-room communication using bridge devices, which are considered as low cost non-PNC devices. Therefore, the parent-child piconet topology does not fulfill this requirement. Second, the second topology is more dynamic than the parent-child piconet topology. Without relaying the timing information via the bridge devices, the adjacent piconets are just independent piconets. The adjacent piconets are aligned together, once a PNC receives the relayed timing information from the adjacent piconet. However, for the parent-child piconet topology, without allocating channel resource by the parent piconet, the child piconet cannot operate at all. Based on the selected mesh topology, the inter-piconet route discovery process will be studied in the next section.

## 8.2 Inter-Piconet Route Discovery

### 8.2.1 Mesh Topology Enhancement

The deployment of RRDs within a home network forms a wireless infrastructure to support the room-to-room communication. They connect several piconets together and coordinate them with the piconet synchronization mechanism explained above. The RRDs might be low-cost devices. Therefore, they are envisioned as non-PNC devices. If there does not exist any PNC-capable devices in between the RRDs, traffic flows cannot be relayed between two non-overlapped piconets. For instance as shown in Figure 8.4 (a), device *A* can not request a route with device *B* because the two piconets are not overlapped. To bridge two non-overlapped piconets, the RRD from the route request direction is defined as a *reduced-function* PNC and it organizes a *reduced-function* piconet which is only used to relay traffic from one RRD to the other RRD, e.g. RRD *i* as shown in Figure 8.4 (b). The

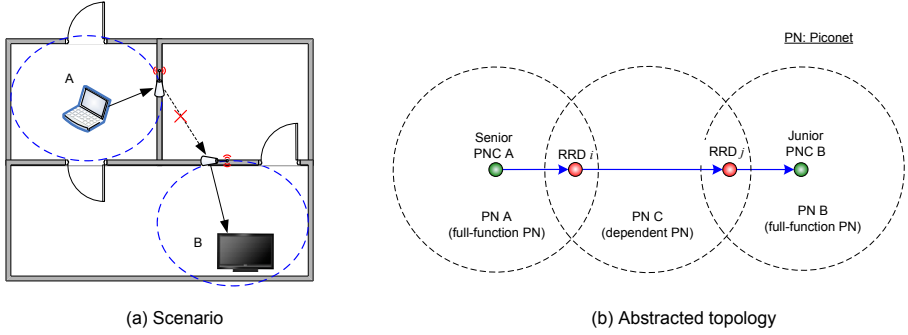


**Figure 8.4:** Using reduced-function piconet to support non-overlapped piconets.

reduced-function PNC does not generate its own beacon. It simply relays the timing information from its parent PNC to organize the reduced-function piconet. In contrast, a piconet is organized by a PNC-capable device, and this piconet is called as *full-function* piconet. The channel time allocation of a reduced-function piconet relies on its parent PNC. Therefore, reduced-function PNC  $i$  sends the channel allocation request to PNC  $A$  and PNC  $A$  allocates channel access time for  $A \rightarrow i$  and  $i \rightarrow j$ . If a PNC-capable device moves in a reduced-function piconet, the reduced-function PNC transfers the PNC role to the PNC-capable device and the piconet upgrades to a full-function piconet.

## 8.2.2 Inter-Piconet Route Discovery Protocols

### RREQ Forwarding

Based on the enhanced mesh network architecture, the inter-piconet route discovery process is investigated using 60 GHz radio. On-demand routing is feasible for home network because of the dynamics of the network topology. Hence, a route discovery process is triggered when a source has a communication request for a specific destination. One of the major features of the 60 GHz radio technology is the use of directional antennas. To set-up directional communication, it is necessary for the devices to know the direction of their neighbors. When directional antennas are used in a route discovery process, devices could cache and refine the directional information of its neighbors. To initialize a route discovery process, the source device sweeps the Route Request (RREQ) messages in all the possible directions. Each intermediate device that receives a RREQ message adds its own address in the path table of the RREQ and forwards it directionally. If a device is already recorded in a RREQ, it simply drops the packet to avoid routing loop. When the destination device receives the RREQ, it generates a Route Reply (RREP) for the source device and unicasts it back according to the path recorded in the RREQ. Compared to the omni-directional transmission, the



directional transmission of RREQ messages generates more overhead. To achieve high performance route discovery, corresponding packet forwarding optimization strategies should be devised. There are three RREQ Forwarding Algorithms (FA) which are studied in this chapter:

- FA1: The azimuth plane of a device is divided into  $N_B$  sectors,  $N_B = \frac{2\pi}{\theta}$  and  $\theta$  is the antenna beamwidth. When a device receives a RREQ, it sweeps the packet from each beam sector. FA1 is a pure directional flooding.
- FA2: When a device receives a RREQ, it estimates the receiving direction  $\alpha$  using a Direction of Arrival (DoA) technique and maps it into a certain beam sector  $i$ , where  $i = \lceil \frac{\alpha}{\theta} \rceil$ . It broadcasts the RREQ from all the beam sectors except the receiving sector  $i$ .
- FA3: is similar to FA2, but it broadcasts from the beam sectors except the receiving one and its two adjacent sectors  $[i - 1, i, i + 1]$ .

### RREP Compaction

The route discovery process is executed within the CAP of a superframe, and the medium access is based on CSMA/CA. Due to the contention and back-off based nature of CSMA/CA and directional sweeping, it is possible that the route discovery time of a sub-optimized path is faster than the shortest path. On the condition that the destination replies all the received RREQs, the first arrived RREP at the source device might not be the RREP from the shortest path. Therefore, to increase the chance of finding the best path, referring the path with shortest hop count, a RREP forwarding optimization mechanism is proposed as follows. During the route discovery process, each device caches and updates its one-hop neighbors' information during the neighbor discovery process. After an intermediate device receives a RREP, it forwards the RREP to the device on the next hop, which is recorded in the path in the RREP. Before forwarding, it firstly checks the path table. If an intermediate device (e.g.  $i$ ) along the path is its one-hop neighbor but not the one it forwards the RREP to, the device removes the intermediate devices from the path table in-between itself and  $i$ , and then it forwards the RREP to  $i$  directly.

### 8.2.3 Simulation Model

The entire route discovery protocol is implemented based on the IEEE 802.15.3 MAC implemented in Section 3.7. The simulation related MAC and PHY layer parameters are listed in Table 8.1. A flat-top antenna pattern is used in the simulation and the antenna gain is given as  $10\log(2\pi/\theta)$ , where  $\theta$  is the antenna beamwidth. Because piconet synchronization is not the focus of this work, it is assumed that all the piconets are already synchronized with each other in the simulation. They follow the same superframe length, beacon period, CAP and CTAP durations.

**Table 8.1:** *Simulation related MAC and PHY parameter specifications*

	Parameters	Value
MAC	Beacon frame	832 bits
	pPHYSIFSTime	0.2 $\mu$ s
	BIFS	1.2 $\mu$ s
	Slot time	1.2 $\mu$ s
	Guard band	0.1 $\mu$ s
	CAP Duration	1 ms
	MCTA Duration	0.15 ms
	CTAs Duration	25.6 ms
PHY	Data rate	1 Gbps
	Carrier frequency	60 GHz
	Transmission power	10 mW
	Path loss at 1m ( $PL_0$ )	68 dB
	Path loss exponent ( $n$ )	2
	Noise figure (NF)	1
	Antenna beamwidth ( $\theta$ )	30° and 60°

### Radio Propagation Model

To simulate the indoor environment, a multi-wall model is taken into account in the radio propagation model (6.1) as,

$$P_r(d) = P_t + G - (PL_0 + 10n \log(d) + X_\sigma) - D_w \times N_w \quad (8.1)$$

where,  $D_w$  is the attenuation caused by a wall and  $N_w$  is the number of the walls between the transmitter and the receiver. The attenuation of 1 cm concrete wall is set as 3 dB for 60 GHz radio and the thickness of each wall is 5 cm.

### Simulation Scenario

An office scenario is deployed in OPNET as shown in Figure 8.5 (a), in which the red points represent the RRDs that are deployed through the walls to relay signals from room to room. Due to the lack of the simulation support for indoor environment in OPNET, the simplified network topology is shown in Figure 8.5 (b), in which, a dashed circle represents the coverage range of a piconet and the blue lines represent the existing radio links between RRDs.

### Performance Metrics

During each simulation, the route discovery process is triggered only once at the source device and each simulation is iterated 1000 times. Three metrics are used to evaluate the directional route discovery performance:

- Route discovery latency

To study the route discovery latency especially for discovering the best path, the destination replies to all the received RREQs. The route discovery latency is

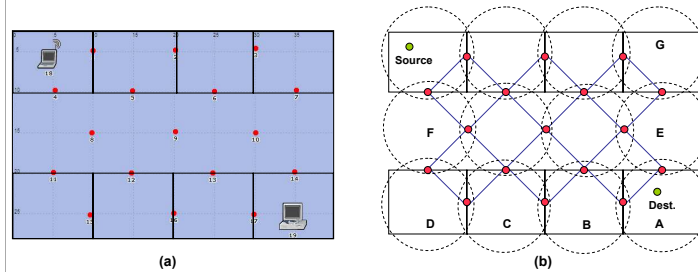


**Figure 8.5:** *Indoor office scenario and corresponding network topology.*

defined as the time duration from the moment the source device generates the first RREQ to the moment the source receives the RREP from the path with minimum hop count. What should be noticed is that, the path with the minimum hop count is not necessary to be the shortest path. This is because the RREQ or RREP from the shortest path might be missing due to the deafness problem caused by the antenna beam-forming or transmission collisions.

- Route discovery overhead

The route discovery overhead refers to the total number of generated RREQs and RREPs within one run of simulation. It indicates the efficiency of a route discovery protocol.

- Shortest path discovery ratio

As mentioned before, a source cannot always find the shortest path in a route discovery process. The shortest path discovery ratio is defined as the ratio of the number of times that a route discovery process can find the shortest path to the total number of simulation iterations.

### Simulation Model Validation

The one-hop transmission latency of a RREQ includes two parts: medium access delay and queuing delay. The medium access delay is caused by the CSMA/CA based MAC mechanism. If a device senses that the channel is busy, it waits until the channel is free and attempts to access the channel again. The queuing delay is induced because of directional sweeping. The device begins to transmit the RREQs by randomly picking up a beam sector, e.g.  $n_i$  ( $n_i \in [1, \frac{2\pi}{\theta}]$ ), and sequentially transmitting the RREQs in all the possible directions. If a device  $s$  is located in the  $n_s$  sector, the RREQ that can be received by  $s$  has to be queued in the buffer until the RREQs have been transmitted in the previous  $|n_i - n_s|$  sectors. Because the transmission of RREP is unicast, the involved latency is only related to the medium access delay. Therefore, the route discovery latency

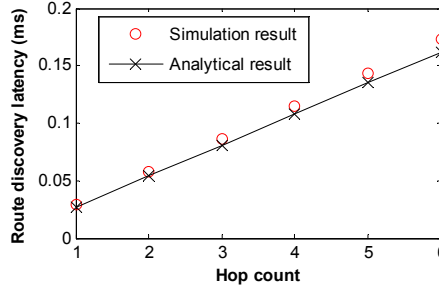


**Figure 8.6:** The validation of the simulation model, with  $\theta = 60^\circ$  and  $N_{win} = 7$ .

$T$  for a path with hop count  $H$  is the summation of the RREQ latency  $T_{rreq}$  and the RREP latency  $T_{rrep}$ , which is given as:

$$\begin{aligned}
 T &= T_{rreq} + T_{rrep} \\
 &= H \times \left( \sum_{n_i=1}^{\frac{2\pi}{\theta}} p_i (1 + |n_i - n_s|) + 1 \right) \times (t_{BIFS} + t_{slot} \cdot \sum_{N_{bf}=1}^{N_{win}} p_{bf} N_{bf})
 \end{aligned} \tag{8.2}$$

where,  $p_i$  is the possibility to chose  $n_i$  as the initial beam sector to transmit RREQ.  $N_{bf}$  is the randomly selected backoff window size,  $N_{bf} \in [1, N_{win}]$ ,  $t_{slot}$  is the slot time, and  $p_{bf}$  is the possibility to select  $N_{bf}$ . A batch of devices are aligned in a line, and the destination is changed according to the number of hop counts. To validate the simulation model, the simulation and analytical results are compared in Figure 8.6, which uses  $60^\circ$  antenna and the backoff window size  $N_{win}$  being 7.

### Performance Analysis

Based on the IEEE 802.15.3 MAC, the route discovery process is only executed within the CAP of a superframe. If the route discovery process cannot finish within one superframe, it continues in the CAP of the next superframe. Therefore, the route discovery latency might also be influenced by the CAP length. If the CAP is too short, a route discovery process needs several superframes to be accomplished. If the CAP length is increased, the channel access time used for data transmissions is decreased. The CAP length is set as 1 millisecond (ms) in the simulation, hence the MAC efficiency is 95.7%. In this circumstance, the performance of the route discovery process with single transmission pair is examined. The positions of the source and the destination are shown in Figure 8.5.

- RREP compaction

To illustrate the performance of RREP compaction mechanism, the route discovery latency using and not using compaction mechanisms is depicted in Figure 8.7,

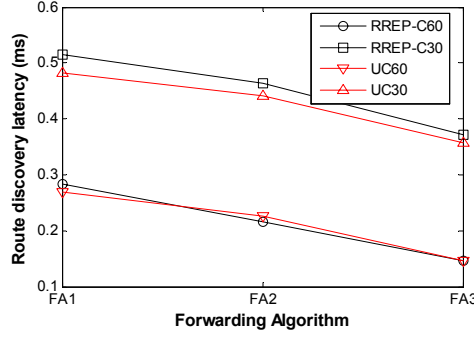


**Figure 8.7:** Performance of RREP compaction using FA1.

and the shortest path discovery ratio is listed in Table 8.2. It is observed that, the compaction mechanism has negligible influence on the route discovery latency, but the shortest path discovery ratio has dramatic improvement, especially when  $30^\circ$  antenna is used. Hence, the following simulation is executed with RREP compaction.

**Table 8.2:** The shortest path discovery ratio

	FA1	FA2	FA3
RREP-Compaction $60^\circ$ (RREP-C60)	0.9439	0.9389	0.9409
RREP-Compaction $30^\circ$ (RREP-C30)	0.9439	0.9459	0.948
Un-Compaction $60^\circ$ (UC60)	0.9139	0.9129	0.9409
Un-Compaction $30^\circ$ (UC30)	0.8759	0.8799	0.8959

- RREQ forwarding algorithms comparison

Based on the RREP compaction mechanism, three RREQ forwarding algorithms are compared together. The route discovery latency and the involved overhead for different algorithms are depicted in Figure 8.8, in which, the position of the destination is changed from piconet A to C as shown in Figure 8.5 (b). In Figure 8.8, the third forwarding algorithm (FA3) has the best performance. It has the shortest route discovery latency and the fewest overhead. When the same forwarding algorithm is used, the  $60^\circ$  antenna outperforms the  $30^\circ$  antenna. In some works, for instance [106], it is reported that a narrower antenna beamwidth can achieve lower route discovery latency. This is because the influence of the environment is not considered in [106]. In general, narrower beamwidth could get longer transmission range. Therefore, using narrower antenna beamwidth leads to fewer hops to reach the destination. However, in an indoor scenario, even with narrow beamwidth, it is still difficult for 60 GHz radio to penetrate the walls. Hence, the

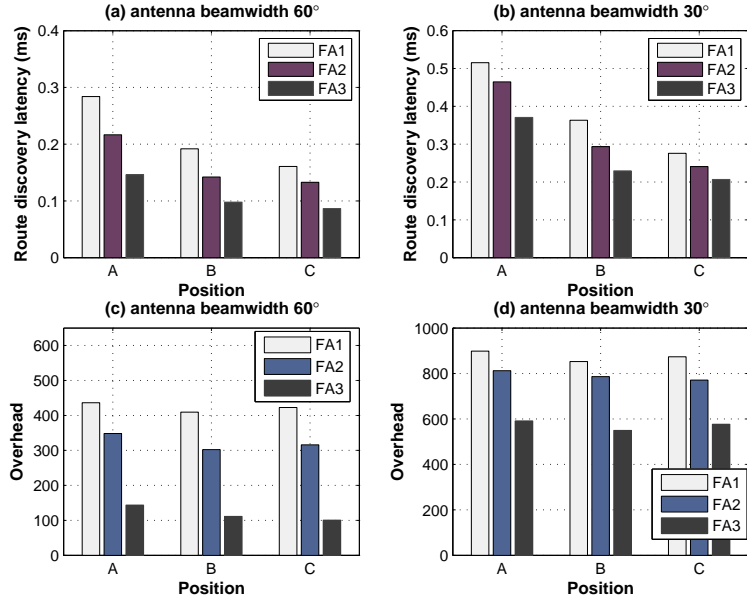


**Figure 8.8:** Route discovery latency and involved overhead with different destination position.

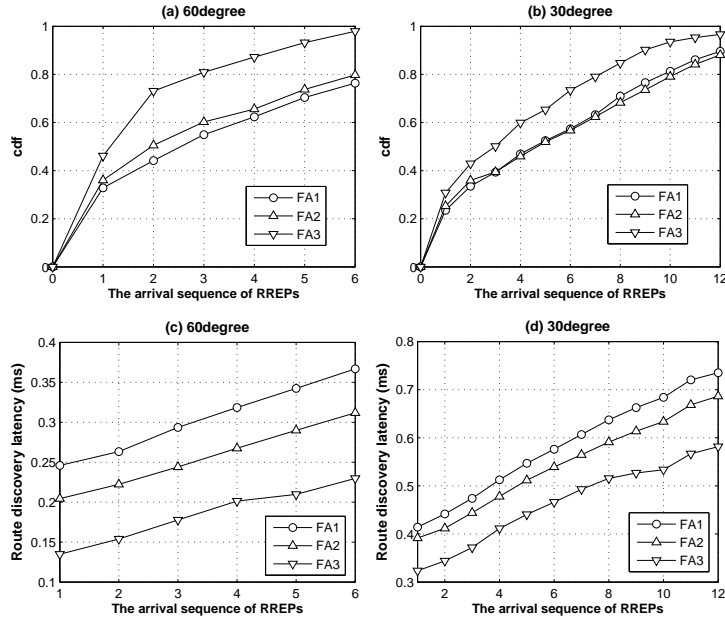


**Figure 8.9:** The cdf and the corresponding route discovery latency to find the best path.

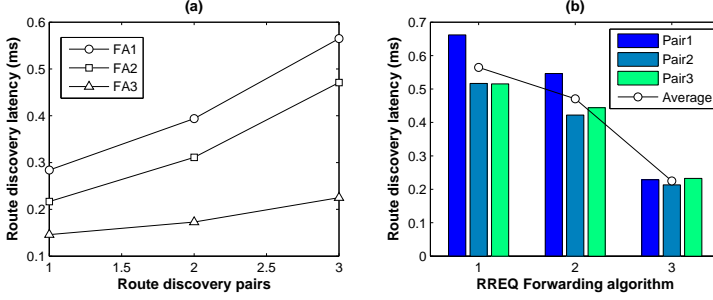


**Figure 8.10:** Multiple route discovery pairs, with  $\theta = 60^\circ$ .

radio coverage range is limited only within a room. Therefore, narrower beamwidth cannot have advantage in route discovery process, and conversely, antennas with smaller beamwidth have to sweep more beam sectors, which involves more overhead and slows down the route discovery process.

During a route discovery process, the source could receive a sequence of RREPs replied from the destination. The probability that the  $x^{th}$  arrived RREP is from the path with minimum hop count is defined as  $f(x)$ . Figure 8.9 (a) and (b) plots the cumulative distribution function (cdf)  $F(x)$  of  $f(x)$  with different antenna beamwidth, where,  $F(x) = \sum_{x \leq \frac{2\pi}{\theta}} f(x)$ . Sub-figure (a) is for  $60^\circ$  antennas. It indicates that after waiting for the arrival of 6 RREPs, the probability to receive the RREP from the path with minimum hop count can be as high as 98%. Sub-figure(b) with  $30^\circ$  antennas indicates that after waiting for the arrival of 12 RREPs, the probability to receive the RREP from the path with minimum hop count is 96.6%. The corresponding route discovery latencies for different sequence of arrived RREPs are shown in Figure 8.9 (c) and (d). Based on Figure 8.9, it can be summarized that after a source receives the first arrived RREP, it calculates the route discovery latency  $T_{RD1}$  and waits another  $T_{RD1}$  for receiving the other sequentially arrived RREPs, which can guarantee that the probability to find the optimized route is higher than 98% for  $60^\circ$  antennas and higher than 96.6% for  $30^\circ$  antennas.

- Multiple transmission pairs

To examine the parallel executed route discovery processes, the second route discovery pair is added with the source in piconet G and the destination in piconet D, and the third pair with the source in piconet F and destination in piconet E as shown in Figure 8.5. The simulation results using  $60^\circ$  antenna are shown in Figure 8.10. The subplot (a) compares the route discovery latency using different RREQ forwarding algorithms when the number of route discovery pairs is increased from 1 to 3. FA3 performs better than FA1 and FA2, and the route discovery latency using FA3 does not change dramatically when the number of route discovery pairs increases. The subplot (b) plots the latency for each route discovery

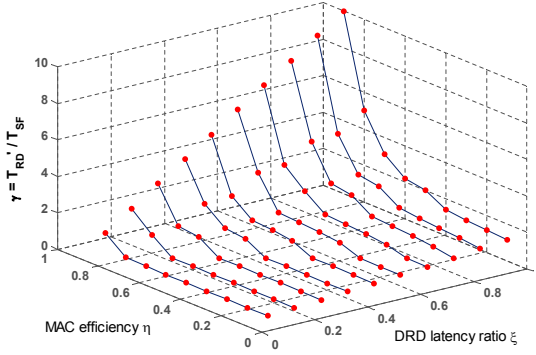


**Figure 8.11:** *Route discovery latency with superframe structure influence.*

pair when there are three route discovery pairs in the network, which indicates that the average route discovery latency is only around 0.2 ms using FA3. Being different with large-scale networks, e.g., ad-hoc sensor network, routing in a home network might not require a long path. Therefore, a directional route discovery process can be easily completed within one CAP length.

- Superframe influence on route discovery latency

If a route discovery process cannot finish within one CAP, the superframe structure involves extra delay on the route discovery latency. The total required time for a route discovery process to find the best path is defined as  $T_{RD}$ . Hence, if  $T_{RD}$  is bigger than  $T_{CAP}$ , the route discovery process has to be executed within  $x$  continuous superframes, where  $x = \left\lceil \frac{T_{RD}}{T_{CAP}} \right\rceil$  and  $\lceil \cdot \rceil$  represents the ceiling function. The MAC efficiency  $\eta$  is defined as the proportion of a superframe that is allocated for data communication, where  $\eta = T_{CTA}/T_{SF}$ , where  $T_{CTA}$  is the CTAs duration and  $T_{SF}$  is the superframe duration. The exact route discovery latency  $T'_{RD}$  with the superframe structure influence is given by:

$$T'_{RD} = \left\lfloor \frac{T_{RD}}{T_{CAP}} \right\rfloor \cdot T_{SF} + \left[ \frac{T_{RD}}{T_{CAP}} - \left\lfloor \frac{T_{RD}}{T_{CAP}} \right\rfloor \right] \cdot T_{CAP} \quad (8.3)$$

where,  $T_{CAP} = (1 - \eta)T_{SF}$  and  $\lfloor \cdot \rfloor$  represents the flooring function.  $T_{RD}$  and  $T'_{RD}$  are normalized as  $\xi = T_{RD}/T_{SF}$  and  $\gamma = T'_{RD}/T_{SF}$ , respectively. In Figure 8.11, it depicts  $\gamma$  as a function of  $(\eta, \xi)$ , from which it can be seen that, when the MAC efficiency is high, the channel resource allocated for route discovery is small, which could lead to a longer time for route discovery.



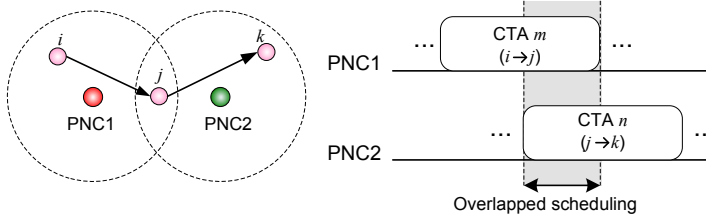


**Figure 8.12:** *Channel resource reservation collision.*

### 8.3 Joint QoS Routing and Resource Reservation

As mentioned before, adjacent piconets can be inter-connected by bridge devices, which are the devices located within the overlapped area of two piconets. A common problem in such inter-connected piconets is the interference caused to the devices that can receive from both piconets. Hence, an interference-free resource allocation mechanism should be devised in order to support the inter-piconet communication. A joint QoS routing and resource reservation mechanism is devised in this section. To avoid possible reservation collisions among inter-connected piconets, the resource reservation is embedded with the route discovery process. Meanwhile, our routing mechanism takes into account the available channel resource within a piconet for route selection. The use of directional antennas brings spatial diversity in WPANs. Hence this framework is also integrated with a transmission scheduling algorithm that uses directional antennas to enable spatial reuse TDMA. The advantages of our proposal are shown via extensive simulation studies.

#### 8.3.1 QoS Routing

##### Problem Definition

The main challenge to enable inter-piconet communication is to allocate the channel resource for a traffic flow passing through multiple piconets. Although piconets can be synchronized together using bridge devices, PNCs still manage their piconets independently. It is possible that the PNCs of two overlapped piconets reserve the same channel access time for a bridge device which is used to connect them together. For example as shown in Figure 8.12, there are two piconets inter-connected by device  $j$ , and there is a multi-hop path  $i \rightarrow j \rightarrow k$  going through the two piconets. According to the IEEE 802.15.3 MAC, to reserve channel access time, device  $i$  transmits request to PNC1 to reserve channel resource for link  $i \rightarrow j$  from PNC1, and device  $j$  transmits request to PNC2 to reserve channel resource for link  $j \rightarrow k$ . Suppose the transmitter and the receiver cannot operate at the same time and if the allocated CTAs for link  $i \rightarrow j$  and  $j \rightarrow k$  are overlap-

ped, the transmission and reception at device  $j$  will be disordered. This problem is termed as *channel resource reservation collision*. The hinge of enabling high performance inter-piconet communication is to prevent the inter-piconet channel resource reservation collisions.

### Notations and Definitions

Let  $G(V, E, X)$  denote a network topology, where  $V$  represents the set of devices within the network,  $E$  represents the set of radio links between devices, and  $X$  represents the set of piconets.  $V_x$  represents the set of devices that are members of piconet  $x$ , where  $V_x$  is a subset of  $V$ ,  $\forall x \in X$ .  $E_x$  represents the set of transmission links within piconet  $x$ , and  $E_x$  is a subset of  $E$ . The half duplex mode is assumed in this work, which is a valid assumption for the devices that have single front-end. Therefore, at any instant for a certain device, e.g. device  $v$ , its available capacity  $C_v$  could be characterized by the amount of traffic that it receives and the amount of traffic that it transmits.  $C_v$  is a normalized factor, which is defined as

$$C_v = 1 - \left( \sum_{u \rightarrow v \in E^{v,i}} \frac{B_{uv}}{R_{uv}} + \sum_{v \rightarrow w \in E^{v,o}} \frac{B_{vw}}{R_{vw}} \right), \quad (8.4)$$

where,  $E^{v,i}$  and  $E^{v,o}$  represent the set of incoming links to  $v$  and the set of outgoing links from  $v$ , respectively.  $R_{uv}$  and  $R_{vw}$  are the achievable data rates on link  $u \rightarrow v$  and  $v \rightarrow w$ .  $B_{uv}$  and  $B_{vw}$  are the required bandwidth from link  $u \rightarrow v$  and  $v \rightarrow w$ , respectively, and they are subjected to  $B_{uv} \leq R_{uv}$  and  $B_{vw} \leq R_{vw}$ . The first summation in the bracket in (8.4) represents the total fraction of the reserved channel resource for the incoming flows to  $v$ . The second summation term is the total fraction of the reserved channel resource for the flows going out from  $v$ . Because of half duplex nature, the summation of all the channel resource allocated for a device, receiving and transmitting, cannot exceed the capacity of this device,

$$\sum_{u \rightarrow v \in E^{v,i}} \frac{B_{uv}}{R_{uv}} + \sum_{v \rightarrow w \in E^{v,o}} \frac{B_{vw}}{R_{vw}} < 1, \quad (8.5)$$

and in turn  $C_v$  is also within the range  $[0,1]$ . For a certain piconet  $\epsilon$ , its available capacity is given by:

$$C_{PN_\epsilon} = \eta - \sum_{r \rightarrow s \in E_\epsilon} \frac{B_{rs}}{R_{rs}}, (r, s \in V_\epsilon), \quad (8.6)$$

where the summation represents the total allocated channel resource for all the flows passing through piconet  $\epsilon$ .  $\eta$  is the MAC efficiency factor which is already defined in the previous section. The QoS routing issue is formulated as finding a path from a source to a destination which satisfies the bandwidth constraint,

while the end-to-end delay is kept minimum (bandwidth-constraint shortest path). Based on the piconet topology, the available capacity of a link is constrained by the available capacity of the nodes on the link and the available capacity of the piconet which the link belongs to. For instance, there is a link  $v \rightarrow u$  within piconet  $\epsilon$ , its capacity  $C(v, u)$  is given by:

$$C(v, u) = \min(C_v, C_u, C_{PN_\epsilon}). \quad (8.7)$$

### Channel Resource Aware Route Discovery

In previous section, several mechanisms have been discussed to reduce the overhead influence of the directional route discovery process. To guarantee the required bandwidth, a link might be selected as part of a route only if it can support the required capacity to forward the traffic. Therefore, one more mechanism is proposed here, which could further reduce the overhead for inter-piconet route discovery. When an intermediate device receives a RREQ, instead of simply re-broadcasting the RREQ, it estimates the channel resource in *two-hop* range. For instance, assume that device  $v$  connects two piconets  $x$  and  $y$ . When device  $v$  receives a RREQ from device  $w$ , ( $v, w \in V_x$ ), device  $v$  performs resource estimation as follows:

- Estimation for incoming link: Device  $v$  firstly checks if it has sufficient capacity to support the traffic on the link  $w \rightarrow v$ . According to the achievable data rate  $R_{wv}$ , device  $v$  can calculate the required channel access time as  $C_{req}(w, v) = B_{wv}/R_{wv}$ . If  $C_{req}(w, v) \leq \min(C_v, C_{PN_x})$ , which means that the PNC of this piconet is able to provide sufficient channel resources and  $v$  has enough capacity to handle this communication. Otherwise, it drops the RREQ.
- Estimation for forwarding link: If there is sufficient channel resource for the incoming link,  $v$  should also estimate the channel resource for the forwarding link. Device  $v$  uses the maximum achievable data rate on a link, denoted as  $R_{max}$ , to find whether it is possible to provide the channel access time  $C_{est}$  for the next hop in piconet  $y$ , where  $C_{est} = \frac{B_{wv}}{R_{max}}$ . If  $C_{est} \leq \min(C_v - C_{req}(w, v), C_{PN_y})$ ,  $v$  forwards the RREQ in piconet  $y$  with certain modifications. It adds its own information  $\langle \text{IntID}, \text{IntPNID} \rangle$  to the RREQ, where IntID represents the intermediate device ID and IntPNID is the piconet ID of the intermediate device. Otherwise, it drops the RREQ.

### Route Selection

The link capacity is used to assign the weight for each link as  $w(v, u) = 1/C(v, u)$ . Therefore, route selection problem can be formulated as

$$\arg \min_{i \in I} \sum_{x=1}^{n_i} w_x, \quad (8.8)$$

where  $w_x$  is the weight factor for the  $x^{th}$  hop,  $n_i$  is the hop count for the  $i^{th}$  path, and  $I$  represents the set of all the possible paths from source to destination, which are recorded in the arrived RREQs at the destination.

### 8.3.2 Inter-piconet Channel Resource Allocation

#### Route Reply Triggered Resource Reservation (RTR)

Devices within a piconet reserve channel access time from their PNC, which is responsible to manage channel resource and schedule transmissions. A PNC maintains an admission table to record the scheduled channel access requests. Every entity of the table contains the source ID, the destination ID, the arranged CTA block ID and the allocated channel access time. When a transmission is scheduled, the PNC updates the admission table correspondingly. As mentioned in Section 8.3.1, reservation collisions could happen during inter-piconet resource allocation. Such collisions could disturb the inter-piconet communication and severely affect the network performance. The main cause for reservation collision is that a PNC is not aware of the reservations in its adjacent piconets. Therefore, two PNCs could reserve the overlapped channel access time for the same bridge device. Here, a Route-reply Triggered Resource-reservation (RTR) mechanism is proposed to resolve this problem. In RTR, the resource reservation for a route passing several piconets is triggered by the transmission of RREP from the destination node. Our approach includes three features:

- Relaying RREP via PNC: Instead of transmitting a RREP to the previous intermediate device, a device transmits the RREP to the PNC and the PNC relays the RREP to the next hop device.
- Piggybacking reserved time-slots with RREP: Once a PNC receives a RREP but it is not on the route, it reserves the channel access time for the device that transmitted the RREP and its previous device recorded in the path table. The PNC piggybacks the information of the allocated time-slots with the RREP and transmits the RREP to the previous device.
- Updating the resource reservation status at a bridge device proactively: If a bridge device is reserved by a PNC within one piconet, the bridge device should inform all the adjacent PNCs to update their admission tables to record the time-slots that the bridge device is already engaged. With the use of this mechanism, a PNC has sufficient information to allocate channel resource properly.

The example shown in Figure 8.12 is taken to explain the RTR joint routing and resource reservation mechanism, and the corresponding message sequence chart is shown in Figure 8.13. If multiple RREQs arrive at a piconet simultaneously, the channel resource estimation might not be accurate enough, because the device cannot sense the parallel estimations from other devices in the same piconet.



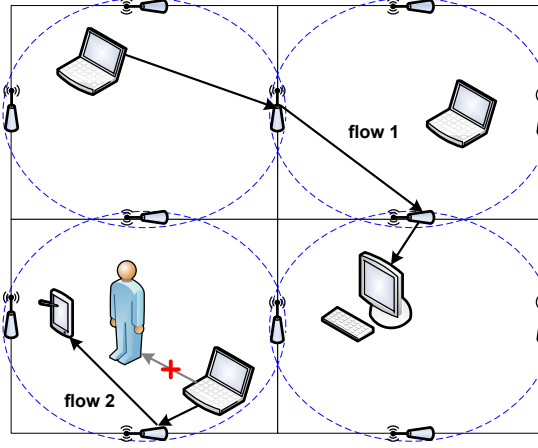


**Figure 8.14:** *Simulation scenario with  $2 \times 2$  piconets and 12 bridge devices.*

analysis, it is supposed that the data rate amongst the bridge devices with direct links to each other is  $R_{max}$ . However, our approach can also support variable data rates. In each simulation run, the transmission pairs are randomly picked up. If the selected source and destination are within the same piconet, it is considered as intra-piconet communication. Otherwise, it is considered as inter-piconet communication. To take consideration of LOS link blockage problem which is mentioned in Chapter 5, it is defined that the link blockage happens for intra-piconet communication with probability  $p_\kappa$ . If a direct link is blocked, the transmitter uses bridge devices to relay traffic, like flow 2 illustrated in Figure 8.14. Normally, it is recommended to mount bridge devices at high positions to reduce the link blockage probability. Therefore, it is assumed that the link between two bridge devices cannot be blocked.

Network capacity is our primary investigated parameter. Not losing the generality, the accumulated capacity within the entire network is defined as a normalized factor  $C$ , which is given by,

$$C = \sum_{i \in I} \frac{B_i}{R_{max}}, \quad (8.9)$$

where  $B_i$  is the required bandwidth (in Mbps) of flow  $i$ . It is assumed that the superframe length  $L_{SF}$  is fixed. In order to support a flow with  $B_i$ , each link along the route needs to reserve a CTA block with length  $T_{CTA}$ , where  $T_{CTA} = B_i L_{SF} / R_{max}$ . If each flow requires the same bandwidth, the number of CTA block in one superframe could be calculated as  $N_{CTA} = \left\lceil \frac{\eta L_{SF}}{B_i} \right\rceil$ , where  $\lceil \cdot \rceil$  is the ceiling function. All the following simulation results are the mean of 10000

**Table 8.3:** *Specifications for the proposed schemes*

Scheme	Routing	Resource Allocation
S1-D	Dijkstra	Random w/o RTR
S1-QD	QoS Dijkstra	Random w/o RTR
S2-D	Dijkstra	N-P
S2-QD	QoS Dijkstra	N-P
S3-D	Dijkstra	RTR
S3-QD	QoS Dijkstra	RTR

iterations.

### Simulation Schemes

To compare with our proposed RTR, the other two channel resource allocation mechanisms are introduced as follows:

- Random w/o RTR: A PNC randomly picks up a free CTA block for the request link, if the channel resources are sufficient. Randomly selecting CTA blocks could reduce the chance of reservation collisions, but it cannot be avoided. Especially when the traffic load is high, the possibility for reservation collision is also high.
- Normal and Public CTAs (N-P): This refers to the mechanism proposed in [104], where the CTAs are segregated into two parts: normal CTAs and public CTAs. The normal CTAs are used for the links outside the overlapped area. For the links within the overlapped area, channel resources can only be allocated from the public CTAs. If two piconets have overlapped area, the PNCs should negotiate with two non-overlapped public CTAs to separate the reservation time for the devices within the overlapped area. To compare this mechanism with our proposal, the ratio between the length of the normal CTAs and public CTAs is set as 1 : 4, and the adjacent piconets have the same length of public CTAs.

Our proposed QoS routing scheme is also compared with the shortest-path routing, which uses hop-count as the link weight metric. Combining the routing and channel resource allocation mechanism together, there are six schemes which are listed in Table 8.3. In this table, Dijkstra is the algorithm used for finding the path with minimum hop count. The proposed QoS routing mechanism is used to specify the weight factor for each link, and use Dijkstra to find a route with minimum accumulated weight factor, which is denoted as QoS Dijkstra.

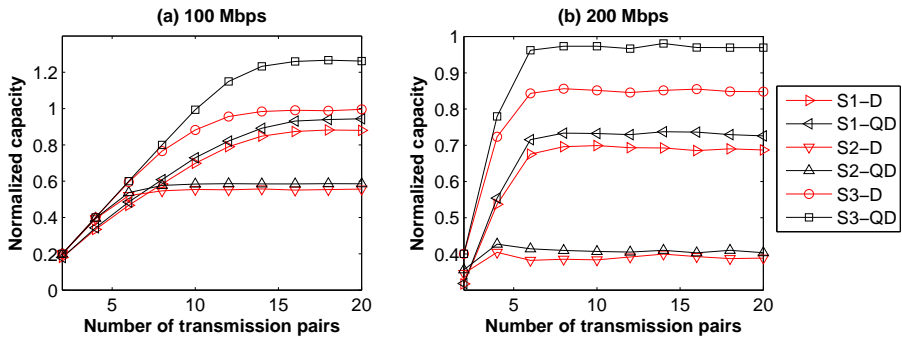


**Figure 8.15:** The normalized capacity as a function of the number of transmission pairs within  $2 \times 2$  piconets,  $\eta = 90\%$ ,  $p_\kappa = 0.1$ .

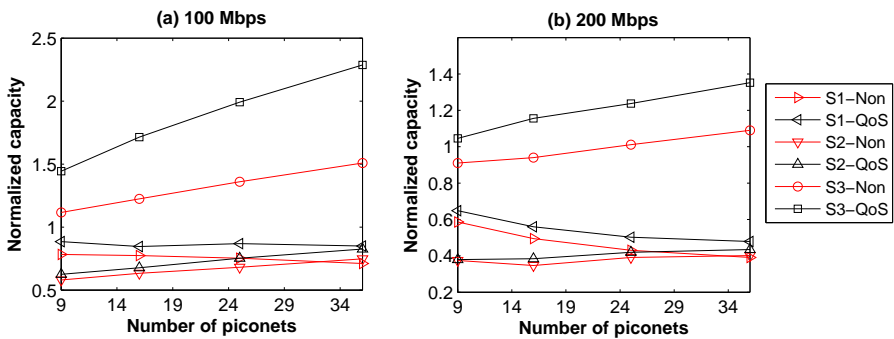


**Figure 8.16:** The normalized capacity as a function of the number of piconets,  $\eta = 90\%$ ,  $p_\kappa = 0.1$ .



### Performance of Channel Resource Allocation Mechanisms

Figure 8.15 evaluates the different simulation schemes in terms of normalized capacity within  $2 \times 2$  piconets. The transmission scheduling is based on FCFS. As shown in this figure, all the QoS-based schemes perform better than non-QoS based schemes. This indicates the effectiveness of our QoS based routing mechanism. The subplot (a) shows the performance when the traffic load  $B_i$  is 100 Mbps, and the subplot (b) is for 200 Mbps. In both figures, the QoS routing mechanism with the proposed RTR outperforms the other resource reservation algorithms. The reason is that the QoS based routing scheme can balance the traffic load to increase the entire system capacity. Moreover, RTR increases the system capacity by preventing resource reservation collisions. Figure 8.16 depicts the saturated capacity of all the schemes as a function of the number of piconets. With the increase in the number of piconets, Random w/o RTR and N-P have similar performance. However, Random w/o RTR suffers from channel resource reservation collisions, which can decrease the network capacity. Although N-P can mitigate reservation collisions, it is less dynamic than our proposed RTR.

### Performance of Transmission Scheduling Algorithms

In this section, the performance of two transmission scheduling algorithms, namely FCFS and DTS, are compared based on the proposed RTR channel resource allocation mechanism. In Figure 8.17 and 8.18, FCFS-D and DTS-D denote the FCFS and DTS algorithms when Dijkstra routing algorithm is used. Similarly, FCFS-QD and DTS-QD correspond to the case where QoS Dijkstra routing approach is used. Figure 8.17 depicts the system capacity with the increase in the number of transmission pairs in  $2 \times 2$  piconets, in which, DTS-QD exhibits the best performance in both subplots. Figure 8.18 shows the capacity variance and the resource utilization ratio per piconet when the traffic load is 100 Mbps. The capacity is defined in (8.9), and resource utilization ratio is defined as  $\zeta = C/N_{PN}$ , where  $C$  is the network capacity and  $N_{PN}$  is the number of piconets. The mean hop-counts for different algorithms and different network sizes are listed in Table 8.4. By exploiting spatial reuse capability in WPANs with directional antennas, the DTS algorithm combined with the QoS routing scheme improves the network capacity and channel resource utilization considerably. Figure 8.19 illustrates the impact of MAC efficiency factor  $\eta$  on the network capacity when DTS-QD is used. As mentioned before, this value expresses the proportion of channel resource used for data communication. When  $\eta$  increases from 70% to 90%, the network capacity increases 43.12% for  $N_{PN} = 9$ , and 67.16% for  $N_{PN} = 36$ . However, it does not mean that  $\eta$  should be as large as possible, because the proportion of  $1 - \eta$  is used for command packet like neighbor discovery, route discovery, network maintain, etc. If  $1 - \eta$  is too small, it might be difficult to maintain the entire network.

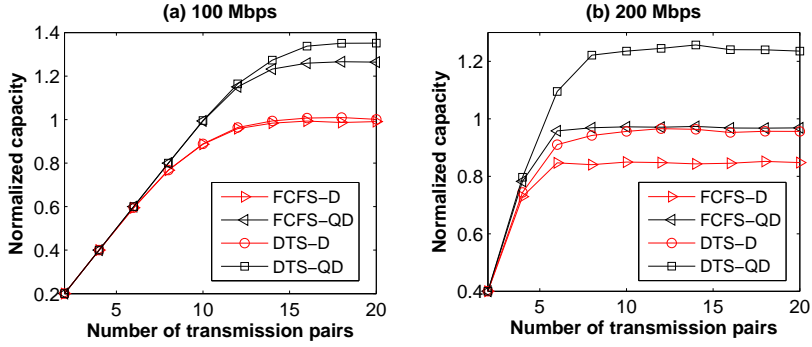


**Figure 8.17:** The performance of joint transmission scheduling and routing algorithms within  $2 \times 2$  piconets,  $30^\circ$  directional antennas,  $\eta = 90\%$ ,  $p_\kappa = 0.1$ .

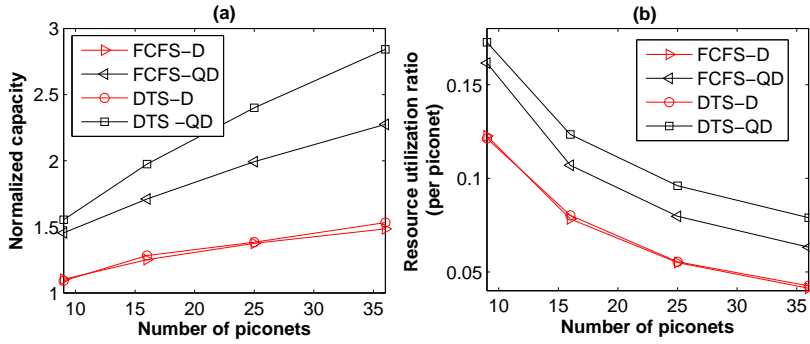


**Figure 8.18:** The performance of joint transmission scheduling and routing algorithms with the variant number of piconets,  $30^\circ$  directional antennas,  $\eta = 90\%$ ,  $p_\kappa = 0.1$ .

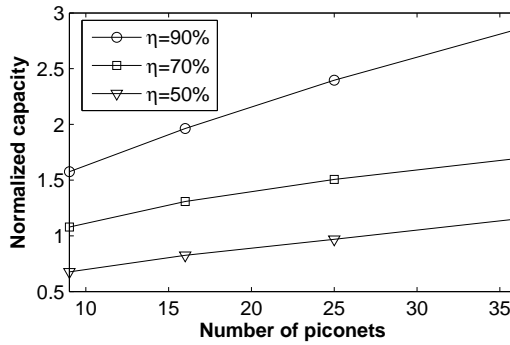


**Figure 8.19:** The impact of the MAC efficiency factor  $\eta$  on the network capacity, considering DTS-QD,  $30^\circ$  directional antennas.

**Table 8.4:** *The mean hop-count for various network sizes*

$N_{PN}$	FCFS-D	FCFS-QD	DTS-D	DTS-QD
$3 \times 3$	2.91	3.03	2.93	3.08
$4 \times 4$	3.83	4.01	3.84	4.07
$5 \times 5$	4.76	4.96	4.76	5.10
$6 \times 6$	5.70	5.88	5.64	6.03

## 8.4 Chapter Summary

Due to the severe propagation attenuation and absorption properties of the 60 GHz radio, ultra high data rate transmissions can only be achieved within a short range. To extend the 60 GHz radio coverage range, radio relay devices could be used to bridge the inter-piconet communication. To provide a better support for room-to-room communication, a systematic study has been provided to investigate the feasibility to enable inter-piconet route discovery process in 60 GHz WPANs. It has been reviewed that by intelligently designing the RREQ and RREP forwarding mechanisms, the directional broadcast overhead can be dramatically mitigated and the route discovery latency can be effectively reduced. To coordinate inter-piconet channel resource allocation, a cross layer framework has been proposed in this chapter, which could effectively resolve the inter-piconet channel resource reservation collisions. During a route discovery process, if the resource availability is taken into account, proper paths can be selected beforehand to optimize the entire system capacity with QoS provisioning.



# Chapter 9

## Conclusions

“When *vision* looks inward it becomes a *duty*. When *vision* looks outward it becomes an *aspiration*. When *vision* looks upward it becomes a *faith*. When *vision* looks forward it becomes a *reality*.”

- Anonymous

*This chapter presents an overview of the major contributions obtained from previous chapters. It is our **duty** to first look inward to provide a valuable summary insights into the filed of 60 GHz wireless communication. It is our **aspiration** in the sense that it tries to resolve the research challenges in 60 GHz radio. It is our **faith** it will become a **reality**. To continue the research in the area of 60 GHz wireless communication, it is also our **duty** to elaborate a number of research issues that are unresolved yet.*

## 9.1 Recapitulation

To cater to the emerging wireless multimedia applications like uncompressed high-definition video streaming, it is necessary to increase the wireless transmission data rate to the order of Gigabits per second (Gbps). Currently, the available wireless technologies, for instance IEEE 802.11x WLAN, can not meet this data rate requirement. Therefore, researchers have begun to look for possible solutions on the spectrum which is centered around 60 GHz. Up to 7 GHz spectrum near 60 GHz has been allocated worldwide for unlicensed use. As a promising technology that can handle multi-Gbps data rate, 60 GHz radio is expected to play an important role in the fourth-generation (4G) wireless system. The main focus of this dissertation is to enable high-capacity and high-reliability communication in WPANs using 60 GHz radio technology. The unique properties of 60 GHz radio pose special research challenges, which are identified in Section 1.4. To overcome these hurdles, it requires a novel network architecture design with innovative proposals on the Medium Access Control layer (MAC) and the Network layer. Hence, this dissertation aims to provide an in-depth view of the following aspects of 60 GHz networks: (1) self-organization of the network (2) medium access control (3) maintenance of connectivity (4) system coexistence (5) multi-hop communication (6) QoS provisioning. In this section, we provide a summary of the results obtained under each aspect listed here.

### • Self-organization of the Network

A network is self-organized, if it is organized and maintained without any external infrastructure, central dedicated control entity, system administrator, or users. In-home wireless communication networks are expected to deliver the services for the users without letting them be aware of the technicalities. Hence, network self-organization is a crucial factor to achieve user friendly man-machine interaction experience. Network initialization, neighbor discovery, route discovery, connection setup and topology management are the major factors to enable network self-organization. Hence, the network self-organization is a theme running through the entire dissertation. The main difficulty in realizing self-organization in 60 GHz radio based wireless networks is the use of directional antennas. Although directional antennas offer many advantages over omni-directional antennas, their deployment is very challenging for the MAC and Network layer protocols. To set up connections, devices are expected to know the direction information of their neighbors. Therefore, Directional Neighbor Discovery (D-ND) process has been investigated in Chapter 2. A comprehensive theoretical model has been deduced for different Neighbor Discovery (ND) protocols (one-way ND and handshake-based ND) combined with different antenna transceiver modes (DO mode and DD mode). Our proposed model is accurate for the D-ND with the assumption of an idealized flat-top antenna pattern without interference consideration from the antenna side lobes. To

address a more sophisticated antenna pattern and its side lobe influence on a D-ND process, a uniform circular array antenna system and a refined link probability model have been introduced in our work. With the knowledge of the identities and directions of the neighbors, medium access using directional antennas has been studied in Chapter 3. The IEEE 802.15.3 standard defines a well-accepted MAC for high data rate WPAN due to its capability to support QoS for multimedia applications. However, this MAC protocol is designed for omni-directional antennas. To support directional antennas in IEEE 802.15.3 based WPANs, a Directional Transmission Scheduling (DTS) algorithm and corresponding resource management scheme have been proposed to schedule concurrent directional transmissions in 60 GHz WPANs. We have shown the improvement in the system capacity by exploiting the spatial reuse capability of directional antennas. Chapter 7 investigates the topology management and information dissemination processes, and Chapter 8 studies route discovery, establishment and multi-hop resource management schemes.

- **Medium Access Control**

MAC transmission efficiency is a crucial factor to evaluate the performance of a MAC protocol. It can be simply defined as the proportion of the channel access time used for data communication within a system. Automatic repeat request is a MAC layer mechanism using Acknowledgment (ACK) and timeouts to increase transmission reliability in error-prone wireless channels. Due to the fact that the data rate considered here is in the order of Gbps, the transmission overhead caused by the ACK and timeout mechanism severely impacts the capacity of 60 GHz systems. There are two mechanisms identified in this dissertation to increase the capacity of 60 GHz systems. The first one is exploiting the spatial reuse capability using directional antennas as mentioned in Chapter 3. This is an indirect way to alleviate the impact of the overhead. In comparison with the first method, the second method uses the frame aggregation mechanism to reduce the impact of overhead. Two frame aggregation mechanisms have been studied in Chapter 4, i.e. standard frame aggregation and low latency frame aggregation. We have proposed an analytical model to access the performance of these two aggregation mechanisms in terms of system capacity and packet delivery delay. It has been shown that the standard frame aggregation mechanism effectively improves the system capacity when the channel quality is sufficiently high. However, the improved capacity comes at the price of the prolonged delay. Hence the low latency frame aggregation mechanism has been investigated to support the services like delay-sensitive applications.

- **Maintenance of Connectivity**

High-reliability is a crucial requirement for wireless communication to support multimedia-oriented applications. A direct reflection of reliability is

the connectivity of a radio link. Due to the weak penetration and reflection properties, 60 GHz communication highly relies on the LOS link. Therefore, in an indoor environment, a moving person or any obstacle passing through two 60 GHz radio components can easily block the LOS connection. The LOS link blockage problem has been addressed in Chapter 5. Thanks to the beam-forming capability of adaptive antenna array systems, it is possible to manually switch the antenna's transmitting or receiving direction. Hence, in Chapter 5, Beam Switching (BS) based mechanisms are proposed to resolve the link blockage problem. To support different usage models, the BS mechanisms are classified into two categories: BS based on instant decision and BS based on environment learning. The instant decision based BS is suitable for portable devices without fixed positions. It is observed that combining the directional information of a beam path with the received SNR makes a better instantaneous BS decision. The environment learning based BS uses the earlier switching experiences and the current measured data to make a switching decision, which is suitable for the devices with fixed positions, like HDTV, VRD, etc. Once there is no alternative beam path that can be used to maintain connectivity, transmitter and receiver can be linked via the third party in a multi-hop fashion, which has been investigated in Chapter 8.

- **System Coexistence**

From Chapter 2 to Chapter 5, the network organization, medium access and connectivity maintenance are addressed to enable high-capacity and high-reliability communication within a single WPAN. Now the stage is set to extend the communication ability from one-WPAN to multi-WPANs. Due to the stringent link budget to achieve Gbps-based transmission, 60 GHz radio is very fragile to the Co-Channel Interference (CCI). However, it is possible for several WPANs coexist with each other within a certain area, for instance, conference room, exhibition hall, etc., because of the limit coverage range of 60 GHz radio. Hence, it is essential to devise a CCI mitigation mechanism in order to provide high performance 60 GHz communication in the coexisting environment. Synchronization (sync) frame is used in the IEEE 802.15.3c standard to mitigate CCI. Chapter 6 reported a thorough investigation to examine the performance of using sync frame within coexisting WPANs. The beacon and sync frame range is a hinge factor to decide the achievable piconet capacity, since the spatial reuse capability (the number of coexisting piconets in a certain area) is inversely proportional to the amount of CCI. To obtain the relationship between the beacon and sync frame range with CCI, special concerns have been placed in our proposed theoretical model. Wherein, the log-normal radio propagation model is used to model the CCI in each piconet. It is observed that communication within a single WPAN can be effectively protected from other coexisting WPANs using sync frames.



The system coexistence issue is also addressed in Chapter 8, in which, radio relay devices, which are also called as bridge devices, are introduced to provide infrastructure mode in wireless in-home networks. Because of the weak penetration property of 60 GHz radio, the concrete walls and floors of a building are natural boundaries for room-based piconets. Radio relay devices are capable of acting as bridges to enable room-to-room communication.

- **Multi-Hop Communication**

Due to the limited coverage range of 60 GHz radio, it is necessary to address multi-hop communication in 60 GHz systems. In this dissertation, multi-hop communication is taken into account from two aspects. First, to explore the impact of directional antennas on multi-hop communication, the fundamental investigations have been undertaken in Chapter 7 in terms of topology control and message dissemination. We concluded that the neighbor attachment policies that focus on the interference reduction may fail to improve system capacity in ad-hoc networks. Moreover, directional message dissemination processes have been studied in different network graphs with different antenna modes and dissemination algorithms. It has been shown that using directional transmitting and directional receiving (DD mode) does not always perform worse than directional transmitting and omni-directional receiving (DO mode). On the contrary, DD mode can help to speed up the message dissemination process due to its extended coverage range.

Second, to enable multi-hop communication for in-home network amongst multiple piconets, bridge devices are involved in the infrastructure design. The bridge devices provide the feasibility for room-to-room communication via 60 GHz radio. Moreover, with the deployment of the bridge devices, it is also possible to resolve the link blockage problem via multi-hop solution. While extending the range of WPANs, bridge devices become the capacity bottlenecks for these connected piconets. An un-optimized resource allocation mechanism involving the bridges could severely degrade system performance. After examining the inter-piconet route discovery process using directional antennas, a novel inter-piconet channel resource reservation mechanism has been proposed in Chapter 8. In our proposed scheme, resource allocation cooperates with the route discovery process to mitigate possible inter-piconet resource reservation collisions. Simulation studies show that our approach significantly increases network capacity.

- **QoS Provisioning**

Catering to the applications like uncompressed high-definition video streaming, 60 GHz systems are envisaged to be capable of providing QoS for multimedia applications. The IEEE 802.15.3 MAC defines a centrally controlled network topology, in which the PNC manages QoS by scheduling peer-to-

**Table 9.1:** *Overview of the main contributions and corresponding research criteria*

	Self-organization	Medium access control	Connectivity maintenance	System coexistence	Multi-hop	QoS
Ch2. D-ND	✓					
Ch3. Enhanced 802.15.3 MAC	✓	✓				✓
Ch4. Frame aggregation		✓				✓
Ch5. Beam switching	✓		✓			
Ch6. Interference mitigation	✓	✓		✓		
Ch7. Dir-antenna impact on multi-hop	✓				✓	
Ch8. In-home multi-hop	✓	✓	✓	✓	✓	✓

peer communication via TDMA based medium access mechanism. However, the IEEE 802.15.3 MAC lacks fairness and multi-class traffic support. In Chapter 3, a QoS-aware transmission scheduling algorithm with fairness consideration is devised to support heterogeneous services in WPANs. This proposal can be considered as an add-on to the IEEE 802.15.3 MAC. Our proposal can substantially improve system performance in terms of the delay-based fairness and job failure ratio. Moreover, QoS provisioning is addressed in Chapter 4, in which, low frame aggregation mechanism has been studied to support delay-sensitive multimedia applications.

As we know, the IEEE 802.15.3 MAC lacks the capability to support multi-hop communication. In Chapter 8, a joint routing and channel resource allocation mechanism has been proposed to resolve the inter-piconet resource reservation and routing issues. Moreover, our routing mechanism is QoS aware by considering the available channel resource within a piconet for route selection.

In summary, 60 GHz radio technology is a very attractive candidate for short-range wireless communication, but it is also challenging at the same time. Therefore, this dissertation is dedicated to resolve the challenges that are raised by enabling the 60 GHz WPANs, in which, the MAC and Network layers are the main focuses. The overview of the contributions of each chapter and the important research criterion addressed by each of them are listed in Table 9.1.

## 9.2 Directions for Future Work

Based on our investigation so far, it has been shown that 60 GHz radio is capable to be used for high-performance wireless communication. However, we believe that it is still a long way to adopt 60 GHz radio for future home networks, which is envisioned with ambient intelligence. Therefore, we raise a number of issues that are worthy for the future investigation.

- **Cross-layer Optimization**

Protocol-wise solutions for 60 GHz networks should be service-oriented. As introduced in Chapter 1, the usage models are classified into five categories according to the IEEE 802.15.3c activities, and different categories have different requirements regarding transmission data rate, channel quality, and QoS constraint. Hence it is an interesting aspect to investigate protocol-wise adaptations according to the delivered service via cross-layer optimization approach. For instance, link reliability is an essential factor that influences the quality of experience of users. LOS blockage is a problem for 60 GHz network which severely influences the link reliability. A beam switching mechanism is proposed in this dissertation to resolve the LOS link blockage problem. However, it is possible that the alternative NLOS link cannot provide sufficient link budget for high speed communication. For the sake of reliability maintenance, it is necessary to adjust QoS requirements according to the current channel status. For instance, to adapt uncompressed video stream to compressed video stream, which is a resource management issue involves cross-layer optimizations.

- **Coexistence of Multiple Standardizations**

Without any doubt, 60 GHz radio technology offers tremendous opportunities for our society. To facilitate the research development of 60 GHz radio technology and its interconnection with industry area, a number of non-profit international standardization groups and industry-led efforts have emerged to unify and standardize the use of 60 GHz radio technology. In the future market, it is possible that an overabundance of 60 GHz electronic products featured by different standardization incurs the multi-standard coexistence issue.

- **Coexistence of Multiple Technologies**

According to Moore's Law, the number of components in a semiconductor chip doubles every year. According to the prediction of the WWRF meeting, seven trillion wireless devices will serve seven billion people by 2017, which means there will be 1000 wireless devices providing services for one person [107]. Within this mega-trend of wireless technology development, the future network components, including portable personal consumer electronic devices, are envisaged to be capable to support multi-technology with

multi-interface. Hence it is worth to investigate how to maximize the 60 GHz system capability by acquiring the assistance and cooperation with other technologies. For instance, In Chapter 5 we have proposed the BS based mechanisms to resolve the link blockage problem in 60 GHz radio systems. Assuming that a device has multiple radio interfaces, once the 60 GHz radio connectivity is blocked, the device may easily switch to a low frequency band for instance 2.4 or 5 GHz, to maintain the connectivity. Moreover, the combination of radio-over-fiber technology with 60 GHz radio technology may solve the mobility and handover hurdles which cannot be easily addressed by 60 GHz radio alone.

### • Integration of Technology and User Behavior

The essential and ultimate purpose of technology is to improve the quality of everyday life of people. During the development period, different technologies may compete with each other to gather a significant market share. After the progressive improvement and maturity, technologies will be in the relationship of mutual interdependence and mutual complementarities. In the future ambient intelligent home and office environment, there will be a seamless integration of multi-scale networks, for instance, sensor network, wireless mobile networks, home entertainment systems, etc. Consumer electronic devices do not simply provide service according to the users' requirements. They could also sense, learn and self-adapt to fulfill the users' needs via day-to-day man machine interactions. Therefore, the integration mentioned here does not simply refer to the cooperation between different devices or different technologies. The essential issue is how to give a "soul" for a technology such that it knows the habits of users, learns emotions of users and enriches ambient life of users with *intelligence* and *empathy*.

## 9.3 Epilogue

60 GHz radio is a promising technology on the block which breaks the barriers of Gbps-based wireless communication. While doing so it is expected to totally change user experience with wireless technology. At the end of this dissertation, we would like to emphasize our contributions to the wireless communication using 60 GHz radio technology as a whole. The motivation of this dissertation was to design *high-capacity* and *high-reliability* 60 GHz system to support in-home wireless communication. This dissertation spans from MAC layer protocol design to Network layer protocol design, from single hop communication to multi-hop communication. To achieve high-capacity, we investigated how to improve the system capacity by exploiting special reuse capability using directional antennas. We also studied the performance of frame aggregation mechanism to overcome the impact of overhead. To achieve high-reliability, a beam switching based mechanism is proposed to against the link blockage problem in 60 GHz systems. Moreover, a

multi-hop communication scheme is involved in this dissertation to assure room-to-room communications. While we agree that there are many solutions already in this domain, we also stand out (if not *outstanding*) with our contributions. Gbps-based wireless communication is the mega-trend for future in-home networks. We have tried here to come up with the best possible solutions to enable 60 GHz radio for in-home networks. We do not claim to have done everything to achieve a future proof architecture as well as technology to realize the grand vision of a 60 GHz home networks. While there are many issues to deal with as mentioned in the previous section, *pari passu*, we would like to state that the results we have provided here are some of the important steps towards realizing our grand vision.

## A Parting Note

*60 GHz radio breaks the barrier of data rate bottleneck of wireless transmission. Is Gigabit the upper-limit for wireless communication? Or, are we just one step away from Terabit transmission?*



## Occupancy Problem in Directional Neighbor Discovery

In this appendix, the occupancy problem in one-way directional transmitting and omni-directional listening neighbor discovery (DO-ND) process is discussed. In one round of scanning during a DO-ND process, if device  $m$  is in the receiving state, the number of directional advertising messages that arrive at  $m$  in the  $x^{th}$  slot of one frame is denoted as  $n_x$ . Hence we have  $n_1 + n_2 + \dots + n_{N_b} = w$ , where  $N_b$  is the number of beam sectors which is also equal to the number of slots in one frame, and  $w$  is the number of neighbors that are in the transmitting state. This problem is an occupancy problem that randomly place indistinguishable  $r$  balls into  $n$  cells, where  $r_1 + r_2 + \dots + r_n = r$ , and the number of elements in one cell can be zero. The number of ways to separate  $r$  elements into  $n$  sub-groups is given by [42],

$$\begin{aligned}
& \binom{r}{r_1} \binom{r-r_1}{r_2} \binom{r-r_1-r_2}{r_3} \dots \binom{r-r_1-\dots-r_{n-2}}{r_{n-1}} \binom{r_n}{r_n} \\
&= \frac{r!}{r_1!(r-r_1)!} \frac{(r-r_1)!}{r_2!(r-r_1-r_2)!} \\
&\quad \times \frac{(r-r_1-r_2)!}{r_3!(r-r_1-r_2-r_3)!} \dots \frac{(r-r_1-\dots-r_{n-2})!}{r_{n-1}!(r-r_1-r_2-\dots-r_{n-1})!} \\
&= \frac{r!}{r_1!r_2!\dots r_n!}. \tag{A.1}
\end{aligned}$$

Denote  $w$  as the maximum number of balls in one cell, where  $w = \max(r_n)$ . Therefore, we have  $n_0 + n_2 + \dots + n_w = n$ , where  $n_i$  is the number of cells which contain  $i$  balls in them,  $0 \leq i \leq w$ . According to (A.1), the number of ways to

participate in cells is given by,

$$\frac{n!}{n_0!n_1!\dots n_w!} \quad (\text{A.2})$$

Therefore, the total number of distributions of the occupancy numbers with  $\mathcal{N}_n = [r_1, r_2, \dots, r_n]$  is given by,

$$\mathbb{N}_{r,n} = \frac{r!}{r_1!r_2!\dots r_n!} \times \frac{n!}{n_0!n_1!\dots n_w!} \quad (\text{A.3})$$

In total, there are  $n^r$  possible placements which are equiprobable, hence the probability  $p$  to obtain the given occupancy number  $\mathcal{N}_n$  is  $p = \mathbb{N}_{r,n}n^{-r}$ .



## Implementation of Enhanced IEEE 802.15.3 MAC

OPNET employs a hierarchical structure to model communication networks, which is comprised of network, node and process models. The network model defines the overall simulated system that includes communication links, devices or sub-networks. A device can be mapped into a specific node model that represents its internal protocol structure. The OPNET node model uses an analogous concept of layer-based protocols described by the OSI reference model. In the node model, each layer has a corresponding processor module, and these modules only exchange data with the adjacent layers over packet streams. The process models in OPNET use a Finite State Machine (FSM) paradigm to express model behaviors. FSMs are represented by a state transition diagram approach which contains state objects and transition objects. States are used to represent the significant modes of a process. Each state has an attribute called as status which is used to designate the state as forced or unforced. A forced state is one which is necessarily traversed without any simulation time elapsing. An unforced state is one in which a process can remain after having been invoked to respond to an interrupt.

At the beginning of simulation, each queue or processor has only a single process that is automatically created by the kernel. This process is termed as *root process*. During simulation, the root process or any processes can dynamically create additional processes within a queue or processor. The newly created process is called as *child process*. The process which created a child process is referred as *parent process*. On modeling a complicated system or protocol, usually single process model is not enough to clearly represent the required functionalities. Therefore, it is recommended by OPNET modeling methodology to decompose different functionalities into different process models. In our designed WPAN\_MAC module, it contains one root process and three children processes. The child

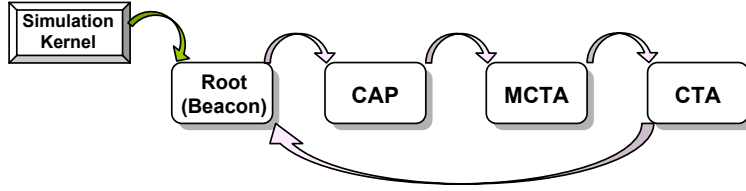


**Figure B.1:** *Dynamic process design for IEEE 802.15.3 MAC in OPNET.*

processes are invoked by their parent processes according to the time sequence shown in Figure B.1. When the simulation begins, the simulation kernel invokes the root process of each node, which is also called as beacon process. In the root process, the PNC generates and broadcasts beacon that contains the timing and management information which specifies the beginning time of the CAP, MCTA and CTAP in the current superframe. Other DEVs in the piconet synchronize themselves with the PNC by receiving the beacons. At the end of beacon period, beacon process invokes the CAP process, MCTA process is invoked at the end of the CAP, and CTA process is invoked at the end of MCTA. When the CTA period is over, it triggers the execution of the beacon process again to schedule the next superframe.

## B.1 Root Process Modeling

The diagram in Figure B.2 illustrates the FSM for root (beacon) process. It includes a main process state `Tx_Beacon`. This state is used for the PNC to schedule channel access time for the DEVs within its piconet for the current superframe. By leaving this state, PNC schedules a self interrupt to invoke CAP. When the current superframe is over, the `SF_END` state resets the overdue parameters and triggers the beginning of the next superframe. The color of a forced state is green and an unforced state is red.

## B.2 CAP Process Modeling

### Medium Access Control Mechanism

The MAC mechanism during the CAP is based on CSMA/CA, the basic operation procedure of which is shown in Figure B.3. The PHY layer of the node model is featured with the Clear Channel Assessment (CCA) capability, which can be used to detect the busy or idle state of the channel. According to the CSMA/CA, a transmitter is required to perform channel sensing before medium access to avoid possible collisions. This process of waiting before transmission is called as *backoff*. Before transmitting a data frame, the remaining time in the CAP needs

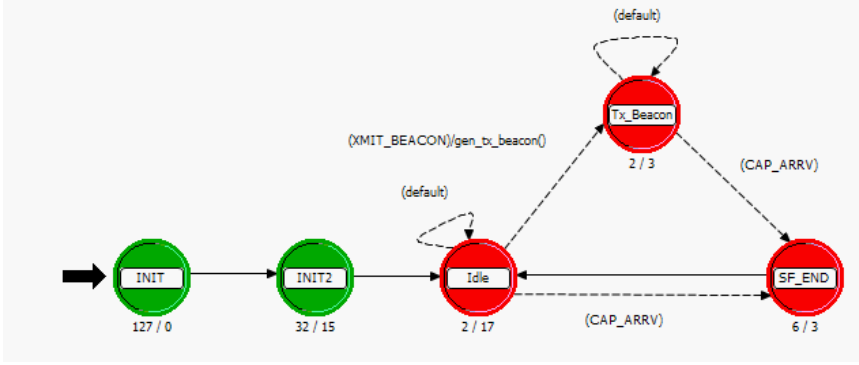


Figure B.2: FSM diagram for *Root(beacon)* process.

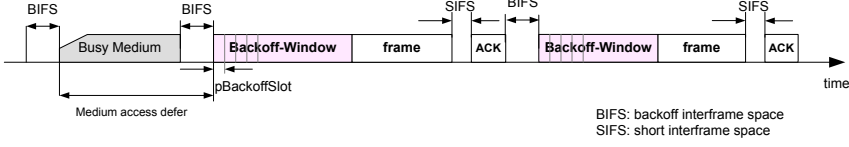
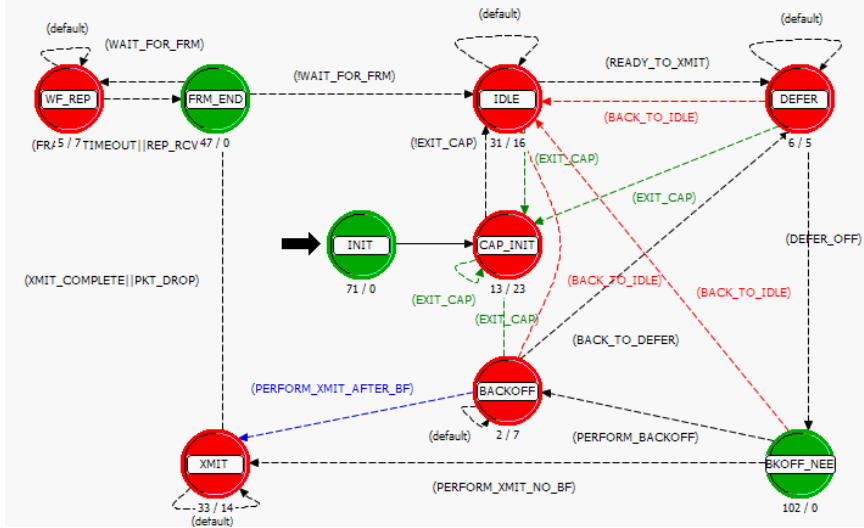


Figure B.3: CSMA/CA medium access diagram.

to be long enough to accommodate the current frame, 2 SIFS times and the Imm-ACK frame when the Imm-ACK retransmission mechanism is used [3]. In no case a DEV or the PNC extend its transmission that was started during the CAP into the MCTA. The FSM diagram for the CAP process is illustrated in Figure B.4.

### Backoff Algorithm

During the CAP, a DEV is allowed to transmit a data frame after the backoff procedure. The backoff mechanism applies to every frame attempting for medium access during the CAP except for the Imm-ACK frames. According to the number of retransmission times, the backoff process requires the transmitter to choose an integer in the range of 0 to 3, which acts as an index in a table with the values [7, 15, 31, 63]. The device then generates a random integer between 0 and the selected value, termed as the backoff counter. The backoff counter is decremented by one only when the medium is sensed idle for the entire duration of a backoff slot. Whenever the channel is busy, the backoff counter is suspended. The channel should be sensed idle for the duration of a Backoff Inter-Frame Space (BIFS) period before the backoff slot countdown is resumed. Once the counter reaches zero, the transmitter is allowed to transmit. The counter is suspended outside the CAP period.

Figure B.4: *FSM diagram for CAP process.*

### B.3 MCTA Process Modeling

The PNC and DEVs play different roles in the MCTA period. DEVs transmit Channel Time Request (CTR<sub>q</sub>) frames to the PNC to reserve the channel access time in the next Superframe. Whilst the PNC in the MCTA period is in charge of receiving those CTR<sub>q</sub> frames and hence execute admission operation depending on whether the current superframe remainder is enough for the requested reservation time, though PNC also reserves channel time for itself if necessary. The PNC transmits back a Channel Time Response (CTR<sub>p</sub>) frame to the requesting DEV using *reason\_code* field inside a CTR<sub>p</sub> frame to inform the DEV whether the reservation request has been scheduled or not. The PNC certainly checks its own reservation need and carryout similar steps without the involvement of command frame CTR<sub>q</sub> or CTR<sub>p</sub>.

#### Medium Access Control Mechanism

Slotted ALOHA is the access mechanism in MCTA. The access to MCTA shall be controlled by a contention window  $CW_a$  maintained by each DEV. The contention window shall be derived from the number  $a$ , where  $a$  is the number of retransmission attempts made by the DEV. For the first access attempt,  $a$  is set to zero. The size of the contention window  $CW_a$  is defined by the following formula:

$$CW_a = \begin{cases} 256 & \text{if } 2^{a+1} \geq 256 \\ 2^{a+1} & \text{if } 2^{a+1} < 256 \end{cases}$$



CTA process. The whole process is basically split into two parts: transmit and receive. In the CTA period, certain channel access time has been allocated for a transmission pair. The timing related information (e.g. CTA sequence number, CTA begin time and CTA end time) is specified in the beacon packet at the beginning of the superframe.

### **Directional Antenna Control**

At the beginning of each allocated CTA block, the transmitter and receiver point the main lobe of their directional antennas to each other to achieve high data rate transmission. At the end of the allocated CTA block, their antenna modes change back from directional to omni-directional.

# IEEE 802.15.3c Physical Layer Specification

The millimeter wave PHY defined by IEEE 802.15.3c working group [7] operates in the frequency band of 57-66GHz, as allocated by the regulatory agencies in Europe, Japan, Canada, the United States. Three PHY modes are defined in IEEE 802.15.3c, the Single Carrier (SC) mode, the High Speed Interface (HSI) mode and the Audio/Video (AV) mode. Without loss of generality, we will use SC mode as the PHY layer to study the performance of the higher layer protocols.

PHY layer simulation is performed to obtain the BER performance under real 60 GHz residential environments. The transceiver function block diagram used in the PHY layer is shown in Figure C.1. To protect the transmitted data in the presence of noise, channel coding is performed to encode the raw bit stream. The considered forward error correction code is the Reed-Solomon code that encodes 239 octets to 255 octets, giving a code rate of 0.937. The supported modulation schemes included BPSK, QPSK, 8PSK and 16QAM, and their corresponding modulation levels  $L_m$  are denoted as 1,2,3 and 4. The pulse filtering strategy is root-raised cosine in both the transmitter and receiver with roll-off factor of 0.25. The 60 GHz power amplifier at the front end of the transmitter has a power output backoff of 3 dB for LOS environment and 5 dB for NLOS environment. Particularly in multipath (NLOS) environment, the receiver employs the Minimum Mean-Square Error (MMSE) Frequency Domain Equalization (FDE) to mitigate multipath fading using guard interval of 128 chips prepended to the data. The Fast Fourier Transform (FFT) block for the FDE is 512 symbols. Within IEEE 802.15.3c activities, several Channel Models (CM) are proposed for residential, office, library, etc. environments [108]. Especially for the residential environment, the LOS and NLOS are considered in CM1.3 (close to Additive White Gaussian Noise (AWGN)) and CM2.3, respectively, which are based on the

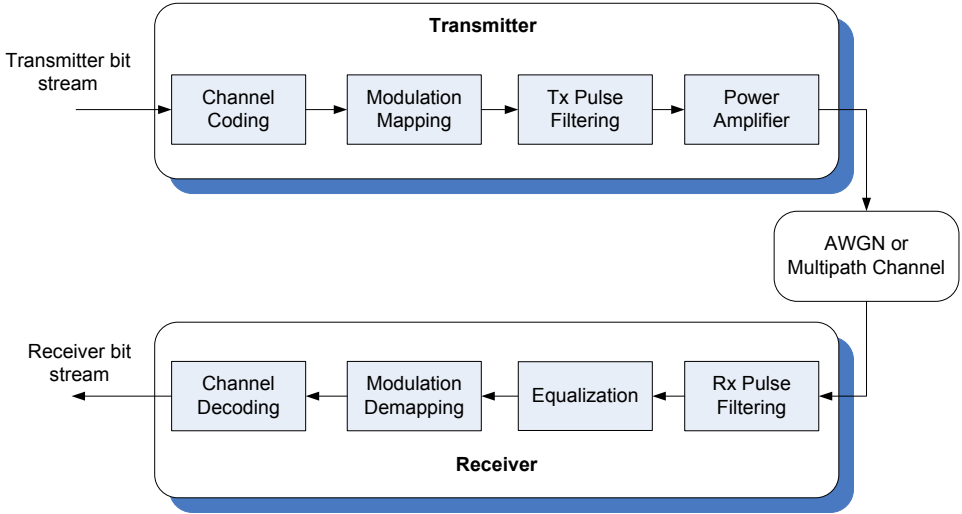


**Figure C.1:** *The transceiver block diagram illustration.*

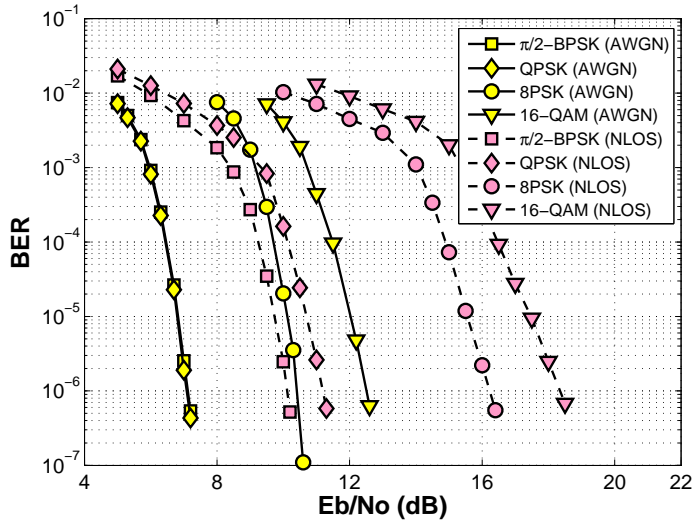


**Figure C.2:** *The BER performance for AWGN and residential NLOS channel [67].*



**Table C.1:** *Parameters of different PHY Modes*

	Modulation	Spreading Factor	Data rate
Mode 1	$\pi/2$ BPSK	1	1.61 Gbps
Mode 2	QPSK	1	3.23 Gbps
Mode 3	8PSK	1	4.86 Gbps
Mode 4	16QAM	1	6.48 Gbps

real measurement.

According to the draft standard, the symbol rate is 1.728 Gs/s and the corresponding PHY data rates is 2.83 Gbps due to the impact of PHY layer overhead such as pilot symbols. The resultant BER performance is shown in Figure C.2. The achievable data rate by using different modulation scheme is listed in Table C.1.



# Bibliography

- [1] Wi-Fi Alliance. [Online]. Available: <http://www.wi-fi.org/>
- [2] Bluetooth. [Online]. Available: <http://www.bluetooth.com>
- [3] *Wireless Medium Access Control (MAC) and Physical Layer (PHY) Specifications for High Rate Wireless Personal Area Networks (WPANs)*, IEEE Std. 802.15.3-2003 Std.
- [4] ZigBee Alliance. [Online]. Available: <http://www.zigbee.org/>
- [5] D. T. Emerson, “The work of Jagadis Chandra Bose: 100 years of millimeter-wave research,” *IEEE Transactions on Microwave Theory and Techniques*, vol. 45, pp. 2267–2273, 1997.
- [6] P. Smulders, H. Yang, and I. Akkermans, “On the design of low-cost 60-GHz radios for multigigabit-per-second transmission over short distances,” *IEEE Communications Magazine*, vol. 45, pp. 44–51, 2007.
- [7] *IEEE 802.15 WPAN Millimeter Wave Alternative PHY TG3c.*, Std. [Online]. Available: <http://www.ieee802.org/15/pub/TG3c.html>
- [8] WirelessHD, “Wirelesshd specification overview,” August 2009.
- [9] IEEE 802.11ad. [Online]. Available: [http://www.ieee802.org/11/Reports/tgad\\_update.htm](http://www.ieee802.org/11/Reports/tgad_update.htm)
- [10] Wireless Gigabit Alliance. [Online]. Available: <http://wirelessgigabitalliance.org/>
- [11] *High Rate 60 GHz PHY, MAC and HDMI PAL*, ECMA International, ECMA 387, 1st Edition Std., Dec. 2008.

- [12] A. Sadri, "Summary of the usage models for 802.15.3c," Nov. 2006, doc. IEEE 802.15-06-0369-09-003c.
- [13] Federal Communications Commission, *Amendment of Parts 2, 15 and 97 of the Commission's Rules to Permit Use of Radio Frequencies Above 40 GHz for New Radio Applications*, FCC 95-499, ET Docket No. 94-124, RM-830, Dec. 1995.
- [14] K. Obara, "Millimeter wave frequency allocation in Europe," Sept. 2003, doc. IEEE802.15.3/0360r0.
- [15] K. Hamagushi, "Japanese regulation for 60 GHz band," Sept. 2003, doc. IEEE802.15.3/0351r1.
- [16] S. Q. Xiao, M. T. Zhou, and Y. Zhang, Eds., *Millimeter Wave Technology in Wireless PAN, LAN, and MAN*. Auerbach Publicatio, 2008.
- [17] H. Friis, "A note on a simple transmission formula," in *Proc. of IRE*, 1946.
- [18] H. A. Kues, S. A. D'Anna, R. Osiander, W. R. Green, and J. C. Monahan, "Absence of ocular effects after either single or repeated exposure to 10 mW/cm<sup>2</sup> from a 60 GHz CW source," *Bioelectromagnetics*, vol. 20, pp. 463–473, 1999.
- [19] J. Winters, "Smart antennas for wireless systems," *IEEE Personal Communications*, vol. 5, pp. 23–27, Feb. 1998.
- [20] A. N. Zadeh, B. Jabbari, R. Pickholtz, and B. Vojcic, "Self-organizing packet radio ad hoc networks with overlay (SOPRANO)," *IEEE Communications Magazine*, June 2002.
- [21] S. K. Yong, M. E. Sahin, and Y. H. Kim, "On the effects of misalignment and angular spread on the beamforming performance," in *Proc. IEEE Consumer Commun. and Networking Conf. (CCNC'07)*, Jan. 2007.
- [22] K. Sohrabi, J. Gao, V. Ailawadhi, and G. J. Pottie, "Protocols for self-organization of a wireless sensor network," *IEEE Personal Communications*, vol. 7, no. 5, pp. 16–27, Oct. 2000.
- [23] S. Vasudevan, J. Kurose, and D. Towsley, "On neighbor discovery in wireless networks with directional antennas," in *Proc. of IEEE INFOCOM'05*, vol. 4, March 2005, pp. 2502–2512.
- [24] L. Galluccio, G. Morabito, and S. Palazzo, "Analytical evaluation of a tradeoff between energy efficiency and responsiveness of neighbor discovery in self-organizing ad hoc networks," *IEEE Journal on Selected Areas in Communications*, vol. 22, no. 7, pp. 1167–1182, September 2004.

- [25] N. Shi, X. An, and I. Niemegeers, "Performance analysis of the link layer protocol for UWB impulse radio networks," in *Proc. of the 3rd ACM international workshop on Performance evaluation of wireless ad hoc, sensor and ubiquitous networks (PE-WASUN'06)*, October 2006, pp. 136–140.
- [26] M. J. McGlynn and S. A. Borbash, "Birthday protocols for low energy deployment and flexible neighbor discovery in ad hoc wireless networks," in *Proc. of the 2th ACM international symposium on MOBIHOC*, October 2001, p. 137145.
- [27] Y. Ko, V. Shankarkumar, and N. H. Vaidya, "Medium access control protocols using directional antennas in ad hoc networks," in *Proc. of IEEE INFOCOM'00*, vol. 1, March 2000, pp. 13–21.
- [28] S. Yi, Y. Pei, and S. Kalyanaraman, "On the capacity improvement of ad hoc wireless networks using directional antennas," in *Proc. of the 4th ACM international symposium on MOBIHOC*, 2003, pp. 108 – 116.
- [29] R. Ramanathan, "On the performance of ad hoc networks with beamforming antennas," in *Proc. of the 2th ACM international symposium on MOBIHOC*, 2001, pp. 95 – 105.
- [30] M. Takai, J. Martin, A. Ren, and R. Bagrodia, "Directional virtual carrier sensing for directional antennas in mobile ad hoc networks," in *Proc. of the 3th ACM international symposium on MOBIHOC*, 2002, pp. 183 – 193.
- [31] R. R. Choudhury, X. Yang, R. Ramanathan, and N. Vaidya, "Using directional antennas for medium access control in ad hoc networks," in *Proc. of the 8th annual International Conference on Mobile Computing and Networking (MobiCom'02)*, Atlanta, Georgia, USA, 2002, pp. 59 – 70.
- [32] S. Singh, F. Ziliotto, U. Madhow, E. M. Belding, and M. Rodwell, "Blockage and directivity in 60 GHz wireless personal area networks: From cross-layer model to multihop MAC design," *IEEE Journal on Selected Areas in Communications, Special Issue on Realizing Gbps Wireless Personal Area Networks*, 2009.
- [33] Z. Zhang, "Performance of neighbor discovery algorithms in mobile ad hoc self-configuring networks with directional antennas," in *Proc. of Military Communications Conference (MILCOM'05)*, Oct. 2005, pp. 1–7.
- [34] J. Ning, T. S. Kim, and S. V. Krishnamurthy, "Directional neighbor discovery in 60 GHz indoor wireless networks," in *Proc. of the 12th ACM international conference on Modeling, analysis and simulation of wireless and mobile systems (MSWiM'09)*, 2009.

- [35] F. Yildirim and H. Liu, "A cross-layer neighbor-discovery algorithm for directional 60-ghz networks," *IEEE Trans. on Vehicular Technology*, vol. 58, pp. 4598–4604, 2009.
- [36] *IEEE standard definitions of terms for antennas (IEEE Std 145-1983)*, Std., June 1983.
- [37] C. A. Balanis, *Antenna theory : analysis and design*. Wiley-Interscience, 2005.
- [38] R. Schmidt, "Multiple emitter location and signal parameter estimation," *IEEE Trans. Antennas Propagation*, vol. AP-34, pp. 276–280, March 1986.
- [39] R. Roy and T. Kailath, "ESPRIT-estimation of signal parameters via rotational invariance techniques," *IEEE Transactions on Acoustics, Speech and Signal Processing*, vol. 37, pp. 984–995, 1989.
- [40] H. Yang, P. F. M. Smulders, and M. H. A. J. Herben, "Channel characteristics and transmission performance for various channel configurations at 60 GHz," *EURASIP Journal on Wireless Communications and Networking*, 2007.
- [41] P. F. Smulders, "Exploiting the 60-GHz band for local wireless multimedia access: Prospects and future directions," *IEEE Communications Magazine*, vol. 40, no. 1, pp. 140–147, Jan. 2002.
- [42] W. Feller, *An Introduction to Probability Theory and its Applications*, 3rd ed. John Wiley and Sons, 1968, vol. 1.
- [43] A. Chandra, V. Gummalla, and J. O. Limb, "Wireless medium access control protocols," *IEEE Communications. Surveys and Tutorials*, vol. 3, 2000.
- [44] N. Abramson, "The ALOHA system - another alternative for computer communication," in *Proc. of 1970 Fall Joint Computer Conference, AFIPS Press*, 1970.
- [45] *Wireless LAN Medium Access Control (MAC) and Physical Layer (PHY) Specifications*, IEEE Standard 802.11 Std., June 1999.
- [46] A. Nasipuri, S. Ye, J. You, and R. E. Hiromoto, "A MAC protocol for mobile ad hoc networks using directional antennas," in *Proc. of IEEE Wireless Communications and Networking Conference (WCNC'00)*, Sep. 23-28, 2000.
- [47] J. Zander, "Slotted aloha multihop packet radio networks with directional antennas," *Electronics Letters*, vol. 26, no. 25, pp. 2098–2100, Dec. 1990.

- [48] T. Elbatt, T. Anderson, and B. Ryu, "Performance evaluation of multiple access protocols for ad hoc networks using directional antennas," in *Proc. of IEEE Wireless Communications and Networking Conference (WCNC'03)*, March 2003, pp. 982–987.
- [49] T. Korakis, G. Jakllari, and L. Tassiulas, "A MAC protocol for full exploitation of directional antennas in ad-hoc wireless networks," in *Proc. of the 4th ACM international Symposium on MOBIHOC*, June 2003, pp. 98–107.
- [50] H. Gossain, C. Cordeiro, T. Joshi, and D. Agrawal, "Cross-layer directional antenna MAC protocol for wireless ad hoc networks: Research articles," *Wireless Communications and Mobile Computing*, vol. 6, pp. 171–182, March 2006.
- [51] P. Bjorklund, P. Varbrand, and D. Yuan, "Resource optimization of spatial tdma in ad hoc radio networks: A column generation approach," in *Proc. of IEEE INFOCOM'03*, 2003, pp. 818–824.
- [52] H. Yin and H. Liu, "Performance of space-division multiple-access (SDMA) with scheduling," *IEEE Transactions on Wireless Communications*, vol. 1, pp. 611–618, Oct. 2002.
- [53] L. X. Cai, L. Cai, X. Shen, and J. W. Mark, "Efficient resource management for mmwave WPANs," in *Proc. of IEEE Wireless Communications and Networking Conference (WCNC'07)*, Mar. 2007, pp. 3816–3821.
- [54] C. Chou, "On the design of medium access control for multi-gbps wireless networks in 60-GHz bands," in *Proc. of IEEE Consumer Communications and Networking Conference (CCNC'09)*, Jan. 2009.
- [55] L. Godara, "Application of antenna arrays to mobile communications, part II: Beam-forming and direction-of-arrival considerations," in *Proc. of IEEE*, vol. 85, no. 8, 1997, pp. 1195–1245.
- [56] OPNET. [Online]. Available: <http://www.opnet.com/>
- [57] U. Rizvi, G. Janssen, and J. Weber, "Impact of rf circuit imperfections on multi-carrier and single-carrier based transmissions at 60 GHz," in *Proc. of IEEE Radio and Wireless Symposium'08*, 2008, pp. 22–25.
- [58] K. H. Liu, H. Rutagemwa, X. Shen, and J. W. Mark, "Efficiency and goodput analysis of Dly-ACK in IEEE 802.15.3," *IEEE Transactions on Vehicular Technology*, vol. 56, pp. 3888–3898, Nov. 2007.
- [59] F. Kojima, C. Pyo, Z. Lan, H. Harada, S. Kato, and H. Nakase, "Necessary modifications on conventional IEEE 802.15.3b MAC to achieve IEEE 802.15.3c millimeter wave WPAN," in *Proc. IEEE PIMRC'07*, Sept. 2007.

- [60] K. Sato and T. Manabe, "Estimation of propagation-path visibility for indoor wireless LAN systems under shadowing condition by human bodies," in *Proc. of the 48th IEEE Vehicular Technology Conference (VTC'98)*, May 1998, pp. 2109–2113.
- [61] S. K. Yong and C. C. Chong, "An overview of multigigabit wireless through millimeter wave technology: potentials and technical challenges," *EURASIP Journal on Wireless Communications and Networking*, Jan. 2007.
- [62] S. Collonge and G. Zaharia, "Influence of the human activity on wide-band characteristics of the 60 GHz indoor radio channel," *IEEE Tran. on Wireless Communications*, vol. 3, Nov. 2004.
- [63] M. Flament and A. Svensson, "Virtual cellular networks for 60 GHz wireless infrastructure," in *Proc. of IEEE International Conference on Communications (ICC'03)*, May 2003.
- [64] M. Unbehauen and J. Zander, "Infrastructure density and frequency reuse for user-deployed wireless LAN systems at 17 GHz in an office environment," in *Proc. of IEEE ICC'01*, 2001, pp. 2535–2539.
- [65] J. Wang, Z. Lan, C. W. Pyo, T. Baykas, C. Sum, M. A. Rahman, J. Gao, R. Funada, F. Kojima, H. Harada, and S. Kato, "Beam codebook based beamforming protocol for multi-Gbps millimeter-wave WPAN systems," *IEEE Journal on Selected Areas in Communications*, 2009.
- [66] K. Kimura and J. Hirokoshi, "Prediction of millimeter-wave multipath propagation characteristics in mobile radio environment," *IEICE Transactions on Electronics*, vol. E82-C, pp. 1253–1259, July 1999.
- [67] C. S. Sum, R. Funada, J. Wang, T. Baykas, M. A. Rahman, and H. Harada, "Error performance and throughput evaluation of a multi-Gbps millimeter-wave WPAN system in multipath environment in the presence of adjacent and co-channel interference," *IEEE Journal on Selected Area of Communications*, vol. 27, Oct. 2009.
- [68] K. Sato, H. Sawada, Y. Shoji, and S. Kato, "Channel model for millimeter wave WPAN," in *Proc. of the 18th Annual IEEE International Symposium on Personal, Indoor and Mobile Radio Communications (PIMRC'07)*, 2007.
- [69] S. Kato, C. Sum, T. Baykas, and Z. Lan, "Common mode signaling (CMS) for intersystem coexistence enhancement," March 2009, IEEE 802.15-09-192-003c.
- [70] L. Chen, T. Sun, and M. Gerla, "Modeling channel conflict probabilities between IEEE 802.15 based wireless personal area networks," in *Proc. IEEE ICC'06*, June 2006, pp. 343–348.



- [71] A. Mehbodniya and S. Aissa, "Coexistence between DS-UWB and MB-OFDM: Analysis and interference mitigation," in *Proc. IEEE Global Telecommunications Conference (GLOBECOM'07)*, Nov. 2007, pp. 5200–5204.
- [72] G. Pasolini, "Analytical investigation on the coexistence of bluetooth piconets," *IEEE Communication Letters*, vol. 8, March 2004.
- [73] M. C. H. Chek and Y. K. Kwok, "Design and evaluation of practical coexistence management schemes for bluetooth and IEEE 802.11b systems," *Computer Networks*, vol. 51, no. 8, June 2007.
- [74] M. Vu, S. Ghassemzadeh, and V. Tarokh, "Interference in a cognitive network with beacon," in *Proc. of IEEE Wireless Communications and Networking Conference (WCNC'08)*, 2008, pp. 876–881.
- [75] A. A. M. Saleh and R. A. Valenzuela, "A statistical model for indoor multipath propagation," *IEEE Journal on Selected Areas in Communications*, vol. 5, pp. 128–137, 1987.
- [76] H. Hashemi, "The indoor radio propagation channel," in *Proc. of IEEE*, vol. 81, no. 7, 1993, p. 943968.
- [77] R. Hekmat, *Ad-hoc Networks: Fundamental Properties and Network Topologies*. Springer, Oct. 2006.
- [78] M. Abramowitz and I. A. Stegun, Eds., *Handbook of Mathematical Functions*. Dover Publications, Inc., New York, 1968.
- [79] A. A. Abu-Dayya and N. C. Beaulieu, "Outage probabilities in the presence of correlated log-normal interferers," *IEEE Transactions on Vehicular Technology*, vol. 43, pp. 164–173, 1994.
- [80] L. Fenton, "The sum of log-normal probability distributions in scatter transmission systems," *IRE Transactions on Communications Systems*, pp. 57–67, 1960.
- [81] Z. Huang, Z. Zhang, and B. Ryu, "Impact of topology control on end to end performance for directional manets," in *Proc. of Military Communications Conference (MILCOM'06)*, Oct. 2006.
- [82] C. Hu, Y. Hong, and J. Hou, "On mitigating the broadcast storm problem with directional antennas," in *Proc. of IEEE ICC'03*, May 2003, pp. 104–110.
- [83] J. Shen, I. Nikolaidis, and J. Harms, "Dynamic 802.15.3 wpan scheduling using maximal matching," in *Proc. IEEE Global Telecommunications Conference (GLOBECOM'06)*, Nov. 2006.

- [84] O. Dousse, F. Baccelli, and P. Thiran, "Impact of interference on connectivity in ad hoc networks," in *Proc. of IEEE INFOCOM'03*, vol. 3, April 2003, pp. 1724–1733.
- [85] R. Sollacher, M. Greiner, and I. Glauche, "Impact of interference on the wireless ad-hoc networks capacity and topology," *Wireless Networks*, vol. 12, no. 1, pp. 53–61, Feb. 2006.
- [86] D. M. Blough, M. Leoncini, G. Resta, and P. Santi, "The k-neighbors approach to interference bounded and symmetric topology control in ad hoc networks," *IEEE Transactions on Mobile Computing*, vol. 5, no. 9, pp. 1267–1282, Sep. 2006.
- [87] R. Hekmat and P. V. Mieghem, "Interference power statistics in ad-hoc and sensor networks," *Wireless Networks*, vol. 14, pp. 591–599, Jan. 2007.
- [88] K. Moaveni-Nejad and X. Li, "Low-interference topology control for wireless ad hoc networks," *Ad Hoc and Sensor Wireless Networks*, vol. 1, pp. 41–64, March 2005.
- [89] M. Burkhart, P. von Rickenbach, R. Wattenhofer, and A. Zollinger, "Does topology control reduce interference," in *Proc. of the 5th ACM international Symposium on MOBIHOC*, 2004, pp. 9–19.
- [90] N. Li, J. C. Hou, and L. Sha, "Design and analysis of an MST-based topology control algorithm," in *Proc. of IEEE INFOCOM'03*, vol. 3, 2003, pp. 1702–1712.
- [91] R. Wattenhofer, L. Li, P. Bahl, and Y. Wang, "Distributed topology control for power efficient operation in multihop wireless ad-hoc networks," in *Proc. of IEEE INFOCOM'01*, vol. 3, 2001, pp. 1388–1397.
- [92] J. Wozencraft and I. Jacobs, *Principles of Communication Engineering*. New York : Wiley, 1965.
- [93] S. Ni, Y. Tseng, Y. Chen, and J. Sheu, "The broadcast storm problem in a mobile ad hoc network," in *Proc. of the 5th annual International Conference on Mobile Computing and Networking (MobiCom'99)*, Aug. 1999, pp. 151–162.
- [94] Z. J. Haas, J. Y. Halpern, and L. Li, "Gossip-based ad hoc routing," in *Proc. of IEEE INFOCOM'02*, vol. 3, 2002, pp. 1707–1716.
- [95] P. Kyasanur, R. R. Choudhury, and I. Gupta, "Smart gossip: an adaptive gossip-based broadcasting service for sensor networks," in *Proc. of IEEE International Conference on Mobile Adhoc and Sensor Systems (MASS'06)*, 2006.

- [96] Y. Sasson, D. Cavin, and A. Schiper, "Probabilistic broadcast for flooding in wireless mobile ad hoc networks," in *Proc. of IEEE Wireless Communications and Networking Conference (WCNC'03)*, March 2003, pp. 1124–1130.
- [97] M. J. Lin and K. Marzullo, "Directional gossip: Gossip in a wide area network," in *Proc. of European Dependable Computing Conference*, 1999, pp. 364–379.
- [98] J. Cartigny and D. Simplot, "Border node retransmission based probabilistic broadcast protocols in ad-hoc networks," *Telecommunication Systems*, vol. 22, pp. 189–204, 2003.
- [99] G. Grimmett, *Percolation*. Springer-Verlag, 1989.
- [100] X. Chen, J. Lu, and Z. Zhou, "An enhanced high-rate WPAN MAC for mesh networks with dynamic bandwidth management," in *Proc. IEEE Global Telecommunications Conference (GLOBECOM'05)*, Dec. 2005, pp. 3408–3411.
- [101] Z. Yin and V. Leung, "Third-party handshake protocol for efficient peer discovery in IEEE 802.15.3 WPANs," in *Proc. IEEE International Conference on Broadband Networks (BroadNets'05)*, Oct. 2005, pp. 840–849.
- [102] P. F. Smulders, "Broadband wireless lans: A feasibility study," Ph.D. dissertation, Eindhoven University of Technology, The Netherlands, 1995.
- [103] Z. Genc, B. L. Dang, J. Wang, and I. Niemegeers, "Home networking at 60 GHz: challenges and research issues," *Annals of Telecommunications*, vol. 63, pp. 501–509, 2008.
- [104] P. Xue, P. Gong, and D. Kim, "Enhanced IEEE 802.15.3 MAC protocol for efficient support of multiple simultaneously operating piconets," *IEEE Trans. on Vehicular Technology*, vol. 57, pp. 2548–2559, July 2008.
- [105] F. daCosta, *Dynamic Beacon Alignment in Simultaneously Operating Piconets (SOP) Using the Heart Beat Approach*, IEEE Std. P802.15-04/135r0 Std., Mar. 2004.
- [106] R. Choudhury and N. Vaidya, "Impact of directional antennas on ad hoc routing," in *Proc. of International LNCS Conference on Personal and Wireless Communication*, 2003.
- [107] N. Jefferies, "Global vision for a wireless world," in *Proc. of the 18th meeting of WWRf, Helsinki, Finland*, 2007.
- [108] S. K. Yong, "TG3c channel modeling sub-committee final report," Nov. 2006, IEEE 802.15-06-0195-07-003c.



## List of Abbreviations

ACK	Acknowledgment
ASIE	Application Specific Information Element
AWGN	Additive White Gaussian Noise
BER	Bit Error Rate
Blk-ACK	Block ACK
BPSK	Binary Phase Shift Keying
BS	Beam Switching
C/I	Carrier to Interference ratio
CAP	Contention Access Period
CCI	Co-Channel Interference
cdf	cumulative distribution function
CMOS	Complementary Metal Oxide Semiconductor
CSMA	Carrier Sense Multiple Access
CSMA/CA	CSMA with Collision Avoidance
CTA	Channel Time Allocation
CTAP	Channel Time Allocation Period
CTRp	Channel Time Response
CTRq	Channel Time Request
CTS	Clear to Send
DA	Directional Advertising
DD	Directional transmitting and Directional receiving
DEV	Device
Dly-ACK	Delayed ACK

D-ND	Directional Neighbor Discovery
DO	Directional transmitting and Omni-directional receiving
DoA	Direction of Arrival
DS-UWB	Direct Sequence UWB
DTS	Directional Transmission Scheduling
ECMA	European Computer Manufacturers Association
EMA	Exponential Moving Average
FA	Forwarding Algorithms
FCC	Federal Communications Commission
FCFS	First Come First Served
FCS	Frame Check Sequence
FCSL	Frame Convergence SubLayer
FDE	Frequency Domain Equalization
GaAs	Gallium Arsenid
Gbps	Gigabits per second
GCS	Giant Component Size
GSM	Global System for Mobile communications
HDMI	High Definition Multimedia Interface
HDTV	High Definition TeleVision
ICT	Information and Communication Technolog
Imm-ACK	Immediate ACK
InP	Indium Phosphide
LCT	Link Coexistence Test
LOS	Line-of-Sight
MAC	Medium Access Control
MB-OFDM	Multi-band Orthogonal Frequency Division Multiplexing
MCS	Modulation and Coding Scheme
MCTA	Management CTA
MSDU	MAC Service Data Unit
MST	Minimum Spanning Tree
ND	Neighbor Discovery
NF	Noise Figure
NLOS	Non Line-of-Sight
OFDM	Orthogonal Frequency Division Multiplexing
OPNET	Optimized Network Engineering Tools
OSI	Open System Interconnection
PER	Packet Error Rate
PHY	Physical Layer
PNC	Piconet Coordinator
PSTN	Public Switched Telephone Network
QoS	Quality of Service
QPSK	Quadrature Phase Shift Keying
RERR	Route Error
RF	Radio Frequency
RIFS	Retransmission Inter-Frame Space

RRD	Radio Relaying Device
RREP	Route Reply
RREQ	Route Request
RTR	Route-reply Triggered Resource-reservation
RTS	Request to Send
RWP	Random Way Point
SAP	Service Access Point
SIFS	Short Inter-Frame Space
SINR	Signal to Interference plus Noise Ratio
SRF	Spatial Reuse Factor
TDMA	Time Division Multiple Access
UCA	Uniform Circular Array
UMTS	Universal Mobile Telecommunications System
UWB	Ultra Wide Band
VHT	Very High Throughput
VoIP	Voice over Internet Protocol
WLAN	Wireless Local Area Networks
WMAN	Wireless Metropolitan Area Networks
WPAN	Wireless Personal Area Networks
WWAN	Wireless Wide Area Networks





# Publications by the Author

## Journal Publications

- [J1] X. An, C. S. Sum, R. V. Prasad, H. Harada, and I. Niemegeers, “Impact of Antenna Pattern and Link Model on Directional Neighbor Discovery in 60 GHz Networks,” submitted to IEEE Transactions on Wireless Communications.
- [J2] X. An, C. S. Sum, R. V. Prasad, H. Harada, and I. Niemegeers, “Performance Analysis of Synchronization Frame based Interference Mitigation in 60 GHz WPANs,” IEEE Communications Letters, May 2010, 14(5), pp. 471-473.
- [J3] J. Wang, R.V. Prasad, X. An, and I. Niemegeers, “A study on wireless sensor network based indoor positioning systems for context-aware application,” Wiley Wireless Com. and Mobile Computing, Jan. 2010.
- [J4] R. Hekmat and X. An, “Relation between Interference and Neighbor Attachment Policies in Ad-hoc and Sensor Networks,” International Journal of Hybrid Information Technology (IJHIT) Journal, Vol.1 No.2, April 2008.

## Conference Publications

- [C1] X. An, R. V. Prasad, H. Harada, and I. Niemegeers, “Neighbor Discovery Investigation in Wireless Personal Area Networks using 60 GHz Radio Technology,” IEEE International Symposium on a World of Wireless, Mobile and Multimedia Networks (WoW-MoM), Industry Track, June 2010.

- [C2] T. Baykas, X. An, C. S. Sum, M. A. Rahman, J. Wang, Z. Lan, R. Funada, and H. Harada, "Investigation of Synchronization Frame in Multi-Gbps 60 GHz WPANs," IEEE Wireless Communications and Networking Conference (WCNC'10), Sydney, Australia, April 2010.
- [C3] X. An, J. Vazifehdan and R. Hekmat, R. V. Prasad, H. Harada, and I. Niemegeers, "Extending 60 GHz based WPANs to Support Multi-hop Communications with QoS," IEEE Consumer Communications and Networking Conference (CCNC'10), Jan. 2010.
- [C4] X. An and R. Hekmat, "Probabilistic-based Message Dissemination in Ad Hoc and Sensor Networks using Directional Antennas," IEEE International Conference on Mobile Ad-hoc and Sensor Systems (MASS'09), Oct. 2009, Macau, P.R. China.
- [C5] T. Baykas, X. An, C.S. Sum, J. Wang, M. Rahman, Z. Lan, R. Funada, H. Harada, "Effect of Beacon Design to WPAN Throughput," IEICE conference on Radio Communication Systems (RCS), Oct. 2009, Kyoto, Japan.
- [C6] X. An, C. S. Sum, J.Y. Wang, Z. Lan, J. Wang, R.V. Prasad, R. Hekmat, H. Harada, and I. Niemegeers, "Beam Switching Support to Resolve Link-Blockage Problem in 60 GHz WPANs," IEEE Personal, Indoor and Mobile Radio Comm. Conf. (PIMRC'09), Sept. 2009, Tokyo, Japan. (**Best Student Paper Award**)
- [C7] X. An, Z. Lan, R. V. Prasad, R. Hekmat, H. Harada, and I. Niemegeers, "Performance Analysis of the Frame Aggregation Mechanisms in IEEE 802.15.3c," IEEE PIMRC'09, Sept. 2009, Tokyo, Japan.
- [C8] C.S. Sum, X. An, Z. Lan, T. Baykas, J. Wang, R. Funada, M. Rahman, H. Harada, S.Kato, "A Synchronization-Frame-Aided Interference Mitigation Mechanism for Millimeter-wave WPAN," IEEE PIMRC'09, Sept. 2009, Tokyo, Japan.
- [C9] X. An and R. Hekmat, "Inter-Piconet Route Discovery to Support 60 GHz based Wireless Mesh Network," WiMesh, conjunction with IEEE SECON'09, June 2009, Rome, Italy.
- [C10] X. An and R. Hekmat, "A QoS-aware and Fair Resource Allocation Scheme for WPANs," IEEE CCNC'09, Jan. 2009, Las Vegas, USA.
- [C11] X. An, S. Zhang, and R. Hekmat, "Enhanced MAC Layer Protocol for Millimeter Wave based WPAN," IEEE PIMRC'08, Sept. 2008, Cannes, France.

- [C12] R. Hekmat and X. An, "On the Performance of Ad-hoc and Sensor Networks," ICT-MobileSummit'08, June 2008, Stockholm, Sweden.
- [C13] X. An and R. Hekmat, "Directional MAC Protocol for Millimeter Wave based Wireless Personal Area Networks," IEEE Veh. Technol. Conf. (VTC'08-Spring), May 2008, Singapore, pp. 1636-1640.
- [C14] R. Hekmat and X. An, "Effects of Neighbor Attachment Policies on Interference in Ad-hoc and Sensor Networks," International Conference on Future Generation Communication and Networking (FGCN'07), Jeju Island, South Korea, Dec. 2007, pp.152-156.
- [C15] R. Hekmat and X. An, "A Framework for Performance Evaluation of Wireless Ad-hoc and Sensor Networks", the 15th IEEE International Conference on Networks (ICON'07), Adelaide, Australia, Nov. 2007, pp. 412-418. **(Best Paper Award)**
- [C16] X. An and R. Hekmat, "Self-Adaptive Neighbor Discovery in Ad Hoc Networks with Directional Antennas," the 16th IST Mobile and Wireless Communications Summit, Budapest, Hungary, July 2007.
- [C17] J. Wang, X. An and R. V. Prasad, I.G.M.M. Niemegeers, "RF-OPT: A Range-Free Online Person Tracking System," the 1st ACM International Conference on Pervasive Computing Technologies for Healthcare 2006 , Innsbruck, Austria, Nov. 2006
- [C18] N. Shi, X. An and I.G.M.M. Niemegeers, "Performance Analysis of the Link Layer Protocol for UWB Impulse Radio Networks," the 3rd ACM PE-WASUN, conjunction with MSWiM 06, Oct. 2006, Malaga, Spain, pp. 136-140.
- [C19] X. An, J. Wang, R. V. Prasad and I.G.M.M. Niemegeers, "OPT - Online Person Tracking System for Context-awareness in Wireless Personal Network," REALMAN, conjunction with MobiHoc 06, May, 2006, Florence, Italy, pp. 47-54.

## Demo

- [D1] X. An, J. Wang, R. V. Prasad and I.G.M.M. Niemegeers, "OPT - Online Person Tracking System for Context-awareness in Wireless Personal Network (Demo)," REALMAN, conjunction with MobiHoc 06, May, 2006, Florence, Italy.

**Relation to This Dissertation**

This thesis is based on the previously published publications. The table on this page depicts the relation between the publications and the chapters of the dissertation, in which, “●” represents major relation, “○” represents minor relation.

Pub.	Chap.2	Chap.3	Chap.4	Chap.5	Chap.6	Chap.7	Chap.8
J1	●						
J2					●		
J3							
J4						●	
C1	●						
C2					●		
C3							●
C4						●	
C5					○		
C6				●			
C7			●				
C8					○		
C9							●
C10		●					
C11		●					
C12						○	
C13		●					
C14						●	
C15						○	
C16	○						
C17							
C18							
C19							
D1							

## Curriculum Vitae

Xueli An was born in Harbin, China, on May 23, 1980. She graduated with her Bachelor of Engineering (B.Eng.) degree from Harbin Institute of Technology (HIT), China, in July 2003. She graduated with M.Sc degree in Electrical Engineering from Delft University of Technology, the Netherlands, in July 2005. In Sept. 2006, she started her research work as a PhD candidate at the Wireless and Mobile Communications (WMC) group, faculty of Electrical Engineering, Mathematics and Computer Science (EEMCS), Delft University of Technology, the Netherlands. From March 2009 to June 2009, she took an internship in the Ubiquitous Mobile Communications Group, National Institute of Information and Communications Technology (NICT), Yokosuka, Japan. Her research work in TU Delft, which is presented in this dissertation, focused on the medium access control layer and network layer design for 60 GHz featured wireless personal area networks.

She was awarded Delta Scholarship from TU Delft in Sept. 2003. She received the Best Paper Award at the 15th IEEE International Conference on Networks (ICON'07), Adelaide, Australia, 2007. She was the winner of the Best Student Paper Award at the 20th IEEE International Symposium on Personal, Indoor and Mobile Radio Communications (PIMRC'09), Tokyo, Japan, 2009. She was awarded the Travel Grant from IEEE International Conference on Mobile Ad-hoc and Sensor Systems (MASS'09), Macau, P.R. China, 2009.